

Programa de Doctorado en Ciencia y Tecnología

Tesis Doctoral

**THE CIRCULAR ECONOMY PRINCIPLES OF REPAIR, RECYCLE,
AND REDUCE APPLIED TO THE DEVELOPMENT OF
STYRENE-BUTADIENE RUBBER COMPOSITES**

JAVIER ALEJANDRO ARAUJO MORERA

INSTITUTO DE CIENCIA Y TECNOLOGÍA DE POLÍMEROS

2021

Programa de Doctorado en Ciencia y Tecnología

Tesis Doctoral

**THE CIRCULAR ECONOMY PRINCIPLES OF REPAIR, RECYCLE,
AND REDUCE APPLIED TO THE DEVELOPMENT OF
STYRENE-BUTADIENE RUBBER COMPOSITES**

JAVIER ALEJANDRO ARAUJO MORERA

Ingeniería de Materiales

Directores

Dra. Marianella Hernández Santana

Dra. Raquel Verdejo Márquez

INSTITUTO DE CIENCIA Y TECNOLOGÍA DE POLÍMEROS

A mi familia

"It is our choices, that show what we truly are, far more than our abilities"

J. K. Rowling

Agradecimientos

Quisiera expresar mi mayor y más sincero agradecimiento a mis directoras de Tesis, *Dra. Raquel Verdejo Márquez* y *Dra. Marianella Hernández Santana*. A *Raquel* por todo el tiempo que me has dedicado, por tu amabilidad, empatía e interés siempre. A *Marianella*, por haber confiado en mí y darme la oportunidad de desarrollarme en este mundo. ¿Quién diría que, aunque el correo que te envié al llegar a Madrid hace 6 años se extravió, te convertirías en mi Directora de Tesis? Como dice el refrán, “Cuando te toca, ni aunque te quites; cuando no te toca, ni aunque te pongas”. Gracias a ambas por su inestimable ayuda, dedicación, positivismo, por la confianza que depositaron en mí, por el ánimo en todo momento a lo largo de esta aventura y enseñarme el significado de la constancia y la dedicación.

A todos los miembros y compañeros del *Grupo de Compuestos Poliméricos* del Instituto de Ciencia y Tecnología de Polímeros (ICTP), con los que he podido compartir espacios y experiencias: *Rubén Sánchez, Mario Hoyos, Said El Khezraji, Suman Thakur, Raúl Doral, Ornella Ricciardi* y *Sergio González*. Y especialmente a *Mónica Peñas, Amparo Fernández, Alberto Santiago* y *Jordy Guadalupe* por las risas en el laboratorio y los momentos de catarsis.

Quisiera expresar un agradecimiento muy especial al *Dr. Javier Carretero González* y *Dr. Miguel Ángel López Manchado*, por ser una fuente de inspiración, por sus consejos, apoyo, comentarios constructivos y demostrarme y transmitirme la pasión por la ciencia.

A *Saúl Utrera*, por siempre estar dispuesto a ayudarme, por tu buena actitud, apoyo y positivismo. Gracias por compartir conocimientos, experiencias y muchas risas.

A *Reyes Verdugo*, por ser mi fuente de alegría y energía en este último tiempo. Gracias por animarme, ayudarme y apoyarme constantemente, por dedicarme bonitas palabras, transmitirme tus buenas vibras y tu buena actitud. Gracias por tantas risas y confidencias.

A todos aquellos que contribuyeron en esta Tesis. Al Servicio de Caracterización del ICTP: *Carolina García, Esperanza Benito, Pilar Posadas, Isabel Muñoz, David Gómez* y *Patricia Sampedro*. Al Servicio de Mantenimiento de Equipos, Infraestructura e Informática del ICTP: *Manuel Rus, Alberto Hernando* y *Carlos Álvarez*. Al Servicio de Gerencia y Administración, especialmente a *María Jesús de Benito*. Gracias a todos por su buena disposición siempre.

A compañeros y amigos de otros grupos de investigación del ICTP, que de forma incondicional me echaron una mano.

Al *Grupo de Ingeniería Macromolecular*, en especial, *Marta Fernández, Daniel López, Laura Peponi, Coro Echeverría, Agueda Sonseca, Alexandra Muñoz, Sandra Santaolalla, Adrián Leonés, Marina Arrieta, Gema Rodríguez, Castor Salgado y Alberto Chiloeches*. Gracias por el apoyo y siempre tener buenas palabras hacia mí.

Al *Grupo de Elastómeros*, en especial, *Antonio González, Alberto Fernández, Rodrigo Navarro, Rebeca Herrero y Juan López Valentín*. Gracias por transmitirme su cariño, ilusión, por su apoyo tanto a nivel profesional como personal y hacerme sentir siempre querido y parte de su grupo.

A los "*Forasteros en El Mundo*", aquellos compañeros que pasaron por el ICTP durante una temporada y se convirtieron en muy buenos amigos. En especial, *Albanelly Soto, Francisco Rivera, Francisco González y Daniel Canales*. Gracias por el apoyo, las charlas, las reuniones y salidas de "tranquis". Los recuerdo con mucho cariño.

A mis amigos y que por mucho tiempo fueron mi grupo de comida: *María Puertas, Ana Mora, Jorge Montero, Estela Sanzhorcajo y Vanesa Yuste*. Gracias por tantas charlas, risas, anécdotas y buenas energías.

A todos aquellos amigos, que, sin estar vinculados a la Tesis, me han acompañado a lo largo de estos últimos años con palabras de ánimo: *Jonathan González, Josmari Cuenda, Andrea Salas, Gabriela Garzón, José Jiménez, Santiago De Laguno, Dina Castro, Vanesa Suaza, Laura Pericet, y Linda Díaz*. Quiero agradecer especialmente a *Lorenzo Chichiricco, Rosa Martínez, Antonio Capezza y Wolfgang Suárez*, por su apoyo e interés en todo momento. Gracias por su amistad y brindarme todo su cariño.

A *María José Perdomo (Majo)*, por ser mi amiga y confidente, por tus consejos y ser un apoyo incondicional, animarme, escucharme y estar siempre, en las buenas y en las malas.

I would like to thank *Fabian Grunert (Fabi)* for your friendship, kindness, since the day we met, for your advices and for your support.

A *Pilar Bernal (Pi)*, por todas las experiencias vividas, los paseos, fiestas, desayunos, cafecitos, risas y comilonas. Por ser mi amiga, confidente, animarme, ayudarme y ser un apoyo para mí siempre. Ya son 7 años y contando.

A mi *familia*, por sus buenos deseos y siempre apoyarme en los caminos y decisiones que he tomado.

A mis niños, *Piloto, Owen y Panxito, (P.O.P)*, por ser los mejores y más fieles compañeros que he podido tener. Gracias por recargarme de energía y llenarme de amor durante este largo viaje y por la compañía durante la escritura de la Tesis.

A *Hugo Intriago*, por ser mi compañero de vida, mi cómplice, y un apoyo incondicional desde el inicio de esta aventura. Gracias por los viajes, las escapadas, los momentos de diversión y todas las risas. Por nosotros y por muchos momentos más juntos. ¡Te quiero!

A mi madre, *Mercedes Morera*, por ser mi modelo a seguir, un apoyo incondicional y por todo el amor y comprensión que siempre me has dado. Por tener siempre la fortaleza de seguir adelante a pesar de las dificultades. Todo lo que soy te lo debo a ti. ¡Te amo!

Javier

Table of contents

Abstract	7
Resumen	15
1. Introduction	31
1.1. The tire industry.....	33
1.2. Circular economy applied to tires	37
1.2.1. Redesign.....	37
1.2.2. Renew.....	39
1.2.3. Reduce	43
1.2.4. Reuse	46
1.2.5. Repair	48
1.2.6. Recover	51
1.2.7. Recycle	54
1.3. References	62
2. Materials and methods	73
2.1. Materials.....	73
2.2. Preparation of SBR composites	81
2.2.1. Formulation.....	81
2.2.2. Mixing	81
2.2.3. Vulcanization.....	83
2.3. Experimental techniques	84
2.3.1. Physico-chemical properties	84
2.3.2. Mechanical properties.....	91
2.3.3. Dynamic properties	92
2.3.4. Self-healing properties	94
2.4. References	97
3. “R” as Repair - Healing of SBR Compounds	101
3.1. Effect of the vulcanization system	103
3.2. Optimization of the self-healing protocol.....	108
3.3. Effect of the vulcanizing additives	119
3.3.1. Effect of sulfur content	120
3.3.2. Effect of ZnO/SA content	127
3.4. Understanding the self-healing mechanism.....	134
3.5. Summary	139
3.6. References	141

4. “R” as Recycle - Healing of SBR/GTR Composites	146
4.1. Experimental.....	148
4.1.1. Grinding protocols.....	148
4.1.2. Particle Size Distribution.....	149
4.1.3. Surface Modification.....	149
4.1.4. Hydrophilicity Test.....	150
4.1.5. Payne effect.....	150
4.2. SBR composites preparation.....	152
4.3. Modification and characterization of GTR.....	154
4.3.1. As-received GTR.....	154
4.3.2. Cryo-grinding of GTR.....	157
4.3.3. Surface modification of GTR.....	158
4.4. Development of SBR/GTR composites.....	170
4.4.1. Characterization of SBR/GTR composites.....	170
4.4.2. Self-healing SBR/GTR composites.....	182
4.5. Development of hybrid reinforced SBR composites.....	187
4.5.1. Characterization of hybrid reinforced SBR composites.....	188
4.5.2. Self-healing of hybrid reinforced SBR composites.....	197
4.6. Summary.....	202
4.7. References.....	204
5. “R” as Reduce – Dynamics of SBR/GTR Composites	211
5.1. Experimental.....	213
5.1.1. Broadband dielectric spectroscopy (BDS).....	213
5.1.2. Dynamic-mechanical analysis (DMA).....	216
5.1.3. Microscopic network damage.....	220
5.2. BDS analysis. Evaluation of pristine composites.....	220
5.2.1. Effect of sulfur content.....	220
5.2.2. Effect of curing system.....	222
5.2.3. Effect of filler type and content.....	227
5.2.4. Effect of coupling agent (CA).....	236
5.3. DMA analysis. Evaluation of pristine composites.....	241
5.4. Dynamics of self-healing SBR composites.....	247
5.4.1. Analysis of network damage.....	247
5.4.2. Correlating dynamics and structure with healing.....	250
5.4.3. Healing as part of the magic triangle of tires.....	257
5.5. Summary.....	261

5.6. References	262
6. Summary and final remarks	269
6.1. General conclusions	269
Repair	269
Recycle	269
Reduce.....	270
6.2. Outlook and future work	271
Appendix	277
Publications related to this Doctoral Thesis	277
Other articles.....	278
Dissemination articles	279
Oral contributions	280
Dissemination activities.....	280

ABSTRACT

Abstract

Introduction

The world is currently undergoing a radical transformation. The more stringent environmental regulations and the fluctuating price of raw materials are leading society to develop more responsible consumption habits. The society is moving from the currently linear economy model (extract-manufacture-consume-dispose) to a circular economy (CE) model, that replaces the notion of “dispose” with “restore”, which has the potential to deliver benefits at all scales, from individual citizens to the global economy, and society. The circular economy (CE) model aims at extending the lifetime of resources through their rational and efficient use in order to generate value repeatedly, reducing costs and waste. The main principles of the CE are based on 7 basic notions (Redesign, Renew, Reduce, Reuse, Repair, Recover and Recycle).

Elastomers are a special class of polymeric materials with a wide range of applications. They are extensively used in industrial sectors like the aerospace or the biomedical industry. However, a large proportion of their production is used in the transport sector as tires. Thanks to their inherent stable covalently bonded three-dimensional molecular network, elastomers can sustain large deflections with little or no permanent deformation. Nonetheless, rubbers can also fail through fracture and fatigue processes. As a consequence of this weakness, one of the most serious environmental problems facing society today is the accumulation of large quantities of end-of-life tires (ELTs) in landfill sites, and the increasing automotive production over the years continuously aggravates it.

Recycling and recovering used tires can be considered reasonable strategies to solve this concern. However, there are some limitations to overcome, since a tire is composed of various materials and additives incorporated in the rubber compound, turning it into a very complex system. Meanwhile, the approach of self-healing materials, characterized by the ability to recover fully or partially their performance after suffering damage, is more than ever attractive. However, applying such concept to attain healing in rubbers is especially challenging, since the restrictions imposed by crosslinks prevent the polymer chains from forming new bonds across previously damaged areas, theoretically blocking their self-healing capability.

Objectives

The main objective of this Doctoral Thesis is the development of sustainable styrene-butadiene rubber (SBR) composites, since SBR is one of the main elastomers used in tires, combining self-healing properties with the inclusion of ELTs as a sustainable alternative to traditional reinforcing fillers, to address the tire waste management issue, and following the CE principles of Repair, Recycle and Reduce.

Self-healing capability will be achieved through the restoration of crosslinks across damaged surfaces, extending the rubber lifetime. Sustainability will be given by the addition of reclaimed tires as filler, providing alternative usage of rubber waste, reducing the demand of non-renewable resources and contributing to the restoration of degraded ecosystems. Therefore, this Doctoral Thesis serves as a starting point for the development of new economically, energetically and environmentally convenient elastomeric systems, with potential use in the tire industry, and at the same time, defines an environmentally friendly scenario for addressing the rubber waste disposal issue.

This Doctoral Thesis has been divided into 6 chapters. Chapter 1 introduces the state of the art of the route followed by tires from the CE perspective. From the early stages of production to the post-consumption step, the path that tires trail within this CE model evidences the commitment and efforts towards the development of effective management schemes for achieving a real sustainable mobility. Chapter 2 details the materials and the general experimental techniques and methods that have been used throughout the preparation and characterization of the developed rubber composites. Chapter 3 explains the validation of self-healing concepts in a SBR matrix and provides details of the effect of different vulcanization systems on the self-healing capability of the rubber compounds. Chapter 4 addresses the incorporation of tire waste, traditional fillers and hybrid filler systems to the self-healing matrix for enhancing its mechanical properties and for achieving a good trade-off between mechanical properties and self-healing capability. Chapter 5 focuses on the evaluation of the molecular dynamics of the developed rubber composites to comprehend the effect of different systems on the relaxation mechanisms and healing capability of the rubber matrix. And finally, the conclusions of the thesis and future outlook are given in Chapter 6.

Conclusions

In this doctoral thesis, SBR eco-friendly composites that combine self-healing properties with the use of ELTs as alternative filler were developed, following CE principles. The main results have served for defining an environmentally friendly scenario for addressing the rubber waste disposal problem, extending service life of products and reducing rubber waste by re-bonding the damaged materials. Combining the inclusion of rubber tire waste as alternative filler, and the self-healing capability of the rubber composites will contribute to the future of the tire industry and the mobility of tomorrow, where technological and sustainability demands are growing every day.

Repair

This work presents experimental results that validate self-healing concepts in SBR compounds. The healing mechanism arises from the combination of two different processes. First, the chain interdiffusion and formation of physical entanglements take place, during the initial stages of healing process. Second, long-range interactions and disulfide exchange reactions, as intrinsic self-healing mechanism, result in the almost full recovery of mechanical stress. Hence, vulcanizing additives, such as zinc oxide (ZnO) and stearic acid (SA), affect healing in its early stages. Meanwhile, sulfur (S) is the fundamental component that promotes the almost full recovery of a macroscopic damage when applying a healing protocol of 130 °C for 1 h.

Temperature and time also affect the repair mechanism, achieving higher healing efficiencies as time and/or temperature increased, thanks to the enhanced mobility and interdiffusion of molecular chains. Moreover, the SBR compound herein developed exhibited repeatable healing after multiple cycles, resulting an acceptable recovery of tensile strength of 60 % after 3 cycles.

Recycle

A fundamental, extensively and systematic study has been carried out to understand the healing mechanism of SBR composites and the influence of cryo grounded GTR (c-GTR) and modified GTR (m-GTR) as sustainable filler in the rubber properties of the developed composites. A successful mechano-chemical modification of GTR was accomplished with a combination of a cryo-grinding process and a chemical treatment. The cryo-grinding

Abstract

process was successfully optimized, reducing the average particle size of the departing material up to 100 – 150 μm . The most effective modification of the GTR particles was performed with sulfuric acid (H_2SO_4), corroborated by the increase in oxygen content on the surface of the GTR. The c-GTR and m-GTR composites showed a good balance between tensile strength and healing capability when applying 130 $^\circ\text{C}$ during 5 h, and confirm the great potential of c-GTR and m-GTR as sustainable filler in rubber materials. A good compromise between healing efficiency and mechanical performance was promoted by the combination of disulfide bonds and reversible ionic bonds, which come from the functional groups on the surface of the m-GTR. The use of a coupling agent (CA) provided better filler dispersion and interaction with the SBR matrix, leading to an increase in mechanical strength, but limiting the healing capability. Hybrid reinforcing SBR composites, combining m-GTR and conventional fillers such as carbon black (CB) and silica (Si), were also developed in order to overcome the limitations of c-GTR and m-GTR. The hybrid system consisting of 20 phr m-GTR and 20 phr CB turned out as the best SBR composite with a positive balance between mechanical strength and healing efficiency.

Reduce

The “magic triangle” is defined by three main material-specific requirements relevant to the tread (rolling resistance, wet grip, and abrasion resistance). The rolling resistance (fuel consumption) and wet grip (driving safety) are intimately linked to the viscoelastic properties of the tire tread material. Therefore, it is of great interest to study molecular dynamics at a scale close to molecular processes. In this work, the magic triangle of tires was customized, substituting wear resistance for healing ability. It was demonstrated that the good properties of the m-GTR₂₀-CB₂₀ sustainable composite had some limitations when applied in tire tread composites. However, in presence of a CA, the three triangle indices were optimized, overcoming the delicate balance between rolling resistance, wet grip, and healing efficiency; hence, reducing fuel consumption, increasing driving safety and extending lifetime.

Correlations between the dynamics and the molecular structure of the developed composites were also established in an attempt to understand the physical properties and the possible repair mechanism at the microscopic scale. The presence of CA, fillers and high S content tend to restrict the segmental dynamics of the SBR matrix due to the formation of a more cross-linked network. Meanwhile, accelerants affect the inter- and intra-molecular interactions between the rest of the additives, fillers and rubber matrix.

Selected composites were analyzed under three different conditions: pristine, damaged by cyclic deformation, and thermally healed. When damaged, the composites show faster dynamics; meanwhile, after the application of the healing protocol, the dynamics tends to slow down, and the rubber network becomes more heterogeneous due to the chain interdiffusion and reversibility of disulfide bonds, which enable the full recovery of stiffness at different temperature regions (-80 °C and 30 °C). Moreover, it was found that a microscopic damage requires shorter periods of healing to achieve a high healing efficiency, if compared to macroscopic damaged composites.

RESUMEN

Resumen

Introducción

Actualmente el mundo está experimentando una transformación radical. Las estrictas regulaciones ambientales y el precio fluctuante de las materias primas están conduciendo a la sociedad a desarrollar hábitos de consumo más responsables. La sociedad está pasando del actual modelo de economía lineal basado en el principio de “extraer-fabricar-consumir-desechar” a un modelo de economía circular (EC) reemplazando la noción de “desechar” por “restaurar”, que tiene el potencial de generar beneficios en todas las escalas de la sociedad y en la economía global. El modelo de EC tiene como objetivo alargar la vida útil de los recursos mediante su uso racional y eficiente, con el fin de generar valor de forma repetida, reduciendo costes y residuos. Los principios de la economía circular se basan en 7 nociones básicas (Rediseñar, Renovar, Reducir, Reutilizar, Reparar, Recuperar y Reciclar).

Los elastómeros son una clase especial de materiales poliméricos con una amplia gama de aplicaciones. Estos materiales se utilizan en sectores industriales como el aeroespacial o la industria biomédica. Sin embargo, gran parte de su producción se utiliza en el sector del transporte como neumáticos. La red molecular tridimensional enlazada covalentemente de los elastómeros les permite soportar grandes deflexiones con poca o ninguna deformación permanente. No obstante, los elastómeros también pueden fallar por procesos de fractura y fatiga. Como consecuencia de esta debilidad, uno de los problemas ambientales más graves que enfrenta la sociedad actual es la acumulación de grandes cantidades de neumáticos al final de su vida útil (NFVU) en vertederos, agravado continuamente por el aumento de la producción automotriz a lo largo de los años.

En este contexto, el reciclaje de los NFVU puede considerarse una estrategia razonable para abordar esta problemática. Sin embargo, existen algunas limitaciones que superar, ya que un neumático está compuesto por diversos materiales y aditivos incorporados en el compuesto elastomérico, convirtiéndolo en un sistema muy complejo. Por otra parte, el enfoque de los materiales autorreparables, caracterizados por la capacidad de recuperar total o parcialmente su rendimiento después de sufrir un daño, es más atractivo que nunca. Sin embargo, aplicar tal concepto para lograr la reparación en elastómeros es especialmente desafiante, ya que las restricciones impuestas por los

entrecruzamientos evitan que las cadenas de polímero formen nuevos enlaces en áreas previamente dañadas, teóricamente bloqueando su capacidad de autorreparación.

Objetivos

El objetivo principal de esta Tesis Doctoral es el desarrollo de compuestos de caucho de estireno-butadieno (SBR), dado que el SBR es uno de los elastómeros más utilizados en neumáticos, combinando propiedades de autorreparación con el uso de NFVU como carga alternativa para abordar la problemática de la gestión de los desechos de neumáticos, y siguiendo los principios de la EC (Reparar, Reciclar y Reducir).

La capacidad de autorreparación se logrará mediante la restauración de los enlaces en las superficies dañadas, lo que prolongará la vida útil del caucho y reducirá la generación de desechos de neumático. La sostenibilidad vendrá dada por la adición de NFVU como carga, proporcionando un uso alternativo de los desechos de neumáticos, reduciendo la demanda de recursos no renovables y contribuyendo a la restauración de ecosistemas degradados. Por lo tanto, esta Tesis Doctoral está diseñada para servir como punto de partida para el desarrollo de nuevos sistemas elastoméricos viables económica, energética y ambientalmente, con uso potencial en la industria del neumático, y al mismo tiempo, define un escenario sostenible para abordar el problema de la gestión de NFVU.

Esta Tesis Doctoral se ha dividido en 6 capítulos. El capítulo 1 presenta el estado del arte de la ruta seguida por los neumáticos desde la perspectiva de la EC. Desde las primeras etapas de producción hasta la etapa de post-consumo. El camino que recorre el neumático dentro de este modelo CE evidencia el compromiso y el esfuerzo hacia el desarrollo de esquemas de gestión efectivos para lograr una verdadera movilidad sostenible. En el Capítulo 2 se detallan los materiales y las técnicas y métodos experimentales generales que se han utilizado a lo largo de la preparación y caracterización de los compuestos elastoméricos desarrollados. El Capítulo 3 explica la validación de los conceptos de autorreparación en una matriz de SBR y proporciona detalles del efecto de diferentes sistemas de vulcanización sobre la capacidad de autorreparación de los compuestos elastoméricos. En el Capítulo 4 se aborda la incorporación de NFVU, cargas de refuerzo tradicionales y sistemas reforzantes híbridos a la matriz autorreparable para mejorar sus propiedades mecánicas y lograr un buen equilibrio entre el desempeño mecánico y la capacidad de autorreparación. El Capítulo 5 se centra en la evaluación de la dinámica molecular de los compuestos de caucho

desarrollados para comprender el efecto de diferentes sistemas sobre los mecanismos de relajación y la capacidad de reparación de la matriz de caucho. Finalmente, las conclusiones de la tesis y las perspectivas de futuro se presentan en el Capítulo 6.

Conclusiones

En esta tesis doctoral se desarrollaron compuestos sostenibles de SBR que combinan propiedades de autorreparación con el uso de NFVU como carga alternativa, siguiendo los principios de economía circular. Los principales resultados han servido para definir un escenario respetuoso con el medio ambiente para abordar el problema de la eliminación de desechos de caucho, prolongando la vida útil de los productos y reduciendo los desechos de neumáticos. La combinación de usar NFVU como carga alternativa junto con la capacidad de autorreparación de los compuestos elastoméricos contribuirán al futuro de la industria de los neumáticos y a la movilidad del mañana, donde las demandas tecnológicas y de sostenibilidad aumentan día a día.

Reparar

Este trabajo presenta resultados experimentales que validan los conceptos de autorreparación en compuestos de SBR. El mecanismo de reparación surge de la combinación de dos procesos diferentes. Primero, la interdifusión de las cadenas poliméricas y la formación de entrecruzamientos físicos que tienen lugar durante las etapas iniciales del proceso de reparación. En segundo lugar, las interacciones de largo alcance y las reacciones de intercambio de disulfuros, como mecanismo intrínseco de autorreparación, dan como resultado la recuperación casi completa del esfuerzo mecánico. Por lo tanto, los aditivos del sistema de vulcanización, como el óxido de zinc (ZnO) y el ácido esteárico (SA), afectan la reparación en sus primeras etapas. Por su parte, el azufre (S) es el componente fundamental que promueve la recuperación casi total de un daño macroscópico al aplicar un protocolo de reparación de 130 °C durante 1 h.

La temperatura y el tiempo también afectan el mecanismo de reparación, logrando mayores eficiencias de reparación a medida que aumenta el tiempo y / o la temperatura, gracias a la mayor movilidad e interdifusión de cadenas poliméricas. Además, el compuesto de SBR desarrollado en este trabajo exhibió una reparación de múltiples

Resumen

ciclos, resultando valores aceptables de reparación de la resistencia a la tracción del 60 % después de 3 ciclos.

Reciclar

Se ha llevado a cabo un estudio fundamental, exhaustivo y sistemático para comprender el mecanismo de reparación de los compuestos de SBR y la influencia del polvo de neumático de desecho (GTR), molido criogénicamente (c-GTR) y modificado químicamente (m-GTR) como carga sostenible en las propiedades de los compuestos desarrollados. Se logró una modificación mecano-química exitosa del GTR con una combinación de un proceso de crio-molienda y un tratamiento químico. La optimización del proceso de crio-molienda permitió reducir el tamaño medio de partícula del material hasta 100-150 μm . La modificación más efectiva de las partículas de GTR se realizó con ácido sulfúrico (H_2SO_4), corroborado por el aumento del contenido de oxígeno en la superficie de la GTR. Los compuestos cargados con c-GTR y m-GTR mostraron un buen equilibrio entre la resistencia a la tracción y la capacidad de reparación al aplicar un protocolo de reparación de 130 $^\circ\text{C}$ durante 5 h, y confirman el gran potencial de c-GTR y m-GTR como carga sostenible en materiales elastoméricos. La combinación de enlaces disulfuro y enlaces iónicos reversibles, que provienen de los grupos funcionales en la superficie del m-GTR, promovieron un buen compromiso entre la eficiencia de reparación y el rendimiento mecánico. El uso de un agente de acoplamiento (CA) proporcionó una mejor dispersión e interacción de la carga con la matriz SBR, lo que condujo a un aumento de la resistencia mecánica, pero limitó la capacidad de reparación. También se desarrollaron compuestos de SBR híbridos, que combinan m-GTR y cargas reforzantes convencionales como negro de carbono (CB) y sílice (Si), para superar las limitaciones del c-GTR y m-GTR. El sistema híbrido que consta de 20 ppc (partes por cien de caucho) de m-GTR y 20 ppc de CB ($\text{m-GTR}_{20}\text{-CB}_{20}$) resultó ser el mejor compuesto de SBR con un equilibrio positivo entre la resistencia mecánica y la eficiencia de reparación.

Reducir

El triángulo mágico de los neumáticos se define a partir de tres factores de rendimiento del neumático de un automóvil (resistencia a la rodadura, el agarre en mojado y la resistencia al desgaste). Estos principios están asociados al material de la banda de

rodadura de los neumáticos. La resistencia a la rodadura (consumo de combustible) y el agarre en mojado (seguridad en la conducción), están íntimamente ligados a las propiedades viscoelásticas del material de la banda de rodadura del neumático. Por tanto, es de gran interés estudiar la dinámica molecular a una escala cercana a los procesos moleculares. En este estudio se personalizó el triángulo mágico de los neumáticos, sustituyendo la resistencia al desgaste por capacidad de reparación. Se demostró que las buenas propiedades del compuesto sostenible m-GTR₂₀-CB₂₀ tenían algunas limitaciones cuando se aplicaba en compuestos de bandas de rodadura. Sin embargo, en presencia de un CA, los tres índices del triángulo se optimizaron, superando el delicado equilibrio entre la resistencia a la rodadura, el agarre en mojado y la eficiencia de reparación; por lo tanto, logrando una reducción del consumo de combustible, aumentando la seguridad en la conducción y prolongando la vida útil del compuesto.

También se establecieron correlaciones entre la dinámica y la estructura molecular de los compuestos desarrollados en un intento por comprender las propiedades físicas y el posible mecanismo de reparación a escala microscópica. La presencia del CA, las cargas y altos contenidos de S tienden a restringir la dinámica segmental de la matriz de SBR debido a la formación de una red más entrecruzada. Mientras tanto, los acelerantes afectan las interacciones inter- e intra-moleculares entre el resto de aditivos, cargas y matriz de caucho.

Los compuestos seleccionados se analizaron en tres condiciones diferentes: virgen, dañados por deformación cíclica y reparados térmicamente. Cuando se dañan, los compuestos muestran una dinámica más rápida; mientras que, después de la aplicación del protocolo de reparación, la dinámica tiende a ralentizarse y la red de caucho se vuelve más heterogénea debido a la interdifusión de cadenas y la reversibilidad de los enlaces disulfuro, que permiten la recuperación total de la rigidez en diferentes regiones de temperatura (-80 °C y 30 °C). Además, se encontró que un daño microscópico requiere períodos de reparación más cortos para lograr una alta eficiencia de reparación, en comparación con los compuestos dañados macroscópicamente.

PREFACE

Motivation

The world is currently undergoing a radical transformation. The more stringent environmental regulations and the fluctuating price of raw materials are the driving forces for the development of several innovative design, manufacture and recycling technologies. The society is moving from the currently linear economy model (extract-manufacture-consume-dispose) to a circular economy model (extract-manufacture-consume-restore), which has the potential to deliver benefits at all scales, from individual citizens to the global economy, and society. For this reason, this model has been gaining so much attraction over the past years.

Elastomers are a special class of polymeric materials with a wide range of applications. A large proportion of their production is used in the transport sector as tires but they are also extensively used in other industrial sectors like the aerospace or the biomedical industry. Such a widespread usage is due to the unique properties of these materials, namely their large elastic deformation and their excellent noise and vibration damping capabilities, among others. Thanks to their inherent stable covalently bonded three-dimensional molecular network, elastomers can sustain large deflections with little or no permanent deformation. Nonetheless, rubbers can also fail through fracture and fatigue processes. As a consequence of this weakness, one of the most serious environmental problems facing society today is the accumulation of large quantities of used tires in landfill sites, and the increasing automotive production over the years continuously aggravates it.

Recycling and recovering used tires can be considered reasonable strategies to solve this concern. However, there are some limitations to overcome, since a tire is composed of various materials and additives incorporated in the rubber compound, turning it into a very complex system. One of the main ways to consume tire waste is in the production of technically less demanding rubbers by mixing the rubber powder (i.e. grinding the rubber waste to form granulates) with new rubbers (or plastics). The recycling of waste tires has important implications in energy conservation, environmental protection, costs reduction, and in promoting the circular economy model.

Meanwhile, the approach of self-healing materials, characterized by the ability to recover fully or partially their performance after suffering damage, is more than ever attractive. However, applying such concept to attain healing in rubbers is especially challenging, since the restrictions imposed by crosslinks prevent the polymer chains from forming new

bonds across previously damaged areas, theoretically blocking their self-healing capability. Although this field of research is growing and getting worldwide attention, self-healing rubbers are still far from satisfactory and basic research is still needed to be able to extrapolate them to real life applications, especially because of their lower mechanical strength with respect to pristine and fully cured rubbers.

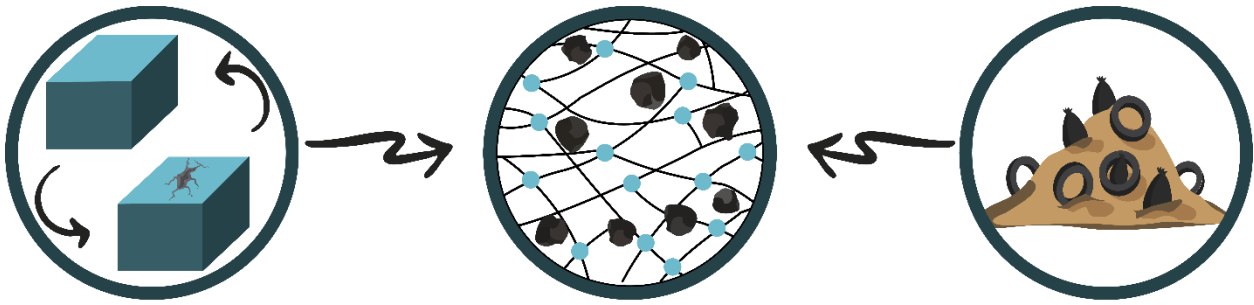
This Doctoral Thesis carries out the still required basic research analyzing different strategies and seeks to build up the knowledge necessary to develop eco-friendly tires. Therefore, it focuses on one of the main elastomers used in this application, styrene-butadiene rubber (SBR) and aims to combine self-healing properties with the use of waste rubber as alternative filler to improve the overall mechanical performance. Thus, this research is designed to follow the circular economy principles and to serve as a starting point for the development of new economically, energetically and environmentally convenient rubbers with potential use in the tire industry, and as an alternative strategy for the management of end-of-life vehicles.

Main Objectives

The main objective of this Doctoral Thesis is the development of sustainable self-healing SBR composites. Self-healing capability will be achieved through the restoration of crosslinks across damaged surfaces, extending the rubber lifetime. Sustainability will be given by the addition of reclaimed tires as filler, providing alternative usage of rubber waste, reducing the demand of non-renewable resources and contributing to the restoration of degraded ecosystems. The combination of reclaimed tires plus self-repair ability will lead to an up grading of the processed elastomeric wastes. These up graded composite materials will contribute to the future of the tire industry, and the mobility of tomorrow, where technological and sustainability demands are growing every day. The following scheme represents the main objective of this Doctoral Thesis.

Self-healing ability

Tire rubber waste



Sustainable SBR composites

To fulfill this main objective, this research has focused on the following specific aspects:

- The first one is related to the validation of self-healing concepts in SBR. A detailed study of the effect of different curing systems and healing protocols on the self-healing capability of rubber compounds has been assessed.
- Secondly, the incorporation of tire waste and traditional fillers to a self-healing SBR matrix to achieve enhanced mechanical properties without sacrificing the healing effectiveness. Since the self-healing capability and the mechanical performance of rubbers tend to be antagonistic properties, the incorporation of fillers arises as a viable option to overcome this issue. The advantages of this strategy will be two-fold. By using recycled rubber, it will be possible to improve the overall performance of self-healing materials, while giving a considerable amount of used tires a second lifecycle.
- Thirdly, the evaluation of the dynamics of self-healing rubber composites has been accomplished by means of broadband dielectric spectroscopy (BDS) and dynamic mechanical analysis (DMA). The rubber composites were investigated by both techniques under three different conditions -virgin, damaged under cyclic deformation and repaired- to comprehend the effect of the rubber structure on the relaxation mechanisms and healing capability of the SBR matrix. Also, the three major indices of the magic triangle of tires (fuel economy, driving safety, and lifetime) have been assessed.

Structure

This Doctoral Thesis has been divided into six chapters:

Chapter 1 introduces the state of the art of the route followed by tires from the circular economy (CE) perspective. From the early stages of production to the post-consumption step, the path that tires trail within this CE model evidences the commitment and efforts towards the development of effective management schemes for achieving a real sustainable mobility.

Chapter 2 details the materials and the general experimental techniques and methods that have been used throughout the preparation and characterization of the developed rubber composites.

Chapter 3 explains the validation of self-healing concepts in a SBR matrix and provides details of the effect of different vulcanization systems on the self-healing capability of the rubber compounds.

Chapter 4 addresses the incorporation of tire waste, traditional fillers and hybrid filler systems to the self-healing matrix to enhance its mechanical properties and to achieve a good tradeoff between mechanical properties and self-healing capability.

Chapter 5 focuses on the evaluation of the molecular dynamics of the developed rubber composites to comprehend the effect of different systems on the relaxation mechanisms and healing capability of the rubber matrix.

And finally, the conclusions of the thesis and future outlook are given in **Chapter 6**.



INTRODUCTION

1. Introduction

The linear economy model of “extract-manufacture-consume-dispose” was globally adopted since the industrial revolution (Figure 1.1). This model resulted in a worldwide urban solid waste of approximately 1.300 million ton/year in 2010, which is expected to increase to 2.200 million ton/year by 2025, being plastics an important contributor.[1] This situation put forward a new model, i.e. the circular economy (CE) model, that replaces the notion of “disposability” with “restoration”.

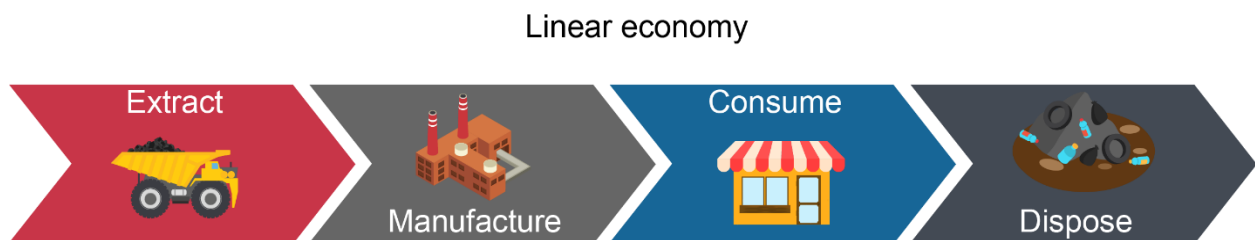


Figure 1.1 Linear economy model

In the CE model the entire system is ready to reuse, repair, restore and recycle resources so that they generate value over and over again, causing their rational and efficient use (Figure 1.2).[2]

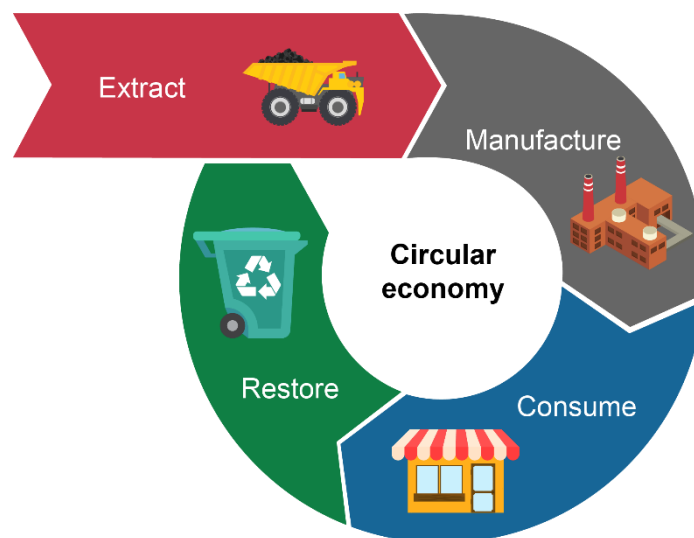


Figure 1.2 Circular economy model.

Initial axioms of the CE model were termed the "3Rs", "R"educing waste, "R"eusing and "R"ecycling resources and products, and have become familiar in many national waste regulations around the world.[3, 4] These basic axioms have now been derived further to broaden the CE approach to the "7Rs" (Redesign, Renew, Reduce, Reuse, Repair, Recover and Recycle), as shown in Figure 1.3.[5]

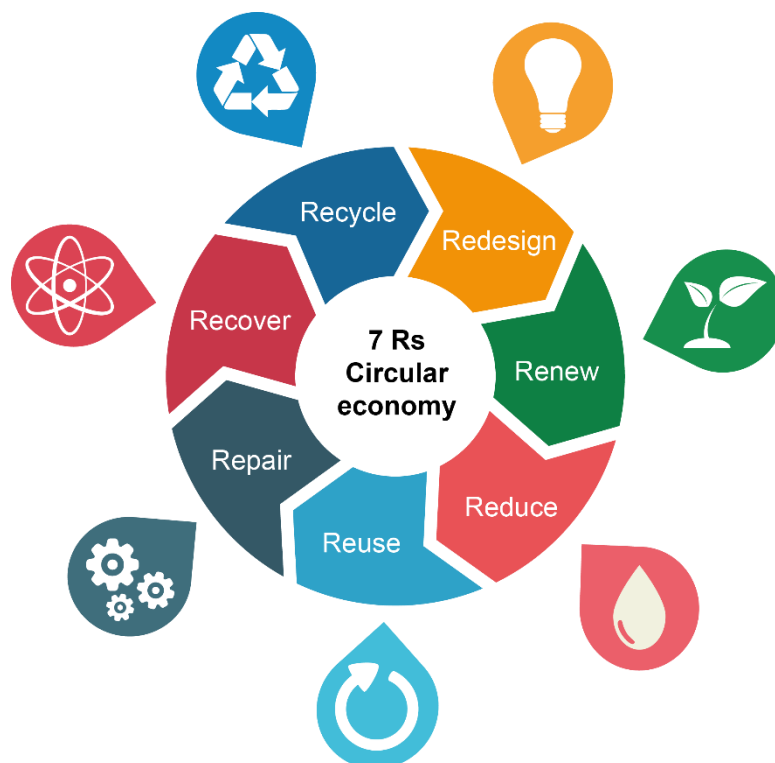


Figure 1.3 7Rs of the circular economy model.

While tires have long provided a circular solution in terms of the 3Rs, the novelty of the CE (and the 7Rs axioms) applied to tires is now determined by product and material circularity, and resource productivity. The product circularity focuses on: i) new and innovative tires with the aim of avoiding safety problems and saving fuel (Redesign); ii) new technologies to extend their useful lifetime (Repair and Reuse); and iii) devulcanization technologies with the aim of obtaining rubber with the same performance as in the fresh/virgin rubber (Recycle). In the case of the material circularity, it focuses on obtaining beneficial by-products (Recover). Meanwhile, the resource productivity focuses on the substitution of petroleum-derived products by other natural or bio-based raw materials (Renew); as well as new technologies for reducing the weight of tires and the benefits they involve (Reduce).

The aim of the present chapter is to analyze tire management considering the 7Rs approach. The chapter starts with a brief analysis of tires and their industry, giving updated consumption and disposal data. Then, it gathers the most relevant studies on the application of the 7Rs to tires, comparing different scientific approaches, as well as their industrial and commercial implementation. It ends with an outlook and some general perceptions. The peer-reviewed literature discussed in this chapter was identified through different professional search engines and databases (Web of Science, Scopus, Google Scholar, etc.), combining several keywords (e.g. tire, elastomer, rubber, green, biobased, redesign, recycle, ground tire rubber, self-healing, reclaim, devulcanization, reuse, pyrolysis, incineration, retread, waste, among others). Collected literature for each R-hierarchy strategy was critically reviewed and assessed, illustrating the drawbacks and feasibility of each “R” approach within the tire industry.

1.1. The tire industry

Tires are essential for mobility, and fundamental for the safety of vehicles. They perform numerous functions: bear the weight of the vehicle, transferring the load to the surface; provide grip between the vehicle and the road for braking and acceleration; and act as vibration absorbers, enhancing road comfort and safety and improving the overall performance of the vehicle.[6]

A tire is manufactured from a variety of materials, including several rubber components, each of which provides a specific and unique purpose. Natural rubber (NR) is used in tire casings requiring high durability, while synthetic rubbers are used in tread materials to provide tire grip. Chemicals (expressed in parts per hundred rubber – phr) serve as antioxidants, curatives, and processing aids; carbon black (CB) and silica are added as reinforcing agents; and cords composed of textile, fiberglass and steel wire (brass, bronze or zinc plated) provide stability and stiffness. About three quarters of the tire correspond to the rubbery compound, which includes the polymer, fillers and chemicals. The composition in weight percentage of raw materials varies depending on the tire type (Figure 1.4).

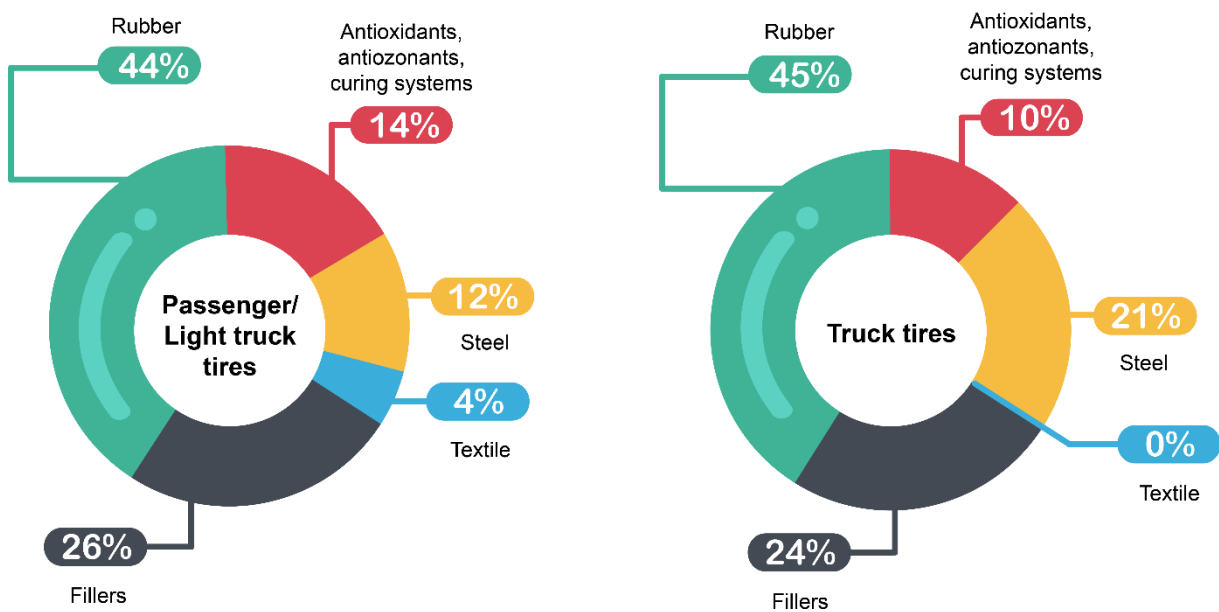


Figure 1.4 Composition of vehicle tires in weight percentages (%).

These materials are selected based on their mechanical and physical characteristics and on their interactions with other constituent materials, providing a broad range of properties.[7] Such composition makes waste management of used tires extremely difficult. Due to their chemical and biological resistance to degradation, tires result in negative environmental impacts. Moreover, in illegal landfilling, tires have the capacity to retain water, which provides a breeding ground for different disease vectors such as mosquitoes and rats, among others. Additionally, in case of burning, tires produce significant air pollution, contamination of the soil and surface and ground water problems.[8]

World population evolution, rapid urbanization, and increasing consumer spending power have contributed to the growing demand for bicycles, motorcycles, buses, trucks, and airplane and passenger vehicles. According to the International Rubber Study Group (IRSG), the world tire production in 2018 was estimated in 17.1 million ton (Figure 1.5).

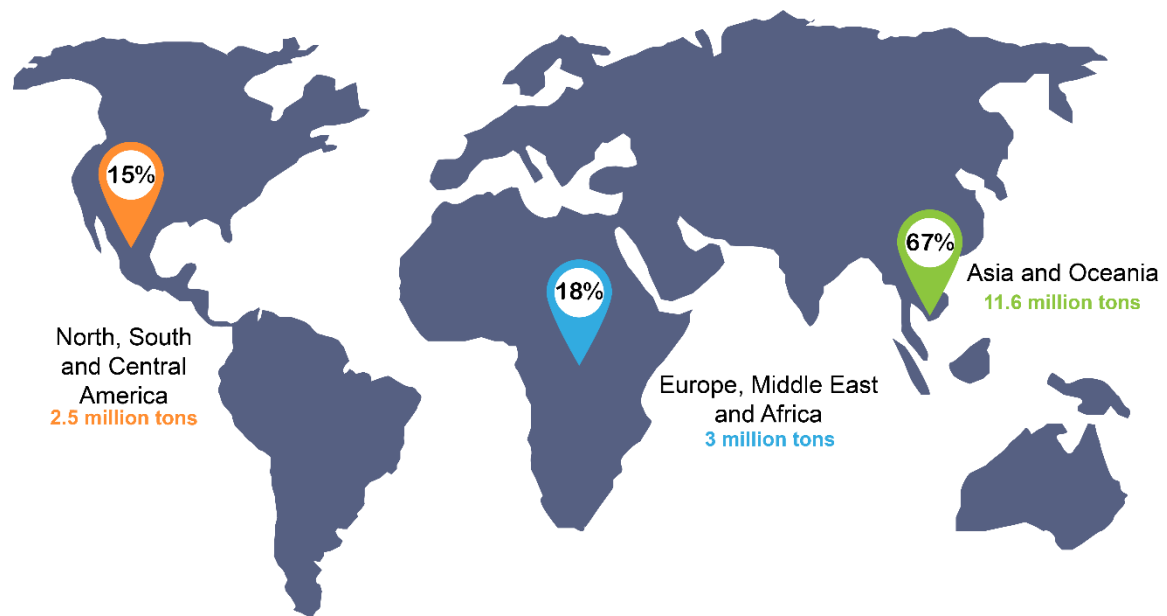


Figure 1.5 Tire production worldwide.[9]

In addition, rising income levels in developing countries will make vehicles more accessible, further increasing tire sales in those markets in the upcoming years.[10] Such global market creates a significant annual demand for tire replacement and, thus, generates a great number of end-of-life tires (ELT). ELT are considered as tires that can no longer serve their original purpose and mostly come from automobiles and trucks. ELT recovery systems can be classified into three groups: material recovery, energy recovery, civil engineering and backfilling, all of which contribute to the industry efforts to build a circular economy. Figure 1.6 shows ELT generated by country/region: China, Europe (countries covered by the European Tire & Rubber Manufacturers Association – ETRMA), India, Japan and USA. The total amount of ELT generated is estimated to be more than 20 million ton, while the amount of ELT recovered rounds up more than 14 million ton/year. Overall, 70 % of the ELT recovered (in ton) by the countries/regions are concentrated in two recovery route sub-categories: production of tire-derived material (TDM), with 52 %, and tire-derived fuel (TDF), with 19 %.[9] Detailed information will be given in the following sections.

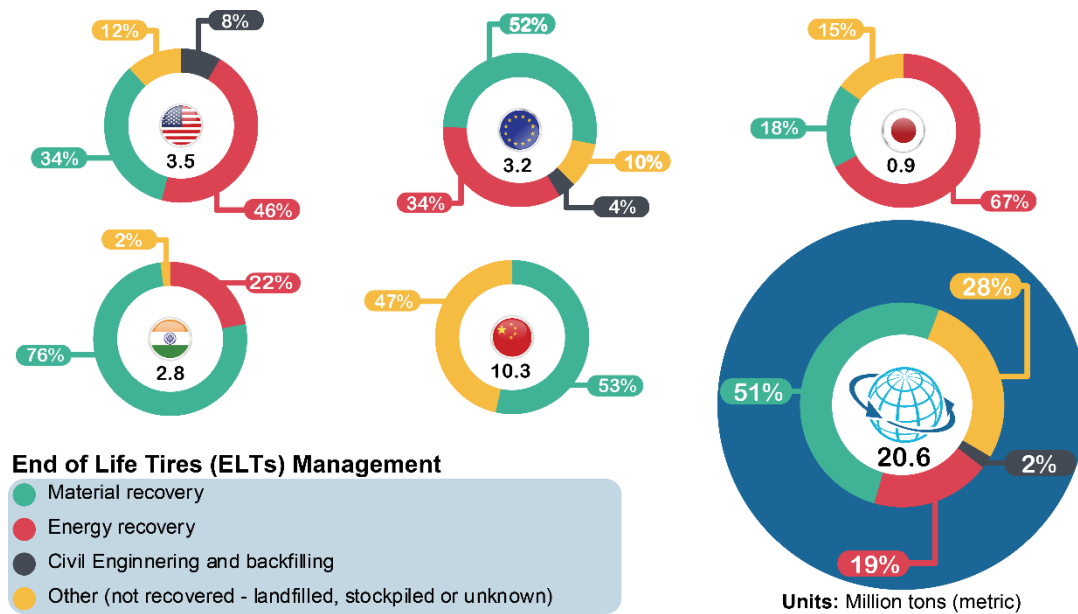


Figure 1.6 ELT management by country/regions.[9]

ELT management is a core activity of the tire industry, like all the other phases of the design and production process, and has three main models worldwide. According to the Extended Produced Responsibility (EPR) model, tire industries are responsible for the management of used tires. This model is very common in the European countries, also used in Brazil, South Africa and South Korea and, recently, Russia and Ukraine.[11] The participants of the system create a non-profit organization that manages the collection and ensures that the mandatory levels of recovery and recycling of waste tires are accomplished. The additional cost is generally passed on to consumers, with an environmental fee (ecological-fee) added to the price of the tire. In the Tax model, the responsibility lies on the State and collection and recovery are financed by a tax on production, passed on to the consumer. Producers or sellers impose a disposal liability, added to the cost of a new tire and paid to the national budget. The management of waste tires is carried out by recovery/recycling organizations and financed by the State. Only a few countries, Denmark, Slovakia and Croatia, run such a system. While the Free Market model considers the profitability of recovery and recycling of tires. It assumes that used tires are a source of valuable raw materials and that the involved companies profit from their management. In this system, the State establishes legislations to have an ELT management plan; however, the responsibility (tax) is not imposed on particular participants. The countries with this system are Argentina, China, India, Indonesia, Japan, Malaysia, Mexico, New Zealand, Saudi Arabia, Thailand, Austria, Switzerland, Germany, the UK and the United States.[9, 12]

1.2. Circular economy applied to tires

The CE model is growing in the tire industry, whether it is for the convenience of opening up new opportunities in the sustainable market, for pure survival in an increasingly demanding environmental legal context, or for the true conviction of companies that are more aware of the need to minimize their environmental impact. Applying the CE model and the 7Rs to tires involve studying and comparing tire management from different perspectives (the scientific, industrial, and commercial), while innovating in search of the right combination of design, materials and advanced engineering. The following sections detail the different studies and approaches developed by these actors according to each of the “Rs” of the CE model.

1.2.1. Redesign

The starting point of the CE is based on the redesign of the products and services themselves, taking into account the environmental consequences. The main objective of these designs has so far focused on reducing fuel consumption and, consequently, pollutant emissions, while maintaining road safety (Figure 1.7). The next challenge is to bring down tire design to individual components or elements to facilitate tire repair or disassemble and reuse in the manufacture of new ones.

These new designs have materialized into innovative products, some of which are already in the market. Airless or non-pneumatic tires that do not deflate under any circumstance use 3-dimensional structures to bear the weight of the vehicle. Goodyear trades airless tires for zero-turn radius mowers, while Michelin offers a line of airless radial tires for construction, recreation and small-scale utility vehicles. Cooper has been active in the development and evaluation of non-pneumatic tire technology for military use. Moreover, Hankook, Bridgestone, Michelin and Goodyear have introduced concept tires that would bring airless tires to the passenger vehicle market. One example is Michelin’s Tweel tire, an airless integrated tire and wheel assembly, in which the rubber tread is fused to the wheel core with polyurethane rods. The Tweel tire targets performance levels beyond what is possible with conventional pneumatic know-how due to its shear band design, additional suspension, and decreased rolling resistance.[13] Michelin also introduced Vision, a biodegradable 3D printed smart concept tire, manufactured using sustainable materials. It is airless and equipped with sensors that offer real time updates on the condition of the tire.[14]

Another line of innovation and redesign considers self-sealing tires. This technology involves the use of a sealant material placed as an inner layer below the tread. When a puncture occurs, the sealant prevents the loss of air pressure by filling the hole. In addition, run-flat tires can travel safely for up to 80 km at 80 km/h even after a tire loses its pressure due to a puncture, according to the manufacturers' specifications. This feature allows drivers to navigate to a safe and convenient place to repair or replace the affected tire. Run-Flat tires also eliminate the need for occasionally used spare tires and rims, preserving materials and freeing up boot space.[15]

Tires can lose about 3 – 6 % of pressure per month without the driver's knowledge. Deflated tires can cause up to 4 % increase in fuel consumption while reducing tire lifespan by 45 %. Many manufacturers are also developing sophisticated and inherent detection systems (chips, tags or sensors) that, integrated into a tire, can wirelessly transmit real-time information, such as pressure, tire temperature and tread wear, warning of malfunctions.[16] Goodyear has implemented the so-called self-inflating tires, i.e. a sensor/pump combination embedded within the tire structure, which could ultimately eliminate the need for drivers to manually control tire pressure. Another example is the Tire Pressure Monitoring Sensor (TPMS), an electronic device that alerts drivers in case of a tire puncture or under inflation below a threshold.[17] This feature improves safety, by improving traction, vehicle handling, decreases fuel consumption, increases braking efficiency, reduces tire wear and extends tire lifespan.[16] Potential applications as sensors by the combination of rigid conductive fillers and flexible and insulating matrices can also be derived from the development of electrically conducting elastomeric compounds.[18] Different studies already published have addressed sensing strain, compression and damage.

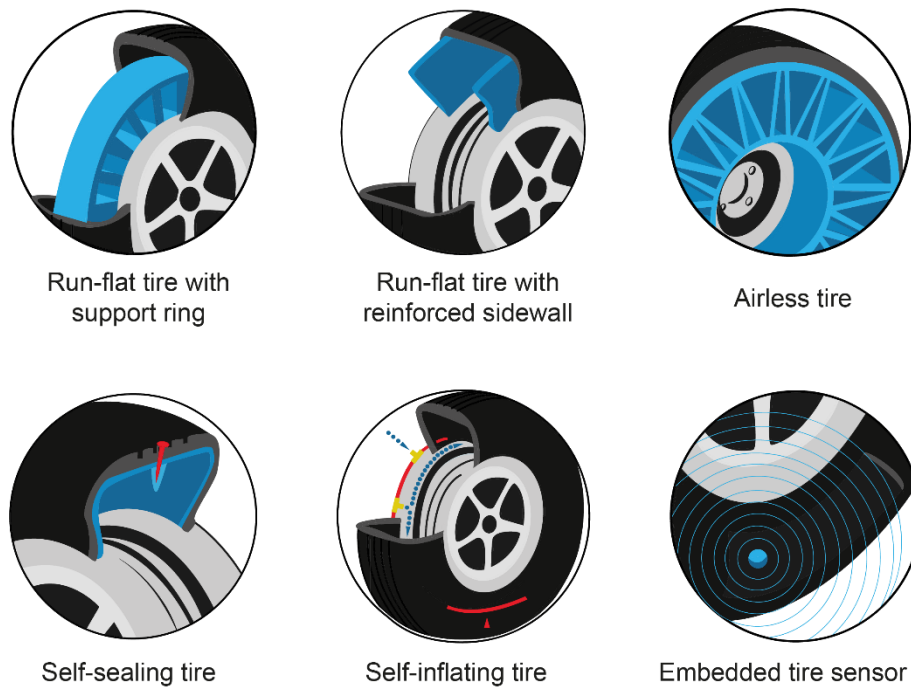


Figure 1.7. Innovative tire concepts and designs.[15]

Summarizing, the incorporation in the tire of sophisticated and inherent detection systems, as well as innovative concepts and designs would remain a challenging issue. In an ideal context, the products must be designed, not only based on performance and aesthetics, but also based on other key aspects derived from their subsequent management. They should be designed to be easily repaired, be able to adapt to the new needs of the client, and when they can no longer be useful, they must be simple to be reused in other production processes. When the design of the products considers these concepts, the following links in the chain of the CE will be developed more easily.

1.2.2. Renew

The manufacture of tires from renewable resources is a clear objective to achieve sustainability and reduce the dependency on fossil fuels.[19] NR has unique reinforcing properties, tear, impact and abrasion resistance, among others. However, the supply of NR from Pará rubber tree (*Hevea brasiliensis*) cannot meet the growing world demand and, thus, new sustainable alternatives are being sought. The two main sources of alternative rubber crops are Russian dandelion (*Taraxacum kok-saghyz*)[20-23] and guayule (*Parthenium argentatum*).[20, 24-26] Russian dandelion is a fast-growing resource and produces large amounts of biomass, emerging as a powerful alternative to

Pará rubber tree since it synthesizes large amounts of high-quality poly(cis-1,4-isoprene) in its roots.[21] Russian dandelion natural rubber (RDNR) shows excellent chemical and physical properties and tires made from RDNR can be as resilient as those made from *Hevea brasiliensis*. [20] However, RDNR has a potential disadvantage since it contains more associated proteins that can lead to allergic reactions, limiting its use to non-medical applications. On the other hand, guayule natural rubber (GNR) has a structural backbone with 99.9 % poly(cis-1,4-isoprene) units and analogous molecular weight and physico-mechanical properties to NR.[24] GNR also undergoes the same degree of strain-induced crystallization of NR; however, its tensile strength is slightly lower.[27] Table 1 shows a comparison of some properties of the different rubber crops.[28] Apart from the physico-mechanical properties, time to harvest and cultivation area are distinctive aspects to be considered when analyzing the potential of the alternative crops. Both NR and GNR are slow-growing crops that take seven and two years to reach maturity, respectively, whereas RDNR is a fast-growing crop, taking only six months. As for location, NR grows in countries near the equator and in Southeast Asia, with 93 % of the world's supply. Meanwhile, GNR is a tree native to arid and semi-arid regions and RDNR grows in harsher climate conditions than NR. These differences allow crops to be moved closer to production facilities.

Table 1. A comparison of NR, RDNR and GNR features.

	NR	RDNR	GNR
Molecular weight	High	High	High
Branching	Yes	Yes	No
Gel	Yes	Yes	No
Protein	High	High	Low
Allergenic protein	Yes	Yes	No
Fatty acid	Low	Low	High
Tensile Strength	High	High	High
Modulus	High	High	Low
Elongation	Medium	Medium	High
Agricultural regions	Tropical	Temperate	Arid
Growing	Slow	Fast	Slow
Rubber location	Tree bark	Roots	Roots

Comparing all these features, GNR and RDNR can be thought as strong raw material alternatives to traditional NR. Unfortunately, it is still too expensive to extract or process the rubber from both RDNR and GNR. Nevertheless, most of the internationally renowned tire companies have now experimental farms in various parts of the world and have conducted significant research on their commercial potential. The development of alternative sources of NR is essential to ensure raw material availability and to reduce the dependence on petroleum-derived products. In this framework, it is mandatory to establish new production processes, improve logistics and promote other initiatives to raise the economic competitiveness of GNR and RDNR as rubber sources.

Another approach to achieve sustainability is to provide substitutes to the other components of the tire, such as the fillers. It is well known that CB is the main reinforcing filler in the tire industry. The traditional methods of production of CB can be classified into two categories: incomplete combustion and thermal decomposition of hydrocarbons, depending upon the presence or absence of oxygen. However, alternative approaches are now being considered to produce renewable CB from biomass products, such as oils and vegetable fats.[29, 30] Peterson *et al.*[29] demonstrated the potential to use renewable CB from birchwood biochar in partially replacing CB without any loss of compounds properties. They made a biochar through slow pyrolysis, which contained 89 % carbon and < 2 % ash. The resulted composites made from SBR filled with 30 % of 50/50 (biochar/CB) showed equal or higher values compared to CB compounds in terms of tensile strength, toughness and elongation properties. Toth *et al.*[30] produced renewable-based CB from the pyrolysis of pine and wood oil in a continuous, high-temperature spray process. In this study, products with similar structures to commercial CB were identified depending on the process temperature. The results showed that at 1300 and 1500 °C, the produced green CB was structurally similar to medium-disperse CB grades. An additional and intense research line is focused on replacing traditional CB by cheap, abundant, and renewable non-petroleum-based fillers.[31-44] Their use would enhance the long-term sustainability and carbon footprint of tire compounds. Unfortunately, not many bio-based renewable fillers have the potential to produce a reinforcement level comparable to that of CB while concomitantly generating more sustainable materials and minimizing pollution. Thus, they can only be used as partial substitutes of CB and/or in combination with other fillers. Some examples of valorized agricultural and industrial residues with comparable reinforcing effects are eggshells,[35] rice husk,[31, 38, 40] chitin,[39] coffee,[36] cellulose,[41] montmorillonite,[42] kaolin,[37, 43] and lignin.[32-34, 44]

Researchers have also focused on the substitution/modification of silica in tire tread compounds. Silica is another reinforcing filler used in the tire industry in combination with CB; it is known for the reduction of hysteresis or energy loss, which leads to a production of energy-saving tires with low rolling resistance and, thus, low fuel consumption. Chuayjuljit *et al.*[31] prepared silica from rice husk ash (RHA silica) with higher specific surface area and lower moisture content than commercial silica. They concluded that NR compounds reinforced with RHA silica were suitable for applications where mechanical properties are desirable but hardness is not the major concern. Other researchers[37] evaluated replacing silica by metakaolin (MK) in the tread rubber compounds. They found a significant reduction of rolling resistance with 75 % and 100 % MK without affecting wet traction. Fathurrohman *et al.*[42] investigated the use of silica-organomodified montmorillonite (MMT) dual filler in the reinforcement of NR truck tire tread compounds. They found that the introduction of MMT (5 phr) enhanced the elastic response of the material (i.e. wet grip and rolling resistance) while maintaining the abrasion resistance. Finally, Mgbemena *et al.*[43] studied the performance of NR/organomodified kaolin compounds for tire sidewalls. The organomodified fillers were prepared from derivatives of rubber seed oil (RSO) and tea seed oil (TSO). Their results showed an increase in tensile strength, fatigue failure and tear strength. NR/TSO compounds filled with 10 phr of modified kaolin were the best material for tire sidewalls considering optimum cure times, maximum torque and tear strength. Figure 1.8 summarizes the sustainable approach of tires from renewable resources and valorized by-products.

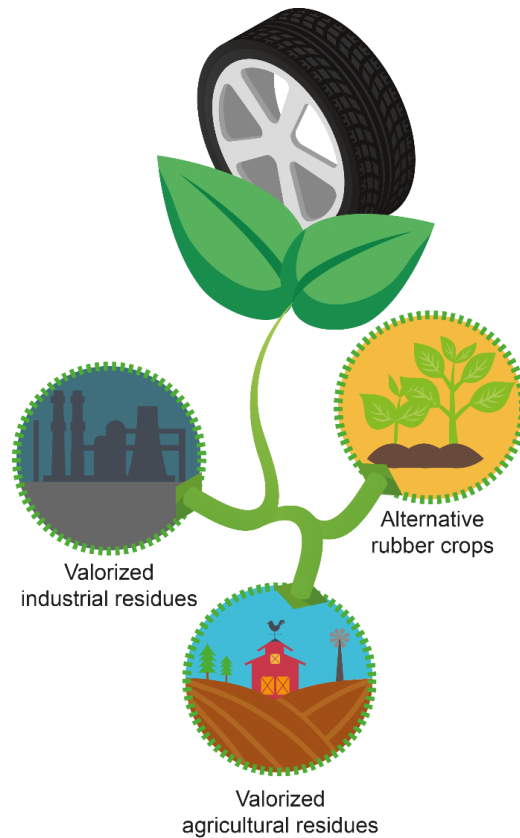


Figure 1.8 Sustainable approach of tires from renewable resources and valorized by-products.

The main tire industries are aware of all these developments and are implementing bio-based components in their production. Bridgestone and Goodyear include soybean oil as a natural ingredient in tire tread compounds, replacing traditional petroleum oil. Firestone commercializes agriculture tires with 10 % soybean oil, which increases the tread life by 10 % and reduces the use of petroleum-based oil by up to 8.5 million gallon/year. Pirelli and Goodyear report the use of silica derived from rice husks, to produce tires with improved rolling resistance. Yokohama uses orange oil, derived from orange peels, instead of petroleum in tires, increasing fuel economy, reducing rolling resistance, while maintaining good traction.[15]

1.2.3. Reduce

Reducing consists in the optimal use of materials. Tire industry targets the weight of the tires to reduce their contribution to the total weight of the vehicle.[45] Such weight reduction also achieves another clear objective, fuel saving. Approximately a quarter of the materials of a tire corresponds to fillers, like CB. Thus, one straightforward approach is the substitution of CB by other reinforcing fillers in lower proportions and/or densities.

Previous studies in the field of rubber nanocomposites have shown that organoclays[46] and other forms of carbon, including graphite, graphene, graphene oxide and carbon nanotubes (CNT) can be considered as effective substitutes of CB.[47-51] These carbon additives with various morphologies have attracted significant attention due to their outstanding properties, such as exceptional modulus and remarkably high electrical and thermal conductivities. Particularizing this approach to tires, Poikelispää *et al.*[52] reported the effect of the partial replacement of CB by MWCNT in tread compounds. They found that by replacing a small amount of CB, the mechanical properties of the tread compound were significantly enhanced. They also observed an increase of the reinforcing effect with MWCNT content, but high loading fractions resulted in poor dispersion of the nanotubes. Shao *et al.*[53] reported a 1.5 % improvement on dry conditions and 6.5 % on wet conditions when substituting 50 phr of CB (N234) by 20 phr of CNT, which was ascribed to the increased hysteresis loss and decreased storage modulus at high frequency domain. Meanwhile, the high specific surface area and strong filler–filler interactions led to a decrease in rolling resistance. They concluded that CNT-filled rubber compounds reduced the tire weight and showed superior handling and traction performances suitable for racing and sport car tires.

One of the most challenging topics in the tire industry is the design of rubber tread compounds with an improved rolling resistance, and without compromising performance in terms of abrasion resistance and wet grip. Tires must operate efficiently under dissimilar conditions, dry, wet, or snow-covered surfaces, while simultaneously fulfil the driver's expectations in terms of acceptable wear resistance, low noise, and good ride quality. Among all the properties considered in the development of tires, these three main properties form the "magic triangle", well known in the tire industry (Figure 1.9).

Two recent reviews on tire design have focused on low rolling-resistance tires.[54, 55] Reducing rolling resistance is an effective method of reducing fuel consumption and CO₂ emissions. When a tire rolls on the road, mechanical energy is dissipated as heat due to friction, which is known as rolling resistance. Rolling resistance, therefore, plays a major role in increasing vehicle fuel consumption.[56] It depends on the type of tire, the nature of the rolling surface, and the operating conditions, i.e. inflation pressure, load and speed. The environmental benefit of low rolling resistance tires is propelling the demand for such products worldwide, with great focus on understanding and modeling such property.

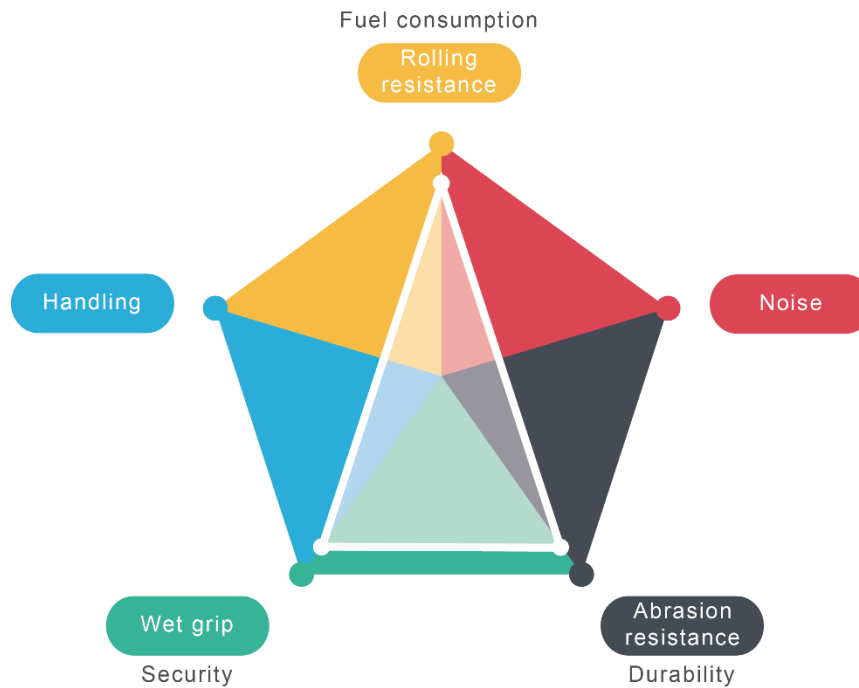


Figure 1.9. Illustration of the “magic triangle” of tires.

Several tire manufacturers have developed green technologies that can reduce CO₂ emissions. Bridgestone has developed Ecopia tires, which reduce carbon footprint of cars by offering exceptionally low rolling resistance, excellent fuel economy, and reducing the frequency of replacement. Continental tires, branded as EcoPlus+ technology, and Firestone's Fuel Fighter technology are focused on reducing rolling resistance while enhancing grip on wet surfaces and improving tread life.[57] Also, the Beijing Tiancheng Linglong Tire company is working on the development of graphene rubber compounds for fuel efficient tires. The graphene-enhanced tire is stated to be produced with only a few minor process adjustments to ensure an industrial viable product. This tire is claimed to be safe and antistatic, and also with low fuel consumption. In addition, its abrasion resistance and thermal conductivity is said to be extremely high.[58] On the other hand, Gratomic is developing graphene-enhanced tires to increase their resistance and reduce friction. The graphene enhanced Gratomic tires are reported to present more than 30 % increase in wear resistance over the “premium tires” from other known trademarks. Tests based on industry standard dynamic mechanical analysis (DMA) showed a significant progress in rolling resistance, indicating more than 30 % improvement in fuel economy. Wet and ice braking distances were also improved by 40 %.[59]

1.2.4. Reuse

Reuse is about giving products an extended useful life before reaching the limiting time to dispose them.[60] The most critical component of the tire is the tread because it determines the final performance. Also, it is the thickest component of the tire that suffers the most due to abrasive loss. The tread ensures the gripping action between the road surface and the whole tire; thus, after several uses, its thickness is reduced and a slippery action takes place on the road surface. At this point consumers have to decide whether to replace the deteriorated tire with a new one (normally expensive) or to retread it, which is a less expensive alternative.[61]

Retreading is a safe re-manufacturing process, which consists of replacing the tread on worn tires, using heat and pressure, preserving the structure, and maintaining its performance.[62] A tire can be retreaded several times depending on the type and conditions; car tires can be retreaded 2 – 3 times; light truck tires 4 – 5 times; heavy truck tires 8 – 9 times; and aircraft tires up to 14 times.[61, 63] Retreading is also a way of reusing that generates energy, material and natural resources savings. It is a safe, low-cost and environmentally friendly solution. Retreading helps to reduce deforestation, decreases land use for the NR industry, reduces particulate air pollution as well as CO₂ emissions, and contributes to reduce waste generation. Figure 1.10 summarizes the main benefits of retreading.

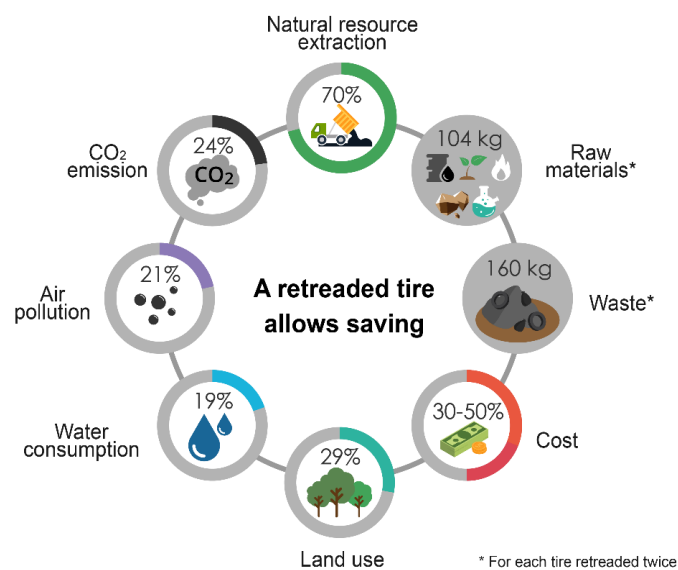


Figure 1.10 Main saving benefits of a retreaded tire.

Most of the retreading market of the commercial vehicle segment is expected to grow 5 % (compound annual growth – CAGR) during the 2021 – 2026 period. In terms of demand, the Asia-Pacific region is expected to account for the highest sales worldwide. Europe is estimated to be the next big market to hold a leading share in the global retreading market followed by North America during the 2018 – 2028 period.[64] Moreover, many leading tire manufacturers are joining the retreading business as they foresee a huge market potential. They are applying innovative manufacturing strategies and processes to remove operational problems to provide high-quality retreaded tires that can closely match the quality of their original ones. From the authors' point of view, retreading is a popular, environmentally friendly, and cost-effective yet high-quality process that should remain in time and should be considered as an alternative to traditional tires. It involves economic and environmental benefits to the society and tire industry and guarantees that tires are not discarded imprudently, contributing to their circular economy.

Certain small-scale projects have also succeeded as alternatives for the productive reuse of scrap tires, using them in their original form without any physical or chemical treatment; and requiring no infrastructure, planning, or regulation.[65, 66] Applications as insulation for the foundations of buildings, art projects, protective barriers along roads and highways, playground equipment, to protect sloping waterfront banks and roadsides, shock absorbers on large vehicles or fenders for boats, artificial reefs (offering protection to marine organisms) are simple and economical uses for scrap tires (Figure 1.11).[67]



Figure 1.11 Other applications for scrap tires.

1.2.5. Repair

Repair forms part of the CE principles whose aim is to extend the lifetime of products. It enables raw materials and energy savings and helps to reduce waste. In this framework, an upfront technology that deserves attention is the development of self-healing materials. This class of smart materials offer the possibility of increasing their useful lifetime and, therefore, helps to decrease the ecological and economic costs of future materials.[68]

Self-healing materials have the capability of recovering their initial properties after suffering damage. White *et al.*[69] pioneering work demonstrated the basic self-healing phenomena in polymers. Since then, research focused on self-healing materials and, especially, self-healing rubbers has rapidly expanded with new concepts and strategies being developed in academic and industrial laboratories around the world. Self-healing materials are generally grouped according to the healing mechanism into two main categories: extrinsic and intrinsic (Figure 1.12). In extrinsic self-healing materials, a so-called healing agent is contained in discrete particles (capsules or fibers) embedded into a polymeric matrix and released upon damage. The discrete healing agent is consumed in the healing reaction and, hence, healing is limited to a single event. On the other hand, intrinsic self-healing polymers make use of moieties becoming an inherent part of the material itself. In this case, multiple healing reactions can take place at a given damage site.[70]

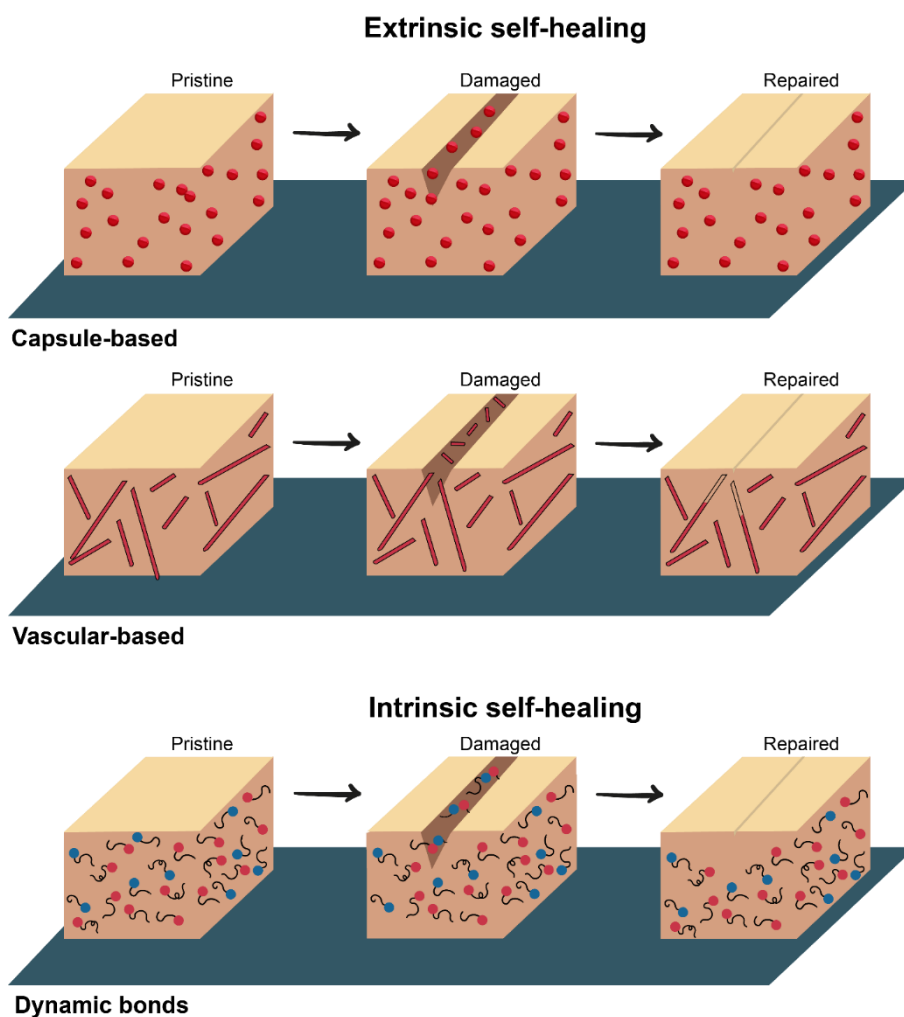


Figure 1.12 Schematic representation of extrinsic and intrinsic self-healing categories.

One of the successful routes for achieving intrinsic self-healing is by promoting physical interactions and/or the formation of dynamic chemical bonds between the interfaces of a damaged zone (i.e. crack).[71] Intrinsic self-healing polymers are capable of repairing molecular and macroscale damages via a temporary local increase in mobility of the polymeric chains, which can occur autonomously or be activated by external stimuli, with the supply of modest amount of energy (heat or radiation), followed by a process of restoration of the chemical or physical bond strength. Nonetheless, attaining such healing in rubbers is especially challenging, since cross-links restrict polymer chains to form new bonds across former (pre-) damaged areas. Different dynamic reversible groups, such as hydrogen bonding,[72, 73] disulfides,[74, 75] Diels-Alder chemistry,[76, 77] and ionic interactions,[78, 79] have attracted growing attention in the self-healing rubber field (Figure 1.13). Moreover, the combination of different self-healing mechanisms (mostly intrinsic) is currently emerging as a strategy to provide an optimal compromise between mechanical performance and reparability.[80]

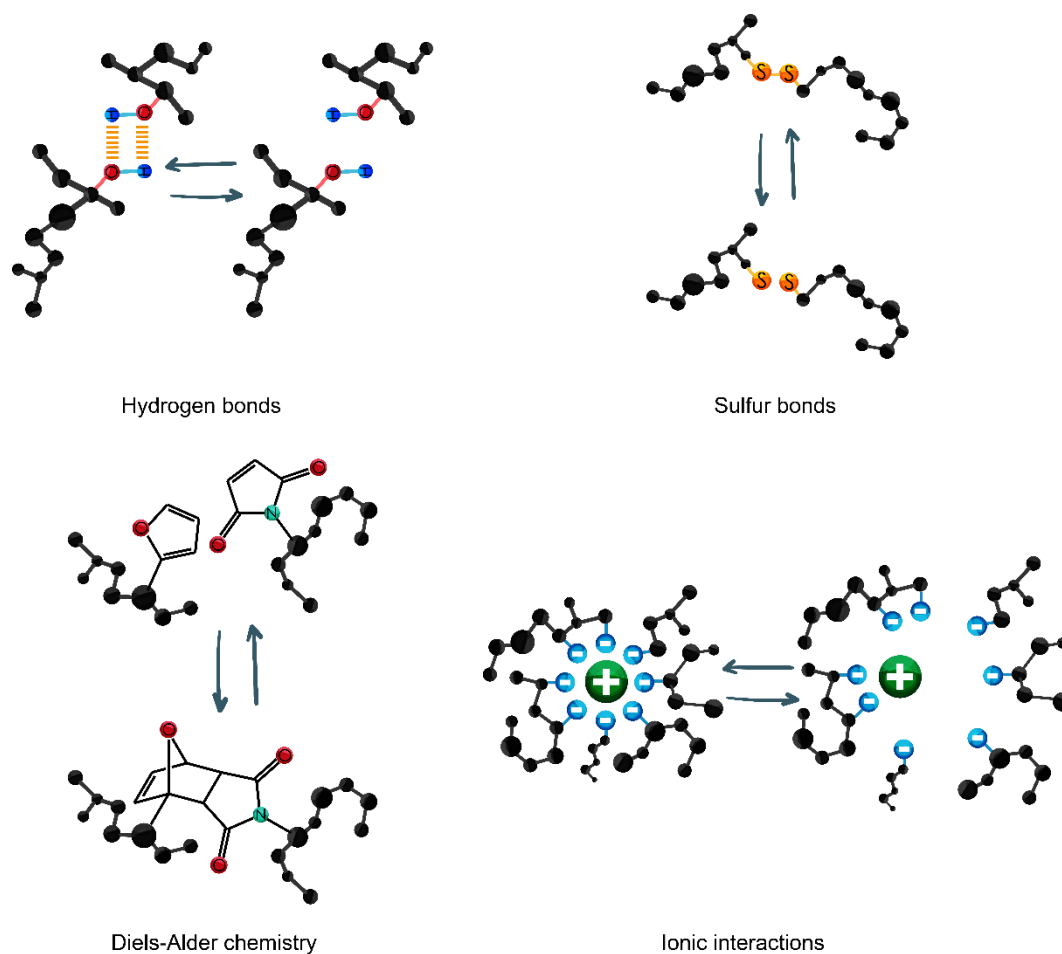


Figure 1.13 Schematic representation of dynamic reversible chemical bonds

Self-healing is an incipient technology when dealing with tires. However, there are several studies already published using the different rubbers contained in a tire, which can pave the way for industrially attractive developments. Vulcanized NR with healing properties was developed by Hernández *et al.*[75] In this work, the authors took advantage of the dynamic character of the disulfides bonds (S–S) naturally present in sulfur-vulcanized rubbers. The disulfide group can introduce a healing functionality at low temperatures, while keeping a reasonable level of bond strength. These bonds can reversibly be cleaved and formed, leading to the renewal of cross-links across damaged surfaces.[81-83] Based on the disulfide exchange reactions, the rubber would accordingly acquire self-healing ability. Reversible ionic cross-links have also been studied as self-healing moieties in NR compounds.[84] The self-healing NR with zinc thiolate recovered 60 % of its initial mechanical properties in 1 min and almost 100 % in 10 min without the aid of any external resources. More recently, Utrera-Barrios *et al.*[73] designed a mechanically robust composite based on ENR filled with thermally reduced graphene oxide (TRGO)

with 85 % of healing efficiency at room temperature, which was promoted by hydrogen bonding interactions with the rubber matrix.

In another investigation, Das *et al.*[78] modified the bromide functionalities of bromobutyl rubber (BIIR) into ionic imidazolium bromide groups, resulting in the formation of reversible ionic associates. The reversibility of these ionic clusters facilitated the healing process due to rearrangements induced by temperature or stress-induced, allowing to preserve the original properties of the network.

Although this field of research is growing and getting attention worldwide, self-healing rubbers are still far from acceptable to be used in the tire industry, due to their low mechanical strength. Adding reinforcing fillers and/or combining different healing strategies[80] is seen as the path to follow for improving the overall mechanical performance of self-healing rubbers without compromising their repair capability.[85, 86]

1.2.6. Recover

Energy and material recovery provide a complementary alternative to address tire waste issues and achieve the goals of sustainable development following CE principles. Pyrolysis, gasification and incineration are thermo-chemical conversion technologies that transform scrap tires into valuable chemical products, fuels, and power.[87, 88] These techniques are particularly useful for ELT, and do not depend on the quality or type of tire.[89, 90] These recovery process offers an environmentally attractive route to reduce the accumulation of waste tires, and represents a valid alternative for a reusable product by converting scrap tires.[67] Volume reduction of waste by more than 90 % and net energy recovery with possible material recovery are the main advantages of these methods. However, generation of toxic gases, disposal of ashes, and so forth are some problems associated with these thermal treatments.[91]

Pyrolysis

Pyrolysis consists in the thermo-chemical decomposition (400 – 1200 °C) of organic compounds into low molecular weight products at reduced or normal pressure and under an inert atmosphere, preventing oxidation and changes of phase or chemical composition.[60, 63, 92, 93]

Pyrolysis of waste tires produces a series of valuable chemical compounds in solid, liquid and gaseous phases, which can become value-added products as additives and starting materials for other products that can be used in the petrochemical, energy or steel industries.[60, 92] Solid products include low grade CB, fly ash, coal, and other inorganic materials as residues of zinc, silicates, iron oxide, sulfides, carbonates, and other impurities.[63] The carbon fraction can be processed to produce activated carbon, recovered CB, and recovered inorganic compounds that can be used as fillers.[94, 95] The liquid fraction contains tar, water, aromatic hydrocarbons and organic substances (oils) with a high calorific value, similar to heavy fuel oil, which are generally mixed with diesel oils and other petrochemical products, after removing sulfur-polluting compounds.[94, 96] Meanwhile, the gas phase is rich in organic compounds (hydrogen (H₂), methane (CH₄), ethylene (C₂H₄), ethane (C₂H₆), carbon monoxide (CO) and carbon dioxide (CO₂), hydrogen sulfide (H₂S)).[63] Once purified, this fraction can be used as an energy source to help carry out the pyrolysis operation.[60]

Although the rising costs of petrochemical raw materials and energy raises the potential of this method, it is less frequently used worldwide than incineration for obtaining energy. Some technological issues must be solved in order to make pyrolysis a more environmentally and economical viable option.[65, 89] Its feasibility is strongly affected by non-competitive prices and the low quality of the obtained products, mainly CB and oil, which prevent their direct use for other manufacturing processes.[87] Furthermore, the high operation and maintenance costs and the absence of a wide market for consumption of the obtained products are the main drawbacks against the implementation of a successful pyrolysis process.[96]

Beston, Mingjie, and Klean Industries are some of the various companies that market their pyrolysis plants and machinery, adjusted to meet the different customers' requirements.[97-99] They customize designs (models), configurations (batch, semi-continuous, and fully continuous), reactor size, capacity, operating pressure, heating materials (charcoal, wood, fuel oil, natural gas, liquefied petroleum gas (LPG)) and patterns (horizontal and rotatory). Moreover, Metso Outotec has developed a patented

process for processing scrap tires to recover oil, non-condensable fuel gas, steel, and commercial grade CB. The process involves an indirectly fired rotary kiln, char handling, steel recovery, grinding and pelletizing circuit, oil condensing system, and gas cleaning system. The capability to generate a CB product appropriate for rubber use enhances the economic feasibility of this process.[100] In our opinion, scientific research and industrial investments should focus on pyrolysis technologies that meet simultaneously the requirements of reliability, automation, security, and durability. The resulting products should widely be used in factories to produce other goods, achieving a real tire circular economy model.

Gasification

Gasification is a partial oxidation process that uses pressure, heat, and a reactive agent (air, oxygen, hydrogen, or steam) to convert tire waste into a gas mixture primarily composed of CO and H₂, with a low calorific value (5 – 6 MJ Nm⁻³),[101] along with CO₂ and light hydrocarbons (CH₄), also known as synthesis gas or syngas. Syngas is dependent on the operating conditions and the concentration of the oxidizing agent. It is used as fuel in fuel cells or gas turbines to obtain a wide range of other fuels and chemicals.[88, 91] Some of the advantages of this treatment are its high conversion performance and energy efficiency of around 34 % (higher than that of incineration). Moreover, syngas contaminants (H₂S, NH₃) can be removed using selected known technologies. Nonetheless, gasification tends to have a slightly higher temperature range than pyrolysis (1200 – 1500 °C).

Incineration

Incineration is the oxidation of combustible material to give inert waste. It is a highly exothermic and spontaneous process that starts at controlled high temperatures (1000 °C) and, once initiated, it becomes self-supporting.[60, 87] This process produces H₂O, O₂, CO₂ and several toxic gases; although the use of high enough temperatures can avoid the formation some of these toxic components, such as dioxin. Incineration is often carried out by the tire industry to dispose of production waste and rejects, and to produce their own energy. Tire manufacturers and retreading companies use this process to produce the steam required in the vulcanization.[94] It is also a common process for providing the energy to power cement kilns for manufacturing Portland cement,[8, 88, 96]

but also in thermal power plants, pulp and paper mills, steel mills, industrial boilers, sewage treatment installations, or farms.[87] In the particular case of the cement industry, the use of very high temperatures ($\sim 2.000\text{ }^{\circ}\text{C}$) ensures the complete combustion of all the tire components, converting the steel to iron oxide and sulfur recovered from rubber to sulfates. These generated salts and metal oxides are useful ingredients in the final cement product.[60]

Energy from incineration is used in many countries with established tire waste management systems[65] and varies in different regions of the world, often due to local considerations such as landfill regulations and the amount of space available. About 45 % and 38 % of postconsumer tires and industrial wastes in the United States and in the EU, respectively, are used as a supplementary non-fossil fuel in some form of energy recovery process.[60] Figure 1.14 summarizes the different technologies that transform scrap tires into valuable chemical products fuels.

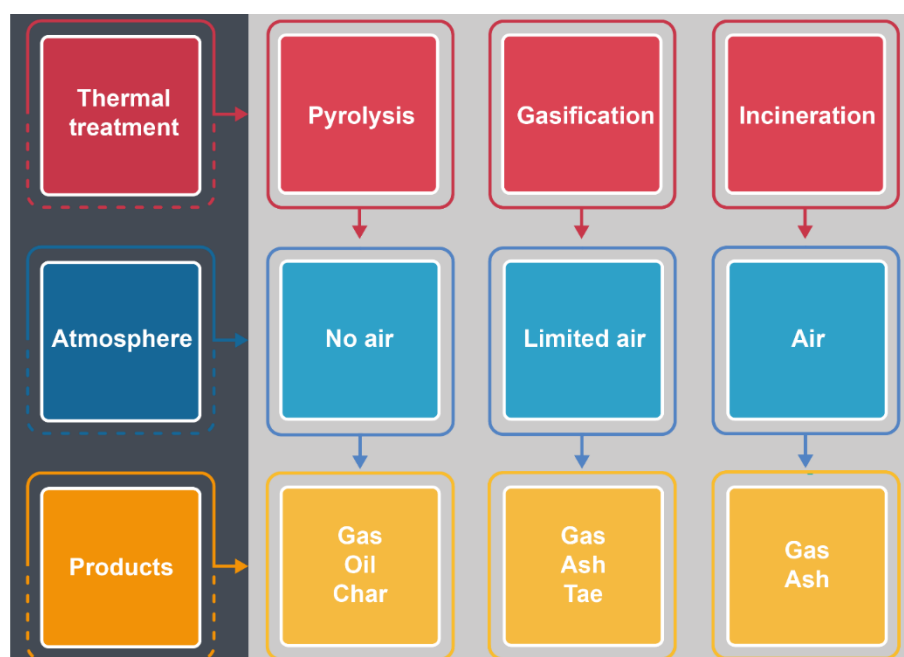


Figure 1.14 Schematic representation of technologies for the transformation of scrap tires into valuable products.

1.2.7. Recycle

Recycling, as defined by the Parliament and Council of the EU,[102] is any recovery operation whereby waste materials are reprocessed into substances, materials or products, either for the original or other purposes. The first step in any tire recycling route

has to consider the production of crumb from scrap tires. This crumb can be produced from whole tires or the remains of tire treads from the retreading process (tread buffings). Using the whole tire as starting material has disadvantages over tread buffings, due to the presence of either fabric or metal particles, which not only contaminate the product but can also act as stress concentration points resulting in premature tears, breaks and cracks.[60] Therefore, removing fabric and metal, in the most efficient way possible during the recycling process, is very important to ensure the quality of the final product.

The utilization of worn tires involves a sub-dividing process that yields a fine granular material denominated ground tire rubber (GTR). There are different techniques by which tire waste can be reduced in size, all of which have practical and technical advantages and disadvantages.[103, 104] These processes are generally carried out by cutting, shearing, or impact (or a combination of these), and may vary in the environmental conditions in which they occur (ambient, wet or cryogenic).[45, 105, 106] The selection of the process depends on different factors, such as the starting form of the waste product, the desired final rubber particles characteristics, the tolerance of residual contamination and the target price. GTR is the starting point for the majority of the reclaiming and devulcanization processes, as will be discussed next.

Uses of GTR

In the framework of direct recycling options, a wide variety of successful applications has been proposed for GTR.[96, 107] It can be used in the manufacture of ground covers in playgrounds, lower layers of floor coverings, walkway tiles, mulch for agricultural purposes, landscape applications and sports surfaces such as running or jogging tracks. Moreover, compounds containing GTR can make up a variety of rubber products, such as conveyor belts, tubes, molded and extruded profiles, shoe soles and heels, car mats, mattresses, sealing plates, battery boxes and other hard rubber goods.[107, 108]

GTR can contain CB, clay, calcium carbonate and silica in its composition and, hence, can act as filler in plastic composites. Blends of GTR with various thermoplastics, mainly polyethylene (PE), polystyrene (PS), polypropylene (PP) and polyvinyl chloride (PVC),[109-113] can be shaped and remelted into a wide range of extruded and molded products. Their mechanical properties will depend on the thermoplastic matrix, GTR content,[114-116] particle size,[117] dispersion degree and GTR-polymer interaction at the interface.[118-120]

GTR can also be incorporated into virgin rubber as semi-active filler. However, the compatibility with the matrix is a major issue. In addition, the type of curing system, the cross-link density of the rubber, and the presence of other ingredients, such as fillers, accelerators,[121] and plasticizers, need to be considered.[105] Usually, the direct incorporation of GTR in rubber composites significantly deteriorates their physical and viscoelastic properties, especially the tensile strength, compared to the virgin composites. This behavior is ascribed to the weak matrix-filler adhesion, between the crumb rubber and the rubber matrix, and the lack of reactive sites on the GTR surface.[122] The curing behavior is also affected by the presence of GTR, through the migration of sulfur or accelerators between the vulcanized GTR and the virgin matrix. Nevertheless, several studies have showed that it is possible to include around 10 – 30 % of GTR to NR and SBR matrices, without sacrificing the essential characteristics of the rubber vulcanizates. Moreover, tangent delta, a direct measure of internal energy dissipation, have been shown to increase with GTR content.[105, 123, 124]

As stated above, GTR particles have limited adhesion to most polymers and form a weak interface, which leads to poor mechanical properties and limited applications. To address this issue, GTR surface have been modified by several methods.[105] Small polar groups on the GTR surface can be attained using plasma[125, 126] or ozone[127, 128], high-energy gamma[129] or ultraviolet irradiation.[130]

Moreover, chemical methods can be used to introduce polar groups and simultaneously produce partial devulcanization. Acids,[116, 131, 132] coupling agents,[118, 133] and chlorination[134] treatments have also been studied.

The use of GTR in the cement and concrete industry is another area of research that has been developed considerably in the last decades.[60, 107, 135, 136] The elasticity given by GTR improves fracture resistance, lowers density, favors heat and sound insulating and energy absorption properties, and reduces cracking and vibration transmission. The asphalt industry also uses GTR as filler for road surface treatment. Blending GTR with asphalt has advantages in the performance of roads and their longevity as it reduces the noise of the vehicles traveling on it, improves crack and skid resistance, and provides a more comfortable ride.[137-139] Finally, in sludge treatment plants, a bed of GTR is effective at absorbing mercury (II) and other heavy metals (the presence of thiol and other sulfur residues can immobilize the metal ions) and organic solvents from waste water runoffs, such as toluene, benzene, ethylbenzene, o-xylene.

Reclaim/Devulcanization

Any process to obtain a low modulus polymer material by breaking the starting permanent tridimensional network is called reclaiming. Reclaim of rubber refers to the recovery of original elastomers in a way that they can be used to replace a fresh polymer.[107] Reclaiming from rubber waste products has the greatest potential in terms of recycling, as vulcanized rubber waste can be mixed, processed, and vulcanized again.[96, 140] Reclaiming deals with the cleavage of carbon-carbon (C-C) bonds on the rubber backbone with the aim of reducing the molecular weight to achieve plasticity.

On the other hand, devulcanization causes the selective breakup of the chemical network. It consists of the cleavage of the intermolecular bonds of the network, such as carbon-sulfur (C-S) and/or sulfur-sulfur (S-S) bonds, that breaks down the macromolecular chains without damaging the backbone network and avoiding material degradation (Figure 1.15). Devulcanization can be carried out by different means, such as chemical,[141] mechano-chemical,[142, 143] ultrasonic,[144-147] microwave,[148-151] biological,[152-155] thermo-mechanical,[156-159] and supercritical CO₂. [160, 161]

The most promising techniques are microwave and ultrasonic devulcanization, due to the good properties of devulcanized material, the possibility of high productivity and ease of implementation. Furthermore, these devulcanization techniques are free of chemical agents during the process that makes them an ecofriendly technology. Microwave devulcanization involve microwave irradiations causing the cross-links breakage in the material network due to the molecular motion and raising the rubber temperature. Whereas ultrasonic devulcanization involves the application of ultrasonic waves to the vulcanized rubber. However, the process conditions must be carefully selected to achieve a selective breaking of chemical links and avoid degradation of the material.[162]

Both reclaiming and devulcanization aim to obtain a rubber compound that can be reprocessed and revulcanized like virgin rubber. However, the difficulty to precisely focus on one type of bond rupture and the simultaneous occurrence of both processes hinders the full recovery of the original properties.[12] Thus, reclaimed/devulcanized rubber can only provide a low-cost material to compounds for less demanding products.[96]

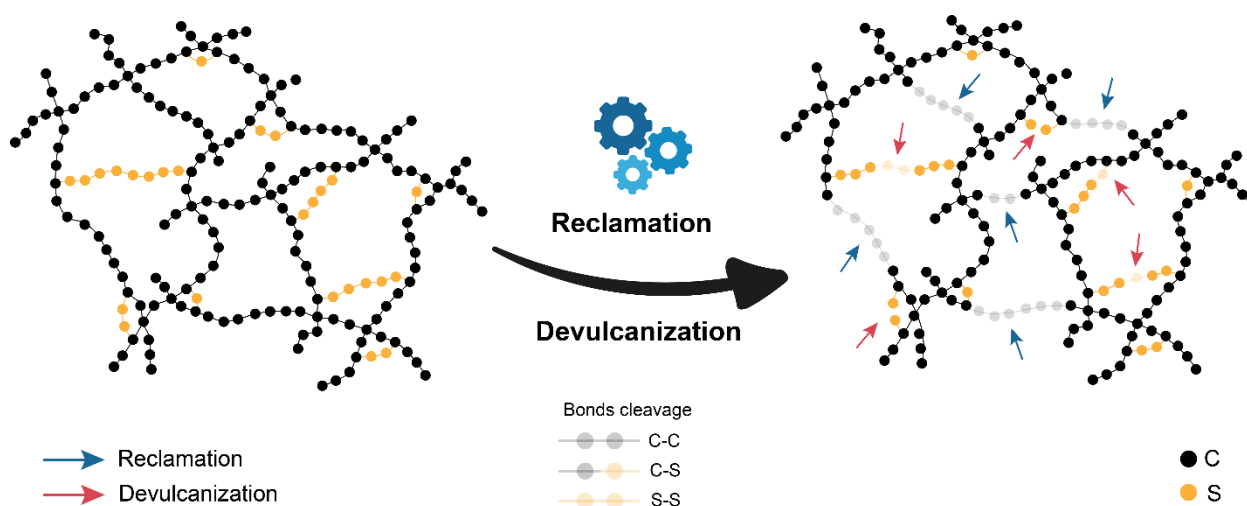


Figure 1.15. Schematic representation of reclamation and devulcanization processes in a cross-linked rubber network.

Conclusions

In this chapter, the management of tires following the different strategies established in the CE model has been exhaustively and critically detailed, comparing scientific perspectives, as well as their industrial and commercial implementation. The path that tires trail within this model, shown in Figure 1.16, evidences the commitment and efforts towards the development of effective management schemes for achieving a real sustainable mobility. In the early stage of production, the optimization of innovative and avant-garde designs will improve tire performance and reduce their environmental impact with the use of alternative renewable raw materials. At the consumption stage, retreading and repairing processes extend the lifetime of tires along with the environmental benefits that these techniques bring. Meanwhile, in the post-consumption stage, the most relevant currently, the main management routes focus on energy and material recovery applications.

To attain the goal of sustainable mobility, it is necessary both to develop a comprehensive used tire management system, and to change the paradigm where ELT are considered as waste to be considered as a resource. In this chapter, the different ELT management systems to reduce landfills and find innovative and environmentally friendly uses has been highlighted, becoming a stronger source of economic and greener growth for industries.

Research and development of both established and emerging tire technologies are of vital importance too. The challenge is to ensure that any process that achieves its

technical objectives is also economically viable and, therefore, has good commercial potential. The use of LCA tools will guarantee such viability. With the optimization of the reclaiming/devulcanization processes, industries would be able to recycle the tire in new tailored made products without having to use any virgin rubber. Likewise, emerging technologies such as the development of self-healing elastomers, whose objective is to extend the useful life of rubber products by reducing waste and saving raw materials and energy, can be seen as an innovative pathway to produce new advanced tires that will lead to the development of sustainable mobility.

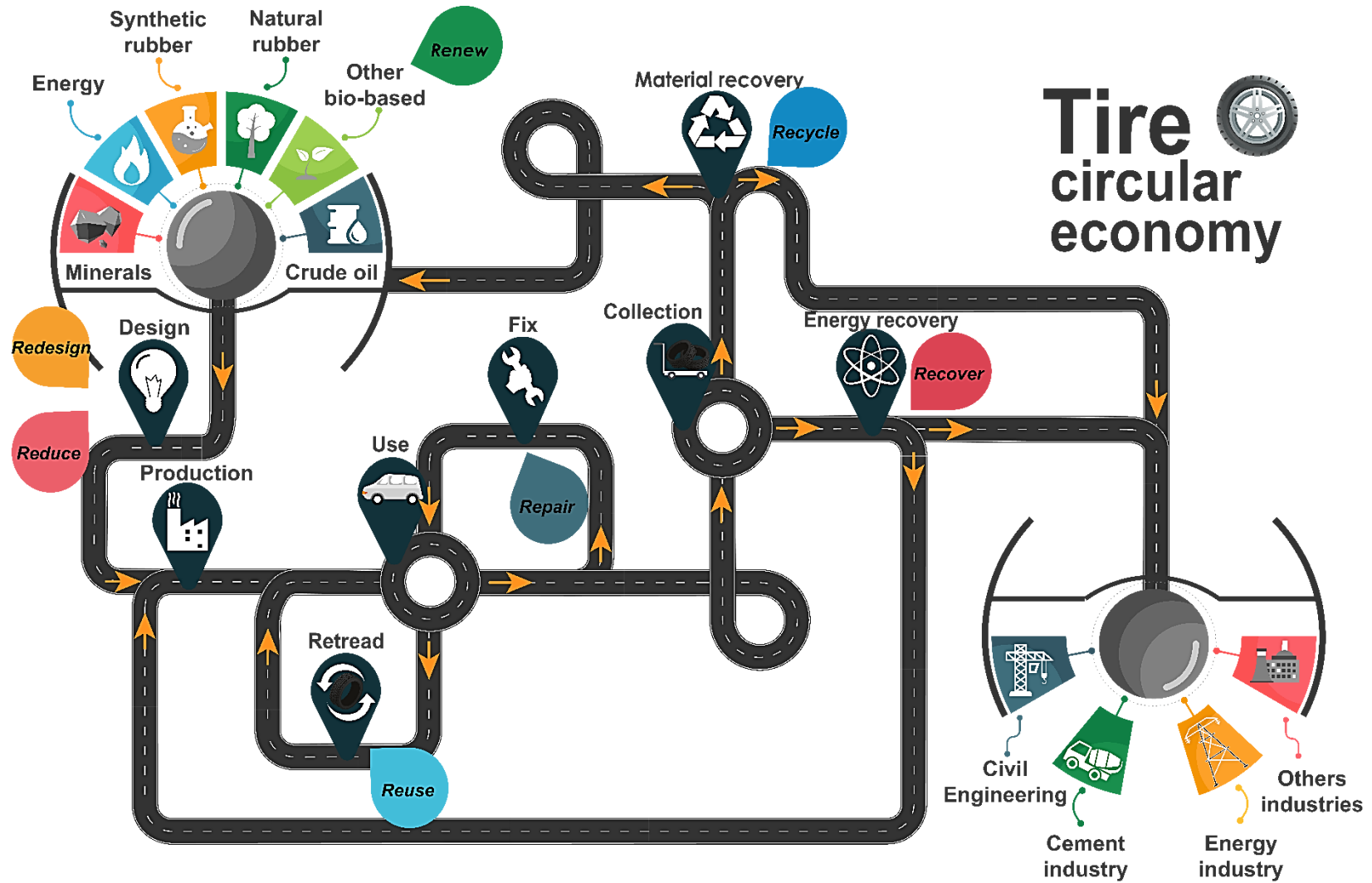


Figure 1.16 Schematic representation of the circular economy path of tires.

Outlook and perspectives

This chapter clearly states the actual commitment and efforts towards the development of effective tire management schemes. Nonetheless, implementing a real sustainable mobility and circular economy model requires a long-term vision based on three main pillars: sustainable use of resources, technological innovation, and economic growth. In this sense, the main tire industries should expand the use of renewable material resources, develop innovative solutions, and invest in groundbreaking technologies to integrate more recycled and renewable materials in its tires, as well as to prolong their useful lifetime. Examples in such direction are already at the core of strategic plans of main tire companies. The Bridgestone Group has set the goal of using 100 % sustainable materials in its products by 2050 and beyond; while Michelin is investing in high technology recycling so that by 2048 tires are 100 % recycled. Likewise, all these actions should generate new business models and lead to sustainable economic growth. The challenge is to ensure that any process that achieves its technical objectives is also economically viable and, therefore, has good commercial potential.

However, industries should not work on their own. Joint actions and cooperation with scientists and government regulatory institutions are needed. Scientific assets will, with no doubt, help in the establishment of research and development programs that will lead to the tire circularity and alleviate the current public concern on the impact of tires on the environment.

1.3. References

1. Segui, L., R. Medina, and H. Guerrero, *Gestión de residuos y economía circular*. 2018, EAE Business School.
2. Ellen MacArthur Foundation. *The Circular Economy In Detail*. 2020. 27/10/2020; Available from: <https://www.ellenmacarthurfoundation.org/explore/the-circular-economy-in-detail>.
3. Gaustad, G., et al., *Circular economy strategies for mitigating critical material supply issues*. *Resour. Conserv. Recycl.*, 2018. **135**: p. 24-33.
4. Vermeulen, W.J.V., D. Reike, and S. Witjes, *Circular Economy 3.0 getting beyond the messy conceptualization of circularity and the 3R's, 4 R's and more*, in *CEC4Europe Factbook*. 2018, Circular Economy Coalition For Europe (CEC4Europe). p. 1-6.
5. Reike, D., W.J.V. Vermeulen, and S. Witjes, *The circular economy: New or Refurbished as CE 3.0? — Exploring Controversies in the Conceptualization of the Circular Economy through a Focus on History and Resource Value Retention Options*. *Resour. Conserv. Recycl.*, 2018. **135**: p. 246-264.
6. The International Market Analysis Research and Consulting Group - IMARC Group. *Tire Market: Global Industry Trends, Share, Size, Growth, Opportunity and Forecast 2020-2025*. 2020. 27/10/2020; Available from: <https://www.imarcgroup.com/tyre-manufacturing-plant>.
7. Anderbilt, T.H.E.V., et al., *Rubber Handbook*. 2010. **06856**(203): p. 853-1400.
8. Beach, D. and J. Schroeder, *An Overview of Tire Technology*, in *Rubber World*. 2000. p. 44-53.
9. World Business Council For Sustainable Development - WBCSD, *Global ELT Management - A global state of knowledge on collection rates, recovery routes, and management methods*. 2018, World Business Council For Sustainable Development - WBCSD.
10. The Freedonia Group, *Global Tires*. 2018, The Freedonia Group. p. 297.
11. European Tyre & Rubber Manufacturers Association - ETRMA. *Circular Economy*. 2019. 27/10/2020; Available from: <https://www.etrma.org/key-topics/circular-economy/>.
12. Sienkiewicz, M., et al., *Environmentally friendly polymer-rubber composites obtained from waste tyres: A review*. *J. Clean. Prod.*, 2017. **147**(February): p. 560-571.
13. Bras, B. and A. Cobert, *Life-Cycle Environmental Impact of Michelin Tweel® Tire for Passenger Vehicles*. *SAE Int. J. Passeng. Cars – Mech. Syst.*, 2011. **4**(1): p. 32-43.
14. The International Market Analysis Research and Consulting Group - IMARC Group. *Global Tire Market to Reach 4.0 Billion Units by 2025, Impelled by Advent of Ecological Tires*. 2019. 27/10/2020; Available from: <https://www.imarcgroup.com/global-tire-market>.
15. Amick, S. *Sustainability: A driving force for the U.S tire manufacturing industry*. 2018. 27/10/2020; Available from: <https://www.ustires.org/sustainability-driving-force-us-tire-manufacturing-industry>.
16. Kuncoro, C.B.D., M.-F. Sung, and Y.-D. Kuan, *Battery Charger Prototype Design for Tire Pressure Sensor Battery Recharging*. *Sensors*, 2019. **19**(1): p. 124.
17. Simonot-Lion, F. and Y. Trinquet, *Vehicel Functional Domains and Their Requirements*, in *Automotive Embedded Systems Handbook*, N. Navet and F. Simonot-Lion, Editors. 2017, CRC Press: Boca Raton, FL. p. 1-22.
18. Aguilar-Bolados, H., M. Yazdani-Pedram, and R. Verdejo, *Chapter 7 - Thermal, electrical, and sensing properties of rubber nanocomposites*, in *High-Performance*

- Elastomeric Materials Reinforced by Nano-Carbons*, L. Valentini and M.A. Lopez Manchado, Editors. 2020, Elsevier. p. 149-175.
19. Barrera, C.S. and K. Cornish, *Novel Mineral and Organic Materials from Agro-Industrial Residues as Fillers for Natural Rubber*. J. Polym. Environ., 2015. **23**(4): p. 437-448.
 20. van Beilen, J.B. and Y. Poirier, *Guayule and Russian Dandelion as Alternative Sources of Natural Rubber*. Crit. Rev. Biotechnol., 2007. **27**(4): p. 217-231.
 21. Niephaus, E., et al., *Uncovering mechanisms of rubber biosynthesis in Taraxacum koksaghyz – role of cis-prenyltransferase-like 1 protein*. Plant J., 2019. **100**(3): p. 591-609.
 22. Ramirez-Cadavid, D.A., et al., *Development of novel processes for the aqueous extraction of natural rubber from Taraxacum kok-saghyz (TK)*. J. Chem. Technol. Biot., 2019. **94**(8): p. 2452-2464.
 23. Cherian, S., S.B. Ryu, and K. Cornish, *Natural rubber biosynthesis in plants, the rubber transferase complex, and metabolic engineering progress and prospects*. Plant Biotechnol. J., 2019. **17**(11): p. 2041-2061.
 24. Rasutis, D., et al., *A sustainability review of domestic rubber from the guayule plant*. Ind. Crop. Prod., 2015. **70**: p. 383-394.
 25. Cheng, F., et al., *Characterization and evaluation of guayule processing residues as potential feedstock for biofuel and chemical production*. Ind. Crop. Prod., 2020. **150**.
 26. Sproul, E., et al., *Integrated techno-economic and environmental analysis of guayule rubber production*. J. Clean. Prod., 2020. **273**.
 27. Mahata, D., et al., *Guayule natural rubber composites: impact of fillers on their cure characteristics, dynamic and mechanical behavior*. Iran. Polym. J., 2020: p. 1-9.
 28. Cornish, K., *Alternative Natural Rubber Crops: Why Should We Care?* Technology & Innovation, 2017. **18**(4): p. 244-255.
 29. Peterson, S.C., S.R. Chandrasekaran, and B.K. Sharma, *Birchwood biochar as partial carbon black replacement in styrene-butadiene rubber composites*. J. Elastomers Plast., 2016. **48**(4): p. 305-316.
 30. Toth, P., et al., *Structure of carbon black continuously produced from biomass pyrolysis oil*. Green Chem., 2018. **20**(17): p. 3981-3992.
 31. Chuayjuljit, S., S. Eiumnoh, and P. Potiyaraj, *Using Silica from Rice Husk as a Reinforcing Filler in Natural Rubber*. J. Sci. Res. Chula. Univ., 2001. **26**(2): p. 127-138.
 32. Snowdon, M.R., A.K. Mohanty, and M. Misra, *A Study of Carbonized Lignin as an Alternative to Carbon Black*. ACS Sustain. Chem. Eng., 2014. **2**(5): p. 1257-1263.
 33. Bahl, K., T. Miyoshi, and S.C. Jana, *Hybrid fillers of lignin and carbon black for lowering of viscoelastic loss in rubber compounds*. Polymer, 2014. **55**(16): p. 3825-3835.
 34. Barana, D., et al., *Lignin Based Functional Additives for Natural Rubber*. ACS Sustain. Chem. Eng., 2018. **6**(9): p. 11843-11852.
 35. Ren, X., et al., *Reinforced Mechanical Properties of Functionalized Silica and Eggshell Filled Guayule Natural Rubber Composites*. Rubber Chem. Technol., 2019. **92**(4): p. 687-708.
 36. Pajtášová, M., et al., *Using of alternative fillers based on the waste and its effect on the rubber properties*, in MATEC Web Conf. 2019. p. 04010.
 37. Gabriel, C., et al., *Tire tread rubber compounds with ternary system filler based on carbon black, silica, and metakaolin: Contribution of silica/metakaolin content on the final properties*. J. Elastomers Plast., 2019. **51**(7-8): p. 712-726.

38. Rahmaniar and T. Susanto, *Impacts of rice husk ash filler loading on curing, morphological characteristics and tensile properties of natural rubber/ethylene propylene rubber blends*, in *IOP Conf. Ser., Mater. Sci. Eng.* 2019.
39. Egbujuo, W.O., P.I. Anyanwu, and H.C. Obasi, *Utilization of chitin powder as a filler in natural rubber vulcanizates: In comparison with carbon black filler*. 2020. **11**(1): p. 43-51.
40. Dominic, M., et al., *Green tire technology: Effect of rice husk derived nanocellulose (RHNC) in replacing carbon black (CB) in natural rubber (NR) compounding*. *Carbohydr. Polym.*, 2020. **230**(November 2019): p. 115620-115620.
41. Ali, S.D., et al., *Novel CNC/silica hybrid as potential reinforcing filler for natural rubber compounds*. *J. Appl- Polym. Sci.*, 2020. **137**(5): p. 48332-48345.
42. Fathurrohman, M.I., et al., *Better balance of Silica-Reinforced Natural Rubber tire tread compound properties by the use of montmorillonite with optimum surface modifier content*. *Rubber Chem. Technol.*, 2020: p. 548-566.
43. Mgbemena, C.O. and C.E. Mgbemena, *Performance Studies of Natural Rubber/Organomodified Kaolin Vulcanizates Developed for Tire Sidewall Applications*. *Arid Zone J. Eng. Technol. Envir.*, 2020. **16**(1): p. 58-64.
44. Mohamad Aini, N., et al., *Lignin as Alternative Reinforcing Filler in the Rubber Industry: A Review*. *Front. Mater.*, 2020. **6**: p. 329-347.
45. Rodgers, B., S.S. Tallury, and W. Klingensmith, *Rubber Compounding: Chemistry and Applications*. 2016: CRC press. 1-60.
46. Arroyo, M., M.A. López-Manchado, and B. Herrero, *Organo-montmorillonite as substitute of carbon black in natural rubber compounds*. *Polymer*, 2003. **44**(8): p. 2447-2453.
47. Hernández, M., et al., *Overall performance of natural rubber/graphene nanocomposites*. *Compos. Sci. Technol.*, 2012. **73**: p. 40-46.
48. Valentini, L., et al., *Nitrile butadiene rubber composites reinforced with reduced graphene oxide and carbon nanotubes show superior mechanical, electrical and icephobic properties*. *Compos. Sci. Technol.*, 2018. **166**: p. 109-114.
49. Bokobza, L., *Natural rubber nanocomposites: A review*. *Nanomaterials*, 2019. **9**(1): p. 12-33.
50. Rathanasamy, R., *A review on the effect of carbon based nanofillers on the properties of elastomers*. *Mater. Sci. Eng. Int. J.*, 2019. **3**(3): p. 89-101.
51. García, D.B., et al., *Effect of carbon nanotubes content on the vulcanization kinetic in styrene-butadiene rubber compounds*. *Polym. Eng. Sci.*, 2019. **59**(s2): p. E327-E336.
52. Poikelispää, M., et al., *The effect of partial replacement of carbon black by carbon nanotubes on the properties of natural rubber/butadiene rubber compound*. *J. Appl- Polym. Sci.*, 2013. **130**(5): p. 3153-3160.
53. Shao, H.-Q., H. Wei, and J.-H. He, *Dynamic properties and tire performances of composites filled with carbon nanotubes*. *Rubber Chem. Technol.*, 2018. **91**(3): p. 609-620.
54. Andersen, L.G., et al., *Rolling resistance measurement and model development*. *J. Transp. Eng.*, 2015. **141**(2): p. 1-10.
55. Aldhufairi, H.S. and O.A. Olatunbosun, *Developments in tyre design for lower rolling resistance: A state of the art review*. *P. I. Mech. Eng. D-J Aunt.*, 2018. **232**(14): p. 1865-1882.
56. Akutagawa, K., *Technology for reducing tire rolling resistance*. *Tribol. Online*, 2017. **12**(3): p. 99-102.
57. Roy, K., S. Debnath, and P. Potiyaraj, *A critical review on the utilization of various reinforcement modifiers in filled rubber composites*. *J. Elastomers Plast.*, 2019. **52**(2): p. 167-193.

58. Linglong Tire. *Linglong Reaches Another Milestone in Graphene Research*. 2019. 27/10/2020; Available from: https://en.linglong.cn/content/details34_38472.html.
59. Gratomic. *Graphene Tires | Gratomic*. 2020. 01/11/2020; Available from: <https://gratomic.ca/graphene-tires/>.
60. Forrest, M.J., *Recycling and Re-Use of Waste Rubber*. 2014: Smithers Rapra Technology Ltd. 1-233.
61. Sharma, A., *Retreading of Tyres*. *Int. J. Eng. Adv. Technol.*, 2013. **2**(6): p. 2249-8958.
62. EY, *The socio-economic impact of truck tyre retreading in Europe*. 2016, EY: <https://www.etrma.org/library/the-socio-economic-impact-of-truck-tyre-retreading-in-europe/>.
63. Imbernon, L. and S. Norvez, *From landfilling to vitrimer chemistry in rubber life cycle*. *Eur. Polym. J.*, 2016. **82**: p. 347-376.
64. Fact MR. *Retread Tire Market Forecast, Trend Analysis & Competition Tracking - Global Review 2018 to 2028*. 2021. 28/02/2021; Available from: <https://www.factmr.com/report/890/retread-tire-market>.
65. Connor, K., et al., *Developing a Sustainable Waste Tire Management Strategy for Thailand*. 2013, Worcester Polytechnic Institute - WPI.
66. Ostoji, S.D., V. Simi, and M. Miljuš, *Used Tire Management: An Overview, Part 1*. 3rd Logistics International conference 25-27 May 2017, 2017: p. 210-215.
67. Sienkiewicz, M., et al., *Progress in used tyres management in the European Union: A review*. *Waste Manage.*, 2012. **32**(10): p. 1742-1751.
68. Geitner, R., et al., *Do You Get What You See? Understanding Molecular Self-Healing*. *Chemistry - A European Journal*, 2018. **24**(10): p. 2493-2502.
69. White, S.R., et al., *Autonomic healing of polymer composites*. *Nature*, 2001. **409**(6822): p. 794-797.
70. Hernández Santana, M., et al., *Routes to make natural rubber heal: A review*. *Polym. Rev.*, 2018. **3724**(4): p. 1-25.
71. Sattar, M.A. and A. Patnaik, *Design Principles of Interfacial Dynamic Bonds in Self-Healing Materials: What are the Parameters?* *Chemistry – An Asian Journal*, 2020. **15**: p. 1-27.
72. Nie, J., et al., *Bio-based epoxidized natural rubber/chitin nanocrystals composites: Self-healing and enhanced mechanical properties*. *Compos. Part. B-Eng.*, 2019. **172**: p. 152-160.
73. Utrera-Barrios, S., et al., *Design of rubber composites with autonomous self-healing capability*. *ACS Omega*, 2020. **5**(4): p. 1902-1910.
74. Imbernon, L., S. Norvez, and L. Leibler, *Stress relaxation and self-adhesion of rubbers with exchangeable links*. *Macromolecules*, 2016. **49**(6): p. 2172-2178.
75. Hernández, M., et al., *Turning vulcanized natural rubber into a self-healing polymer: Effect of the disulfide/polysulfide ratio*. *ACS Sustain. Chem. Eng.*, 2016. **4**(10): p. 5776-5784.
76. Polgar, L.M., et al., *Use of Diels–Alder chemistry for thermoreversible cross-linking of rubbers: The next step toward recycling of rubber products?* *Macromolecules*, 2015. **48**(19): p. 7096-7105.
77. Tanasi, P., et al., *Thermo-reversible crosslinked natural rubber: A Diels-Alder route for reuse and self-healing properties in elastomers*. *Polymer*, 2019. **175**: p. 15-24.
78. Das, A., et al., *Ionic modification turns commercial rubber into a self-healing material*. *ACS Appl. Mater. Inter.*, 2015. **7**(37): p. 20623-20630.
79. Das, A., et al., *Temperature scanning stress relaxation of an autonomous self-healing elastomer containing non-covalent reversible network junctions*. *Polymers*, 2018. **10**(1): p. 94-104.

80. Utrera-Barrios, S., et al., *Evolution of self-healing elastomers, from extrinsic to combined intrinsic mechanisms: a review*. Mater. Horiz., 2020. **7**: p. 2882-2902.
81. Canadell, J., H. Goossens, and B. Klumperman, *Self-healing materials based on disulfide links*. Macromolecules, 2011. **44**(8): p. 2536-2541.
82. Lafont, U., H. van Zeijl, and S. van der Zwaag, *Influence of Cross-linkers on the Cohesive and Adhesive Self-Healing Ability of Polysulfide-Based Thermosets*. Acs. Appl. Mater. Inter., 2012. **4**(11): p. 6280-6288.
83. Pepels, M., et al., *Self-healing systems based on disulfide-thiol exchange reactions*. Polym. Chem., 2013. **4**(18): p. 4955-4965.
84. Thajudin, N.L.N., et al., *Room temperature self-healable natural rubber*. J. Rubber. Res., 2019. **22**(4): p. 203-211.
85. Imbernon, L. and S. Norvez, *From landfilling to vitrimer chemistry in rubber life cycle*. Eur. Polym. J., 2016. **82**: p. 347-376.
86. Sattar, M.A., S. Gangadharan, and A. Patnaik, *Design of dual hybrid network natural rubber-SiO₂ elastomers with tailored mechanical and self-healing properties*. ACS Omega, 2019. **4**(6): p. 10939-10949.
87. Myhre, M., et al., *Rubber Recycling: Chemistry, Processing, and Applications*. Rubber Chem. Technol., 2012. **85**(3): p. 408-449.
88. Ślusarczyk, B., M. Baryń, and S. Kot, *Tire industry products as an alternative fuel*. Pol. J. Environ. Stud., 2016. **25**(3): p. 1263-1270.
89. Li, X., et al., *Comparison of end-of-life tire treatment technologies: A Chinese case study*. Waste Manage., 2010. **30**(11): p. 2235-2246.
90. Martínez, J.D., et al., *Waste tyre pyrolysis - A review*. Renew. Sustain. Energy Rev., 2013. **23**: p. 179-213.
91. Manoharan, P. and K. Naskar, *Recycling of Tire Rubbers and Their Re-usability*, in *Rubber Recycling: Challenges and Developments*, J. Kuk Kim, et al., Editors. 2019, The Royal Society of Chemistry. p. 102-127.
92. Bockstal, L., et al., *Devulcanisation and reclaiming of tires and rubber by physical and chemical processes: A review*. J. Clean. Prod., 2019. **236**: p. 117574-117590.
93. Mavukwana, A.-e. and C. Sempuga, *Recent developments in waste tyre pyrolysis and gasification processes*. Chemical Engineering Communications, 2020: p. 1-27.
94. Torretta, V., et al., *Treatment and disposal of tyres: Two EU approaches. A review*. Waste Manage., 2015. **45**: p. 152-160.
95. Shulman, V.L., *Tire Recycling*. Waste, 2019: p. 489-515.
96. Isayev, A.I., *The Science and Technology of Rubber*, in *Recycling of Rubbers*. 2013, Elsevier Inc. p. 697-764.
97. Beston. *Waste Tire Pyrolysis Plant*. 2021. 28/02/2021; Available from: <https://bestonpyrolysisplant.com/waste-tyre-pyrolysis-plant/>.
98. Mingjie. *Pyrolysis Plant*. 2021. 28/02/2021; Available from: https://www.mingjiegroupp.com/products/Tire_plastic_Pyrolysis_Plant.html.
99. Klean Industries. *Tire Recycling*. 2021. 28/02/2021; Available from: <https://kleanindustries.com/waste-challenges-innovations/tire-pyrolysis-recycling/>.
100. Metso:Outotec. *Tire pyrolysis systems: The true recycling solution*. 2021. 28/02/2021; Available from: <https://www.mogroup.com/portfolio/tire-pyrolysis/>.
101. Ramos, G., F.J. Alguacil, and F.A. López, *The recycling of end-of-life tyres. Technological review*. Rev. Metal, 2010. **47**(3): p. 273-284.
102. European Parliament, C.o.t.E.U., *Directive 2008/98/EC of the European Parliament and of the Council of 19 November 2008 on waste and repealing certain Directives*. 2008, The European Parliament and the Council of the European Union. p. 3-30.

103. Zefeng, W., et al., *Recycling waste tire rubber by water jet pulverization: Powder characteristics and reinforcing performance in natural rubber composites*. J. Polym. Eng., 2018. **38**(1): p. 51-62.
104. Hoyer, S., L. Kroll, and D. Sykutera, *Technology comparison for the production of fine rubber powder from end of life tyres*. Procedia Manuf., 2020. **43**: p. 193-200.
105. Ramarad, S., et al., *Waste tire rubber in polymer blends: A review on the evolution, properties and future*. Prog. Mater. Sci., 2015. **72**: p. 100-140.
106. Wang, Z., Y. Kang, and Y. Cheng, *Multiresponse optimization of process parameters in water jet pulverization via response surface methodology*. Int. J. Precis. Eng. Man., 2017. **18**(12): p. 1855-1871.
107. Rodgers, B. and B. D'cruz, *Recycling of rubber*. Rubber Compounding: Chemistry and Applications, Second Edition, 2015: p. 523-536.
108. Mishra, R., M.K. Aswathi, and S. Thomas, *High Performance Flooring Materials from Recycled Rubber*, in *Rubber Recycling: Challenges and Developments*. 2019, The Royal Society of Chemistry. p. 160-185.
109. Orrit-Prat, J., et al., *Dielectric and mechanical characterization of PVC composites with ground tire rubber*. J. Compos. Mater., 2011. **45**(11): p. 1233-1243.
110. de Sousa, F.D.B., et al., *Blends of ground tire rubber devulcanized by microwaves/HDPE - Part A: Influence of devulcanization process*. Polimeros, 2015. **25**(3): p. 256-264.
111. de Sousa, F.D.B., et al., *Blends of ground tire rubber devulcanized by microwaves/HDPE-Part B: Influence of clay addition*. Polimeros, 2015. **25**(4): p. 382-391.
112. Mujal-Rosas, R., M. Marin-Genesca, and J. Ballart-Prunell, *Dielectric properties of various polymers (PVC, EVA, HDPE, and PP) reinforced with ground tire rubber (GTR)*. Sci. Eng. Compos. Mater., 2015. **22**(3): p. 231-243.
113. Liang, H., et al., *Ground tire rubber (GTR) surface modification using thiol-ene click reaction: Polystyrene grafting to modify a GTR/polystyrene (PS) blend*. Prog. Rubber Plast. Recycl. Technol., 2019. **36**(2): p. 81-101.
114. Zhang, S.L., et al., *Characterization of the properties of thermoplastic elastomers containing waste rubber tire powder*. Waste Manage., 2009. **29**(5): p. 1480-1485.
115. Lima, P., et al., *Rheological properties of ground tyre rubber based thermoplastic elastomeric blends*. Polym. Test., 2015. **45**: p. 58-67.
116. Hernández, E., et al., *Sulfuric acid treatment of ground tire rubber and its effect on the mechanical and thermal properties of polypropylene composites*. J. Appl. Polym. Sci., 2017. **134**(21): p. 1-7.
117. Sonnier, R., et al., *Polyethylene/ground tyre rubber blends: Influence of particle morphology and oxidation on mechanical properties*. Polym. Test., 2007. **26**(2): p. 274-281.
118. Naskar, A.K., S.K. De, and A.K. Bhowmick, *Thermoplastic elastomeric composition based on maleic anhydride-grafted ground rubber tire*. J. Appl. Polym. Sci., 2002. **84**(2): p. 370-378.
119. Formela, M., et al., *Compatibilization of polymeric composition filled with ground tire rubber - short review*. Chem. Chem. Technol., 2014. **8**(4): p. 445-450.
120. Song, P., S. Li, and S. Wang, *Interfacial interaction between degraded ground tire rubber and polyethylene*. Polym. Degrad. Stabil., 2017. **143**: p. 85-94.
121. Formela, K., et al., *Styrene-Butadiene Rubber/Modified Ground Tire Rubber Blends Co-Vulcanization: Effect of Accelerator Type*. Macromol. Sy., 2016. **361**(1): p. 64-72.
122. Yehia, A.A., et al., *Mechano-chemical reclamation of waste rubber powder and its effect on the performance of NR and SBR vulcanizates*. J. Elastomers Plast., 2004. **36**(2): p. 109-123.

123. Han, S.C. and M.H. Han, *Fracture behavior of NR and SBR vulcanizates filled with ground rubber having uniform particle size*. Journal of Applied Polymer Science, 2002. **85**(12): p. 2491-2500.
124. Araujo-Morera, J., et al., *Giving a second opportunity to tire waste: An alternative path for the development of sustainable self-healing styrene-butadiene rubber compounds overcoming the magic triangle of tires*. Polymers, 2019. **11**(12): p. 1-13.
125. Xinxing, Z., et al., *Improvement of the Properties of Ground Tire Rubber (GTR)-Filled Nitrile Rubber Vulcanizates Through Plasma Surface Modification of GTR Powder*. J. Appl- Polym. Sci., 2009. **114**: p. 1118-1125.
126. Cheng, X., et al., *Time effectiveness of the low-temperature plasma surface modification of ground tire rubber powder*. J. Adhes. Sci. Technol., 2015. **29**(13): p. 1330-1340.
127. Cataldo, F., O. Ursini, and G. Angelini, *Surface oxidation of rubber crumb with ozone*. Polym. Degrad. Stabil., 2010. **95**(5): p. 803-810.
128. Cao, X.W., et al., *Structure and properties of deeply oxidized waste rubber crumb through long time ozonization*. Polym. Degrad. Stabil., 2014. **109**: p. 1-6.
129. Herrera-Sosa, E.S., et al., *Waste Tire Particles and Gamma Radiation as Modifiers of the Mechanical Properties of Concrete*. Adv. Mater. Sci. Eng., 2014. **2014**(1): p. 1-7.
130. Shanmugaraj, A.M., J.K. Kim, and S.H. Ryu, *UV surface modification of waste tire powder: Characterization and its influence on the properties of polypropylene/waste powder composites*. Polym. Test., 2005. **24**(6): p. 739-745.
131. Yehia, A.A., et al., *Effect of chemically modified waste rubber powder as a filler in natural rubber vulcanizates*. J. Appl- Polym. Sci., 2004. **93**(1): p. 30-36.
132. Hernández Gámez, J.F., et al., *Mechanical reinforcement of thermoplastic vulcanizates using ground tyre rubber modified with sulfuric acid*. Polym. Compos., 2018. **39**(1): p. 229-237.
133. Aggour, Y.a., *Surface Modification of Waste Tire by Grafting with Styrene and Maleic Anhydride*. Open J. Polym. Chem., 2012. **02**(02): p. 70-76.
134. Rungrodmitchai, S. and D. Kotatha, *Chemically modified ground tire rubber as fluoride ions adsorbents*. Chem. Eng. J., 2015. **282**: p. 161-169.
135. Thomas, B.S. and R.C. Gupta, *Long term behaviour of cement concrete containing discarded tire rubber*. J. Clean. Prod., 2015. **102**: p. 78-87.
136. Youssf, O., J.E. Mills, and R. Hassanli, *Assessment of the mechanical performance of crumb rubber concrete*. Constr. Build. Mater., 2016. **125**: p. 175-183.
137. Shu, X. and B. Huang, *Recycling of waste tire rubber in asphalt and portland cement concrete: An overview*. Constr. Build. Mater., 2014. **67**(PART B): p. 217-224.
138. Wu, X., S. Wang, and R. Dong, *Lightly pyrolyzed tire rubber used as potential asphalt alternative*. Constr. Build. Mater., 2016. **112**: p. 623-628.
139. Hallmark-Haack, B.L., et al., *Ground Tire Rubber Modification for Improved Asphalt Storage Stability*. Energ. Fuel, 2019. **33**(4): p. 2659-2664.
140. Markl, E., M. Lackner, and R. Wintersteller, *Devulcanization Technologies for Recycling of Tire-Derived Rubber: A Review*. Materials, 2020. **13**(5): p. 1246-1246.
141. Sabzekar, M., et al., *Influence of process variables on chemical devulcanization of sulfur-cured natural rubber*. Polym. Degrad. Stabil., 2015. **118**: p. 88-95.
142. Padella, F., et al., *Recycling of scrap tires rubber by mechanochemical devulcanization*. Poly. Recycl., 2001. **6**(1): p. 11-16.
143. Ghorai, S., et al., *Mechanochemical devulcanization of natural rubber vulcanizate by dual function disulfide chemicals*. Polym. Degrad. Stabil., 2016. **129**: p. 34-46.

144. Yun, J., J.S. Oh, and A.I. Isayev, *Ultrasonic devulcanization reactors for recycling of GRT: Comparative study*. Rubber Chem. Technol., 2001. **74**(2): p. 317-330.
145. Yun, J., et al., *Comparative analysis of ultrasonically devulcanized unfilled SBR, NR, and EPDM rubbers*. J. Appl- Polym. Sci., 2003. **88**(2): p. 434-441.
146. Feng, W. and A.I. Isayev, *Recycling of tire-curing bladder by ultrasonic devulcanization*. Polym. Eng. Sci., 2006. **46**(1): p. 8-18.
147. Isayev, A.I., T. Liang, and T.M. Lewis, *Effect of particle size on ultrasonic devulcanization of tire rubber in twin-screw extruder*. Rubber Chem. Technol., 2014. **87**(1): p. 86-102.
148. Seghar, S., et al., *Devulcanization of styrene butadiene rubber by microwave energy: Effect of the presence of ionic liquid*. Express Polym. Lett., 2015. **9**(12): p. 1076-1086.
149. de Sousa, F.D.B., et al., *Devulcanization of waste tire rubber by microwaves*. Polym. Degrad. Stabil., 2017. **138**: p. 169-181.
150. Aoudia, K., et al., *Recycling of waste tire rubber: Microwave devulcanization and incorporation in a thermoset resin*. Waste Manage., 2017. **60**: p. 471-481.
151. Colom, X., et al., *Structural and physico-mechanical properties of natural rubber/GTR composites devulcanized by microwaves: Influence of GTR source and irradiation time*. J. Compos. Mater., 2018. **52**(22): p. 3099-3108.
152. Li, Y., S. Zhao, and Y. Wang, *Microbial desulfurization of ground tire rubber by Thiobacillus ferrooxidans*. Polym. Degrad. Stabil., 2011. **96**(9): p. 1662-1668.
153. Li, Y., S. Zhao, and Y. Wang, *Microbial Desulfurization of Ground Tire Rubber by Sphingomonas sp.: A Novel Technology for Crumb Rubber Composites*. J. Polym. Environ., 2012. **20**(2): p. 372-380.
154. Ghavipankeh, F., Z. Ziaei Rad, and M. Pazouki, *Devulcanization of Ground Tires by Different Strains of Bacteria: Optimization of Culture Condition by Taguchi Method*. J. Polym. Environ., 2018. **26**(8): p. 3168-3175.
155. Kaewpetch, B., S. Prasongsuk, and S. Poompradub, *Devulcanization of natural rubber vulcanizates by Bacillus cereus TISTR 2651*. Express Polym. Lett., 2019. **13**: p. 877-888.
156. Tao, G., et al., *The effect of devulcanization level on mechanical properties of reclaimed rubber by thermal-mechanical shearing devulcanization*. J. Appl- Polym. Sci., 2013. **129**(5): p. 2598-2605.
157. Si, H., T. Chen, and Y. Zhang, *Effects of high shear stress on the devulcanization of ground tire rubber in a twin-screw extruder*. J. Appl- Polym. Sci., 2013. **128**(4): p. 2307-2318.
158. Formela, K., et al., *The influence of feed rate and shear forces on the devulcanization process of ground tire rubber (GTR) conducted in a co-rotating twin screw extruder*. Polimery, 2013. **58**(11-12): p. 906-912.
159. Ujianto, O., et al., *A comparative study of ground tire rubber devulcanization using twin screw extruder and internal mixer*. IOP Conf. Ser., Mater. Sci. Eng., 2017. **223**(1): p. 0-9.
160. Jiang, K., et al., *Complete devulcanization of sulfur-cured butyl rubber by using supercritical carbon dioxide*. J. Appl- Polym. Sci., 2013. **127**(4): p. 2397-2406.
161. Asaro, L., et al., *Devulcanization of natural rubber industry waste in supercritical carbon dioxide combined with diphenyl disulfide*. Waste Manage., 2020. **118**: p. 647-654.
162. Asaro, L., et al., *Recycling of rubber wastes by devulcanization*. Resour. Conserv. Recycl., 2018. **133**: p. 250-262.

2

MATERIALS AND METHODS

2. Materials and methods

Chapter 2 details the materials that have been used in the preparation of the rubber composites studied in this research. In addition, it describes the general experimental techniques and methods that have been used throughout the study to characterize the materials.

2.1. Materials

Styrene-Butadiene Rubber

Styrene-Butadiene Rubber (SBR) is a synthetic rubber which is produced by copolymerization of styrene and butadiene monomers. There are four different basic structural units in SBR; three of them originate from butadiene (Figure 2.1), which can be arranged as cis-1.4, trans-1.4 or 1.2 (vinyl) units.[1] Mutual arrangement of styrene and butadiene units can have random, partially-block or block character.

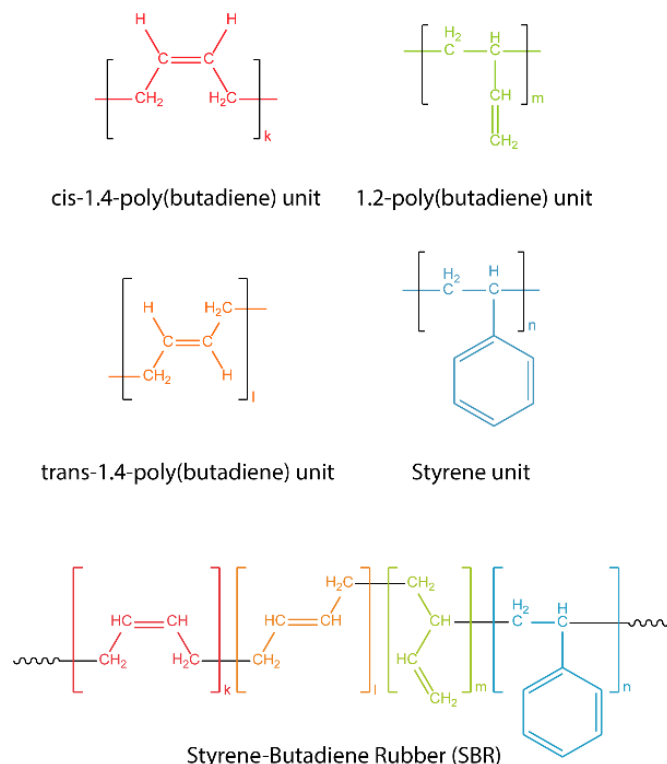


Figure 2.1 Isomeric structures of poly(butadiene), styrene structure and Styrene-Butadiene Rubber structure.

The elastomeric matrix used in this study was a commercial SBR (Buna® SE 1502 H), kindly supplied by Arlanxeo. According to the information provided by the supplier, this elastomer is an emulsion SBR, which is produced via a cold emulsion polymerization, using fatty and rosin soaps as emulsifiers, where the monomers are randomly distributed in the polymer structure. The butadiene fraction is mostly arranged in the trans configuration and has small fractions of cis and vinyl configurations. The raw material properties of the used SBR are shown in Table 2.1.

*Table 2.1 Raw material properties of commercial SBR.**

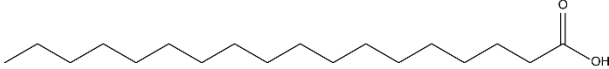
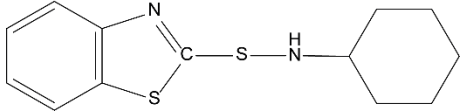
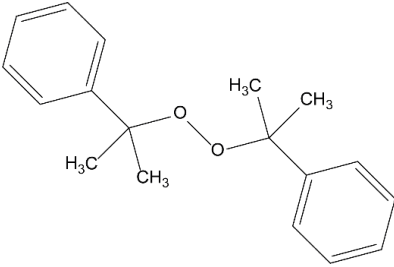
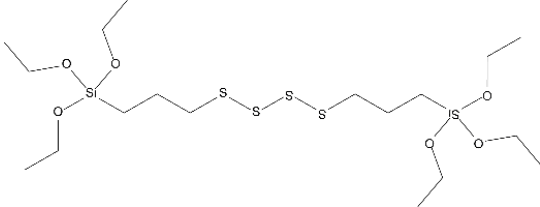
Property	Nominal Value	Test Method
Volatile Matter	max. 0.5 wt %	ASTM D 5668
Mooney Viscosity ML (1+4) 100 °C	53 MU	ASTM D 1646
Free soap	max. 0.5 wt %	ASTM D 5774
Organic acid	6.0 wt %	ASTM D 5774
Bound Styrene	23.5 wt %	ASTM D 5775
Density	0.94 (g/cm ³)	ASTM D 297

** information provided by the supplier*

Vulcanization additives

The ingredients used as vulcanizing additives in the SBR composites are listed in Table 2.2, mentioning their chemical structure, main function within the compound and the supplier.

Table 2.2 Vulcanization additives used in SBR composites.

Additive	Chemical structure	Function	Supplier
Zinc oxide (ZnO)	ZnO	Activator	Sigma Aldrich
Stearic acid (SA)		Activator	Sigma Aldrich
N-cyclohexylbenzothiazole-2-sulfenamide (CBS)		Accelerator	Sigma Aldrich
Sulfur (S)	S ₈	Cross-linking agent	Sigma Aldrich
Dicumyl peroxide (DCP)		Cross-linking agent	Merck KGaA
Bis-(3-triethoxysilylpropyl)tetrasulfide (TESPT)		Coupling agent	Evonik Industries AG

Fillers

Carbon black (CB)

Carbon black (CB) is primarily composed of elemental carbon, in the form of extremely fine particles with an amorphous molecular structure. It is produced by the partial combustion or thermal decomposition of hydrocarbons under controlled conditions. CB is mainly used as reinforcing filler in the rubber industry, especially for tire manufacturing. It is added to improve the processing, strength and durability of tires.[2, 3]

CB exhibits a hierarchical morphology: i) spheroidal primary particles, ii) aggregates, and iii) agglomerates, as shown in Figure 2.2. Primary particles are strongly linked by covalent bonds, forming the aggregates. Thereafter, individual aggregates get together by van der Waals forces to form agglomerates. These agglomerates do not break down into smaller components unless adequate forces are applied.[4]

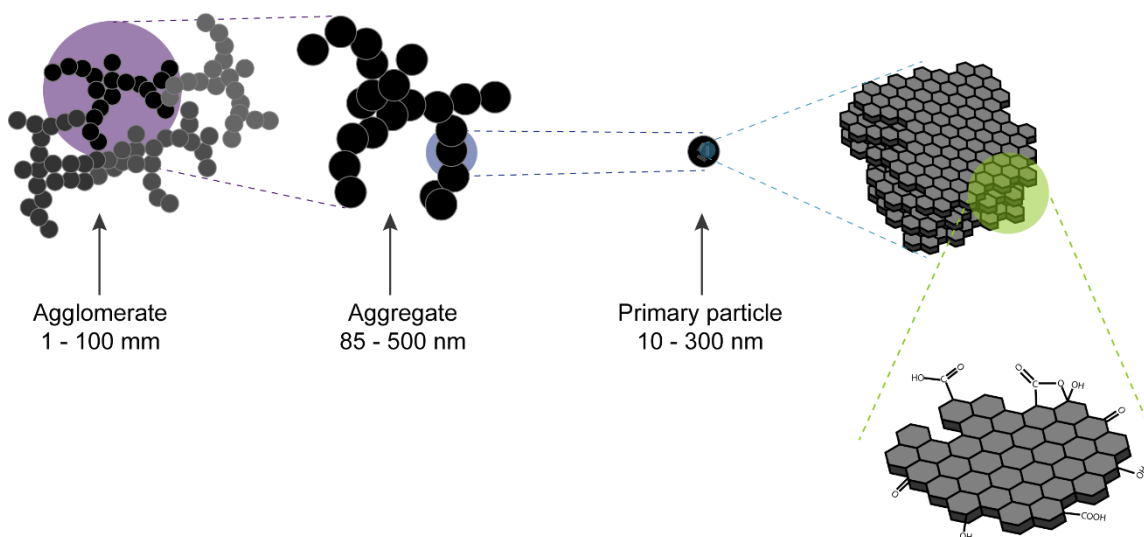


Figure 2.2 Schematic representation of the hierarchical morphology of CB.

The physical properties imparted to a given rubber composite by CB are dominated by three factors: i) the specific surface area, ii) the structure, and iii) the loading. These characteristics determine the static and dynamic within-rubber properties and, therefore, allow customization of the performance of rubber products.

The CB used in this study was a commercial general purpose N330 grade, kindly supplied by Birla Carbon™. According to the information provided by the supplier, this CB offers a good balance of properties, such as medium-high reinforcement, good abrasion

resistance, high elongation, hysteresis, easy processing, and viscosity. Its major applications are tire tread, conveyor belts, rubber mechanical goods, plastic composites, and pigments. The material properties of the used CB are shown in Table 2.3.

Table 2.3 Properties of CB grade N330.*

Property	Value
Appearance	Powder or pellet
Particle size	200 – 300 μm
Density	1.7 – 1.9 g/cm^3

* information provided by the supplier

Silica

Silica has become a high-performance ingredient for rubber composites, acting as reinforcing filler, as well as, providing other requirements such as transparency or a particular color. Precipitated silica is produced in a batch process by adding a mineral acid (normally sulfuric acid) to a water glass (sodium silicate solution). During the precipitation process, primary particles are initially produced, followed by the formation of clusters. The smallest basic silica unit relevant for rubber reinforcement is an aggregate, a three-dimensional structure that consists of primary particles covalently bonded to each other by siloxane bonds.[5]

Silica is incompatible with the non-polar tire polymers due to the high concentration of polar silanol (geminal, isolated and vicinal), and siloxane groups on its surface (Figure 2.3). This polar surface generates a strong silica-silica agglomeration via hydrogen bonding and, at the same time, provides a weak interaction with the rubber.

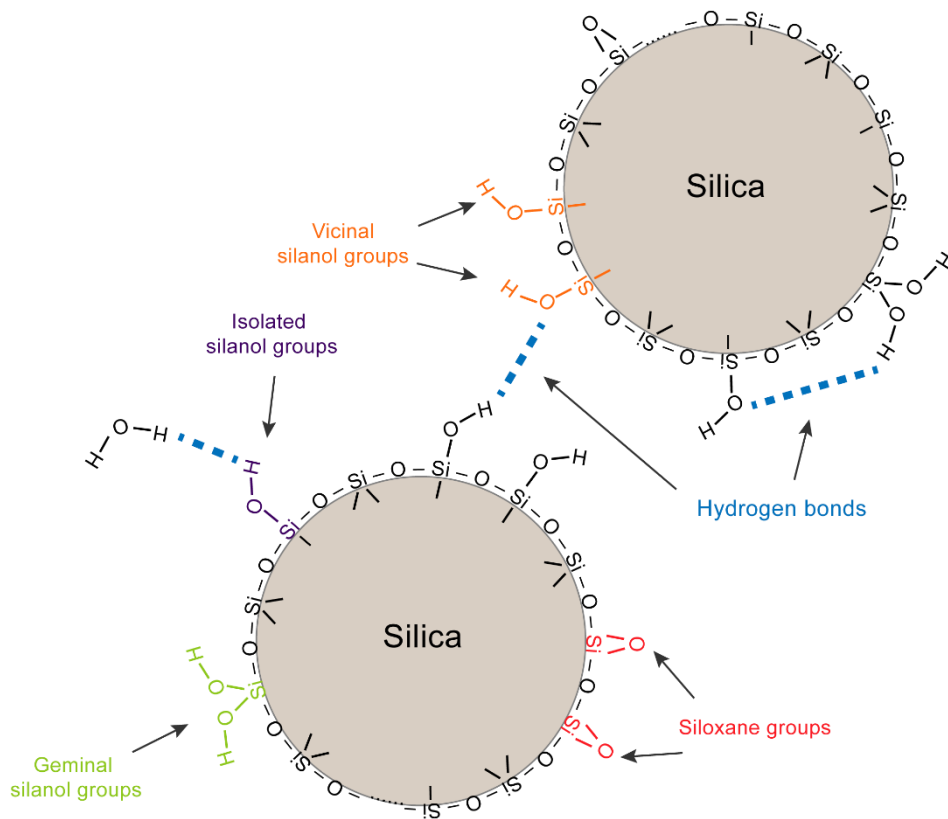


Figure 2.3 Schematic representation of the different types of silanol groups on the silica surface, and the formation of the silica network by hydrogen bonding.

Hence, silica is mainly used in conjunction with bifunctional organosilanes, as coupling agents, to overcome the polarity differences. These coupling agents modify the polar surface of the silica to improve its compatibility and, thus, its dispersion in the rubber matrix (Figure 2.4). Therefore, homogeneously and well-dispersed silica particles are able to provide improved reinforcement for high performance rubber composites.[4]

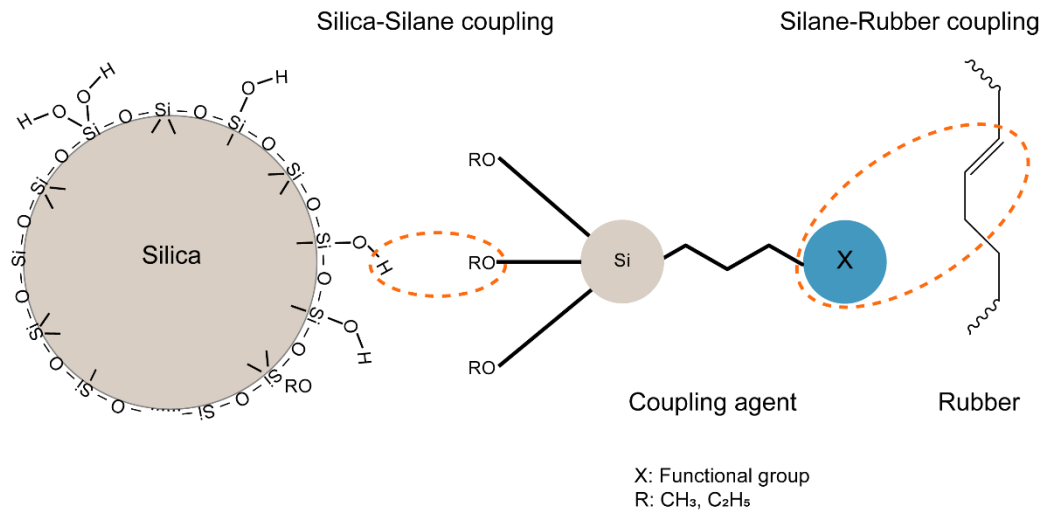


Figure 2.4 Silica-Silane-Rubber coupling scheme.

The silica used in this study was a commercial ZEOSIL[®] 1165 MP, kindly supplied by Solvay. This highly dispersible silica (HDS) micropearls improve tire rolling resistance and grip balance. ZEOSIL[®] 1165MP is used in the manufacturing and reinforcement of rubber goods, as well as, in the manufacturing of plastics products, including compounding, conversion and polymer preparation, and composites. The material properties of the used silica are shown in Table 2.4.

Table 2.4 Silica (ZEOSIL[®] 1165 MP) properties.

Property	Value
Appearance	Micropearls
Particle size	200 – 300 μm
Density	2.1 g/cm ³

Ground tire rubber (GTR)

Ground tire rubber (GTR) is fine granular recycled rubber produced from scrap tires (passenger car, and truck tires). This material is the preferred recycling route for waste tires. A generic profile of the material composition of car and truck tires is shown in Table 2.5.

Table 2.5 Composition by weight of car and truck tires.[6]

Material	Car (%)	Truck (%)
Rubber/Elastomer ¹	± 43	± 45
Carbon black and silica	± 27	± 20
Metals	± 11	± 22
Textiles	± 5	± 1
Vulcanization system ²	± 3	± 3
Additives	± 3	± 3
Aromatic oils	± 8	± 8

¹ Rubber content: truck ± 30 % natural rubber.

² Sulfur, stearic acid, zinc oxide.

The recycling process consists of different stages: grinding, separation (steel, textile), granulation, and classification. There are different grinding conditions such as, ambient, and wet ambient grinding, where the temperature may rise up to 130 °C during milling, and under cryogenic conditions, where the temperature is below its glass transition temperature (T_g).[7] The process choice is based on the final product requirements, such as, particle size and particle size distribution, morphology of the particles, and purity of the GTR.[8] A schematic representation of GTR is shown in Figure 2.5.

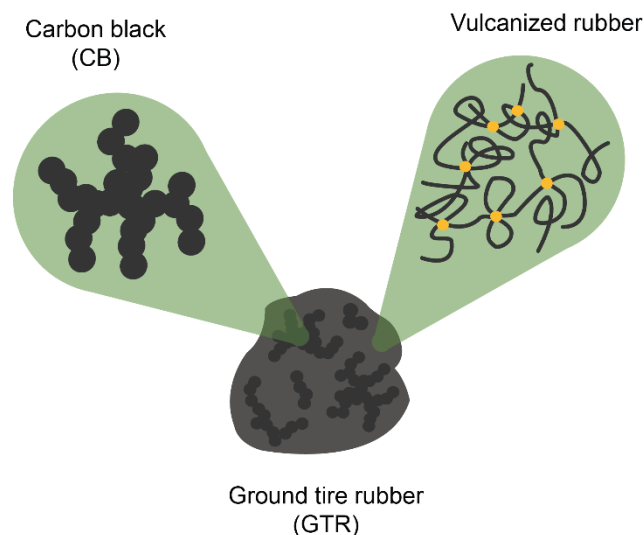


Figure 2.5 Schematic representation of GTR.

GTR obtained by ambient grinding (a blend of truck and passenger car tires), was kindly supplied by Signus Ecovalor. The average particle size of the as-received GTR was 1000 μm . More detailed information about the characterization of GTR will be given in Chapter 4.

2.2. Preparation of SBR composites

The SBR composites were prepared following three stages: formulation, mixing, and vulcanization.

2.2.1. Formulation

The formulations used will be specified in the corresponding chapters. Ingredients are always expressed in "phr", parts per hundred parts of rubber.

2.2.2. Mixing

Rubber composites were mixed in an open two-roll mill (MGN-300S, Comerio Ercole) shown in the Figure 2.6, with cylinders of 15 cm in diameter and 30 cm in length, using a rotor speed ratio of 1:1.5 at room temperature. The cylinders were kept cold, using a water refrigeration system, during the mixing process in order to avoid any pre-vulcanization of the rubber composite. The mixing time was kept constant for all compounds (≈ 20 min). The ingredients were sequentially added in this order: i) rubber, ii) activators, iii) accelerant, iv) filler and v) cross-linking agent.



Figure 2.6 Two-roll mill (MGN-300S Comerio Ercole).

In the case of composites with a coupling agent (TESPT), they were prepared in an internal mixer (Haake™ Rheomix 600, Thermo Fisher Scientific) shown in the Figure 2.7 with a fill factor of 0.7, using a Banbury rotors geometry, a rotor speed of 50 rpm, and an initial temperature of 100 °C. The mixing procedure is shown in Table 2.6.

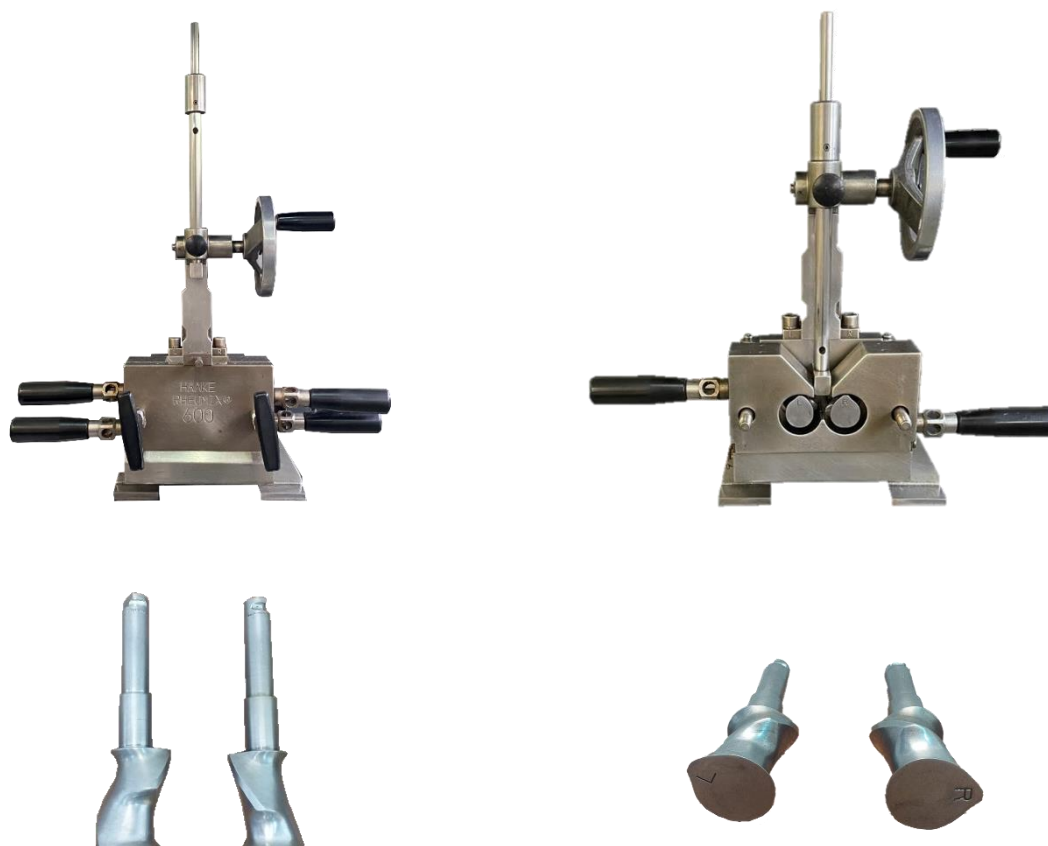


Figure 2.7 Top: Internal mixer (Haake™ Rheomix 600, Thermo Fisher Scientific). Bottom: Banbury rotors geometry.

Table 2.6 Mixing procedure of the rubber composites in an internal mixer.

Time (min)	Action
Pre-heating 100 °C at 50 rpm	
0:00	Addition of rubber, mastication
1:30	Addition of 1/3 filler, 1/2 coupling agent (TESPT)
3:00	Addition of 1/3 filler, 1/2 coupling agent (TESPT)
4:30	Addition of 1/3 filler, ZnO, and SA
6:00	Increase rotor speed to 80 rpm (increase temperature to 130 °C)
15:00	Stop mixing (reaching 140 °C)

After this initial stage, this pre-mixed material was incorporated with the rest of the ingredients (accelerant and cross-linking agent) in the open two-roll mill for further mixing of the rubber composites, following the mixing protocol previously described. After completing the mixing, the uncured compounds were stored at 6 °C in a refrigerator to avoid any premature curing.

2.2.3.Vulcanization

The vulcanization reaction was carried out in an electrically heated hydraulic press (Gumix) shown in the Figure 2.8, at 160 °C with a pressure of 20 MPa. The vulcanization time was determined for each formulation from the t_{90} values, time corresponding to the 90 % of the maximum torque (M_H), according to the curing vulcanization curves. However, in the case of curing curves with a marching trend (those where a constant plateau is not achieved), the time to reach a fixed variation of torque (ΔM) was established as curing time. Steel molds were used for the vulcanization of the rubber composites. Different standard test specimens were vulcanized for their characterization.



Figure 2.8 Left: Press (Gumix). Right: Steel molds for different standard test specimens.

2.3. Experimental techniques

2.3.1. Physico-chemical properties

Scanning electron microscopy (SEM)

The morphological analysis of SBR composites was carried out by scanning electron microscopy (SEM). The samples were cryogenically broken in liquid nitrogen and the fractured ends of the specimens were sputter-coated (Polaron, SC7640) with gold/palladium (Au/Pd) prior to observation. The samples were analyzed by means of an environmental SEM (XL30, Philips) with a tungsten filament with an acceleration voltage of 25 kV. The experimental equipment is shown in Figure 2.9.

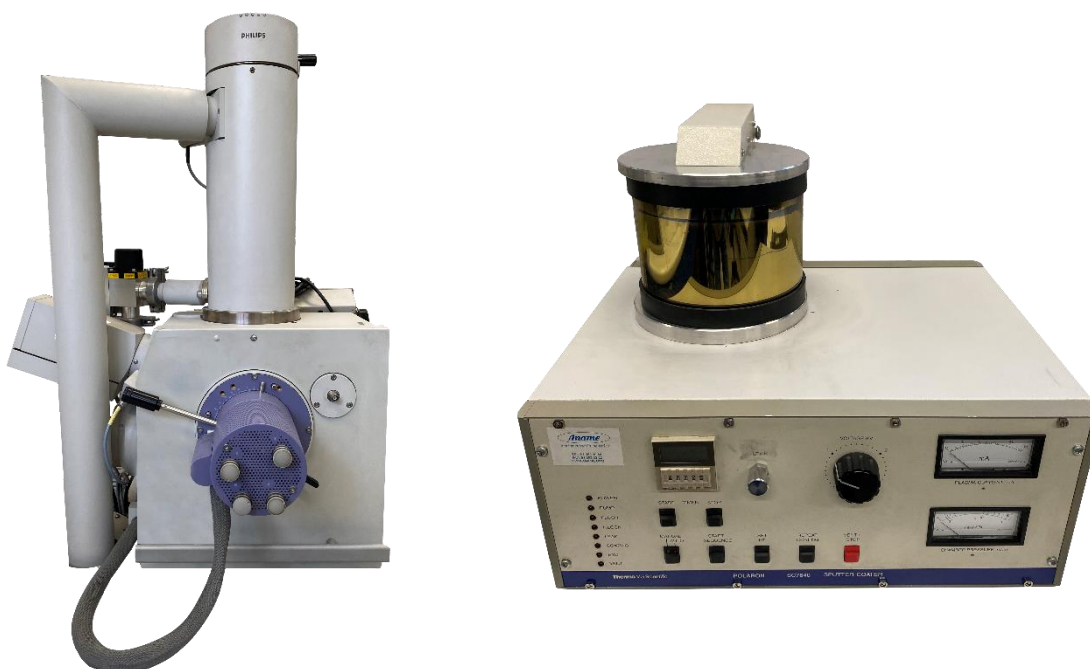


Figure 2.9 Left: Scanning electron microscopy - SEM (XL30, Philips). Right: Sputter coater (Polaron, SC7640).

Fourier-transform infrared spectroscopy (FTIR-ATR)

The infrared spectroscopy is a useful technique to study both the interaction between the polymeric matrix and the ingredients, and the formation of new components. The rubber composites were studied by infrared spectroscopy (PerkinElmer spectrometer UATR Two) shown in the Figure 2.10, from 400 to 4000 cm^{-1} with a resolution of 4 cm^{-1} co-adding 4 scans per spectrum in the ATR mode.



Figure 2.10 FTIR-ATR PerkinElmer spectrometer UATR Two

Differential scanning calorimetry (DSC)

Differential scanning calorimetry DSC 214 Polyma (Netzsch) show in the Figure 2.11, was performed at a scan rate of 10 °C/min in the temperature range from -90 to 160 °C, following a heating/cooling/heating cycle in nitrogen atmosphere. The mid-point of the transition was taken as the value of T_g . The accuracy of the determination was ± 1 °C in each case.



Figure 2.11 DSC 214 Polyma (Netzsch).

Thermogravimetric analysis (TGA)

Thermogravimetric curves were obtained using a thermal analyzer (Mettler-Toledo TA851e). Samples of ~5 mg were heated from 25 to 600 °C under nitrogen atmosphere and in air from 600 to 900 °C with a gas flow of 90 mL/min at a heating rate of 10 °C/min.

Density

The density of GTR samples was determined by hydrostatic weighing method in accordance with the standard ISO 2781.

Rheometric properties

The vulcanization process consists of the transformation of a raw rubber from a linear polymer to a three dimensional macromolecule through the formation of physical or chemical bonds. The determination of the vulcanization parameters is essential for the preparation of appropriate rubber composites.

The vulcanization curves were obtained 24 h after mixing the rubber composites, using a Rubber Process Analyzer (RPA 2000, Alpha Technologies), shown in Figure 2.12, at a frequency of 1.667 Hz, 6.98 % strain and at a vulcanization temperature of 160 °C. Around 5 g of uncured rubber sample were placed into the rheometer chamber. The accuracy of the measurement is ± 3 %.

This equipment records the evolution in the elastic (S') and viscous (S'') components of the torque (S^*) over the time. When the compound vulcanizes, there is an increase in viscosity, which is reflected in an increase in torque. The evolution of S' with time represents the vulcanization curve, and it is directly related to the evolution cross-links formation. Table 2.7 shows the main parameters obtained from a vulcanization curve.



Figure 2.12 Rubber Process Analyzer (RPA 2000, Alpha Technologies).

Table 2.7 Parameters obtained from a typical vulcanization curve.

Parameter	Description
Minimum torque (M_L)	Indicator of the viscosity of the uncured composite.
Maximum torque, (M_H)	Measures the degree of vulcanization (related to the modulus and hardness of the material).
Induction time (t_0)	Time when the torque begins to increase.
Scorch time (t_{s2})	Time necessary for the torque value to rise two units above the minimum.
Optimal vulcanization time (t_{90})	Time at which the torque value reaches 90 % of the maximum.
Torque variation ($\Delta M = M_H - M_L$)	Related to the cross-link density of the rubber.

The vulcanization reaction can take place following three different behaviors. Firstly, if S' achieves a maximum value and it stays constant at a plateau over time, the vulcanization properties are maintained. Secondly, if S' continues to increase (marching modulus), the vulcanization reaction has not reached the equilibrium. And, if S' decreases (reversion), it indicates that some degradation of the material occurs and the compound loses its properties and performance. Figure 2.13 represents the typical vulcanization curves.[9]

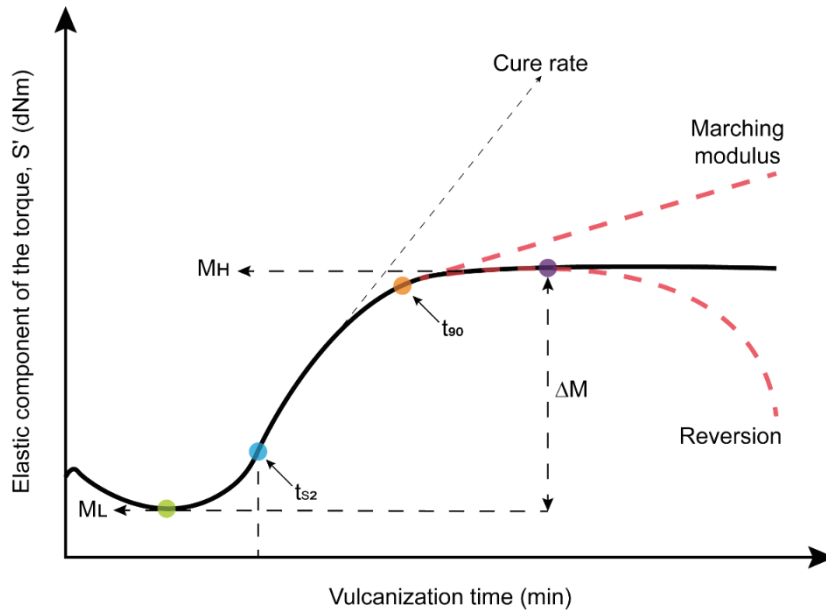


Figure 2.13 Vulcanization curves.[9]

Cross-link density

Cross-link density was determined from the measurements of solvent-swelling in toluene, applying the Flory-Rehner equation[10] and assuming the formation of tetra-functional cross-links during the vulcanization reaction. For each rubber composite, five samples were cut from rubber sheets of approximately 2 mm thickness and were weighed and immersed in toluene at ambient temperature for a period of 72 h. After this time, the samples were blotted with filter paper to remove the excess of solvent and immediately weighed. Finally, the test samples were dried in an oven for 24 h at 60 °C. The cross-link density was calculated according to the following equations:

$$v \left(\frac{\text{mol}}{\text{cm}^3} \right) = \frac{\rho_r}{2Mc} = - \frac{\ln(1 - V_r) + V_r + \chi V^2}{2V_s \left(V_r^{\frac{1}{3}} - \frac{V_r}{2} \right)} \quad (2.1)$$

where Mc is the average molecular weight of the rubber between the cross-links, V_r is the volume fraction of the equilibrium swollen rubber, χ is the Flory-Huggins polymer–solvent interaction parameter, ρ_r is the density of rubber (g/cm^3), and V_s is the molar volume of the solvent used ($106.27 \text{ cm}^3/\text{mol}$ for toluene). The V_f was determined from Equation (2.2).

$$V_r = \frac{\frac{w_d}{\rho_r} - V_f}{\frac{w_d}{\rho_r} - V_f + \frac{w_s - w_d}{\rho_s}} \quad (2.2)$$

where w_d is the weight of the dried sample after evaporation of the solvent, w_s is the swollen weight of the sample, ρ_s is the solvent density (0.867 g/cm³ for toluene), and V_f is the volume fraction of insoluble materials in the rubber composite recipe, determined with Equation (2.3)

$$V_f = f \frac{w_i}{\rho_r} \quad (2.3)$$

where w_i is the initial weight of the sample before swelling and f is the fraction of insoluble materials of the composite recipe, determined from Equation (2.4)

$$f = \frac{w_{ins}}{w_r} \quad (2.4)$$

where w_{ins} is the weight of insoluble materials in the composite and w_r is the total weight of the composite recipe. In this research, ZnO, CB, Silica and GTR were considered as the insoluble fraction in all composites.

Resilience

When a rubber is deformed, an energy input is involved; part of which is returned when the rubber recovers its original shape. The part of the energy that is not returned as mechanical energy is dissipated as heat. The resilience is the ratio between the energy restored, and the total energy applied after a moving mass impacts a rubber specimen. The resilience value is the percentage of energy that the sample is capable of returning. The resilience test has been determined on a rebound pendulum device (Gibitre Instruments, Rebound Check-Resilience) shown in Figure 2.14, at room temperature according to ISO 4662. A minimum of five measurements per specimen were carried out for each composite. The result is expressed as the mean value of the measurements.

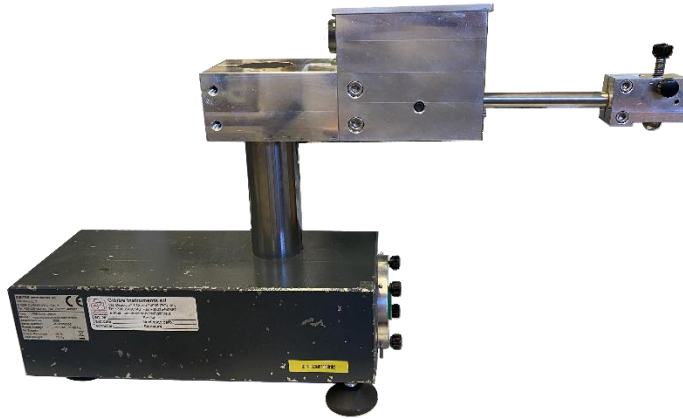


Figure 2.14 Rebound pendulum device (Gibitre Instruments, Rebound Check-Resilience).

Hardness

The hardness is a measure of the resistance a material has to indentation, and depends on the modulus of elasticity and the viscoelastic properties of the studied material. This test is one of the most frequently measured properties in rubbers. The hardness of the rubber samples has been determined using the Shore A method using the durometer (Bareiss, Neurtek) shown in Figure 2.15. The hardness value is determined by the penetration of the durometer indenter foot into the rubber sample with an indentation time of 15 seconds, at room temperature, according to ISO 7619-1. The measurements were made in three different test pieces for each rubber composite. The results are expressed as the mean value of the measurements made.



Figure 2.15 Shore A durometer (Bareiss, Neurtek).

2.3.2. Mechanical properties

Tensile measurements

The tensile stress value is a measure of the stiffness of a rubber sample and one of the most important measures for the evaluation of vulcanizates. Uniaxial tensile strain tests were performed on type 3 dumbbell-shaped samples with a thickness of 2.0 ± 0.2 mm and a width in the narrow section of 4.0 ± 0.2 mm. Tests were performed on a universal mechanical testing machine (Instron 3366) shown in Figure 2.16, equipped with a 1 kN load cell. Samples were stretched until failure at a constant strain rate of 200 mm/min at room temperature according to the UNE-ISO 37. Five specimens are tested for each sample. During the test, the applied load and the resulting elongation were recorded continuously and simultaneously. Figure 2.17 shows a representative stress-strain curve for rubber composites. From these curves, parameters such as the tensile strength, σ_b (stress at break), the elongation at break, ε_b , and the modulus M_x (stress at any given strain) can be determined.



Figure 2.16 Universal mechanical testing machine (Instron 3366).

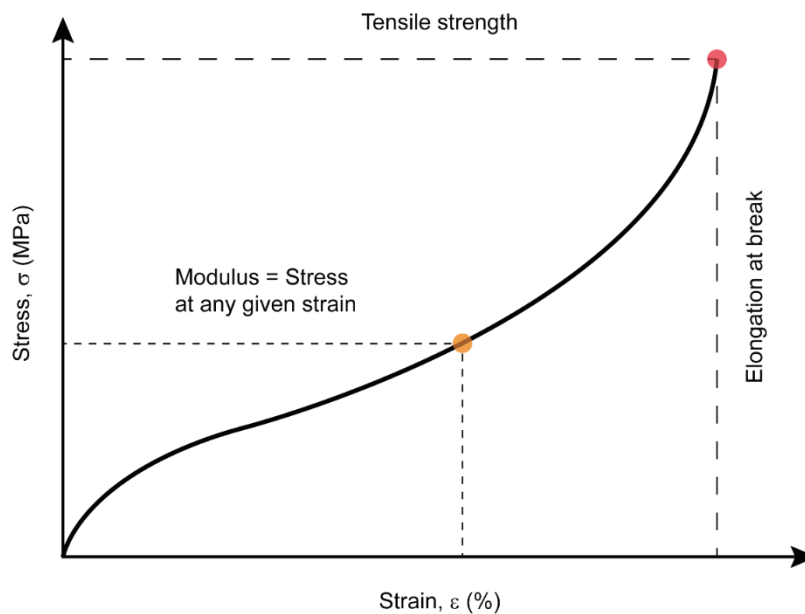


Figure 2.17 Typical tensile-strain curve for rubber composites.

Cyclic deformation testing

Rubber composites were subjected to a cyclic deformation protocol. Tests were done on a universal mechanical testing machine (Instron3366, Grand Rapids) equipped with a 1 kN load cell at room temperature. Type 3 dumbbell-shaped samples with a thickness of 2.0 ± 0.2 mm and a width in the narrow section of 4.0 ± 0.2 mm, and films (50 mm \times 25 mm \times 0.3 mm) were tested during 20 stretching cycles at a speed of 200 mm/min up to 400 % of deformation of each compound.

2.3.3. Dynamic properties

Dynamic-mechanical analysis (DMA)

Dynamic-mechanical analysis measurements of vulcanized samples were carried out in a DMA Q800 device (TA Instruments) shown in Figure 2.18. Dumbbell geometry specimens with 2 mm of thickness were tested in tensile mode at a static preload force of 0.01 N, with a superimposed sinusoidal of 0.5 % strain. The spectra were taken in a temperature range of -100 to 160 °C at a frequency of 1 Hz and “force track” (the ratio of static to dynamic forces) of 125 %. The temperature ramp was 2 °C/min. The accuracy of the measurement is ± 1 %.

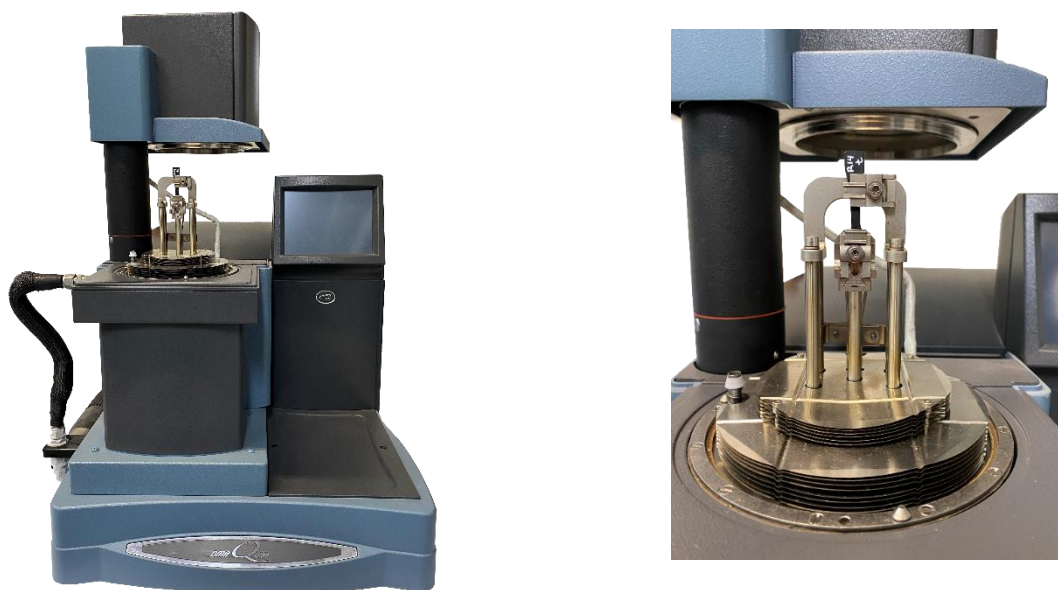


Figure 2.18 DMA Q800 (TA Instruments).

Broadband dielectric spectroscopy (BDS)

Dielectric spectroscopy measurements were carried out on a high-resolution dielectric analyzer ALPHA (Novocontrol Technologies GmbH) shown in Figure 2.19. The film samples with a thickness of 0.30 ± 0.01 mm, were placed in the dielectric cell between two 30 mm diameter parallel gold-coated electrodes. Frequency sweeps between 10^{-1} and 10^6 Hz were performed from -80 to 150 °C with a step of 10 °C.



Figure 2.19 High-resolution dielectric analyzer ALPHA (Novocontrol Technologies GmbH)

2.3.4. Self-healing properties

Self-healing is the ability that materials have to recover or restore their initial properties after being exposed to a damage. This recovery, known as healing efficiency (η), can be calculated as the ratio of certain property (P) in the pristine and healed state, according to equation 2.12.

$$\eta (\%) = \frac{P_{healed}}{P_{pristine}} \times 100 \quad (2.5)$$

Macroscopic damage

In order to evaluate a macroscopic damage (fracture), samples were cut in two with a blade. Then, they were carefully repositioned together by hand, and placed inside a home-built healing device shown in Figure 2.20, to guarantee full contact without subjecting the sample to pressure. The device consists of an endless screw and the size of the sample determines the minimum position necessary to maintain contact. The samples were kept for 30 min at room temperature. After this step, a healing protocol, consisting of different healing times and temperatures, was applied to the rubber composites. Healed samples were re-tested following the uniaxial tensile test conditions described in section 2.3.2. The healing efficiency (η) was calculated as a measure of the recovery of tensile properties. A schematic representation of macroscopic damage is shown in Figure 2.21

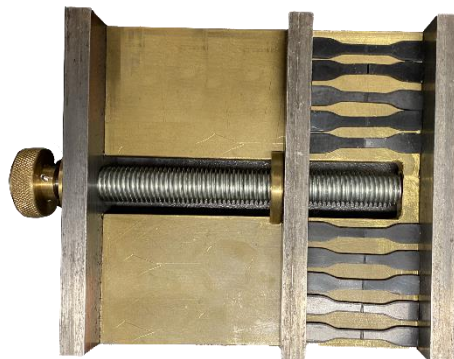


Figure 2.20 Home-built healing device.

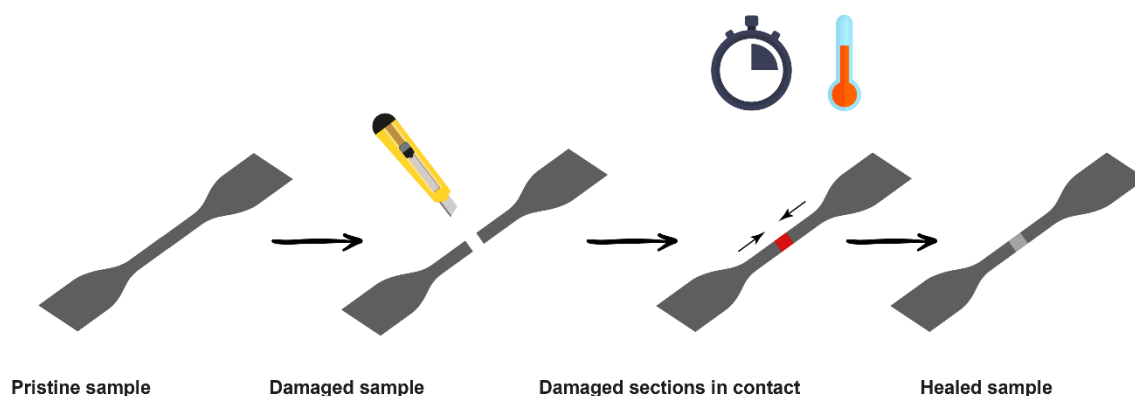


Figure 2.21 Schematic representation of macroscopic damage.

X-ray photoelectron spectroscopy (XPS)

X-ray photoelectron measurements were performed on the surfaces of as-received GTR, cryo-ground GTR (GTR Cryo), and modified GTR (m-GTR) using a spectrometer (MT500, Fisons Instruments) equipped with a hemispherical electron analyzer (CLAM 2) and a Mg Ka X-ray source (1253.6 eV) operated at 300 W. Binding energies were corrected to the carbon 1s peak located at 285 eV.

Data analysis was performed with XPS 4.1 peak software. A Shirley background function was employed to correct the background of the spectra. The full width at half-maximum (FWHM) of each peak was maintained between 1.2 and 1.5 eV. The spectrum fitting was performed using a Gaussian (80 %) – Lorentzian (20 %) peak shape by minimizing the total square-error fit. Atomic ratios (at %) were calculated from experimental intensity ratios and normalized by atomic sensitivity factors (carbon 0.25, oxygen 0.66, silica 0.27, sulfur 0.54, zinc 4.8, and nitrogen 0.42).

The C 1s spectra is deconvoluted into several peaks: C=C sp² with binding energy at 284.5 ± 0.1 eV, C–C sp³ at 285.0 ± 0.1 eV, C–OH at 286 ± 0.1 eV, HO–C=O at 289.0 ± 0.1 eV. The O 1s spectra is deconvoluted into: O=C at 531.2 ± 0.3 , O–C at 532.5 ± 0.2 , and the S 2p spectra is deconvoluted into: S–C 2p_{3/2} at 162.3 ± 0.1 , S–S 2p_{1/2} at 164.0 ± 0.1 , S–O at 165.7 ± 0.1 , and sulfate at 169.2 ± 0.2 eV.

Energy dispersive X-ray spectroscopy (EDS)

GTR samples were analyzed by means of a high-resolution scanning electron microscope FE-SEM (SU8000, Hitachi) with a tungsten filament with an acceleration voltage of 15 kV, and with an EDS detector (XFlash 5030). The samples were sputter-

coated (Quorum Tech, Q 150T ES) with chromium (Cr) prior to observation. The experimental equipment is shown in Figure 2.22.

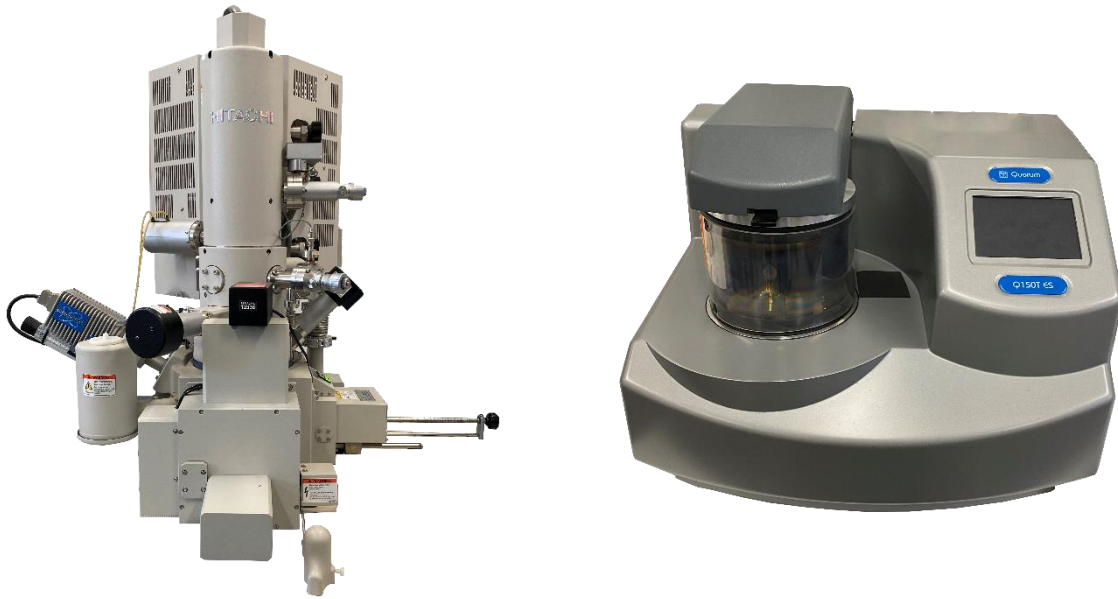


Figure 2.22 Left: High-resolution scanning electron microscope FE-SEM (SU8000, Hitachi). Right: Sputter coater (Quorum Tech, Q 150T ES).

2.4. References

1. Long, J.M., *Commercial Elastomers*, in *The Vanderbilt Rubber Handbook*, M.F. Sheridan, Editor. 2010, R. T. Vanderbilt Company, Inc. p. 67 - 84.
2. Studebaker, M.L., *The Chemistry of Carbon Black and Reinforcement*. Rubber Chem. Technol., 1957. **30**(5): p. 1400-1483.
3. Wampler, W.A., T.F. Carlson, and W.R. Jones, *Carbon black*, in *Rubber Compounding: Chemistry and Applications*. 2004.
4. Byers, J.T. and A.A. McNeish, *Compounding Materials and Uses*, in *The Vanderbilt Rubber Handbook*, M.F. Sheridan, Editor. 2010, R. T. Vanderbilt Company, Inc. p. 492 - 524.
5. Anke, B., et al., *Silica and Silanes*, in *Rubber Compounding: Chemistry and Applications*. 2004. p. 251 - 332.
6. Shulman, V.L., *Tire Recycling*. Waste, 2019: p. 489-515.
7. Forrest, M.J., *Production of Rubber Crumb*, in *Recycling and Re-Use of Waste Rubber*. 2014, Smithers Rapra Technology Ltd. p. 135 - 182.
8. Karger-Kocsis, J., L. Mészáros, and T. Bárány, *Ground tyre rubber (GTR) in thermoplastics, thermosets, and rubbers*. Journal of Materials Science, 2013. **48**(1): p. 1-38.
9. Forrest, M.J., *Analytical Techniques*, in *Rubber Analysis: Characterisation, Failure Diagnosis and Reverse Engineering*. , M.J. Forrest, Editor. 2018, Smithers Rapra.
10. Flory, P.J. and J.R. Jr., *Statistical Mechanics of Cross-Linked Polymer Networks II. Swelling*. The Journal of Chemical Physics, 1943. **11**(11): p. 521-526.
11. Menar, K.P., *Dynamic Mechanical Analysis: A practical introduction*. 2008: CRC Press.
12. Wang, M.-J., *Effect of Polymer-Filler and Filler-Filler Interactions on Dynamic Properties of Filled Vulcanizates*. Rubber Chem. Technol., 1998. **71**(3): p. 520-589.
13. Deshmukh, K., et al., *Dielectric Spectroscopy*, in *Spectroscopic Methods for Nanomaterials Characterization*, S. Thomas, et al., Editors. 2017, Elsevier Inc. p. 237 - 299.

3

“R” AS REPAIR HEALING OF SBR COMPOUNDS

Part of the work described in this chapter has been published in European Polymer Journal. 2018, 106(9), 273-283.

3. “R” as Repair - Healing of SBR Compounds

SBR is a synthetic rubber derived from styrene and butadiene monomers, where the styrene units (between 10 to 25 %) contribute to wearing and bonding characteristics. SBR forms a random copolymer in which the ratio between styrene and butadiene influences the properties of the rubber. The higher this styrene/butadiene ratio is, the harder the polymer is. High styrene content SBR is characterized by excellent abrasion resistance, impact strength, good resilience and high tensile strength, which, together with its good processability, makes it a rubber of choice for the tire industry, which consumes 70 – 80 % of its production.

The dynamic character of disulfides ($-S-S-$), which are naturally present in sulfur vulcanized rubbers, has been proposed as a strategy to develop tailor-made self-healing systems.[1] Disulfides can be reversibly cleaved and formed under thermodynamic control, so the exchange reactions can lead to a renewal of cross-links across damaged surfaces.[2] This approach has successfully been implemented in Natural Rubber (NR), Butadiene Rubber, Chloroprene, Polydimethylsiloxane and Polyurethanes.[3] However, there were no studies on the self-healing ability of SBR compounds reported until now. Since SBR is commonly vulcanized with sulfur, this approach has the potential to produce a self-healing system. Therefore, a detailed description on how the chemical constituents of an SBR formulation affect the healing properties of the vulcanizate is required.

Chapter 3 details the validation of self-healing concepts, quantifying healing efficiency in vulcanized SBR compounds. Different sulfur-based (efficient – EV, semi-efficient – SEV, and conventional – CV), and peroxide-based vulcanization systems, as well as different vulcanizing additives, were studied in order to correlate each system with the mechanical and healing performance of the SBR compounds. Healing conditions (temperature and time) were also varied and optimized to achieve different degrees of healing. A schematic representation on the content of Chapter 3 is shown in Figure 3.1.

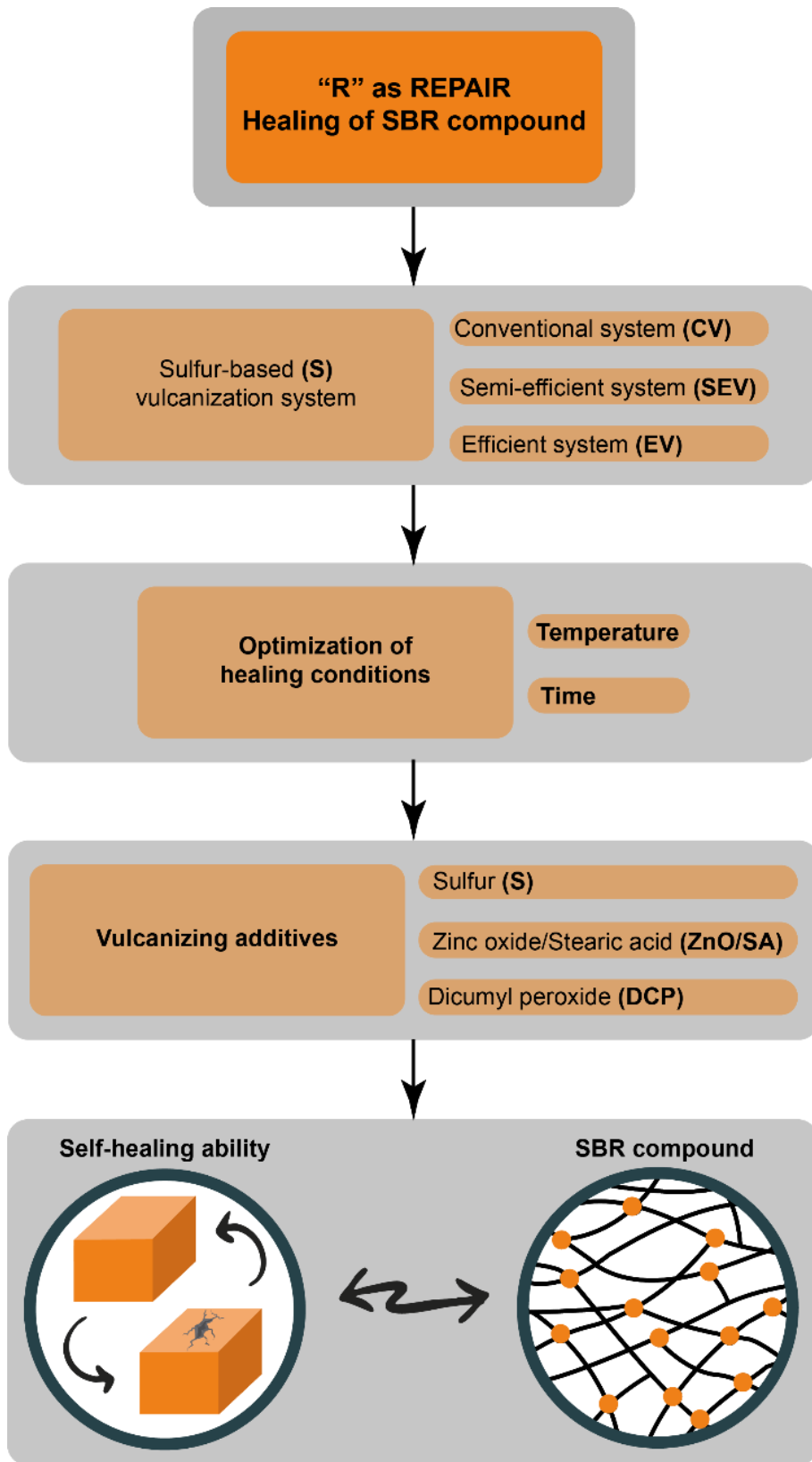


Figure 3.1 Schematic representation of Chapter 3. “R” as Repair – Healing of SBR compounds.

3.1. Effect of the vulcanization system

The most common vulcanization systems for curing polydiene rubbers are based on accelerated sulfur formulations. Depending on the accelerant/sulfur (A/S) ratio, the network of accelerated sulfur vulcanizates is composed of diverse types of cross-links between the elastomeric chains, such as mono-, di-, and poly-sulfides (i.e. more than two sulfur atoms in the cross-link) bonds, among others.[4] Figure 3.2 shows a schematic representation of the typical chemical groups present in a sulfur-vulcanized rubber network.

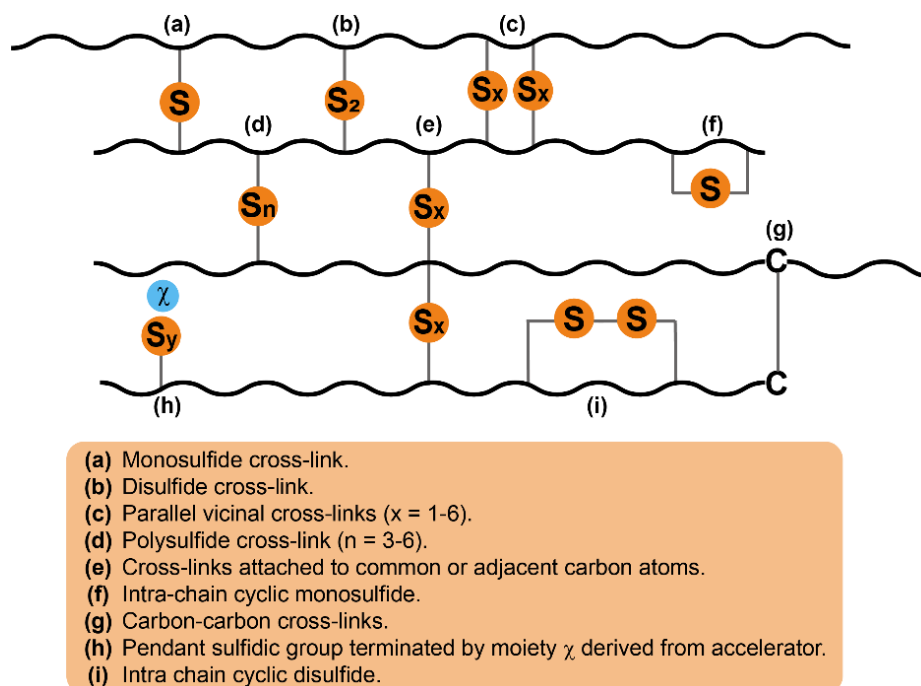


Figure 3.2 A schematic representation of typical chemical groups present in a sulfur-vulcanized rubber network.[5]

Accelerated sulfur vulcanizations are classified as efficient (EV), conventional (CV), and semi-efficient (SEV). The EV system predominantly contains monosulfide ($-C-S-C-$) or disulfide ($-C-S-S-C-$) cross-links, which are obtained using a low level of sulfur and a high level of accelerant. EV systems generate shorter cross-links that enhance the thermal and oxidative resistance of the final compounds, due to their improved thermal stability. Meanwhile, CV systems are composed of a high proportion of highly flexible polysulfide cross-links ($-C-S_x-C-$), obtained when employing low A/S ratios (i.e. higher amount of sulfur than accelerant). The SEV systems are intermediate between the EV

and the CV, composed of nearly equal amounts of sulfur and accelerant. The bonds present in SEV systems are mono-sulfide, as well as di- and poly-sulfides.

In general, the cross-link type (and consequently the A/S ratio) and the degree of cross-link density of a rubber vulcanizate determine its physical properties; by increasing the cross-link density, tensile strength increases, whereas elongation at break decreases.[6] Furthermore, networks containing high proportions of polysulfide cross-links show different mechanical properties than those containing –C–C– or monosulfide cross-links, since the highly flexible and labile –S–S– cross-links are capable of withstanding high stresses. The poly-sulfide cross-links have the ability to reorganize under the influence of external stress and dissipate them without reducing the number of cross-links.[7]

In this research, rubber compounds were prepared according to the compositions shown in Table 3.1 varying the A/S ratio and evaluating its influence on their self-healing capability. The proportion of ZnO, SA, and S was kept constant in all the compositions. Samples are named as CV_x (conventional), SEV_x (semi-efficient) or EV_x (efficient), where “x” corresponds to the proportion of S added. The healing protocol applied was 70 °C for 12 h.

Table 3.1. SBR recipes in phr (parts per hundred parts of rubber), varying A/S ratio content.

Compound	Ingredient (phr)					
	SBR 1502	ZnO	SA	CBS	S	A/S
CV ₁	100	5	1	0.1	1	0.1
SEV ₁	100	5	1	1	1	1
EV ₁	100	5	1	10	1	10

An indirect approach for assessing the vulcanization level is through the rheometer curves. Figure 3.3 shows the curing curves of the SBR compounds at various A/S ratios cured at 160 °C. The changes in torque indicate the different states of vulcanization, where a higher torque is directly related to a higher level of cross-links.

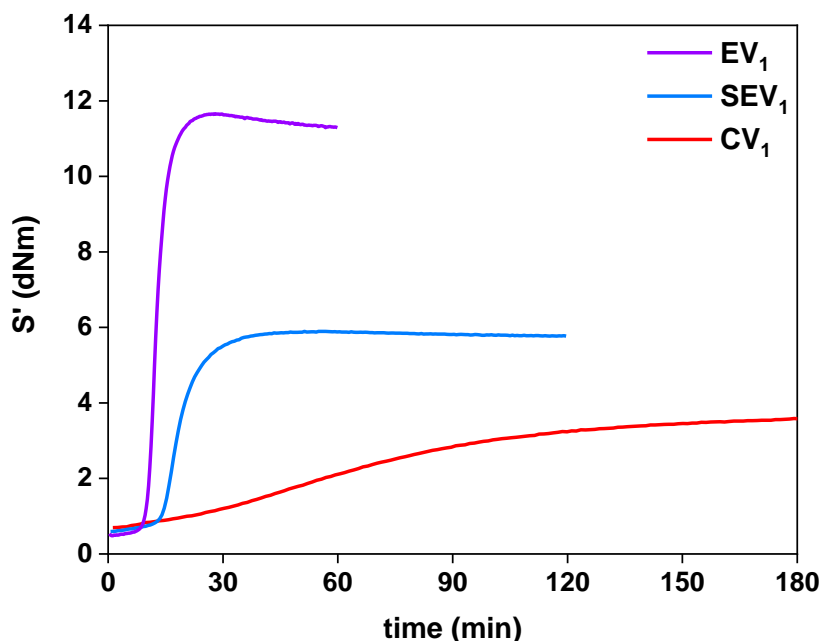


Figure 3.3 Rheometric curves of SBR compounds with different A/S ratios.

The most relevant parameters obtained from the curing curves, such as scorch time (t_{s2}), optimum cure time (t_{90}), minimum torque (M_L), maximum torque (M_H), extent of cure ($\Delta M = M_H - M_L$), are summarized in Table 3.2 and show the well-known fact that an increase of the A/S ratio reduces the length of the sulfur bridges and increases the number of cross-links, as evidenced by the significant increase in ΔM . [8, 9] Table 3.2 also compiles the calculated values of cross-link density (ν) based on swelling tests, and mechanical properties for the different compounds, showing good agreement with the trend shown by the curing parameters. The moduli M_{50} , M_{100} , M_{300} , and M_{500} values correspond to the tensile stress at 50 %, 100 %, 300 %, and 500 % strain, respectively, while σ_b and ϵ_b values correspond to tensile strength and elongation at break. The notorious increase in cross-link density for EV₁ can be ascribed to the higher amount of accelerant. Sulphenamide type accelerants (like CBS), due to the homolytic splitting at the early stages of vulcanization, are able to form two free rubber radicals that can react with sulfur, thus forming cross-links. In this way, such system, once it has split up, has a self-accelerating or auto-catalytic effect. [9] The higher overall cross-link density is the dominating factor for the strength properties, stronger than the well-known ability of the long, polysulfide cross-links to rearrange followed by stress dissipation, and increased tensile strength. [10]

Table 3.2 Physico-mechanical properties of sulfur based SBR compounds.

	Compound		
	CV ₁	SEV ₁	EV ₁
T _g (°C) by DSC	-54 ± 1	-55 ± 1	-51 ± 1
Curing parameters			
M _L (dNm)	0.7	0.7	0.5
M _H (dNm)	3.7	5.8	11.7
ΔM (dNm)	3	5.1	11
t _{s2} (min)	82	17	11
t ₉₀ (min)	143	27	17
Mechanical properties			
M ₅₀ (MPa)	0.40 ± 0.02	0.51 ± 0.01	0.76 ± 0.01
M ₁₀₀ (MPa)	0.48 ± 0.02	0.67 ± 0.02	1.13 ± 0.01
M ₃₀₀ (MPa)	0.57 ± 0.02	0.99 ± 0.01	-
M ₅₀₀ (MPa)	0.67 ± 0.02	1.36 ± 0.03	-
σ _b (MPa)	1.2 ± 0.2	1.6 ± 0.2	1.68 ± 0.04
ε _b (%)	885 ± 119	661 ± 18	198 ± 8
ν × 10 ⁻⁵ (mol/g)	0.55 ± 0.01	2.27 ± 0.03	7.30 ± 0.09

Healed samples are considered specimens in which the restoration of the damaged interface and, thus, mechanical integrity is partially achieved. Figure 3.4 shows the tensile strength values of pristine and healed SBR compounds and their healing efficiency with different A/S ratio. Lower mechanical performance rubber systems show higher healing capability, evidencing the compromise between mechanical properties and healing.[11] The healing efficiency increases in the order: EV₁ (A/S=10) < CV₁ (A/S=0.1) < SEV₁ (A/S=1). EV₁ is a very stable and highly sulfur cross-linked network, making the restoration of the interface less favorable under the studied healing conditions (70 °C and 12 h); while the lower cross-linked networks, the CV₁ and SEV₁ compounds, allow for a substantially higher mobility that favors rubber chain interdiffusion and the rearrangement of broken reversible bonds at the healed interface. Hernández *et al.*[11] reported similar results with a CV natural rubber. Glass transition temperature (T_g) values also support this behavior. Cross-linking increases the T_g of the rubber compound by introducing restrictions on the molecular motions of the rubber chain, as seen in Table 3.2.

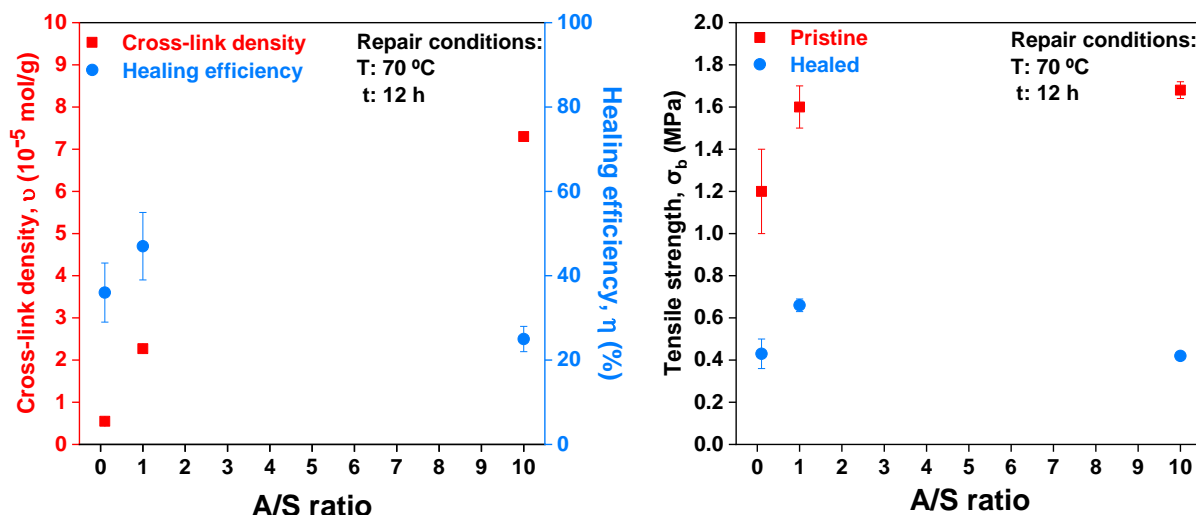


Figure 3.4. Left: Healing efficiency and cross-link density, as function of A/S ratio, Right: Tensile strength of pristine and healed samples.

Figure 3.5 shows a schematic representation of the healing mechanism. A physical damage in a cross-linked network will lead to chain cleavage and/or chain slippage with the subsequent formation of reactive groups (sulfur radicals). Short-range interactions due to entanglements between dangling chains are considered to take place during the initial stage of healing.[12] Followed by a temperature-triggered opening of the di- and poly-sulfide bonds that enable chain mobility in the system facilitating the macroscopic flow required to close the cut.[13]

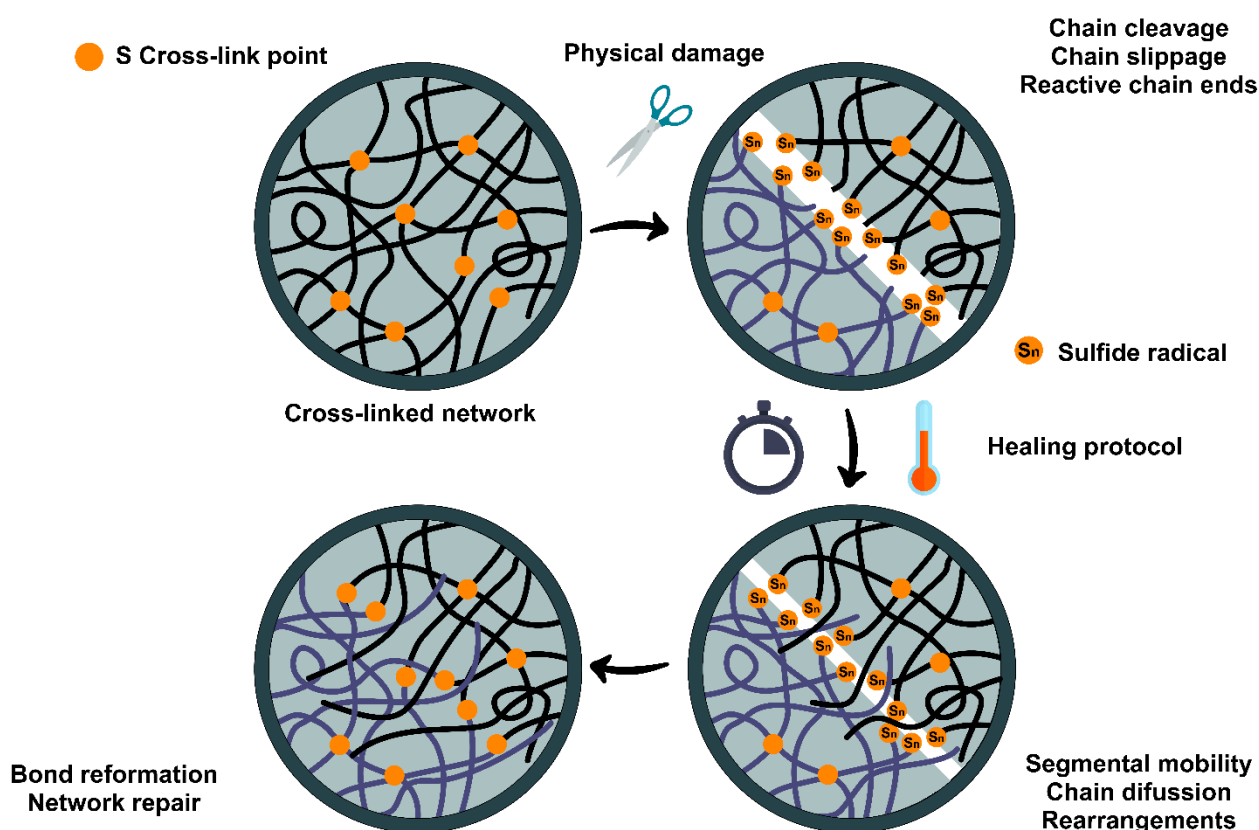


Figure 3.5 Schematic representation of healing mechanism.

The di- and poly-sulfide exchange reactions are thus regarded as the main contributors to the restoration of the mechanical strength; it is presumed that the underlying healing mechanism is determined by the temperature-driven formation of sulfur radicals that bond to each other once the energetic stimulus is removed and allow the formation of new disulfide bridge across the damaged interface.[1, 11, 14-16] It has also been reported that higher healing can be achieved by replacing di-sulfide bonds with tetra-sulfides, as the stability of the $-S-S-$ bridges decreases with increasing number of sulfur atoms beyond two.[13, 17] It would therefore be expected that the lower A/S ratio compounds (CV₁ and SEV₁) with longer length sulfur bridges lead to higher healing. Thus, a combination between lower cross-link density and lower A/S ratio seems to be the reason for the higher healing achieved by CV₁ and SEV₁.

3.2. Optimization of the self-healing protocol

The healing protocol, in terms of time and temperature, was subsequently optimized to maximize the self-healing ability of the SBR compound. Figure 3.6 shows the tensile strength and the healing efficiency as function of selected temperature and time

conditions for the SEV₁ compound. Similar trends were observed for CV₁ and EV₁. As expected, increasing time and/or temperature led to higher healing efficiency and the ultimate full recovery of tensile strength. The strength recovery depends on the formation of new molecular entanglements and the rearrangement of broken reversible bonds, which benefit from high mobility and interdiffusion of rubber molecular chains, which in turn is facilitated by long periods and/or temperatures. The selected conditions for the optimal healing protocol were 130 °C and 1 h. Even though longer times (> 1 h) improve the restoration of the mechanical properties, the selection of the optimal time was based on the possible industrial scalability with an acceptable healing efficiency value ($\approx 80\%$) and low energy consumption. Equivalent results were reported by Feng *et al.*[18] in polyurethane systems. They developed self-healing thermally reversible polyurethanes based on Diels-Alder (DA) reaction (PU-DA). They found that crack shrinkage was faster at higher temperature within a temperature range of 60 °C to 120 °C.

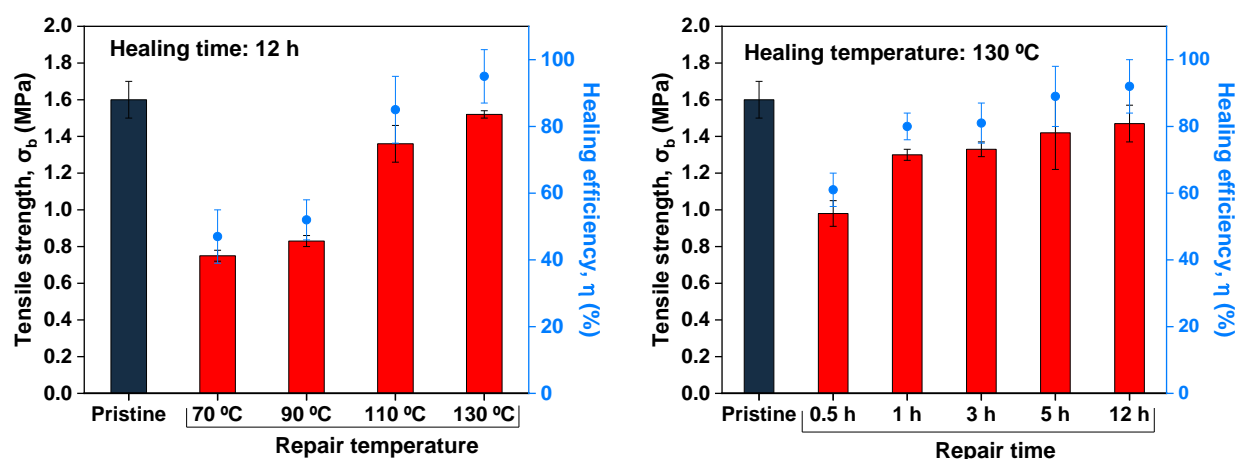


Figure 3.6 Tensile strength and healing efficiency of SBR compound (SEV₁) at different repair temperatures (left) and times (right).

The optimal healing protocol was further corroborated by monitoring the crack closure over time by scanning electron microscopy (SEM). The crack disappeared completely after 1 h of applied healing protocol as shown in Figure 3.7. The change in the surface of the sample, after applying the healing protocol, is related to the migration of zinc stearate – ZnSt₂ domains to the surface.[19]

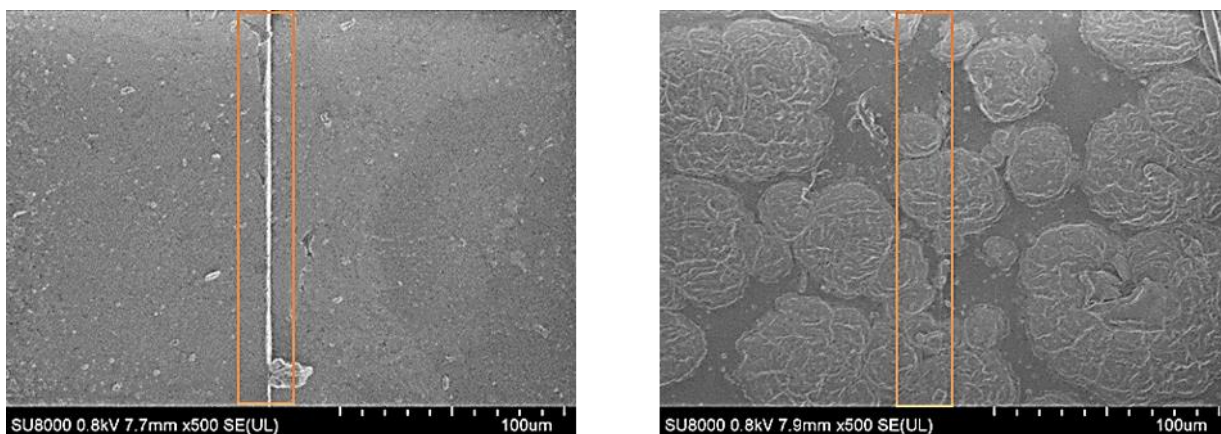


Figure 3.7 SEM micrographs of SEV1 compound before (left) and after (right) applying the optimal healing protocol

The selected healing conditions were also confirmed with a set of mechanical experiments that compared samples with and without the thermal treatment before being damaged (Figure 3.8). The tensile curves of the thermally treated CV₁ and SEV₁ compounds show a slight increase in the moduli M_{50} , M_{100} , M_{300} , and M_{500} compared to pristine samples. This increment may be due to the formation of additional cross-links leading to a change in the network structure. When temperature is applied, a slight oxidation effect can take place. It is known that in SBR compounds, oxidative ageing causes minimum main chain breaking with the subsequent formation of additional cross-links.[10]

It is also worth mentioning the similarity between the thermally treated and the healed curves of the CV₁ and SEV₁ compounds. Both tensile curves follow the same path, indicating that both systems have similar network structure. Hence, the healing efficiency should be calculated with respect to thermally treated samples instead of pristine samples. Current convention of the self-healing community typically calculates healing efficiency as the ratio between the property at the healed state and the pristine state.[20, 21] Such methodology can result in healing efficiencies exceeding 100 %, as observed in Table 3.3. CV₁ and SEV₁ fully recover the tensile stress at low strains (up to 500 % and 300 %, respectively), with unrealistic values of the healing efficiency over 100 % for those calculated based on the pristine sample (η_P). Healing efficiencies based on thermally treated samples (η_T) give scientifically sound values of 64 % (CV₁) and 80 % (SEV₁). The lower healing efficiency attained by the EV₁ compound (36 %) can be attributed to the more restricted mobility of chains due to a higher cross-linked network. Therefore, the

healing efficiency of the following sections will refer to the value calculated based on the thermally treated samples.

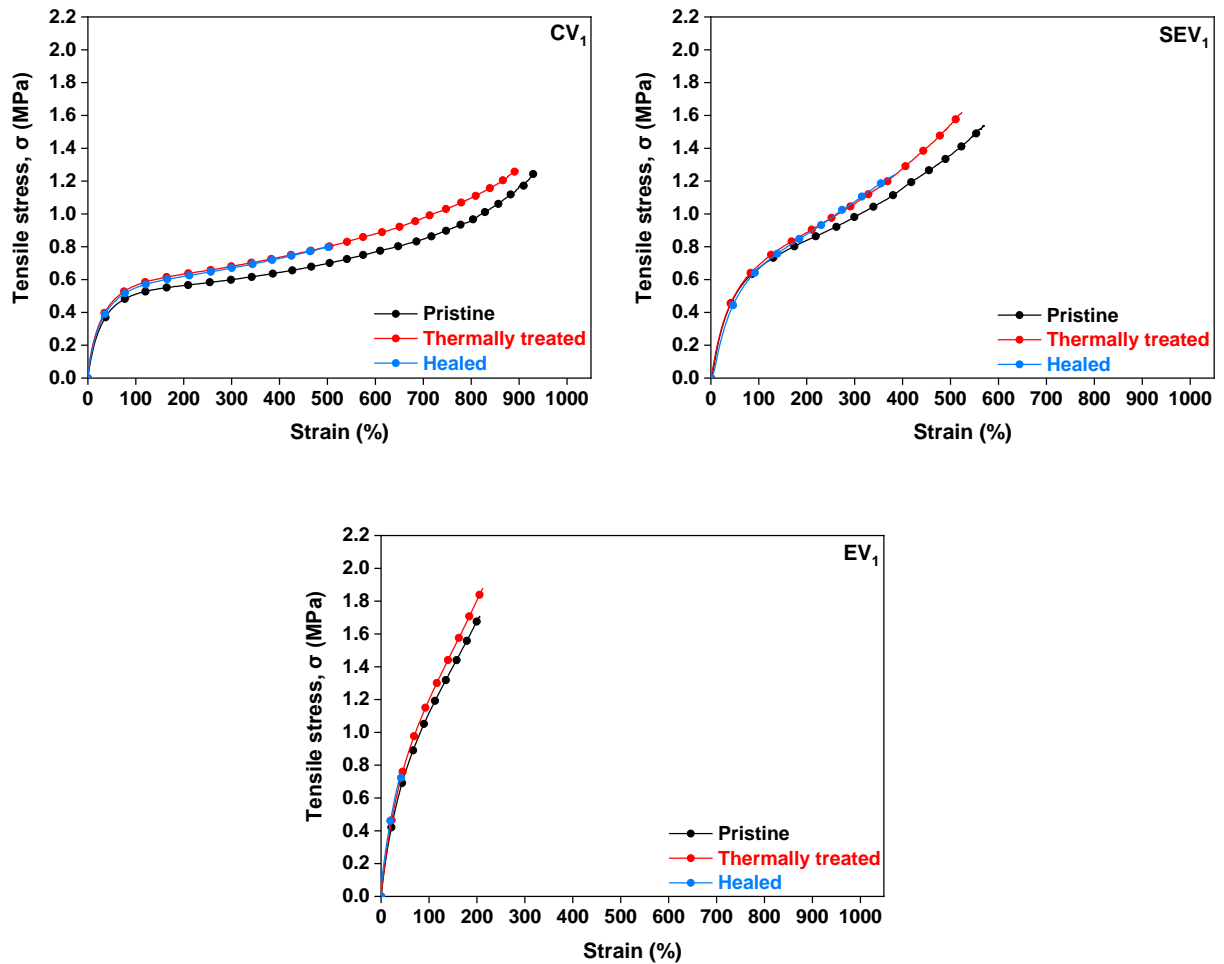


Figure 3.8 Tensile curves of pristine, thermally treated and healed samples as a function of the vulcanization system.

Table 3.3 Physico-mechanical properties and healing efficiency of sulfur based CV₁, SEV₁ and EV₁ systems.

		M ₅₀ (MPa)	M ₁₀₀ (MPa)	M ₃₀₀ (MPa)	M ₅₀₀ (MPa)	σ _b (MPa)	ε _b (%)	υ × 10 ⁻⁵ (mol/g)
CV ₁	Pristine	0.40 ± 0.02	0.48 ± 0.02	0.57 ± 0.02	0.67 ± 0.02	1.2 ± 0.2	885 ± 119	0.55 ± 0.01
	Thermally treated	0.46 ± 0.01	0.56 ± 0.01	0.68 ± 0.01	0.80 ± 0.01	1.2 ± 0.2	869 ± 62	0.54 ± 0.03
	Healed	0.45 ± 0.01	0.55 ± 0.01	0.67 ± 0.01	0.79 ± 0.01	0.8 ± 0.1	485 ± 100	0.54 ± 0.03
	η _P (%)	113 ± 1	114 ± 1	118 ± 1	118 ± 1	65 ± 6	54 ± 11	-
	η _T (%)	99 ± 1	99 ± 1	99 ± 1	99 ± 4	65 ± 6	56 ± 12	-
SEV ₁	Pristine	0.51 ± 0.01	0.67 ± 0.02	0.99 ± 0.01	1.36 ± 0.03	1.6 ± 0.2	661 ± 18	2.27 ± 0.03
	Thermally treated	0.53 ± 0.02	0.69 ± 0.03	1.1 ± 0.1	1.5 ± 0.1	1.61 ± 0.04	527 ± 14	2.48 ± 0.03
	Healed	0.53 ± 0.02	0.68 ± 0.03	1.1 ± 0.1	-	1.3 ± 0.1	290 ± 51	2.48 ± 0.03
	η _P (%)	103 ± 3	102 ± 4	109 ± 7	-	81 ± 4	44 ± 8	-
	η _T (%)	100 ± 3	99 ± 4	100 ± 5	-	80 ± 4	55 ± 10	-
EV ₁	Pristine	0.76 ± 0.01	1.13 ± 0.01	-	-	1.68 ± 0.04	198 ± 8	7.30 ± 0.09
	Thermally treated	0.81 ± 0.01	1.20 ± 0.01	-	-	1.9 ± 0.1	212 ± 15	7.77 ± 0.05
	Healed	-	-	-	-	0.7 ± 0.2	39 ± 13	7.77 ± 0.05
	η _P (%)	-	-	-	-	41 ± 10	20 ± 7	-
	η _T (%)	-	-	-	-	36 ± 18	20 ± 6	-

η_P: Healing Efficiency compared to pristine compound.

η_T: Healing efficiency compared to thermally treated compound.

A significant aspect to study is the contribution of the possible presence of remaining vulcanization system after the vulcanization process on the healing capability of the SBR compounds. To further corroborate the healing capability of SEV₁ compound due to the di- and poly-sulfide exchange reaction, the sample was immersed in toluene at ambient temperature with continuous magnetic stirring for a period of 72 h to remove any unreacted ingredient of the vulcanizing system (i.e. SA, CBS, S, and zinc stearate – ZnSt₂). [22] Figure 3.9 shows the attenuated total reflectance (ATR-FTIR) measurements before and after extraction of unreacted vulcanizing additives. The spectra show the disappearance of the signal at 1540 cm⁻¹, which corresponds to zinc stearate (ZnSt₂) resulting from the reaction of SA and ZnO, corroborating the extraction of all remaining soluble ingredients from vulcanizing system.

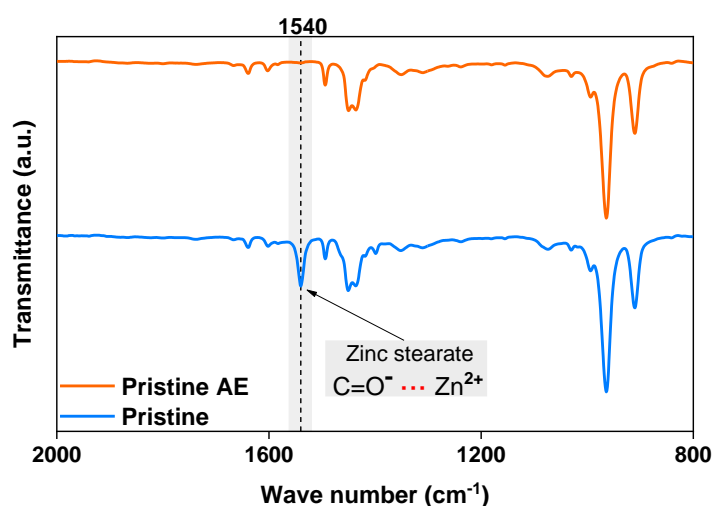


Figure 3.9 ATR-FTIR spectra of SEV₁ compound before (pristine) and after extraction (pristine AE).

After removing all the unreacted and soluble additives, the healing protocol was applied to the SEV₁ AE sample. Figure 3.10 shows the tensile stress curves and healing efficiency of SEV₁ and SEV₁ AE compounds compared to thermally treated and pristine samples. The healing efficiency shows a slight reduction of 10 % in tensile strength after the extraction process, reaching a 70 % of healing efficiency. Therefore, the healing process can be ascribed to the di- and poly-sulfide exchange reaction and not to a possible secondary vulcanization process. However, the partial decrease in ZnSt₂ content could be the reason for the reduction of the healing efficiency after extraction.

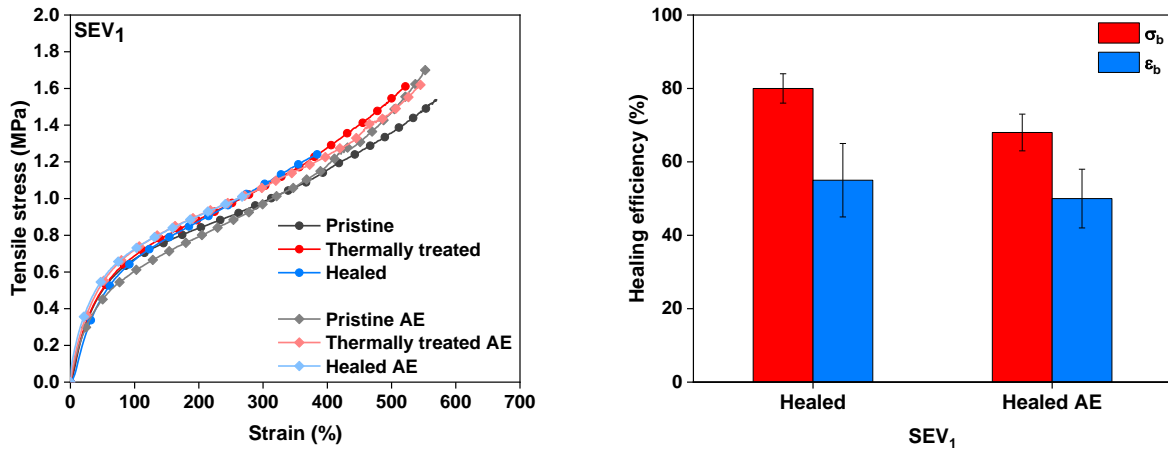


Figure 3.10 Tensile stress and healing efficiency of SEV₁ compounds before and after extraction (pristine AE).

The selected SEV₁ compound was further subjected to several damage/healing cycles in order to quantify how many times it is possible to retain high healing efficiencies. Figure 3.11 shows the tensile stress curves of the SBR samples comparing the thermally treated and 1st, 2nd and 3rd healed states, with the optimal healing protocol conditions selected (130 °C, and 1h). The damage corresponding to the first cycle is the imposed cut with a blade. In the subsequent cycles, the damage is the fracture generated after the tensile test. The similarity between the thermally treated and the healed curves for each cycle could indicate that all systems have the same network structure after the applied healing protocol cycle.

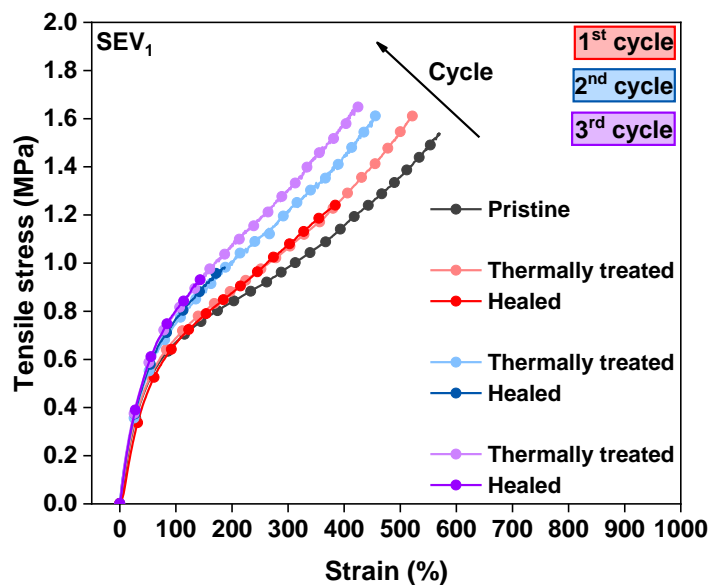


Figure 3.11 Tensile curve of SEV₁ compound at different damage/healed cycles.

The mechanical and physical properties data are listed in Table 3.4. The cross-link density and moduli at M_{50} and M_{100} slightly increase after the healing protocol cycles. Furthermore, the tensile strength and elongation at break values tend to decrease after the first damage/repair cycle. The repetitive thermal healing cycles disrupt the rubber network structure and cause a decrease in the polysulfide cross-links and an increase in monosulfide cross-links. Oxidation-induced cross-links and monosulfide cross-links impart poor strength relative to polysulfide cross-links.[23] Hence, the increment in monosulfide cross-links increases the restriction in the mobility of the rubber chains hindering the bond reformation across the damaged interface, as shown in Figure 3.12.

Table 3.4 Mechanical and physical properties at different damage/healing cycles.

	Compound					
	1 st cycle		2 nd cycle		3 rd cycle	
	Thermally treated	Healed	Thermally treated	Healed	Thermally treated	Healed
M ₅₀ (MPa)	0.53 ± 0.02	0.53 ± 0.02	0.56 ± 0.01	0.55 ± 0.02	0.59 ± 0.02	0.59 ± 0.01
M ₁₀₀ (MPa)	0.69 ± 0.03	0.68 ± 0.03	0.77 ± 0.01	0.78 ± 0.01	0.77 ± 0.03	0.81 ± 0.01
M ₃₀₀ (MPa)	1.1 ± 0.1	1.1 ± 0.1	1.22 ± 0.02	-	1.26 ± 0.03	-
M ₅₀₀ (MPa)	1.5 ± 0.1	-	-	-	-	-
σ _b (MPa)	1.61 ± 0.04	1.3 ± 0.1	1.6 ± 0.1	0.9 ± 0.1	1.6 ± 0.1	0.9 ± 0.1
ε _b (%)	527 ± 14	290 ± 51	445 ± 59	155 ± 23	424 ± 19	136 ± 8
ν × 10 ⁻⁵ (mol/g)	2.48 ± 0.03	2.48 ± 0.03	2.7 ± 0.1	2.7 ± 0.1	2.9 ± 0.1	2.9 ± 0.1

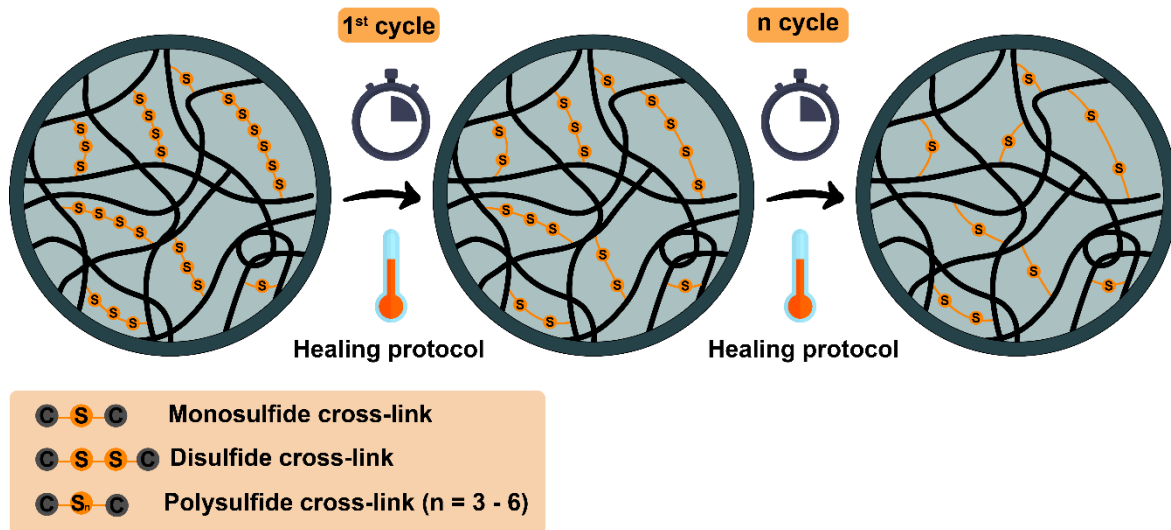


Figure 3.12 Schematic representation of the evolution of polysulfide cross-links after multiple healing cycles.

The variation on the healing efficiency respect to tensile strength and elongation at break after each damaging event is shown in Figure 3.13. This mobility restriction affects the healing capability, although the SEV₁ compound exhibits repeatable healing capability after multiples cycles, resulting an acceptable recovery of tensile strength after 3 cycles of 60 %.

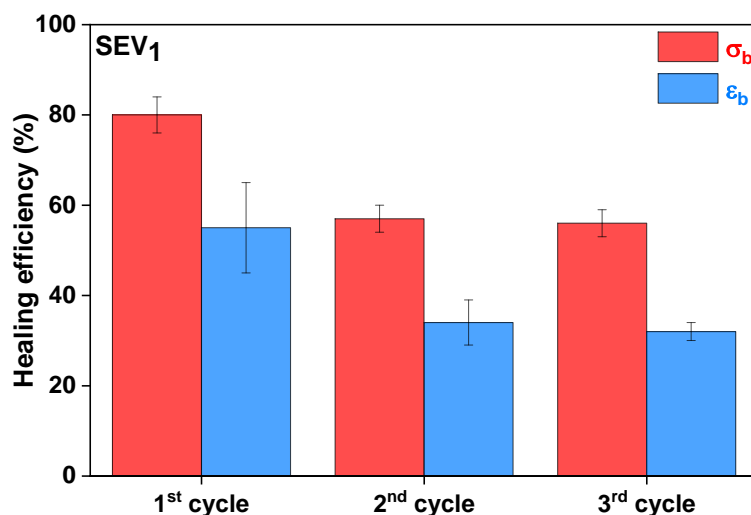


Figure 3.13 Healing efficiency of S₁ compound at different damage/healed cycles.

XPS analyses show a decrease of the S–S–/–S–C– ratio and an increase of the sulfates/–S–C– ratio after successive healing cycles with respect to the pristine material, corroborating the decrease in polysulfide bonds (Table 3.5). S 2p spectra are shown in Figure 3.14. Moreover, the clear loss in –S–S– and notorious increase in sulfates after the 1st cycle evidence that important changes in the network structure mainly occur during the initial thermal treatment. Thus, small variations in healing efficiency should be observed from the 2nd cycle and onwards, as seen in Figure 3.11.

Table 3.5 Ratio between –S–C–, –S–S– and sulfates contributions of S₁ compounds, at different conditions (pristine and after various healing cycles).

	–S–C– (%)	–S–S– (%)	Sulfates (%)	–S–S–/–S–C– Ratio	Sulfate/–S–C– ratio
Pristine	41	50	9	1.22	0.22
1 st cycle	44	24	31	0.54	0.71
2 nd cycle	42	23	35	0.68	1.16
3 rd cycle	35	24	41	0.55	0.85

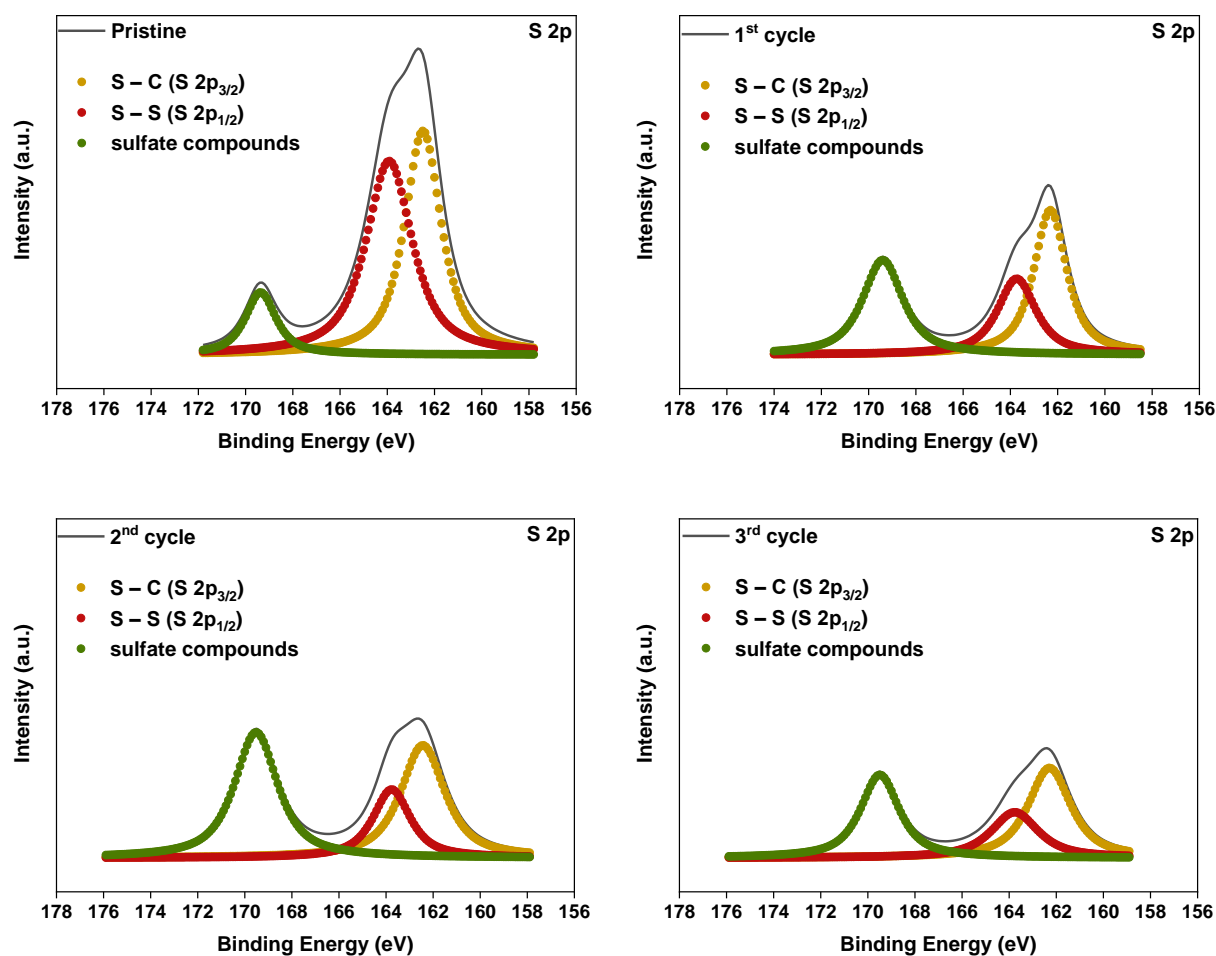


Figure 3.14 The S 2p core spectra of SEV₁ compound at different healing cycles: Pristine; 1st cycle; 2nd cycle and 3rd cycle.

3.3. Effect of the vulcanizing additives

In this section, an exhaustive study of the influence of the different vulcanizing additives on the healing efficiency of SBR compounds was assessed. First, different contents of the curing agent (S) are analyzed in order to determine the optimum amount to obtain the best performance between mechanical properties and self-healing capability. Second, the effect of the amount of ZnO and SA is studied. It is important to highlight the importance of this section, since no other self-healing study has carefully and systematically reported the effect of the various additives of a rubber formulation on its repair capability.

3.3.1. Effect of sulfur content

Several formulations were prepared, varying the S content: 0.4, 0.7, 1, 1.2, 1.6, 2, 3 and 6 phr. The accelerant/sulfur ratio was kept fixed ($A/S=1$), as well as the proportion of, ZnO and SA (5:1). Samples are named as S_x where x is the proportion of S added (Table 3.6). The compound S_1 is equivalent to the SEV_1 compound discussed in the previous section.

Table 3.6 SBR recipes varying S content.

Compound	Ingredient (phr)				
	SBR 1502	ZnO	SA	CBS	S
$S_{0.4}$	100	5	1	0.4	0.4
$S_{0.7}$	100	5	1	0.7	0.7
S_1	100	5	1	1	1
$S_{1.2}$	100	5	1	1.2	1.2
$S_{1.6}$	100	5	1	1.6	1.6
S_2	100	5	1	2	2
S_3	100	5	1	3	3
S_6	100	5	1	6	6

Figure 3.15 shows the vulcanization curves of the compounds. As expected, as the S content increases, the torque increases. Moreover, the increment in ΔM with the S content confirms that a high S content induces higher cross-link densities, resulting in improved tensile properties.[24] At high dosage (6 phr) the rubber shows reversion. This decrease in torque is indicative of degradation, i.e. the breakage of bonds or the presence of secondary reactions taking place after the elastomeric plateau is reached. The occurrence of this process reveals the low thermal stability of the network established at high dosage of curing agent.[5]

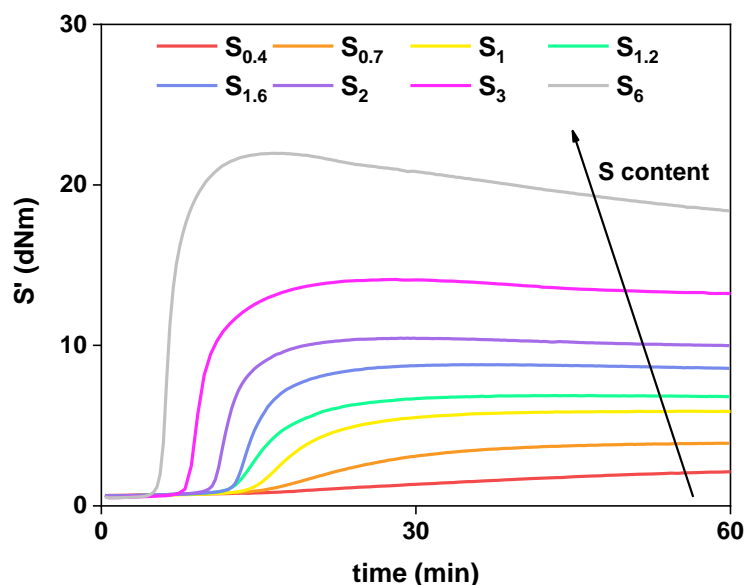


Figure 3.15 Rheometric curves of sulfur based compounds with different S content.

Table 3.7 shows the tensile properties of SBR vulcanizates with different S content. The sample $S_{0.4}$ is a very slightly cross-linked compound, hence, it has a very high elongation at break and the stress values at different strains are similar to each other, indicating that the chains slide as the specimen is deformed. Adding more vulcanizing agent increases the stress required to deform the specimen and the cross-link density, while the elongation at break decreases. At the upper limit content, the vulcanizates become less elastic, favoring crack formation and early breakage of the sample, due to the presence of high cross-linked areas that act as potential points of material fracture.

Figure 3.16 shows the tensile curves. An interesting effect to discuss is the change of trend after 2 phr S content. Opposed to what is observed from 0.4 to 1.6 phr, the thermally treated and the healed curves are below the pristine ones. This behavior can be attributed to a combination of different factors: inhomogeneities in the cross-link network, and a disruption of the rubber network due to the oxidation mechanism during the thermal treatment. In this sense, the formation of inhomogeneities for these compounds could be the result of the presence of chemical groups, such as pendant groups from the accelerator (CBS), which are not taking part in the vulcanization process but just modifying the rubber chains.[25] The presence of these pendant groups is consistent with the high accelerant content of the S_2 , S_3 and S_6 compounds (2, 3, and 6 phr of CBS), respectively. These inhomogeneities together with the thermo-oxidative mechanism

would lead to the degradation of the molecular network in vulcanizates and chain scission in the compounds, which are therefore predominant points of material fracture.

Table 3.7 Physico-mechanical properties and healing efficiency of sulfur based SBR compounds with different S content.

	Compound							
	S _{0.4}	S _{0.7}	S ₁	S _{1.2}	S _{1.6}	S ₂	S ₃	S ₆
Curing parameters								
M _L (dNm)	0.5	0.6	0.7	0.6	0.6	0.6	0.5	0.5
M _H (dNm)	2.4	4	5.8	6.9	8.8	10.5	14.1	22
ΔM (dNm)	1.9	3.4	5.1	6.3	8.2	9.9	13.6	21.5
t _{s2} (min)	-	25	17	14	14	11	9	6
t ₉₀ (min)	67	40	27	24	20	17	15	10
Mechanical properties								
M ₅₀ (MPa)	0.37 ± 0.01	0.48 ± 0.01	0.51 ± 0.01	0.56 ± 0.01	0.67 ± 0.01	0.73 ± 0.01	0.88 ± 0.02	1.4 ± 0.1
M ₁₀₀ (MPa)	0.43 ± 0.01	0.59 ± 0.01	0.67 ± 0.02	0.75 ± 0.01	0.92 ± 0.01	1.05 ± 0.02	1.29 ± 0.03	-
M ₃₀₀ (MPa)	0.44 ± 0.01	0.72 ± 0.01	0.99 ± 0.01	1.17 ± 0.01	1.58 ± 0.03	-	-	-
M ₅₀₀ (MPa)	0.47 ± 0.02	0.87 ± 0.01	1.36 ± 0.03	-	-	-	-	-
σ _b (MPa)	1.3 ± 0.1	1.4 ± 0.3	1.6 ± 0.2	1.6 ± 0.2	1.7 ± 0.1	1.8 ± 0.2	1.7 ± 0.1	1.67 ± 0.02
ε _b (%)	1794 ± 197	864 ± 122	661 ± 18	472 ± 42	326 ± 31	264 ± 42	166 ± 10	65 ± 3
ν × 10 ⁻⁵ (mol/g)	0.09 ± 0.01	0.76 ± 0.01	2.27 ± 0.03	3.21 ± 0.04	4.93 ± 0.05	6.4 ± 0.1	9.71 ± 0.04	20.6 ± 0.3

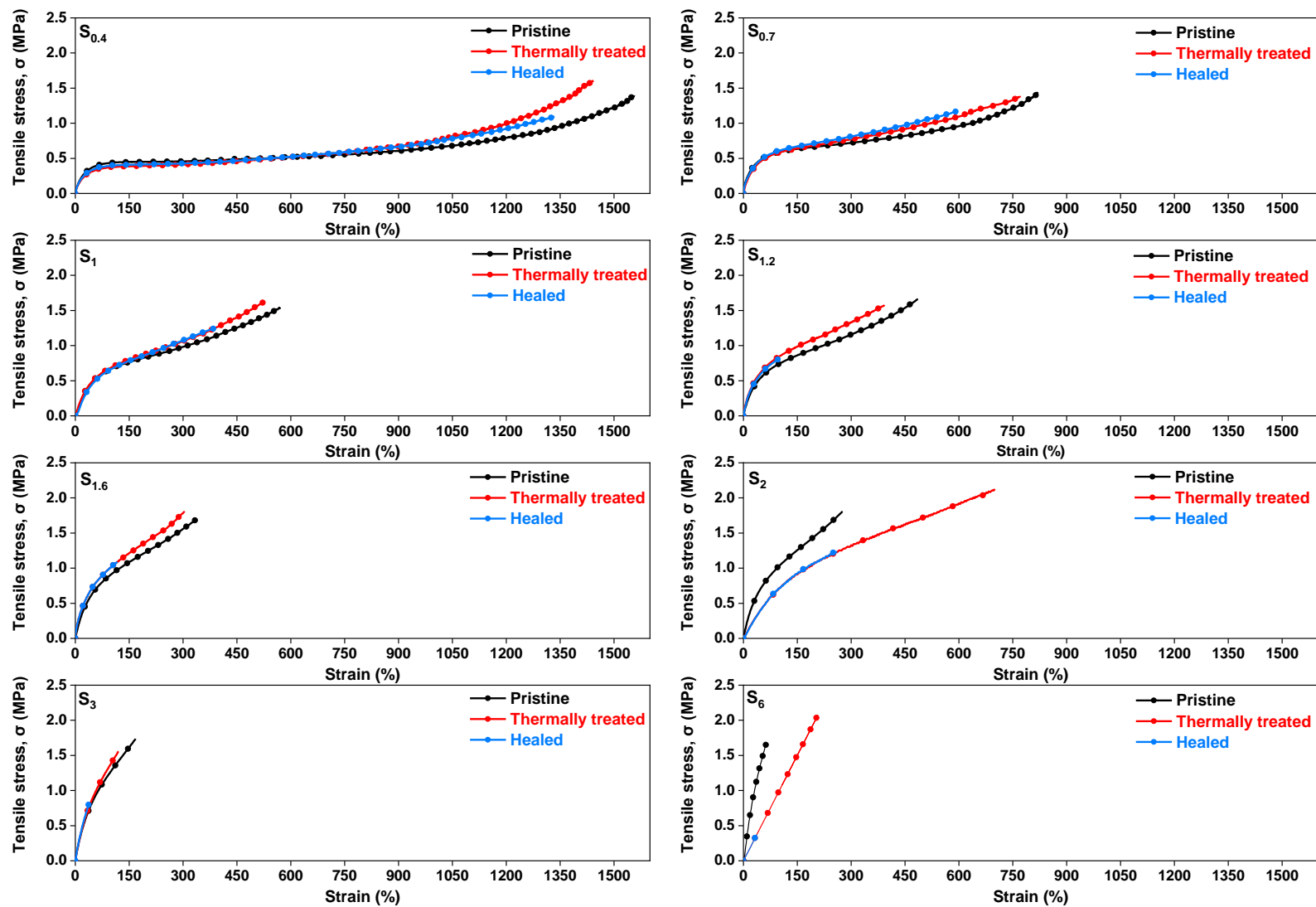


Figure 3.16 Tensile curves of pristine, thermally treated and healed samples of sulfur based SBR compounds with different S content.

The effect of S content on the healing properties can result in two opposite phenomena, as schematically shown in Figure 3.17. On the one hand, as S content increases, more S bridges are present in the rubber network that can participate in the temperature triggered healing mechanism. Therefore, a higher amount of broken rubber chain radicals can be combined and an increase in the healing of the rubber matrix could be expected. On the other hand, the increase in the cross-link density attained with the increment in S content results in a relative more restrained matrix, hindering the recombination of the broken chains. These two opposing trends are clearly seen in Figure 3.18 in compounds with S content above 1phr. Below 1 phr, the increase in cross-link density is not as high as to restrict the mobility of the rubber chains, neither the interdiffusion and the rearrangement of broken reversible bonds at the healed interface; therefore, both properties (cross-link density and healing efficiency) increase simultaneously. These results suggest there is a critical maximum sulfur content and cross-link density for healing to occur effectively. Below 1 phr, the increase in cross-link density is not as high as to restrict the mobility of the rubber chains, neither the interdiffusion and the rearrangement of broken reversible bonds at the healed interface; therefore, both properties (cross-link density and healing efficiency) increase simultaneously. These results suggest there is a critical maximum sulfur content and cross-link density for healing to occur effectively.

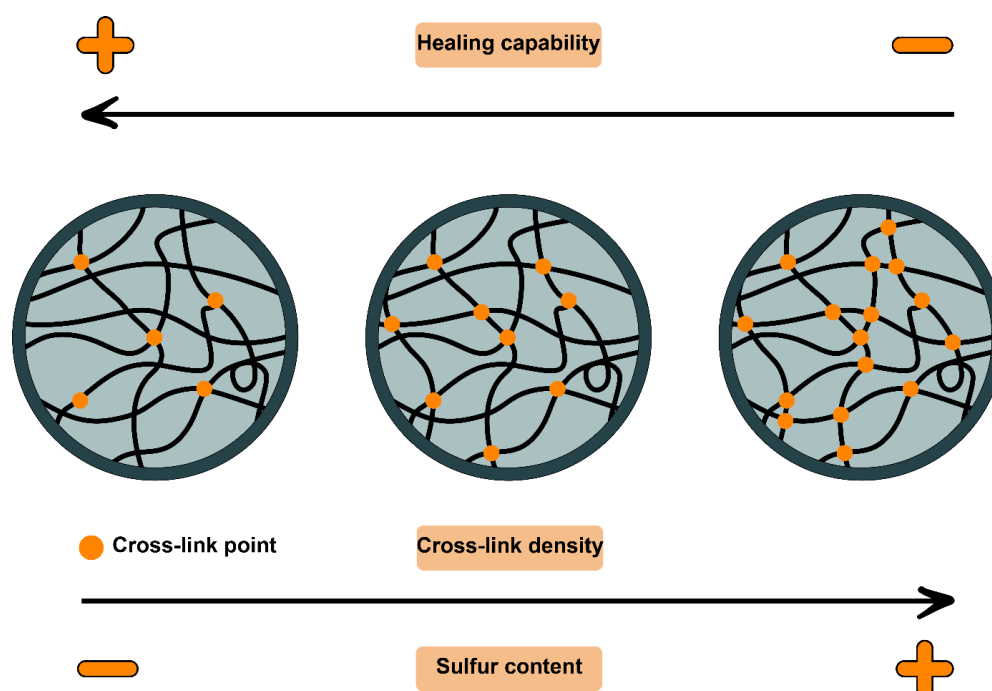


Figure 3.17 Schematic representation of healing capability as function of sulfur content.

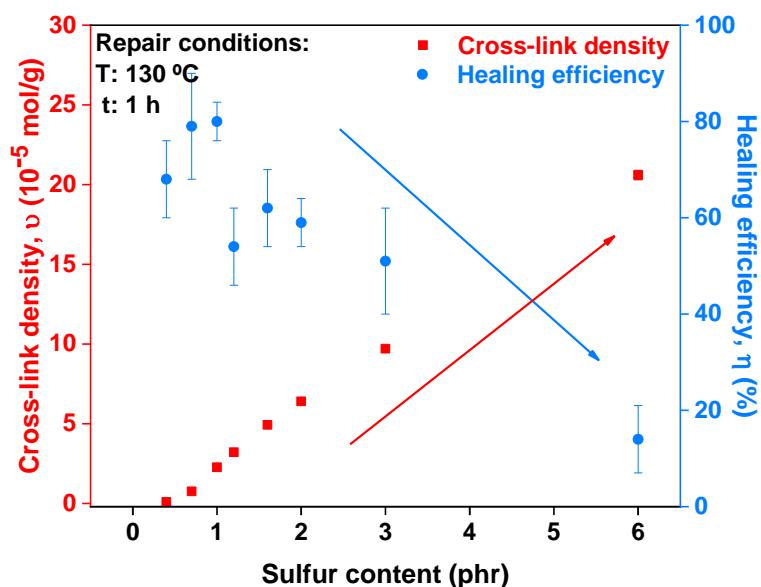


Figure 3.18 Cross-link density and healing efficiency of sulfur based SBR compounds with different S content.

Healing ability can also be determined as the recovery of other properties such as elongation at break. Figure 3.19 shows that good recovery values for elongation are achieved with S contents lower than 1 phr. This result enables us to conclude that the optimum S content for achieving a well-balanced SBR compound with good mechanical properties and healing capability is 1 phr.

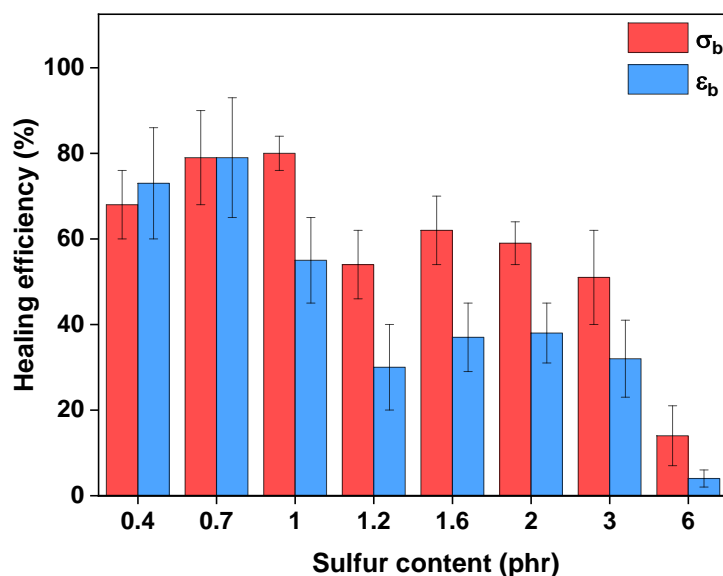


Figure 3.19 Healing efficiency of the elongation at break of SBR compounds with different S content.

3.3.2. Effect of ZnO/SA content

Zinc oxide (ZnO, inorganic activator) and stearic acid (SA, organic activator) are considered an integral and necessary part of the vulcanization system, since the use of these activators improves the efficiency and rate of accelerated sulfur vulcanization.[26] ZnO reacts with SA to form zinc stearate ($ZnSt_2$), which is soluble in the rubber and in this form facilitates the cross-linking process. It forms complexes with accelerants promoting a cross-linking network, resulting in improved sulfur reaction kinetics.[27] Furthermore, it serves as a plasticizer and/or lubricant, reducing the viscosity of the bulk which could eventually contribute to the self-healing capability of the rubber. Therefore, the effect of the amount of ZnO and SA on the healing capability of sulfur/accelerated based systems was studied. The ZnO/SA ratio was kept constant (5:1). Samples are named as S-ZnO_x where “x” corresponds to the proportion of ZnO added (see Table 3.8). The S-ZnO₅ compound is equivalent to the SEV₁ compound previously discussed.

Table 3.8 SBR recipes varying ZnO/SA content.

Compound	Ingredient (phr)				
	SBR 1502	ZnO	SA	CBS	S
S-ZnO ₅	100	5	1	1	1
S-ZnO ₁₀	100	10	2	1	1
S-ZnO ₁₅	100	15	3	1	1
S-ZnO ₂₀	100	20	4	1	1
S-ZnO ₂₅	100	25	5	1	1
S-ZnO ₅₀	100	50	10	1	1

Figure 3.20 shows the vulcanization curves of SBR compounds with different ZnO/SA content. As can be seen in Table 3.9, the increase in the ZnO content slightly reduces the extent of cure and, consequently, the cross-link density also shows a marginal decrease. Nonetheless, samples show an increase in the moduli, tensile strength, and elongation at break with ZnO/SA content (Table 3.9 and Figure 3.21). This behavior can be linked to the individual effect of ZnO and SA. ZnO increases the modulus and tensile strength, since it can act as a semi-reinforcing filler.[28] Meanwhile, SA and $ZnSt_2$ act as internal lubricants between the polymer chains, increasing the elongation at break of the SBR compounds.[29]

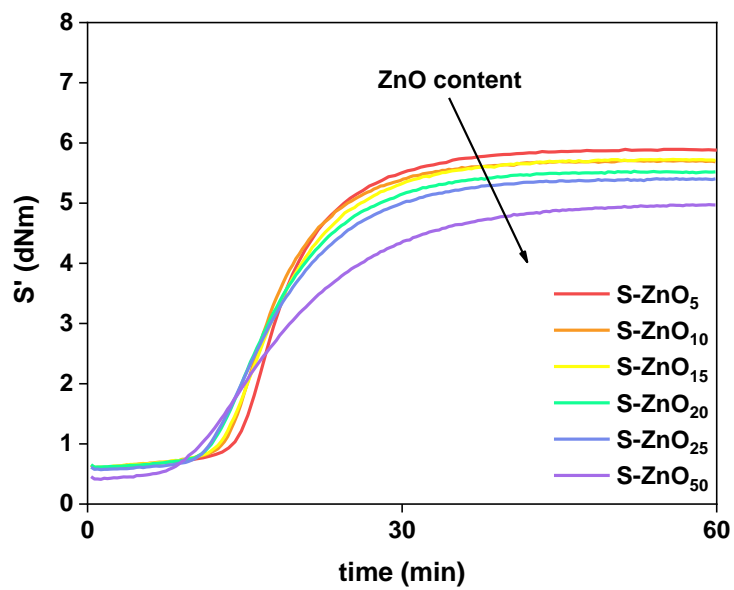


Figure 3.20 Rheometric curves with different ZnO/SA content.

Table 3.9 Physico-mechanical properties and healing efficiency with different ZnO content.

	Compound					
	S-ZnO ₅	S-ZnO ₁₀	S-ZnO ₁₅	S-ZnO ₂₀	S-ZnO ₂₅	S-ZnO ₅₀
Curing parameters						
M _L (dNm)	0.7	0.6	0.6	0.6	0.6	0.4
M _H (dNm)	5.8	5.7	5.7	5.5	5.4	5
ΔM (dNm)	5.1	5.1	5.1	4.9	4.8	4.6
t _{s2} (min)	17	16	17	16	16	17
t ₉₀ (min)	27	27	28	28	29	33
Mechanical properties						
M ₅₀ (MPa)	0.51 ± 0.01	0.53 ± 0.02	0.54 ± 0.03	0.59 ± 0.01	0.58 ± 0.04	0.74 ± 0.04
M ₁₀₀ (MPa)	0.67 ± 0.02	0.68 ± 0.02	0.68 ± 0.03	0.74 ± 0.01	0.72 ± 0.04	0.88 ± 0.04
M ₃₀₀ (MPa)	0.99 ± 0.01	0.97 ± 0.01	0.98 ± 0.03	1.04 ± 0.02	0.99 ± 0.04	1.15 ± 0.05
M ₅₀₀ (MPa)	1.36 ± 0.03	1.33 ± 0.02	1.38 ± 0.02	1.43 ± 0.02	1.38 ± 0.02	1.6 ± 0.1
σ _b (MPa)	1.6 ± 0.2	1.8 ± 0.3	1.8 ± 0.2	2.1 ± 0.3	2.6 ± 0.6	2.9 ± 0.5
ε _b (%)	661 ± 18	633 ± 72	614 ± 34	662 ± 45	705 ± 58	1075 ± 350
ν × 10 ⁻⁵ (mol/g)	2.27 ± 0.03	2.11 ± 0.04	2.11 ± 0.03	2.11 ± 0.05	2.04 ± 0.03	1.58 ± 0.09

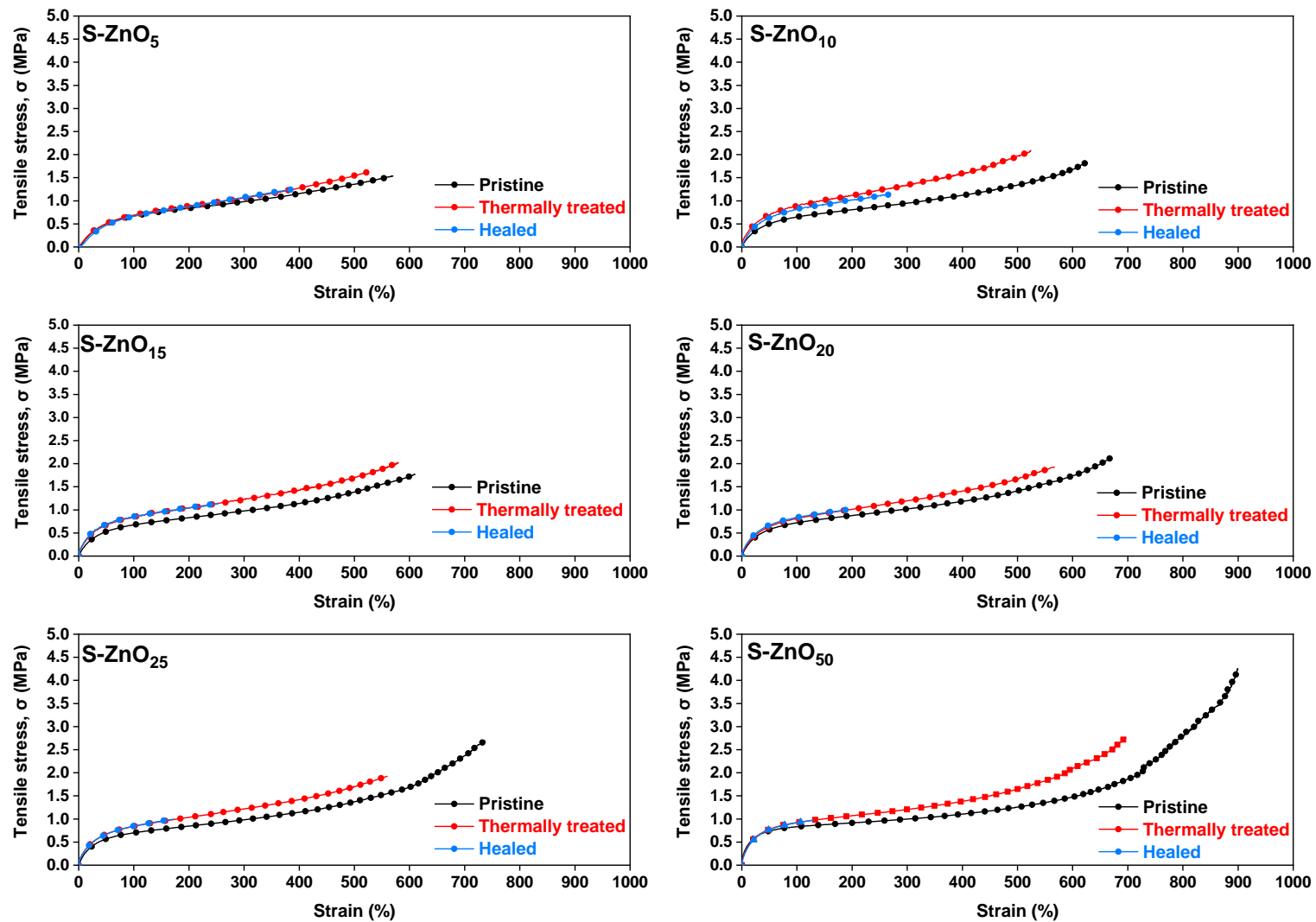


Figure 3.21 Tensile curves of pristine, thermally treated and healed samples with different ZnO/SA content.

The healing efficiency of the compounds as function of ZnO/SA content follows the same trend as the cross-link density (Figure 3.22). This behavior is opposite to what has been discussed in the previous sections, where mechanical performance (i.e. cross-link density) and healing efficiency are antagonistic properties. At the lower and upper ZnO/SA limits, both properties show the highest and the lowest values, respectively. Meanwhile, for intermediate ZnO/SA contents, both properties remain relatively constant.

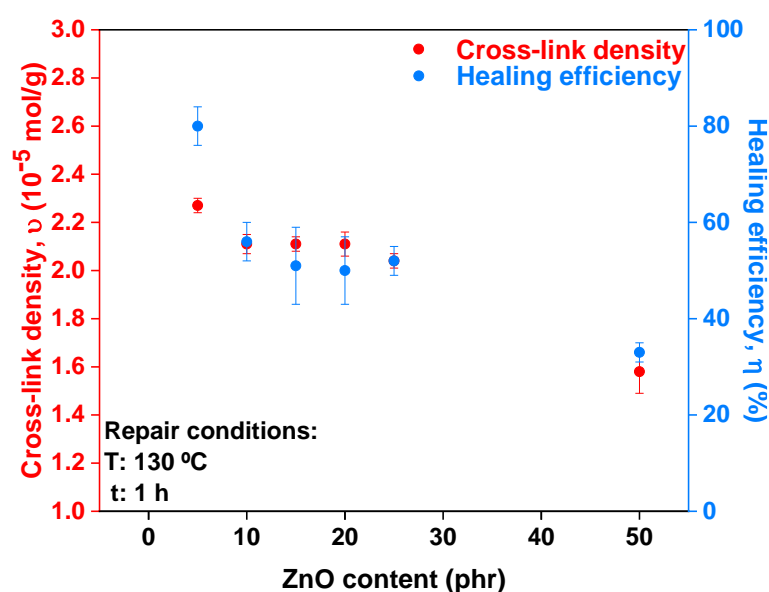


Figure 3.22 Cross-link density and mechanical healing efficiency of sulfur based SBR compounds with different ZnO/SA content.

Two simultaneous contributions seem to be responsible for this behavior, as schematically shown in Figure 3.23. Firstly, ZnO can act as a semi-reinforcing filler, restricts the mobility of the rubber chains; hence, limiting chain interdiffusion and restoration of broken bonds at the damaged interface.[28]

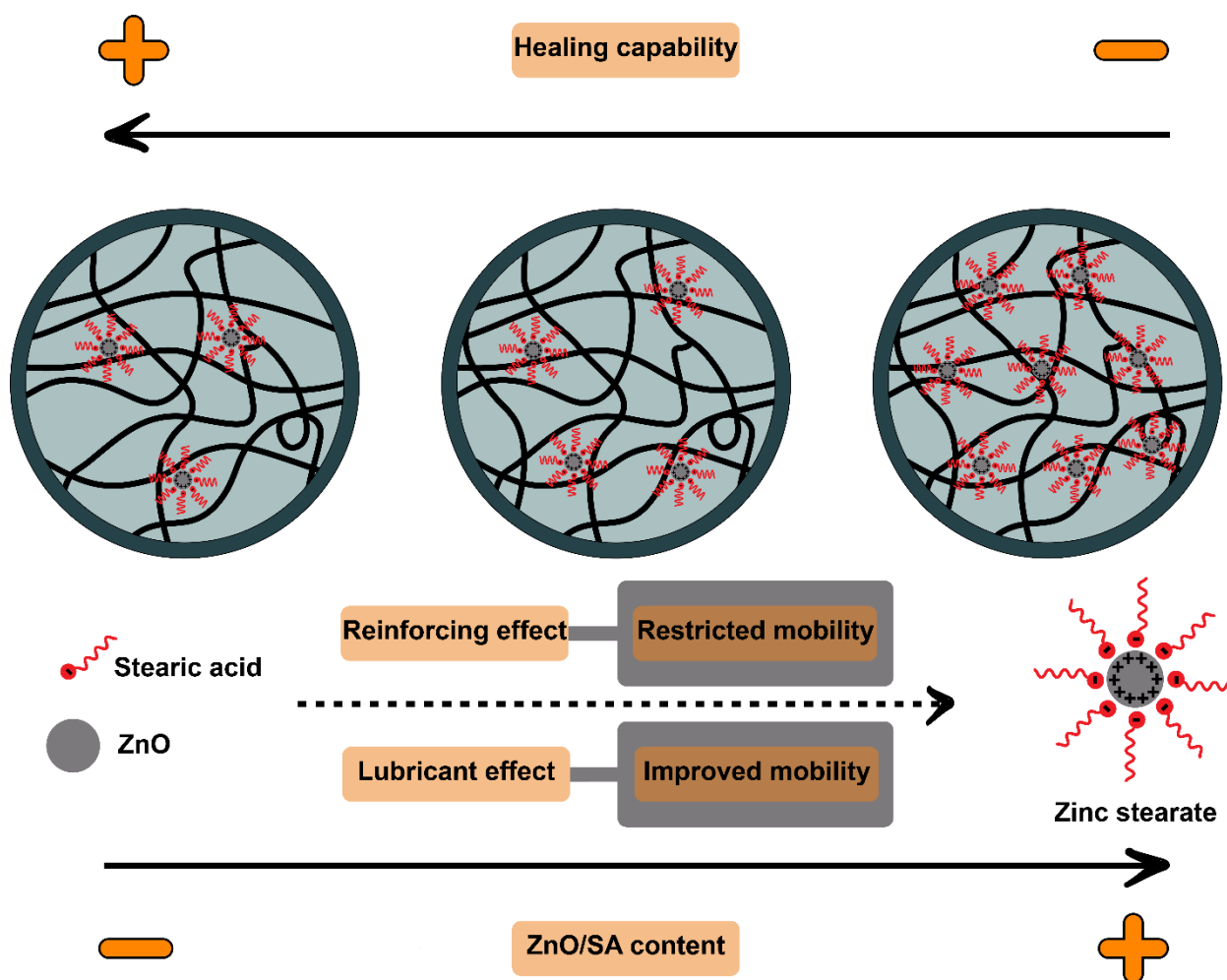


Figure 3.23 Schematic representation of healing capability as function of ZnO/SA content.

Secondly, as ZnO/SA content increases, more ZnSt₂ domains can be formed, up to the extent of forming a percolated network that could improve the rubber chain mobility; hence, contributing to the self-healing capability. At the healing temperature (130 °C), the interdiffusion of rubber chains across the damaged interface is favored thanks to the lubricating effect of the ZnSt₂ followed by the rearrangement of rubber chains. Once the healing cycle ends, ZnSt₂ domains can crystallize near the damage zone enabling the restoration of the initial properties of the rubber network. To corroborate this assumption, DSC measurements of zinc stearate (*Sigma Aldrich*) and SBR compounds with different ZnO/SA contents were performed. Figure 3.24 shows a melting peak around 120 °C that corresponds to the fusion of ZnSt₂ crystalline domains. Similar melting peaks are observed in the SBR compounds where the intensity of the peak increases with ZnO/SA content.

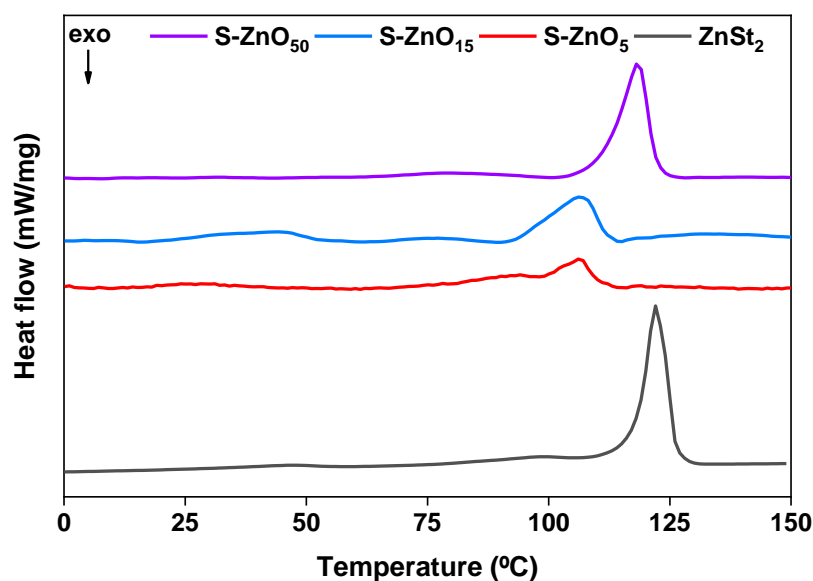


Figure 3.24 DSC thermograms of zinc stearate and SBR compounds with different ZnO/SA content.

To further corroborate the formation of ZnSt_2 domains near the damage zone after applying the healing protocol, scanning electron microscope (SEM) micrographs and energy dispersive X-ray (EDX) elemental mapping at 500x magnification of S-ZnO_5 compound (equivalent to the SEV_1 compound) were assessed. Figure 3.25 shows the presence of rough aggregates of ZnSt_2 domains on the surface and along the crack, after applying the healing protocol (130 °C and 1 h).

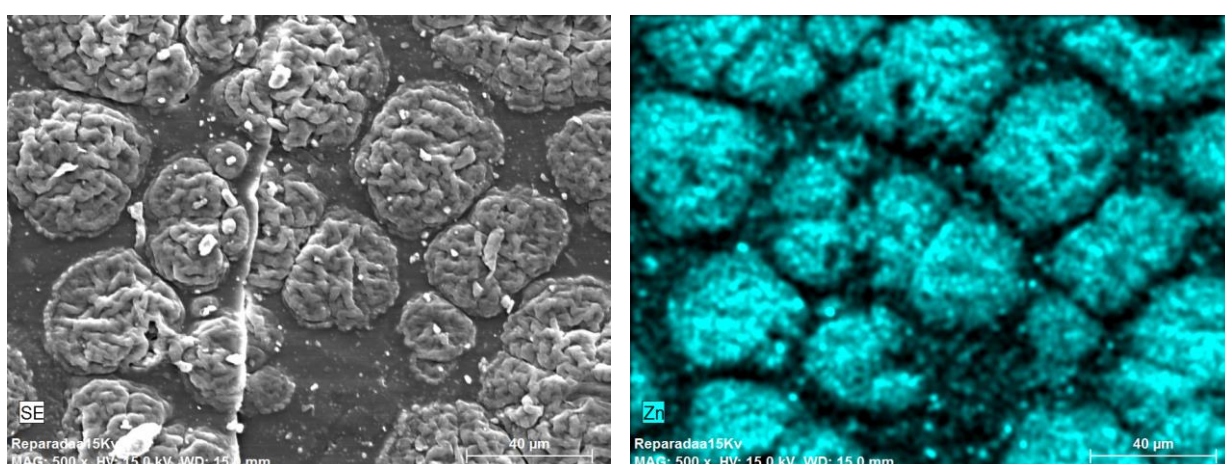


Figure 3.25 Left: Scanning electron microscope (SEM) micrographs, Right: Energy dispersive X-ray (EDX) elemental mapping of S-ZnO_5 (SEV_1) compound at a magnification of 500x.

In conclusion, a balance between the lubricant effect of ZnSt₂ and the reinforcing effect of ZnO seem to be responsible for maintaining acceptable healing efficiencies in the order of 50 – 60 %, while improving tensile strength more than 160 % with respect to the reference compound (SEV₁).

3.4. Understanding the self-healing mechanism

In the previous sections, we have proposed a healing mechanism based on the temperature-triggered opening and recombination of the di- and poly-sulfide bonds, present in sulfur-cured networks. The aim of this last section is to validate such hypothesis. Thus, a dicumyl peroxide-based compound was prepared and compared with a sulfur-based compound, considering equivalent cross-link densities (Table 3.10).

Table 3.10 SBR recipes of sulfur based and dicumyl peroxide based vulcanization systems.

Compound	Ingredient (phr)				
SEV ₁	SBR 1502	ZnO	SA	CBS	S
	100	5	1	1	1
DCP	SBR 1502	ZnO	SA	CBS	DCP
	100	-	-	-	0.1

The cross-link structure of peroxide vulcanizates is relatively simple, consisting of carbon-carbon (–C–C–) bonds between macromolecular chains. Figure 3.26 shows the curing curves of sulfur-based and peroxide-based SBR compounds cured at 160 °C. Unlike the sulfur-based reaction, the peroxide vulcanization occurs without the induction stage. The decomposition of DCP at 160 °C is very fast, giving rise to an immediate increase in the elastic component of the torque, S', due to the creation of covalent bonds between the polymer chains. In general, peroxide vulcanizates present better ageing and oxidation resistance due to the thermal stability of –C–C– bonds, which have higher bond energy than the sulfide bonds (–C–S_x–C–, and –S–S–). The vulcanization with peroxides forms stable cross-links at moderate to high temperatures. Thus, a priori, peroxide-based vulcanizates do not possess a healing ability, since no reversible links are present in the cross-linked structure.

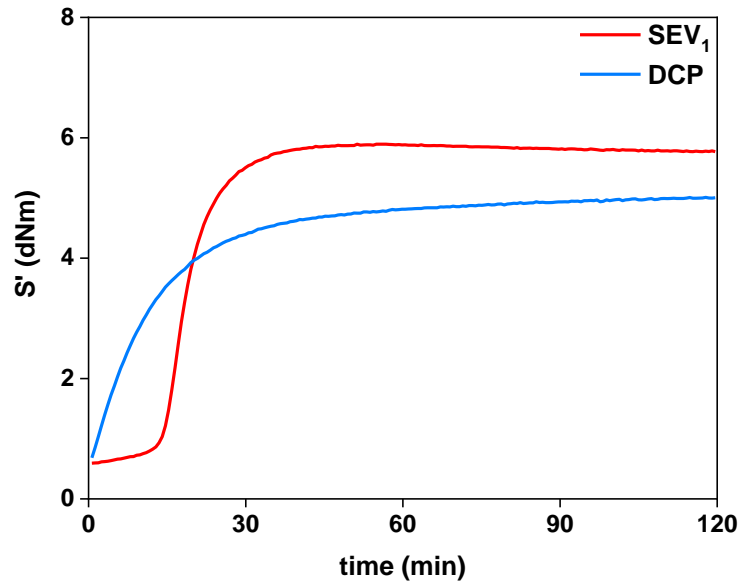


Figure 3.26 Rheometric curves of SEV₁ and DCP compounds.

Figure 3.27 shows the tensile test curves of SEV₁ and DCP compounds. Contrary to what has been discussed for sulfur-based systems, the thermally treated samples of the DCP compound show a slight decrease in the modulus, tensile strength, and elongation at break with respect to the pristine sample. This is somehow an unexpected result that does not correspond to the theoretical predictions, according to which peroxide curing systems lead to the formation of vulcanizates with enhanced heat ageing stability and higher resistance to thermo-oxidative degradation, if compared to sulfur systems.

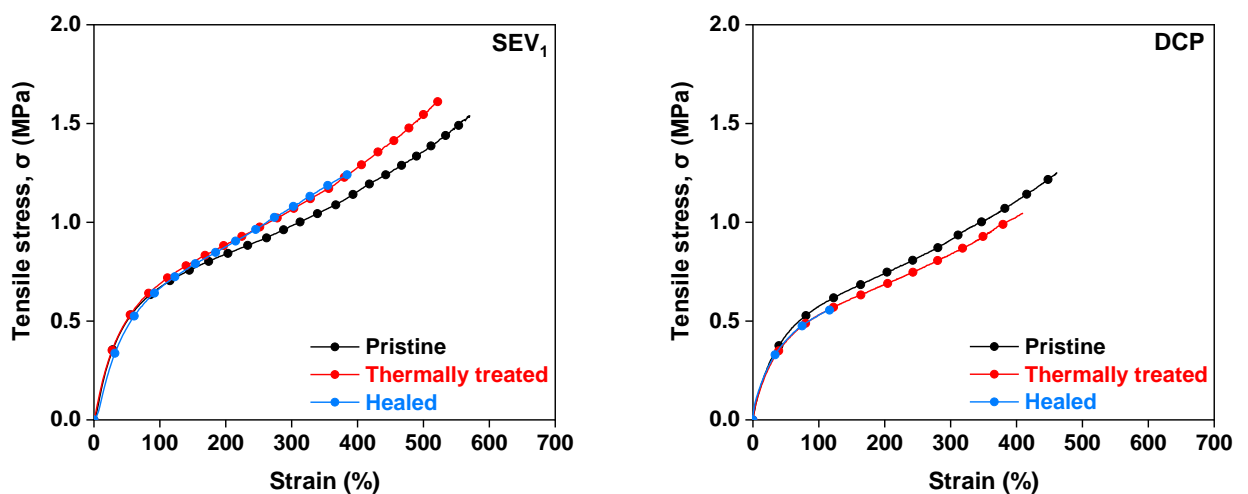


Figure 3.27 Tensile curves of pristine, thermally treated and healed samples of SEV₁ and DCP compounds.

Similar results were reported for NR by Kruželák *et al.*[30] They found a similar negative effect on thermo-oxidative stability of NR compounds vulcanized with DCP. There are some side reactions carried out at the same time as the main vulcanization reaction. The residual and unconsumed peroxide free radical species, from the peroxide decomposition during the vulcanization process, is the main source of oxidative-destructive reactions by producing chain scission reaction.[7] The oxygen molecules present during the healing protocol can be coupled to the rubber backbone radicals to produce peroxide radicals and subsequently hydroperoxides or peroxides, following the thermo-oxidative ageing reaction.[31] Finally, these species undergo chain cleavage reaction decreasing the physical and mechanical properties.

The self-healing capability of the developed compounds was analyzed based on the recovery of tensile strength, as shown in Figure 3.28. The high healing efficiency of the SEV₁ compound, as already discussed, is attributed to the rearrangement of dynamic reversible –S–S– broken bonds at the healed interface. Meanwhile, a healing efficiency of 58 % is unexpectedly observed for the DCP compound. Therefore, since –C–C– bonds are thermally stable and not prone to reversibility, another self-healing mechanism should be taking place. It is important to highlight this finding since, to the best knowledge, no healing has been reported before in fully cured peroxide SBR compounds. Nonetheless, other authors have reported the combination of peroxide with other additives for various healing mechanisms in NR compounds.[32-34]

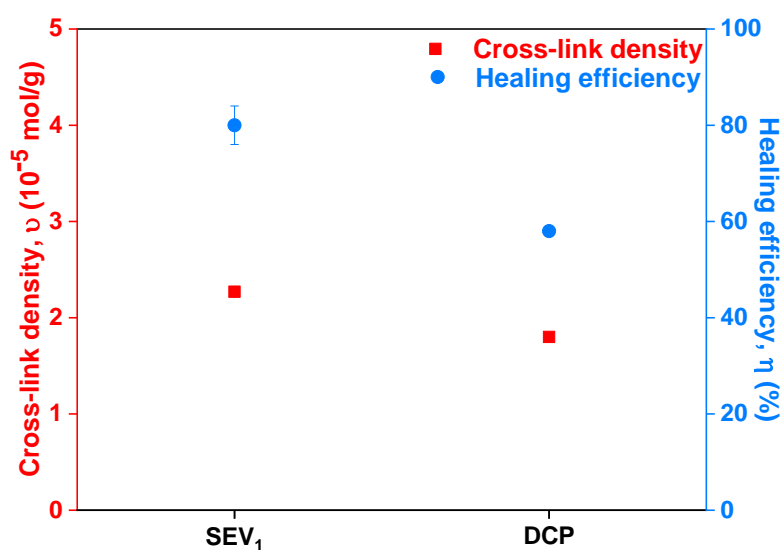


Figure 3.28 Cross-link density and mechanical healing efficiency of SEV₁ and DCP compounds.

According to the theory of Wool *et al.*[35], the overall macroscopic healing process in intrinsic healing polymers consists of three main stages: i) 2D interface (self-adhesion); ii) 3D interphase (long-range diffusion processes at relatively short times); and iii) randomization (homogenization) at long time scales. Short-range physical and/or chemical interactions and molecule/chain interdiffusion take part during the initial steps, being considered as the fundamental principle of physical self-healing.[36] This theory allows considering that the partial recovery of the mechanical strength in the DCP compound results from the interdiffusion of rubber chains and the formation of physical entanglements in the rubber network.

A schematic representation of this physical healing mechanism is shown in Figure 3.29. Upon damage, free dangling end chains occupy the damaged area. Then, healing occurs if the broken interfaces can come into close contact with each other and for a sufficiently long time to ensure adequate molecular movement across the interface. Since the healing temperature (130 °C) is far above the glass transition of SEV₁ (-55 °C), the mobility of these free short and long chains segments is enough to promote chain interdiffusion along the damage surface, the formation of physical entanglements, and then the interpenetration into the matrix rubber compound. The damaged zone gradually disappears recovering the mechanical strength at the interface. Finally, during the randomization step, the complete loss of initial crack interface is achieved facilitating the recovery of the initial properties.[21, 37]

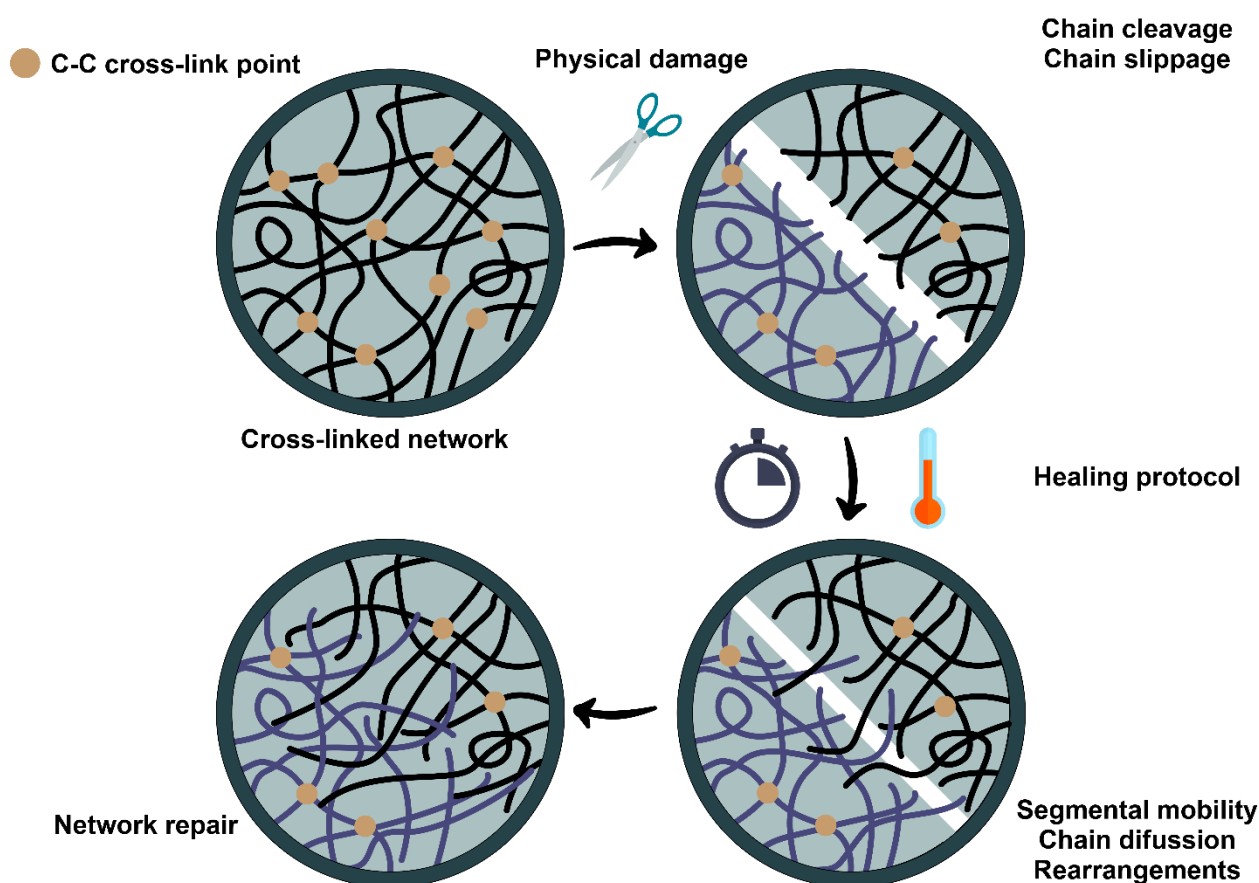


Figure 3.29 Schematic representation of physical healing mechanism.

Another proof of the differences between sulfur-based and peroxide-based compounds arises from the dielectric spectroscopy analysis. The relative permittivity (ϵ^*) increases with temperature for both rubber compounds (Figure 3.30). However, a significant increase (more than 3 orders of magnitude) is seen for the sulfur-based SBR in the selected temperature range. Podgorski *et al.*[38] reported a similar result, and ascribed it to the covalent exchange reactions taking place in dynamic thiol-anhydride covalent adaptable networks (CANs). They discussed that dynamic exchange is a temperature dependent process that facilitates dipole alignment and mobility of the polymeric system. Thus, it is not surprising that the peroxide-based compound, being a non-reversible covalent network, only shows a marginal increase of ϵ^* with temperature. Madsen *et al.*[39] also reported an increase in ϵ^* with the increasing concentration of reversible ionic groups in a self-healing silicone elastomer.

The measurement was repeated three times for the sulphur-based compound, resulting in the same temperature dependence and corroborating that the S₁ compound can support at least three healing cycles (Figure 3.30). Moreover, in all of the cases, the increase in ϵ^* starts at 60 °C, guaranteeing that the healing temperatures evaluated ($T >$

70 °C) and optimized (T = 130 °C) in this study enable disulfide exchange reactions to take place.

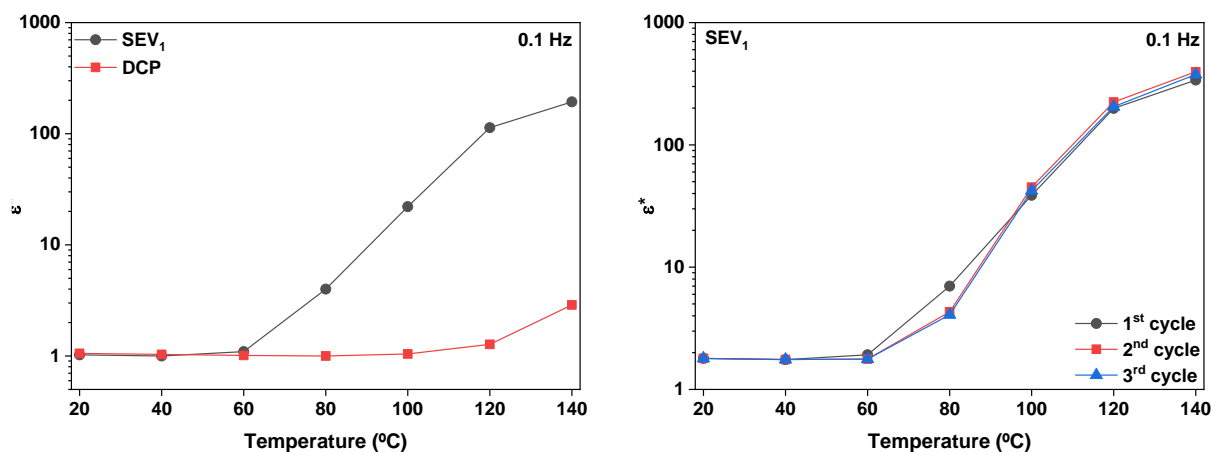


Figure 3.30 Relative permittivity (ϵ^*) vs temperature for: a) S₁ and DCP_{0.1} compounds; b) various heating cycles of S₁ compounds.

3.5. Summary

In this chapter, the self-healing capability of SBR has extensively been studied to gain a thorough understanding of its repair mechanism. The analysis of different healing conditions revealed that pristine materials should be subjected to the same thermal treatment as the healed samples to obtain scientifically sound values of the healing efficiency. The healing mechanism arises from the combination of two different processes. During the initial stages of the healing process, chain interdiffusion and formation of physical entanglements take place, ensuring partial recovery of the interface/interphase. Next, long-range interactions and disulfide exchange reactions are favored, resulting in the almost full recovery of mechanical stress beyond low strains. Thus, S is the fundamental component that promotes the almost full recovery of the mechanical properties; while the other vulcanizing additives, such as ZnO/SA, affect healing in its early stages.

The ratio between the di- and poly-sulfide bridges, resulting from the different A/S ratios, affects the healing performance of the rubber. The semi-efficient vulcanization system (SEV₁) gives the best balance between tensile strength and healing capability. However, depending on the application requirements, the CV system should not be ruled out. Finally, the healing protocol was optimized achieving full recovery of the mechanical

properties when applying 130 °C during 1 h. These conditions were selected aiming to develop a sustainable, and industrially scalable healing process. Meanwhile, the SBR compound exhibited a repeatable healing after multiple cycles, resulting in an acceptable recovery of tensile strength of 60 % after 3 cycles.

3.6. References

1. Imbernon, L., et al., *Chemically crosslinked yet reprocessable epoxidized natural rubber via thermo-activated disulfide rearrangements*. Polym. Chem., 2015. **6**(23): p. 4271-4278.
2. Nevejans, S., et al., *The underlying mechanisms for self-healing of poly(disulfide)s*. Phys. Chem. Chem. Phys., 2016. **18**(39): p. 27577-27583.
3. Utrera-Barrios, S., et al., *Evolution of self-healing elastomers, from extrinsic to combined intrinsic mechanisms: a review*. Mater. Horiz., 2020. **7**: p. 2882-2902.
4. Coran, A.Y., *Chapter 7 - Vulcanization*, in *The Science and Technology of Rubber (Fourth Edition)*, J.E. Mark, B. Erman, and C.M. Roland, Editors. 2013, Academic Press: Boston. p. 337-381.
5. Brydson, J.A., *Reactivity of diene rubbers II: Cross-linking processes*, in *Rubber chemistry*. 1982. p. 194-259.
6. Krejsa, M.R. and J.L. Koenig, *A review of sulfur crosslinking fundamentals for accelerated and unaccelerated vulcanization*. Rubber Chem. Technol., 1993. **66**(3): p. 376-410.
7. Kruželák, J., R. Sýkora, and I. Hudec, *Sulphur and peroxide vulcanisation of rubber compounds — overview*. Chem. Pap., 2016. **70**(12): p. 1533-1555.
8. Brydson, J.A., *Additives I: Curing systems*, in *Rubbery materials and their compounds*. 1988, springer. p. 348 - 374.
9. Hofmann, W., *Vulcanization and vulcanizing agents*, in *Ullmann's Encyclopedia of Industrial Chemistry*. 1967, Maclaren London.
10. Joseph, A., et al., *Current status of sulphur vulcanization and devulcanization chemistry: Process of vulcanization*. Rubber Sci., 2015. **28**: p. 82.
11. Hernández, M., et al., *Turning vulcanized natural rubber into a self-healing polymer: Effect of the disulfide/polysulfide ratio*. ACS Sustain. Chem. Eng., 2016. **4**(10): p. 5776-5784.
12. Yamaguchi, M., et al., *Autonomic healing and welding by interdiffusion of dangling chains in a weak gel*. Polym, Int., 2012. **61**(1): p. 9-16.
13. AbdolahZadeh, M., et al., *Healable dual organic–inorganic crosslinked sol–gel based polymers: Crosslinking density and tetrasulfide content effect*. J. Polym. Sci. A Polym. Chem., 2014. **52**(14): p. 1953-1961.
14. Xiang, H.P., et al., *Crack healing and reclaiming of vulcanized rubber by triggering the rearrangement of inherent sulfur crosslinked networks*. Green Chem., 2015. **17**(8): p. 4315-4325.
15. Hager, M.D., *Self-healing materials*, in *Handbook of Solid State Chemistry*. 2017. p. 201-225.
16. Martin, R., et al., *Dynamic sulfur chemistry as a key tool in the design of self-healing polymers*. Smart Mater. Struct., 2016. **25**(8): p. 084017.
17. Tobolsky, A.V., W.J. MacKnight, and M. Takahashi, *Relaxation of disulfide and tetrasulfide polymers*. J. Phys. Chem., 1964. **68**(4): p. 787-790.
18. Feng, L., et al., *Effect of Heat-Treatment on Self-healing and Processing Behavior of Thermally Reversible Polyurethanes*. J. Polym. Environ., 2020. **28**(2): p. 647-656.
19. Torregrosa-Coque, R., S. Álvarez-García, and J.M. Martín-Martínez, *Migration of Paraffin Wax to Sulfur Vulcanized Styrene–Butadiene Rubber (SBR) Surface: Effect of Temperature*. J. Adhes. Sci. Technol., 2012. **26**(6): p. 813-826.
20. Behera, P.K., S. Mohanty, and V.K. Gupta, *Self-healing elastomers based on conjugated diolefins: a review*. Polym. Chem., 2021. **12**(11): p. 1598-1621.

21. Hernández Santana, M., et al., *Routes to make natural rubber heal: A review*. Polym. Rev., 2018. **3724**(4): p. 1-25.
22. Jay, S., et al., *Solubility of elemental sulfur in toluene between (267.15 and 313.15) K under atmospheric pressure*. J. Chem. Eng. Data, 2009. **54**(12): p. 3238-3241.
23. Hamed, G. and J. Zhao, *Tensile behavior after oxidative aging of gum and black-filled vulcanizates of SBR and NR*. Rubber Chem. Technol., 1999. **72**(4): p. 721-730.
24. Yang, J.-K., et al., *Roles of sulfur and accelerators in the vulcanization of SBR compounds deduced through simulation*. Rubber Chem. Technol., 2018. **91**(3): p. 595-608.
25. Bandzierz, K.S., et al., *Effect of polymer chain modifications on elastomer properties*. Rubber Chem. Technol., 2019. **92**(1): p. 69-89.
26. Ignatz-Hoover, F. and B.H. To, *Vulcanization*, in *Rubber Compounding: Chemistry and Applications*. 2004. p. 461 - 522.
27. Barlow, F.W., *Activators and Retarders*, in *Rubber compounding: principles, materials, and techniques*. 1993, CRC Press. p. 115 - 119.
28. González, N., et al., *Influence of ZnO and TiO₂ particle sizes in the mechanical and dielectric properties of vulcanized rubber*. Mater. Res., 2017. **20**(4): p. 1082-1091.
29. Heideman, G. (2004). *Reduced zinc oxide levels in sulphur vulcanisation of rubber compounds: mechanistic aspects of the role of activators and multifunctional additives*. (Ph.D. Thesis). University of Twente.
30. Kruzalak, J., R. Sykora, and I. Hudec, *Sulfur and peroxide curing of rubber compounds based on NR and NBR. Part II: Thermo-oxidative ageing*. KGK-Kaut. Gummi. Kunst., 2017. **70**(3): p. 41-47.
31. Brydson, J.A., *Reactivity of diene rubbers III: Oxidation and related processes*, in *Rubber chemistry*. 1982. p. 260-294.
32. Rahman, M.A., et al., *Autonomic self-healing in epoxidized natural rubber*. Acs. Appl. Mater. Inter., 2013. **5**(4): p. 1494-1502.
33. Xu, C., et al., *Design of self-healing supramolecular rubbers by introducing ionic cross-links into natural rubber via a controlled vulcanization*. Acs. Appl. Mater. Inter., 2016. **8**(27): p. 17728-17737.
34. Xu, C., et al., *Self-healing natural rubber with tailorable mechanical properties based on ionic supramolecular hybrid network*. Acs. Appl. Mater. Inter., 2017. **9**(34): p. 29363-29373.
35. Wool, R.P. and K.M. O'Connor, *A theory crack healing in polymers*. J. Appl. Phys., 1981. **52**(10): p. 5953-5963.
36. Döhler, D., P. Michael, and W. Binder, *Principles of Self-Healing Polymers*, in *Self-Healing Polymers*. 2013. p. 5-60.
37. Yang, Y. and M.W. Urban, *Self-healing polymeric materials*. Chem. Soc. Rev., 2013. **42**(17): p. 7446-7467.
38. Podgórski, M., et al., *Mixed mechanisms of bond exchange in covalent adaptable networks: monitoring the contribution of reversible exchange and reversible addition in thiol-succinic anhydride dynamic networks*. Polym. Chem., 2020. **11**(33): p. 5365-5376.
39. Madsen, F.B., L. Yu, and A.L. Skov, *Self-Healing, high-permittivity silicone dielectric elastomer*. ACS Macro Lett., 2016. **5**(11): p. 1196-1200.



“R” AS RECYCLE

HEALING OF SBR/GTR COMPOSITES

*Part of the work described in this chapter has been published in *European Polymer Journal*, **2018**, 106(9), 273-283, and in *Journal of Composites Science*. **2021**, 5(3), 68.*

4. “R” as Recycle - Healing of SBR/GTR Composites

Recycling of resources and products is one of the main strategies of the CE model. The most straightforward option in any tire recycling route should consider the production of ground tire rubber (GTR), a fine granular material obtained from worn tires. GTR is generally used as filler substitute in different matrices: thermoplastics, rubber compounds, among others. However, its use in rubber has been, up to now, restricted to the production of technically less demanding goods, since the low compatibility with the matrix is a major issue.

Chapter 4 details the combination of Repair and Recycle CE principles on the development of sustainable, mechanically robust SBR composites. To do so, waste tires were selected as possible reinforcing fillers for the self-healing SBR compound obtained in Chapter 3. The GTR was modified with a combination of mechanical (cryo-grinding) and chemical (oxidizing treatment) processes. Different SBR composites filled with cryo-ground GTR (c-GTR), and chemically modified GTR (m-GTR) were studied in order to correlate each system with the mechanical and healing performance of the SBR composites. In addition, SBR composites with different hybrid reinforcing systems were studied, combining traditional fillers (carbon black – CB, and silica - Si) with m-GTR. The influence of the bis-(3-triethoxysilylpropyl)tetrasulfide (TESPT) as a coupling agent (CA) was also assessed. Healing conditions (temperature and time) were varied and optimized to achieve different degrees of healing. A schematic representation on the content of Chapter 4 is shown in Figure 4.1.

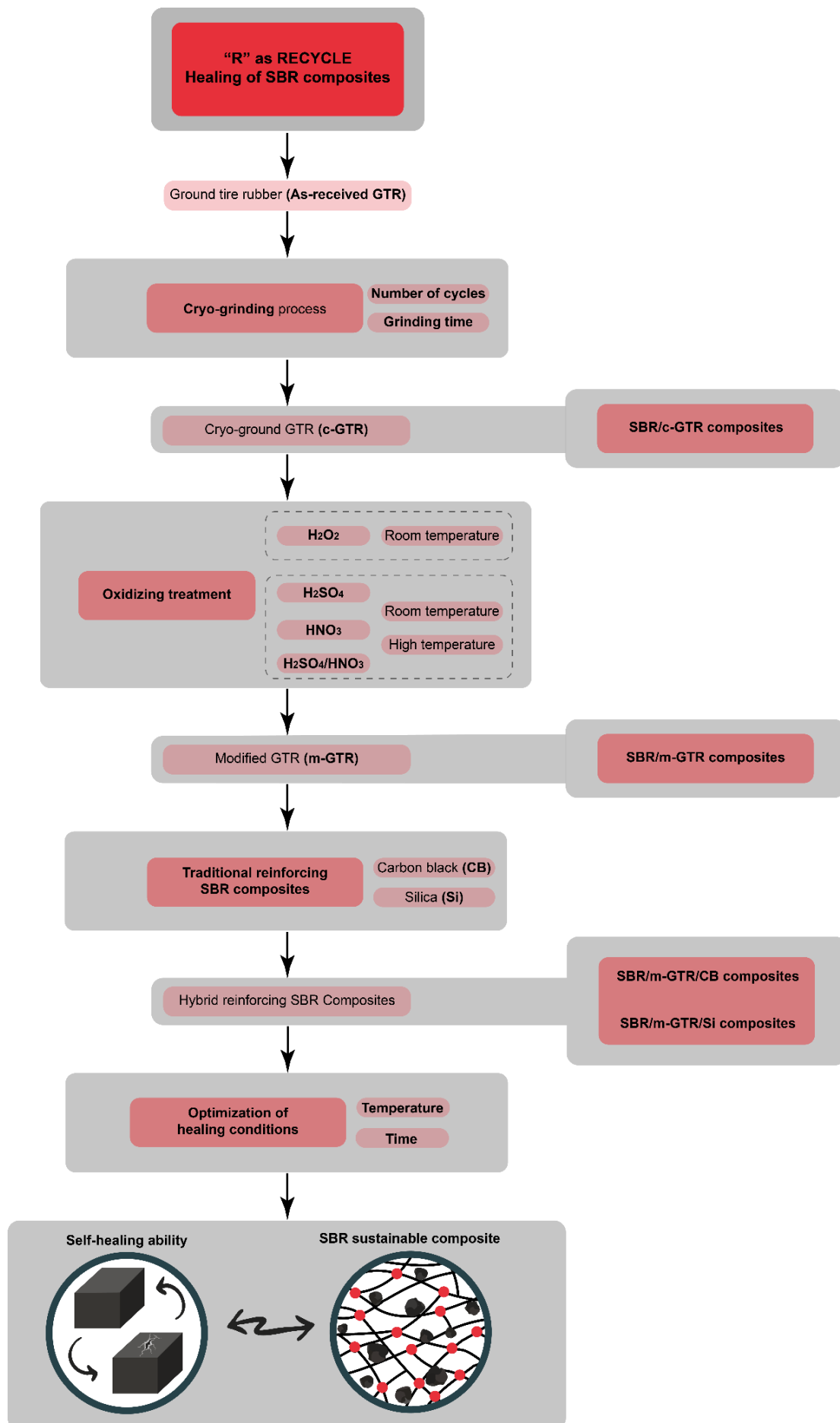


Figure 4.1. Schematic representation of Chapter 4. “R” as Recycle - Healing of SBR/GTR Composites.

4.1. Experimental

4.1.1. Grinding protocols

The as-received ground tire rubber (GTR) was pulverized under cryogenic conditions using a CryoMill (Retsch) shown in Figure 4.2. Three different grinding protocols, varying the number of cycles and grinding time (Table 4.1) were tested in order to reduce the particle size. Figure 4.3 shows the schematic representation of a cryo-grinding and cooling cycle.



Figure 4.2 CryoMill (Retsch).

Table 4.1 Grinding protocols varying number of cycles and grinding time.

Grinding protocol	Number of cycles	Grinding time (min)	Intermediate cooling (min)	Total time (min)
P ₁	18	2	1	54
P ₂	27	1	1	54
P ₃	36	0.5	1	54

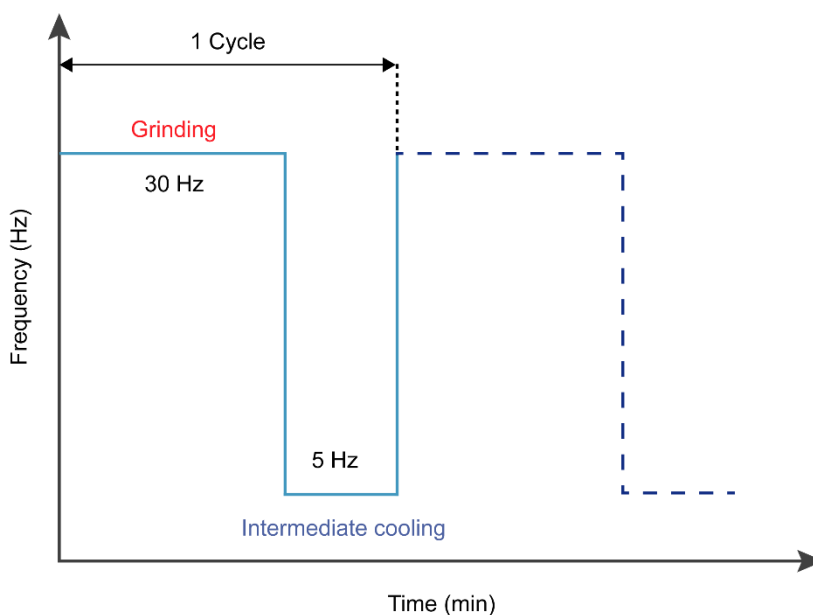


Figure 4.3 Schematic representation of grinding and cooling cycles.

4.1.2. Particle size distribution

GTR powder (~0.05 g) was previously dispersed in 20 mL of water or a water/ethanol 70/30 solution with 0.2 mL of surfactant Triton X-100. The suspension was sonicated in an ultrasound bath (Elmasonic S40H) for about 2 h. The particle size distribution was obtained by means of a laser scattering particle size distribution analyzer (Coulter LS 200). A volume standard cumulative distribution was measured under stabilized conditions. Each sample was subjected to a 60 s optical measurement.

4.1.3. Surface modification

The c-GTR (cryoground according to the optimum grinding protocol) was chemically modified with different oxidizing agents. Sulfuric acid (H_2SO_4) 95 – 98 % pure, pharma grade, and hydrogen peroxide (H_2O_2) 33 % w/v stabilized pure, pharma grade, were supplied by PanReac AppliChem (Spain). Nitric acid (HNO_3) 69 % for analysis was supplied by Emsure (Germany).

A total of 10 g of c-GTR were placed in a 1000 mL round-bottom flask in an ice bath, and then the oxidizing agent was introduced dropwise with continuous magnetic stirring until complete immersion of the GTR. The mixtures were performed at room temperature (RT) and heated to 100 °C (HT), for 3 h for the H_2SO_4 , HNO_3 , and the $\text{H}_2\text{SO}_4/\text{HNO}_3$ mixture (in a 3:1 ratio), and only at RT for H_2O_2 , in order to avoid the early decomposition of the

oxidizing agent and to guarantee the full reaction between the GTR and H_2O_2 ; all procedures utilized magnetic stirring. The modified GTR (m-GTR) was thoroughly washed with purified water at room temperature until the filtrate was colorless and of neutral pH. All the materials were dried in an oven (Digitronic) shown in Figure 4.4 at 70 °C for 24 h.



Figure 4.4. Oven (Digitronic)

4.1.4. Hydrophilicity test

GTR powder (~1 g) was mixed with 10 mL of water. The mixture was sonicated in an ultrasound bath (Elmasonic S40H) for about 10 min. Pictures were taken to analyze the dispersion and hydrophilic nature of the powder.

4.1.5. Payne effect

The filled rubber composites reinforcement is strongly dependent on the interactions between the rubber matrix and the filler, as well as the filler dispersion level in the rubber matrix. Hence, the bound rubber (the polymer chains adsorbed on the surface of a filler), and the strain dependency of the modulus is used to describe the reinforcing behavior.

Figure 4.5 shows the strain-dependence and the strain-independent contributions to the complex modulus (G^*) for filled composites. The reinforcement in filled rubber composites depends on different molecular mechanisms that contributes to the overall strength of the elastomer. The reinforcement is based on four different mechanisms: three strain-independent contributions, i) the polymer network, proportional to the cross-link density,

ii) the hydrodynamics effect, due to the mechanical obstruction to deformation by the presence of (spherical) particles in the polymer matrix, iii) the filler–rubber interactions, where the filler particle acts as poly-functional cross-link site, and parts of the rubber are immobilized in the filler structure contributes to the overall stiffness; and iv) a strain dependent contribution, from the filler–filler interactions (filler network).[1]

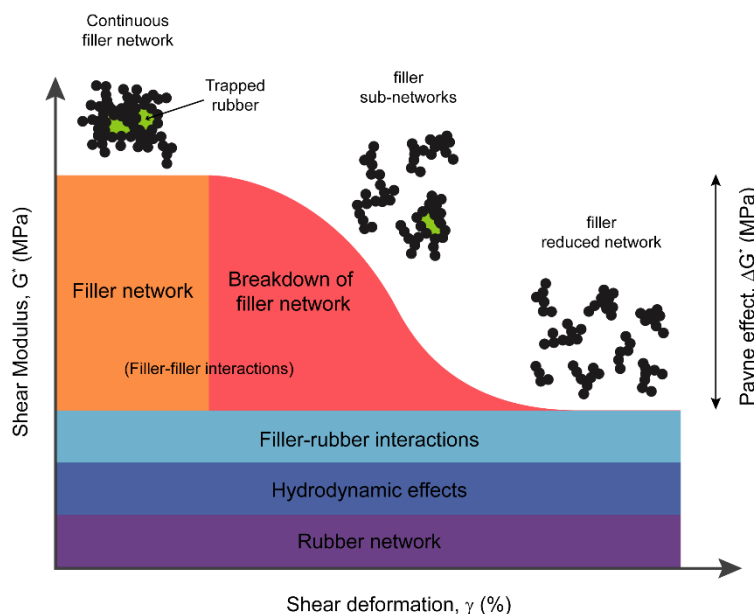


Figure 4.5 The Payne effect concept of filled rubber composites.[2]

The Payne effect consists in the decrease in the G^* of a filled, cross-linked elastomer system with increasing deformation amplitude. This decrease is explained by the continuous breakage of the weak filler–filler interactions (e.g. hydrogen bonds and Van-der-Waals interactions) in a non-linear way resulting in a drop of G^* . Simultaneously, the trapped rubber inside the filler network (occluded rubber) is released and contributes to mobility resulting in a decrease in the complex modulus. The difference between the modulus at low strains and the value at very high strains (ΔG^*), is referred to as Payne effect, and is widely used as an indicator for the filler–filler interaction. This effect is assumed to be reversible when the strain is released, provided that there is enough time for reagglomeration, and it is independent of the type of polymer.[3]

The Payne effect was performed using a Rubber Process Analyzer, (RPA 2000, Alpha Technologies) with strain sweeps from 0.28 to 79.92 %, with a frequency of 1.6 Hz, and at temperature of 60 °C. Beforehand, the samples were cured inside the measuring chamber in accordance with the determined vulcanization conditions. Two identical strain

sweeps were performed directly after each other and the second one was evaluated between a maximum G^* at 79.92 % strain and a minimum G^* at 0.28 % strain. By means of the first strain sweep, it was possible to reduce the effect of flocculation of fillers due to different storage times of the compounds.

4.2. SBR composites preparation

Rubber composites were developed according to the compositions shown in Table 4.2. The accelerant/sulfur ratio was kept fixed ($A/S=1$), as well as the proportion of ZnO and SA (5:1). Throughout this chapter, samples are named as X_y where “x” and “y” correspond to the type and amount of filler, respectively. The unfilled compound is equivalent to the SEV₁ compound previously discussed in Chapter 3.

Table 4.2 SBR composites recipes in phr, varying filler content with and without CA.

Composite	Ingredient (phr)				
	c-GTR	m-GTR	CB	Si	TESPT
Unfilled	-	-	-	-	-
Unfilled-CA	-	-	-	-	5
Sustainable filler					
c-GTR ₁₀	10	-	-	-	-
c-GTR ₂₀	20	-	-	-	-
c-GTR ₃₀	30	-	-	-	-
m-GTR ₁₀	-	10	-	-	-
m-GTR ₂₀	-	20	-	-	-
m-GTR ₃₀	-	30	-	-	-
c-GTR ₁₀ -CA	10	-	-	-	5
c-GTR ₂₀ -CA	20	-	-	-	5
c-GTR ₃₀ -CA	30	-	-	-	5
m-GTR ₁₀ -CA	-	10	-	-	5
m-GTR ₂₀ -CA	-	20	-	-	5
m-GTR ₃₀ -CA	-	30	-	-	5
Traditional reinforcing filler					
CB ₁₀	-	-	10	-	-
CB ₂₀	-	-	20	-	-
Si ₁₀ -CA	-	-	-	10	5
Si ₂₀ -CA	-	-	-	20	5
Hybrid sustainable reinforcing filler					
m-GTR ₂₀ -CB ₅	-	20	5	-	-
m-GTR ₂₀ -CB ₁₀	-	20	10	-	-
m-GTR ₂₀ -CB ₂₀	-	20	20	-	-
m-GTR ₂₀ -CB ₁₀ -CA	-	20	10	-	5
m-GTR ₂₀ -CB ₂₀ -CA	-	20	20	-	5
m-GTR ₂₀ -Si ₁₀ -CA	-	20	-	10	5
m-GTR ₂₀ -Si ₂₀ -CA	-	20	-	20	5

SBR (100 phr), ZnO (5 phr), SA (1 phr), CBS (1 phr), S (1 phr) are common to all composites.

4.3. Modification and characterization of GTR

4.3.1. As-received GTR

Four different batches of as-received ground tire rubber (GTR) obtained by ambient grinding of used tires (combination of passenger car and truck tires of unknown composition) with different particle size were supplied by Signus. As can be seen in Table 4.3, all batches have very similar density values and glass transition temperature (T_g), as calculated by DSC.

Table 4.3 Physical properties of as-received GTR batches.

As-received GTR	Average particle size * (mm)	Density (g/cm ³)	T_g (°C)
GTR ₀	< 0.8	1.12 ± 0.01	-57
GTR ₁	0.8 – 2	1.12 ± 0.01	-56
GTR ₂	2 – 4	1.11 ± 0.01	-57
GTR ₃	4 – 8	1.12 ± 0.01	-58

*Value reported by the supplier.

TGA analysis was done to quantify the relative ratios of rubbers, carbon black and ash present in GTR. One can assume that GTR batches were composed of various blends of NR, SBR and BR as the major polymeric components. Other additives expected to be present (e.g. zinc oxide, stearic acid, accelerant and sulfur), typically included in a tire compound, were not considered. Weight losses at the temperatures of degradation of the rubbers, carbon black and char residue are listed in Table 4.4 and a representative TGA/dTGA curve is shown in Figure 4.6.

Table 4.4 % weight loss and degradation temperature (T_d) of as received GTR batches.

As-received GTR	Initial loss (%)	NR		SBR/BR		CB		Char residue (%)
		(%)	T_d (°C)	(%)	T_d (°C)	(%)	T_d (°C)	
GTR ₀	5	34	403	25	418	30	659	5
GTR ₁	5	35	403	24	421	30	662	6
GTR ₂	5	36	403	24	424	31	663	5
GTR ₃	5	32	403	29	416	31	659	5

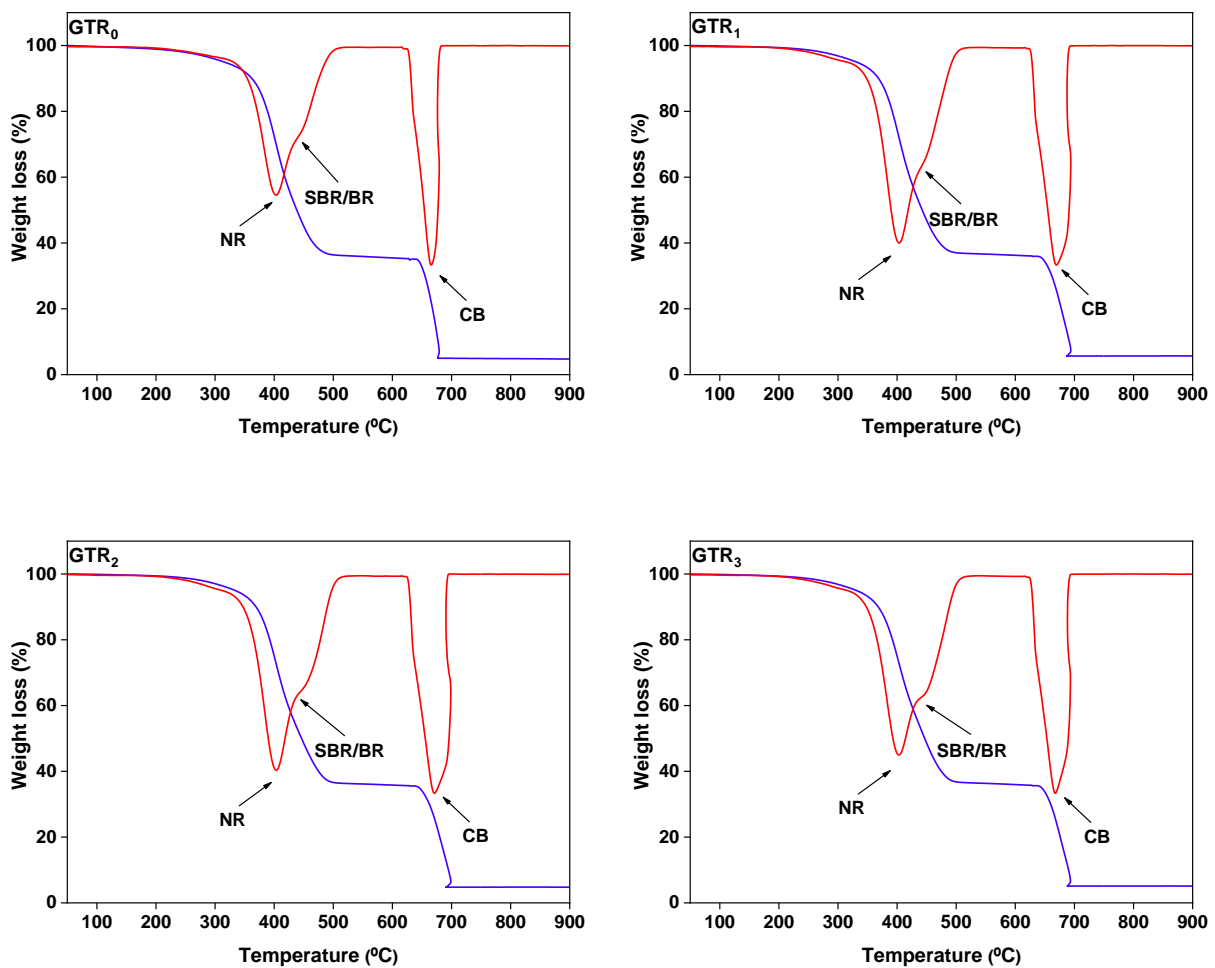


Figure 4.6 TGA/dTGA curves of as received GTR batches.

Major areas of weight loss are observed between 300 and 500 °C in all the samples. These losses took place in an inert atmosphere, suggesting the presence of two rubber matrices. The first peak, starting at around 330 °C, is ascribed to NR while the second peak, starting around 420 °C, can be ascribed to either SBR, BR or a mixture of the two.[4,

5] The third weight loss above 620 °C, in presence of oxygen, is due to carbon black. The weight percentages of the rubbers were converted into phr (parts per hundred parts of rubber) as usually expressed in the rubber industry (see Table 4.5).

Table 4.5 TGA results showing rubber compound composition expressed in phr.

As-received GTR	NR	SBR/BR	CB
GTR ₀	58	42	51
GTR ₁	59	41	51
GTR ₂	60	40	52
GTR ₃	52	48	50

The composition of all the samples studied here seems very similar, independently of the batch: 57 phr NR, 43 phr SBR/BR and 51 phr CB, in average. ATR FT-IR studies were also done as shown in Figure 4.7.

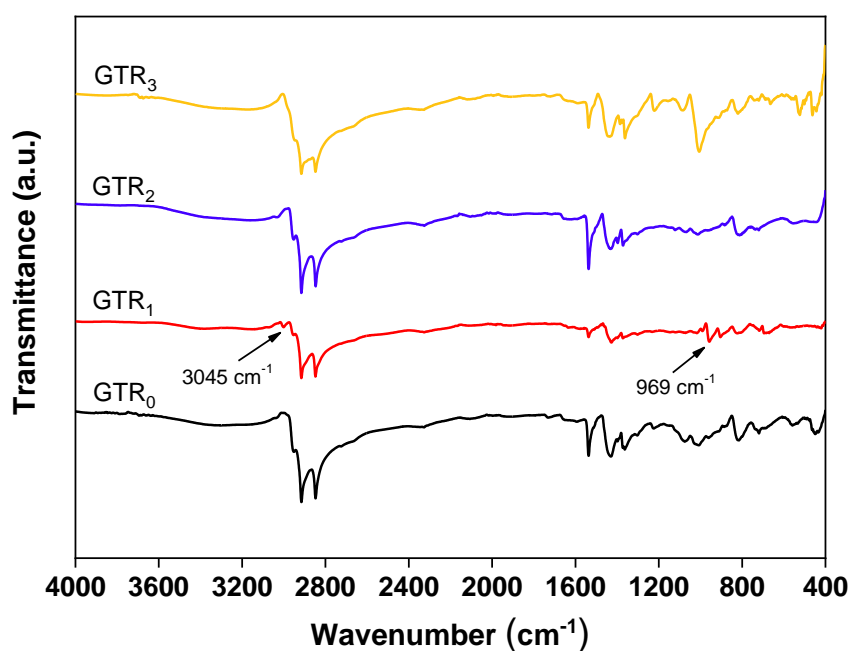


Figure 4.7 ATR FT-IR spectra of different as-received GTR batches.

As expected, all four spectra look very similar. A slight difference could be seen in the spectrum of GTR₁, since two characteristics peaks of SBR appear (the C–CH₂ stretching from trans-butadiene comonomer at 969 cm⁻¹ and the aromatic C–H stretching from

styrene comonomer at 3045 cm^{-1}). The fact that all 4 batches of GTR (coming from 4 different random sources) have similar properties is a promising result for the recycling and reuse of discarded tires. More than the chemical nature of GTR what seems to govern the final properties, as will be discussed next, is the good interaction and compatibility between the rubber powder and a selected matrix. From the 4 batches analyzed, GTR1 was selected as the GTR to be included as alternative filler in SBR compounds.

4.3.2. Cryo-grinding of GTR

As seen in Figure 4.8 and Table 4.6, all of the cryo-grinding protocols used significantly reduce the average particle size of as-received GTR, decreasing it from $1000\ \mu\text{m}$ to $100 - 150\ \mu\text{m}$. Although there does not seem to be a considerable difference between the 3 protocols, P₁ gives a narrower particle size distribution. Hence, P₁ protocol was selected as the optimized cryo-grinding method.

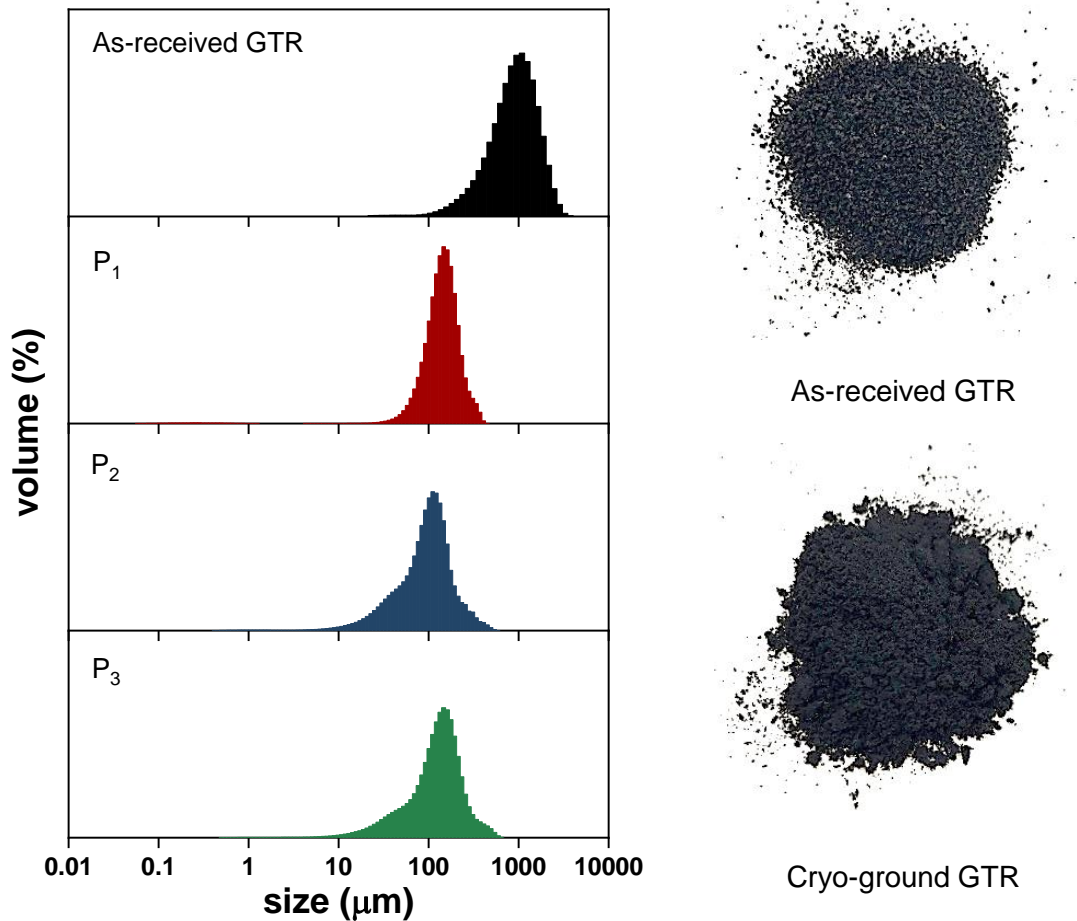


Figure 4.8 Particle size distribution of as-received and cryo-ground GTR according to different grinding protocols.

Table 4.6. Average particle size and diameter on cumulative % of as-received and cryo-ground GTR (c-GTR) according to different grinding protocols.

Grinding protocol	Average particle size (μm)	Diameter on cumulative percentage (μm)		
		10	50	90
As-received	1043	288	744	1439
P ₁	154	81	145	236
P ₂	115	33	99	171
P ₃	147	42	135	254

4.3.3. Surface modification of GTR

The chemical modification of c-GTR reduces the average particle size, especially for the oxidizing treatments with H_2SO_4 , HNO_3 and their mixture, as seen in Figure 4.9 and Table

4.7. In addition, the particle size distribution becomes wider, as a possible evidence of irregular surface modification.

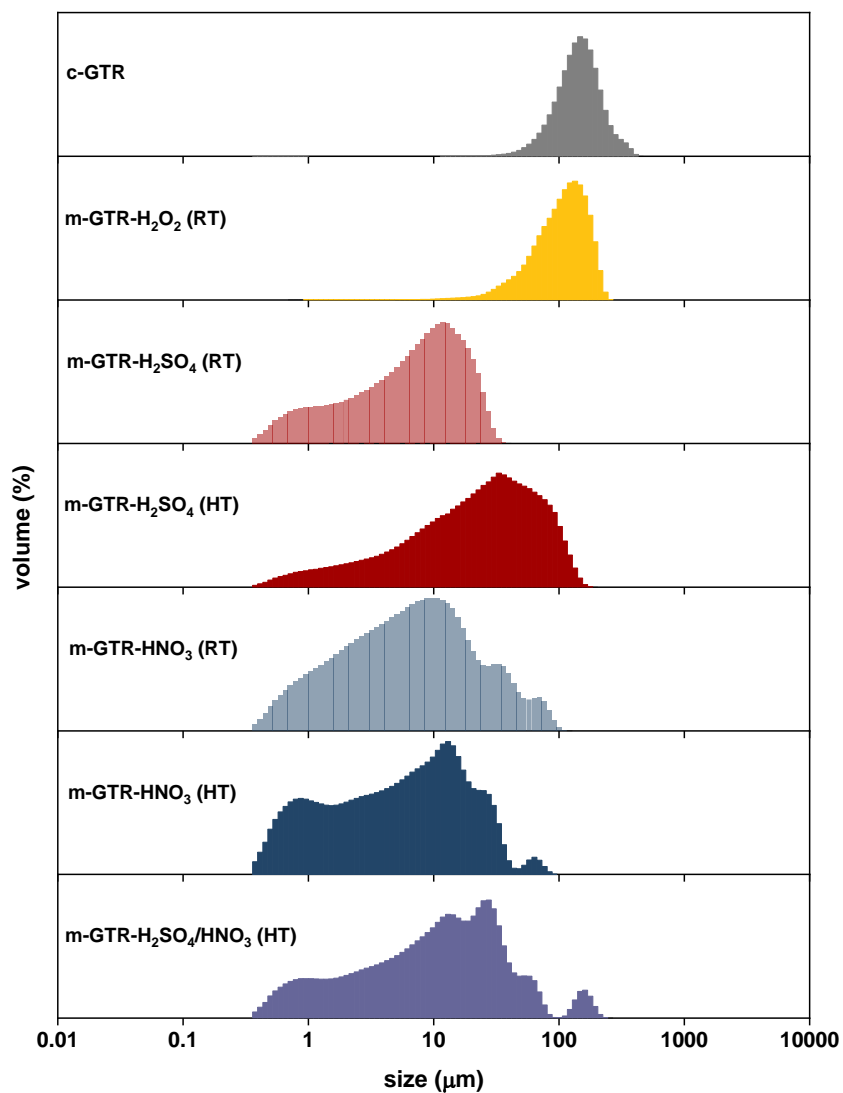


Figure 4.9 Particle size distribution of cryo-ground GTR and chemically modified GTR (m-GTR).

Table 4.7 Average particle size and diameter on cumulative % of c-GTR and chemically modified GTR (m-GTR).

	Average particle size (μm)	Diameter on cumulative % (μm)		
		10	50	90
c-GTR	154	81	145	236
m-GTR-H ₂ O ₂ (RT)	115	50	113	184
m-GTR-H ₂ SO ₄ (RT)	9	1	8	20
m-GTR-H ₂ SO ₄ (HT)	19	9	18	30
m-GTR-HNO ₃ (RT)	13	1	7	34
m-GTR-HNO ₃ (HT)	10	7	10	12
m-GTR-H ₂ SO ₄ /HNO ₃ (HT)	21	14	20	28

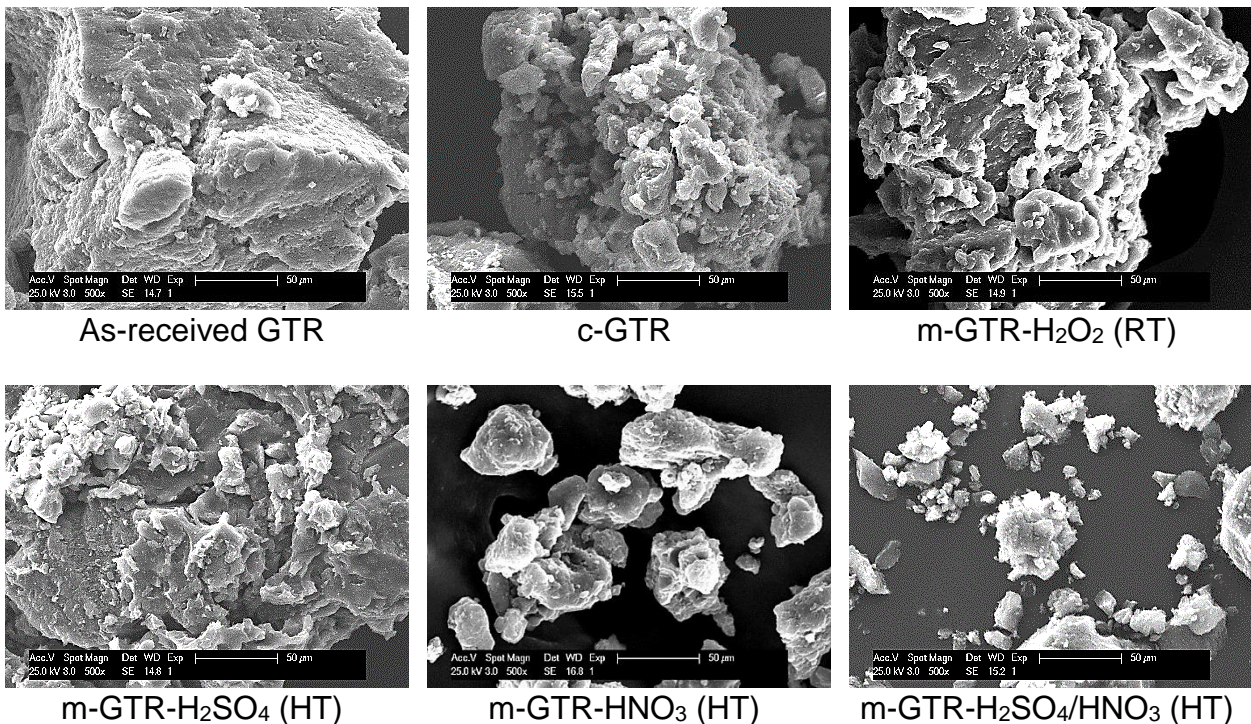


Figure 4.10 Scanning electron microscope (SEM) micrographs of c-GTR and modified GTR (m-GTR) with different treatments at a magnification of 500x.

Figure 4.10 shows SEM micrographs of the surface of all GTR samples at 500x magnification. As-received GTR shows a large, cracked and irregular surface with a rough texture, which is characteristic of tire powders ground under ambient temperature conditions.[6] The cryo-grinding process generates a different morphology showing a smoother fracture surface due to the brittle failure mechanism. Moreover, the cryo-ground

GTR (c-GTR) presents a smaller particle size that is homogeneously distributed.[7] Microcavities and micropores are seen in the modified GTR (m-GTR). These irregularities can be considered as the result of the strong attack of oxidizing agents, which are able to degrade and remove some chemical components of the GTR particles, such as additives and waxes. Also, some sphere-shaped particles are observed at the surface of the treated GTR, which may be zinc oxide (ZnO), silica (Si), or carbon black (CB) added to the tire formulation.[6] As an illustrative example, Figure 4.11 shows the EDX elemental mapping of m-GTR-H₂SO₄ (HT) with uniformly distributed C, O, S, and Zn. Furthermore, it can be inferred that the major proportion of spherical particles corresponds to Si. As it will be discussed in the next section, the new morphology of m-GTR may improve the interfacial adhesion with the SBR matrix and, thus, its dispersion, since the formation of microcavities and pores could significantly increase the surface area and, therefore, its interfacial contact with the matrix.[8, 9]

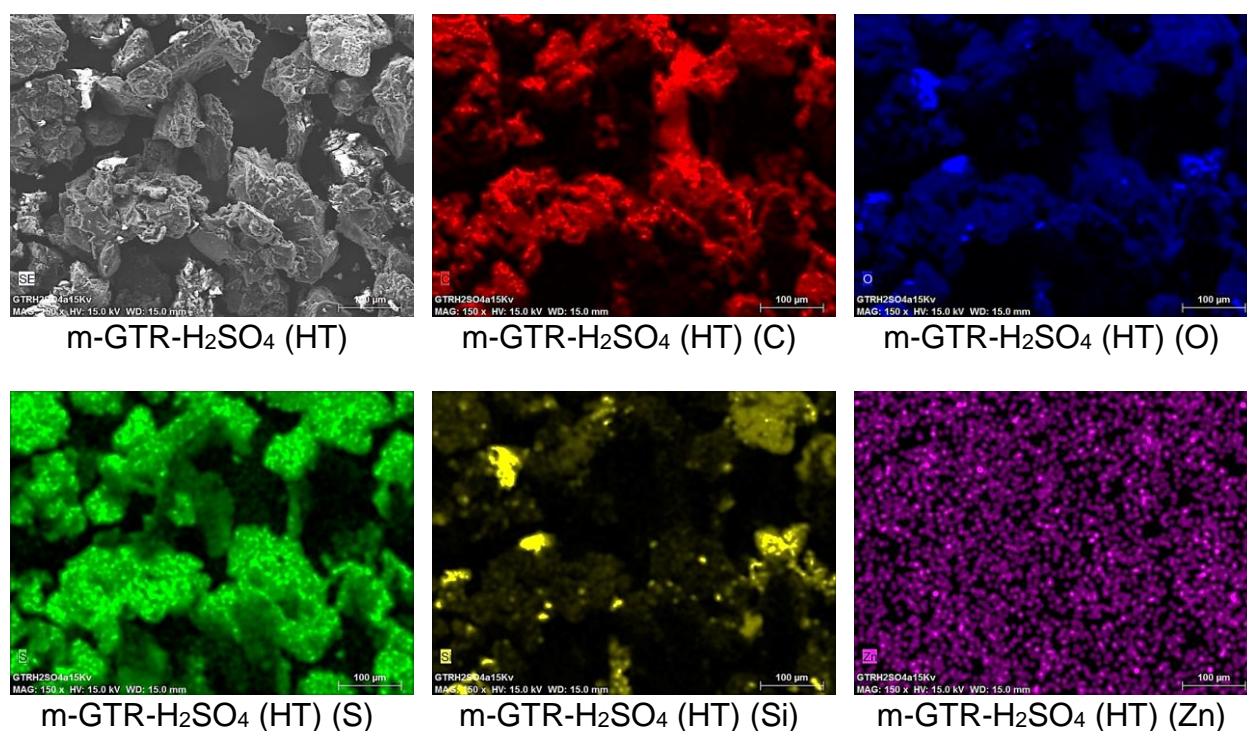


Figure 4.11 EDX elemental mapping of m-GTR sample treated with H₂SO₄ at a magnification of 150X.

FTIR analysis was used to analyze the structure and functional groups present in the m-GTR and to compare the effects of the different oxidizing treatments. Figure 4.12 shows the respective characteristic vibrations before and after the chemical treatments. As-received and c-GTR show signals at 2920 and 2850 cm⁻¹ that are ascribed to the

stretching of C–H. After the chemical treatments, these bands decrease in intensity and new absorption bands are detected; –C=C– at 1640 cm^{-1} and carbonyl groups (–C=O) at 1720 cm^{-1} . The presence of these carbonyl groups is frequently correlated to hydroxyl groups (–OH). The characteristic broad absorption band at 3440 cm^{-1} , corresponding to the stretching vibration of –OH group, results from the oxidation processes, showing a more intense signal when GTR is treated with H_2SO_4 and HNO_3 (RT and HT). A strong band corresponding to C–O stretching is also observed at 1100 cm^{-1} for the m-GTR chemically treated with HNO_3 (RT). Additionally, in the case of the $\text{H}_2\text{SO}_4/\text{HNO}_3$ (HT) treatment, two peaks in the $1000 - 1200\text{ cm}^{-1}$ region are indicative of the O=S=O stretching.[6] These new chemical groups grafted onto the surface of m-GTR could improve the interfacial adhesion with different polymer matrices. These functional groups rise the polarity on the surface of the GTR and, therefore, may increase its reinforcing efficiency due to potential chemical reactions with other suitable functional groups present in the reaction medium.[10] These findings also fit well with the results from the hydrophilicity test, as follows.

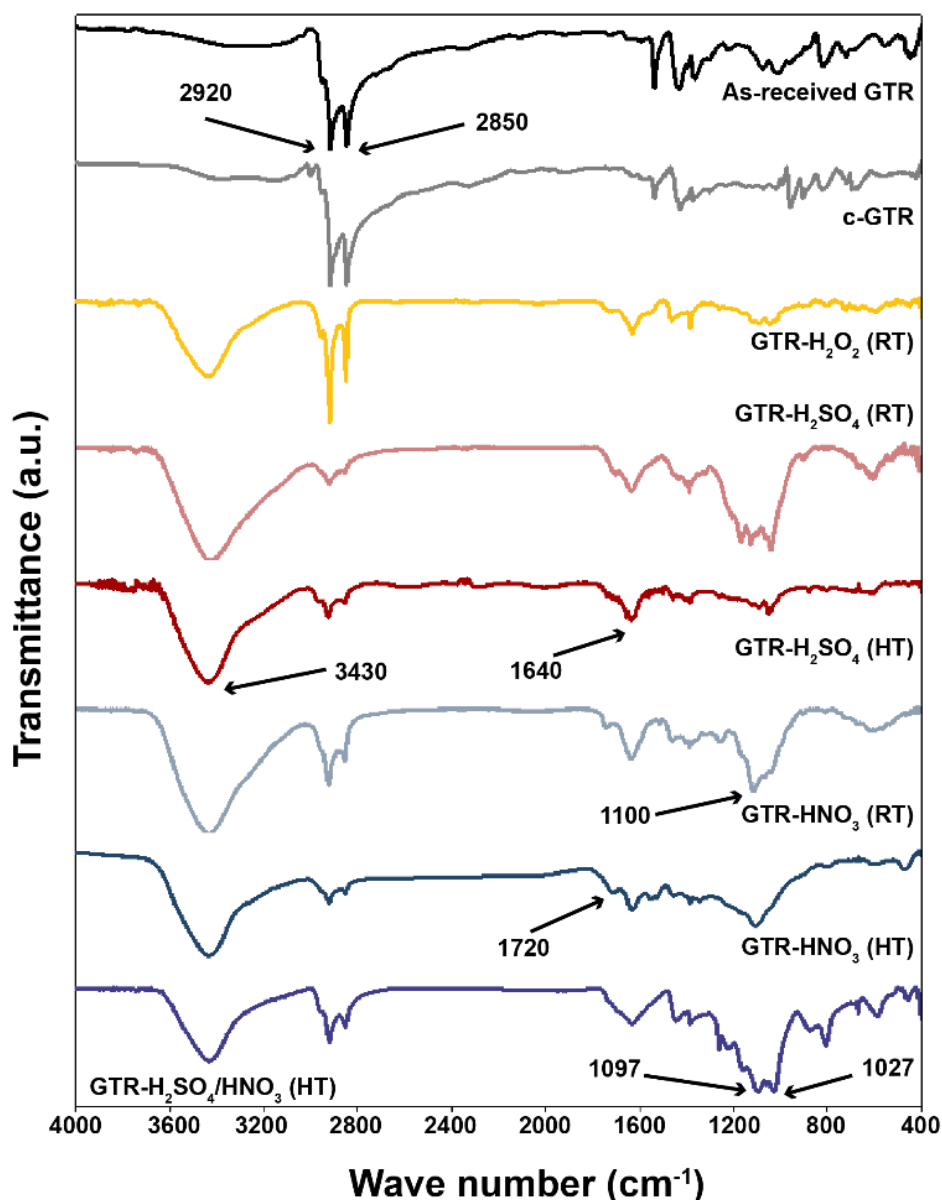


Figure 4.12 FT-IR spectra of as-received, cryground (GTR Cryo) and chemically treated GTR.

Figure 4.13 shows that the as-received, cryo-ground, and H₂O₂ modified GTR are completely hydrophobic, evidenced by their unstable suspension in the water. This can be attributed to the non-polar nature of the untreated GTR, which prevents its interaction with water. After the chemical modification with H₂SO₄, HNO₃, and H₂SO₄/HNO₃, m-GTR disperses uniformly in the water, corroborating the compatibility between the treated GTR and the aqueous medium. The chemical treatment induced a polarity on the surface of the m-GTR that enabled electrostatic interactions with the water. Similar effects have been observed in GTR powder modified through plasma treatment.[11, 12]



Figure 4.13 Hydrophilic behavior of a) as-received, b) c-GTR, c) m-GTR- H_2O_2 (RT), d) m-GTR- H_2SO_4 (RT), e) m-GTR- H_2SO_4 (HT), f) m-GTR- HNO_3 (RT), g) m-GTR- HNO_3 (HT), and h) m-GTR- H_2SO_4/HNO_3 (HT) modified GTR.

XPS analysis was used to analyze the GTR surface after the chemical treatments. Figure 4.14 shows the C 1s, O 1s and S 2p core spectra of unmodified and chemically modified GTR. The C 1s core spectra of as-received GTR and c-GTR show peaks at 284.5 eV (C=C) and 285 eV (C-H) and a very small peak at 286.5 eV (C-OH). The main component at 285 eV is the result of the similarity of carbon surroundings, which remained practically unaltered. [13, 14] This suggests that most of the carbon atoms are of the same nature. After being chemically treated, GTR- H_2SO_4 shows a shift of the C 1s excitation to higher energy due to the presence of oxygen-containing groups.[13] This spectrum is representative of all chemical treatments as they all present the same trend. Two new peaks appear at 287.6 and 288.9 eV binding energies, which can be assigned to the C=O and HO-C=O species, respectively, on the CB surface and/or on polymer chains generated by oxidation during the chemical treatments[13] The C-H bonds of GTR are disrupted, resulting in the dehydrogenation and generation of free radicals. Due to their reactive nature, these radicals can react with oxygen and water in the atmosphere to form peroxide and hydroxyl peroxide species. The introduction of the oxygen-containing polar functional groups onto the GTR surfaces corresponded to the increase in surface energy.[11]

The O 1s core spectra can be deconvoluted into two peaks, showing the combination of oxygen and carbon with both double (O=C) and single (O-C) bonds, at 530 eV and at 532.4 eV, respectively. In all cases, the peak height of O 1s increases after the oxidizing treatment. From these results, it can be confirmed that the GTR surface was successfully modified with oxygen. Meanwhile, the S 2p core spectra reveals peaks at 162.3 eV, 164 eV, 165.7 eV and 169.2 eV, corresponding to S-C, S-S and S-O groups and sulfate compounds, respectively. The cryo-grinding process shows a reduction on the peak area of the S-C and S-S groups and the appearance of the S-O peak. After chemical treatments with the different acids, the S-C bond disappears; meanwhile, the intensity of the S-O and sulfate compounds peaks slightly increased. These observations

demonstrate that the cross-linked sulfur bonds have been partially destroyed during the mechano-chemical modification of GTR to form free chains in the unbound state, and then these active chains converted to sulfate or oxidation products. This could contribute to an increase in oxygen content in m-GTR particles.[15]

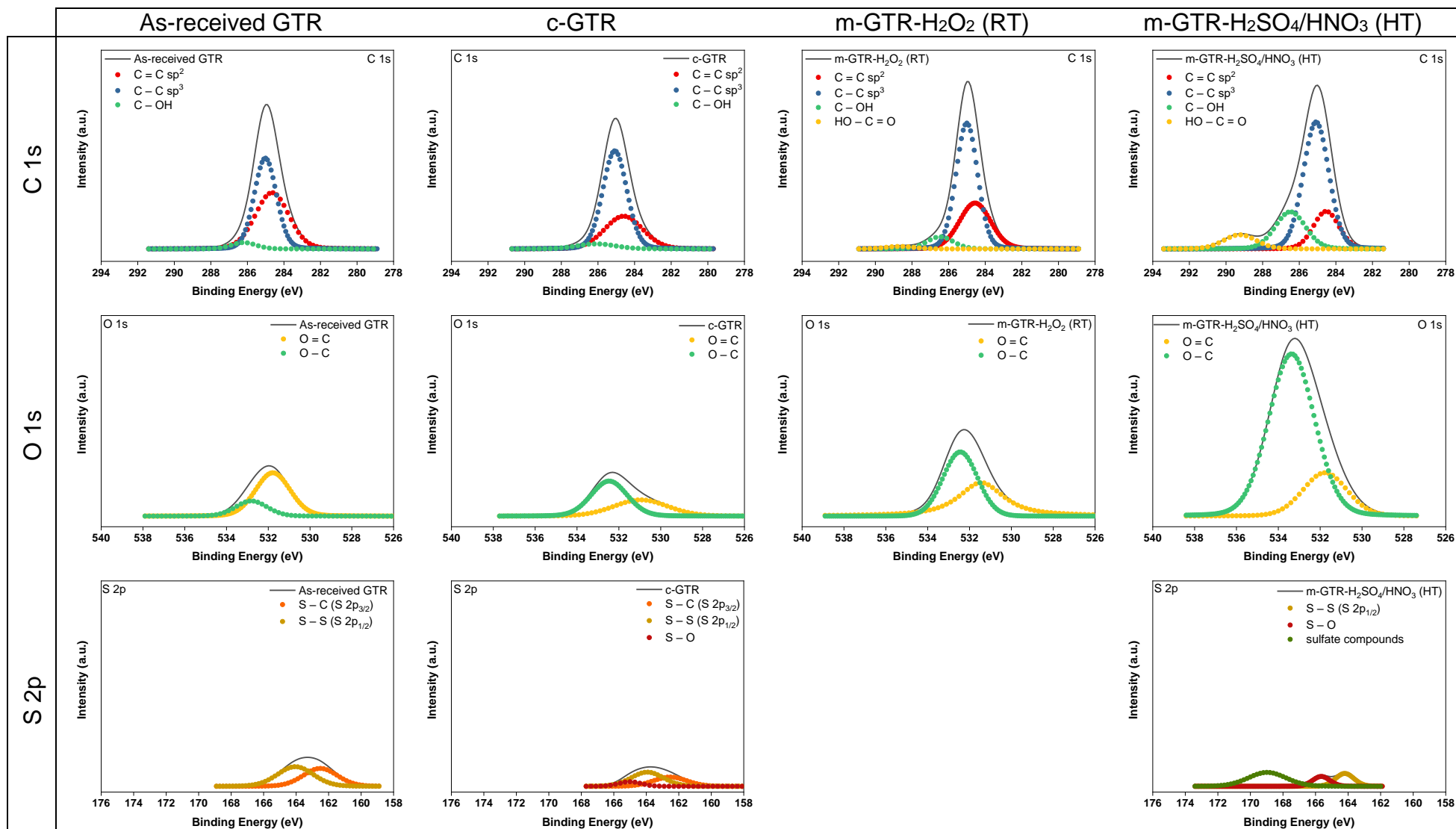


Figure 4.14 C 1s, O 1s and S 2p core spectra of unmodified and chemically modified GTR.

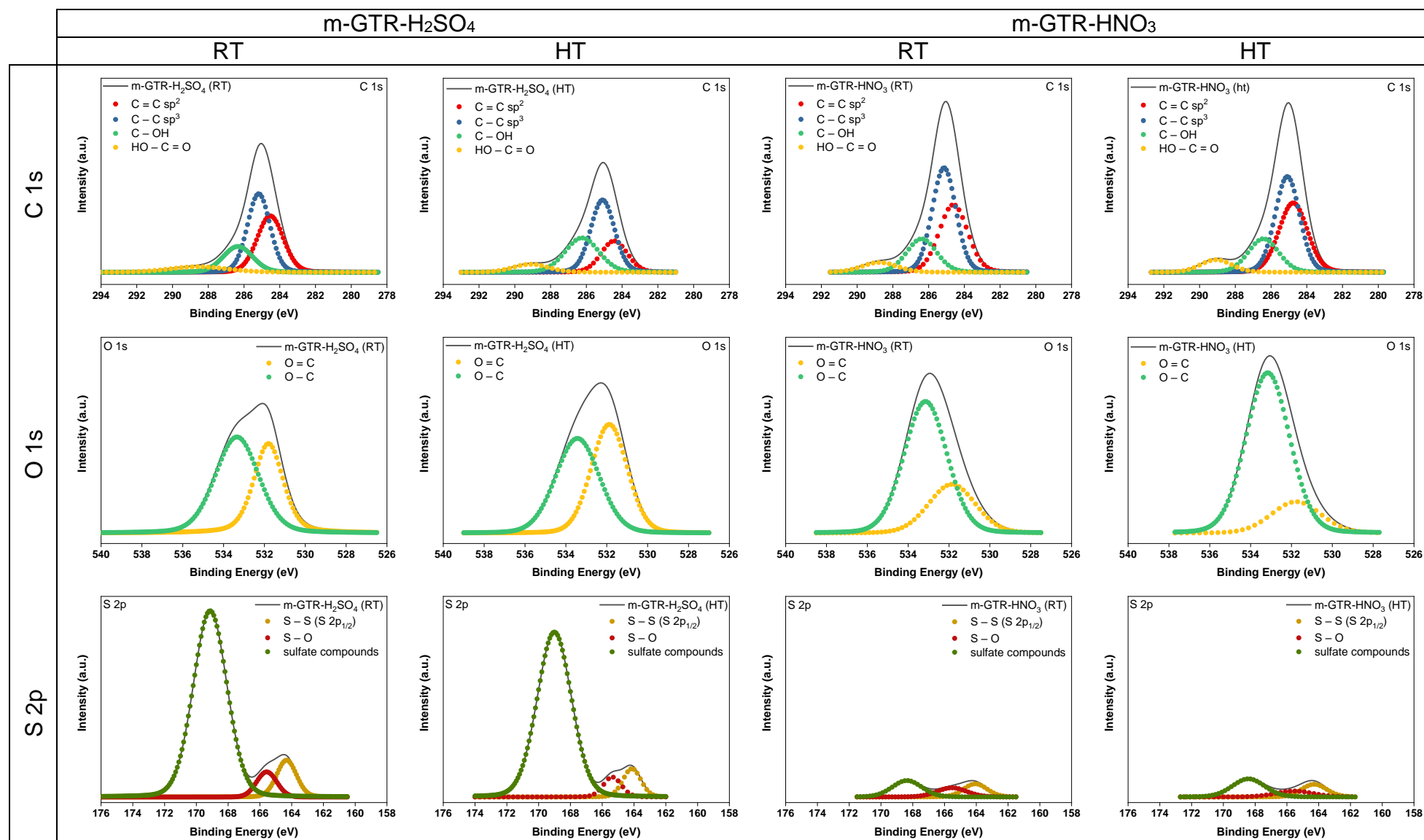


Figure 4.14 C 1s, O 1s and S 2p core spectra of unmodified and chemically modified GTR. (continue)

The surface composition determined through the XPS of the as-received GTR, c-GTR and after chemical treatment is summarized in Table 4.8. S, O, Si, and N elements are present in different amounts depending on the chemical modification. The as-received and c-GTR show subtle changes in their composition. The existence of a lower amount of O in as-received GTR and in c-GTR would be reasonable due to carbonate additives and metal oxides; moreover, the presence of O in modified samples is directly related to the various oxidation treatments.

The O content on the surface of all the chemically treated GTR rises due to the oxidation processes, increasing by 3.53, 9.58, 10.59, 11.76, 11.76, and 15.08 % for H₂O₂ (RT), HNO₃ (RT), HNO₃ (HT), H₂SO₄/HNO₃ (HT), H₂SO₄ (RT), and H₂SO₄ (HT) treatment, respectively, compared to c-GTR. In addition, it can be inferred that the S contribution comes from the vulcanization system and in higher proportion from the H₂SO₄ treatment. However, the m-GTR-H₂O₂ (RT) does not show the S content (derived from GTR) as would be expected. No significant change in silicon (Si) content can be observed. Moreover, the O/C ratio increases with the oxidation process, which might be indicative of increasing –OH groups on the material surface. This proven oxidation reaction occurs between the oxidizing agents and the surface molecules in GTR, introducing oxygen onto the GTR surface. The ratio of O/C increased to 0.133, 0.215, 0.233, 0.251, 0.259 and 0.315 for H₂O₂ (RT), HNO₃ (RT), HNO₃ (HT) H₂SO₄/HNO₃ (HT), H₂SO₄ (RT), and H₂SO₄ (HT) treatment, respectively.

To further confirm the modification of GTR, EDX was used as an analytical method for determining the element composition. According to the results compiled in Table 4.8, all samples contain C, O, Si, S, Fe and Zn. As-received GTR, c-GTR and GTR modified with H₂O₂ have the same composition. Despite the slight variation in the case of the modification carried out by H₂SO₄/HNO₃, the same trend is observed by means of the two techniques (XPS and EDX). After the chemical treatment, the content in O increases due to the oxidation reaction, with the GTR modified with H₂SO₄ (HT) presenting the greatest proportion of oxygen. Thus, this filler (m-GTR-H₂SO₄) was selected for further research, adding it to SBR compounds, as discussed in the following section.

Table 4.8 Analysis of GTR samples by X-ray photoelectron (XPS) (surface relative element content and EDX spectroscopy).

	As-received GTR	c- GTR	m-GTR- H ₂ O ₂ (RT)	m-GTR- H ₂ SO ₄ (RT)	m-GTR- H ₂ SO ₄ (HT)	m-GTR- HNO ₃ (RT)	m-GTR- HNO ₃ (HT)	m-GTR- H ₂ SO ₄ /HNO ₃ (HT)
XPS Analysis								
Element	Normalized Content (%)							
C	91.12	90.19	86.13	75.91	73.02	81.44	79.61	78.31
O	6.95	7.93	11.46	19.69	23.01	17.51	18.52	19.69
S	0.67	0.47	-	2.97	2.70	0.26	0.35	2.97
Si	1.25	1.41	2.40	1.43	1.28	0.79	1.51	1.43
O/C	0.076	0.088	0.133	0.259	0.315	0.215	0.233	0.251
EDX Analysis								
Element	Normalized Content (wt %)							
C	82.97	81.58	82.71	77.55	68.88	72.78	79.39	85.58
O	8.71	10.08	10.64	14.75	21.82	20.8	16.30	11.56
S	1.95	1.68	1.56	6.44	7.26	0.81	0.75	0.67
Si	1.21	0.73	1.08	1.08	1.62	3.34	3.23	1.94
Mg	0.06	0.10	0.05	0.02	0.02	0.07	0.03	0.06
Al	0.18	0.12	0.14	0.06	0.10	0.18	0.12	0.18
Ca	0.55	0.25	0.06	0.01	0.04	0	0.01	0
Fe	1.59	2.60	1.63	0.08	0.09	0.13	0.15	0.01
Zn	2.78	2.86	2.13	0.01	0.17	0.06	0.02	0

4.4. Development of SBR/GTR composites

4.4.1. Characterization of SBR/GTR composites

Rheometric properties

Figure 4.15 shows the vulcanization curves of the SBR composites filled with c-GTR and m-GTR with and without silane coupling agent (CA). The most notorious characteristic is revealed by the m-GTR composites (without CA) presenting a marching modulus behavior. This behavior is characterized by a continue increase of the torque. However, with the addition of the CA, the characteristic marching modulus of SBR-m-GTR composites disappears. Furthermore, the addition of the CA to the SBR-GTR composites show a higher torque, directly associated to a higher level of cross-links.

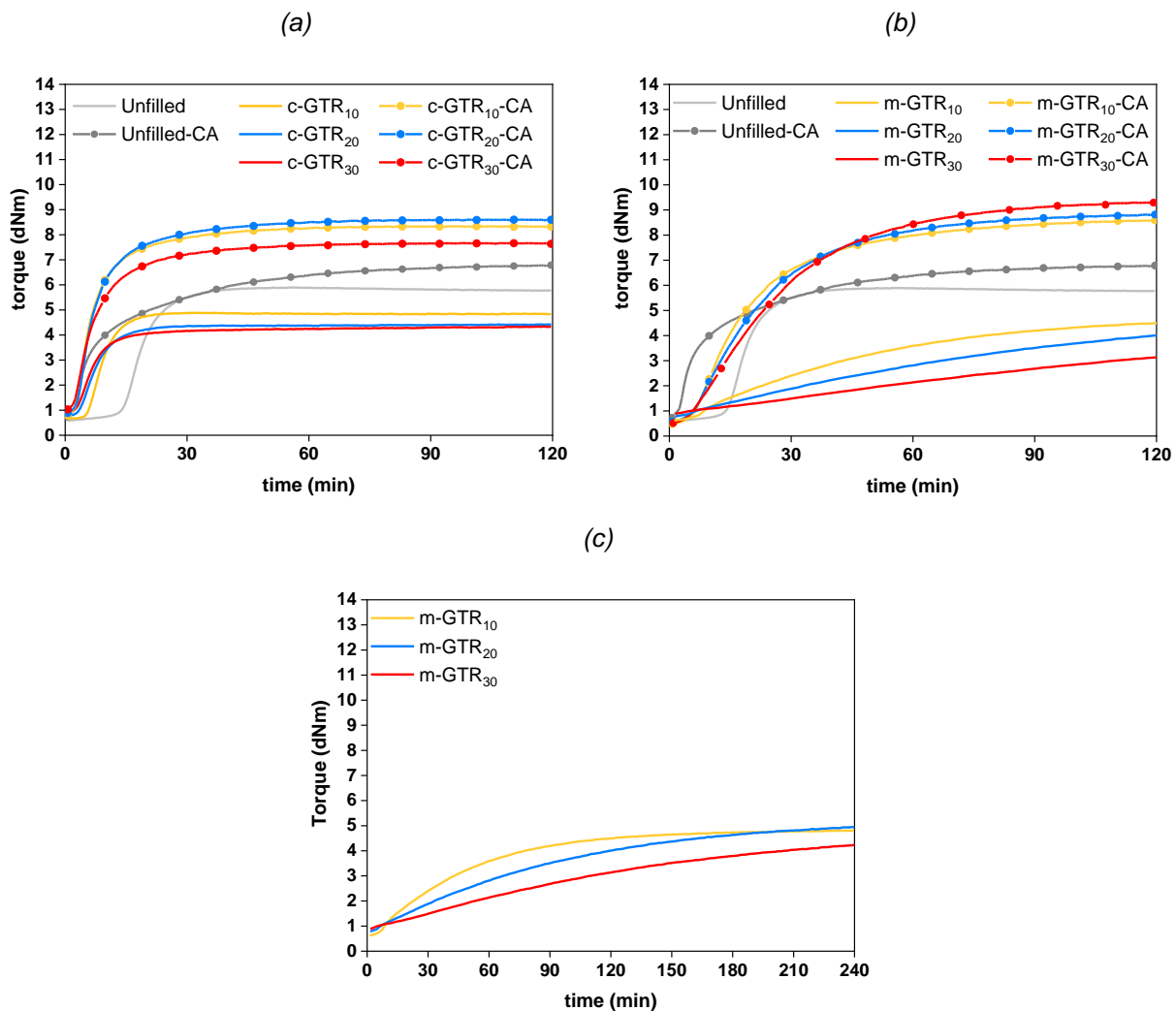


Figure 4.15 Rheometric curves of (a) SBR/c-GTR, (b) SBR/m-GTR composites with and without coupling agent (CA) recorded at 160 °C. (c) Prolongation in time of the m-GTR composite marching curve.

The effect of c-GTR and m-GTR on the vulcanization parameters can be analyzed from the values shown in Table 4.9. M_L slightly increases with increasing c-GTR and m-GTR content, indicating that the filler hinders the compound processing. This behavior may be associated with the agglomeration of tire waste particles in the matrix. A drop in M_H , as well as in ΔM , is also seen. Such trend can be attributed to the migration of sulfur from the elastomeric matrix towards the vulcanized GTR particles, resulting in a lower cross-linking degree.[16] Meanwhile, unreacted cross-linking precursor fragments (accelerants and activators) in the vulcanized waste can migrate towards the virgin matrix. Hence, t_{s2} and t_{90} decrease with the increase in c-GTR content, indicating that the cross-linking reactions start earlier. Similar behavior has been reported by other authors, confirming the effect of the curatives on the rheometric properties of rubber matrices filled with GTR.[16-18] Furthermore, it is possible that for higher filler content, at constant weight of curatives, the amount of curatives per unit volume of rubber decreases. Hence, the curatives diffusion rate within the matrix decreases, resulting in an increase in t_{90} .[19]

Table 4.9 Rheometric properties of SBR-c-GTR and SBR-m-GTR composites.

Composite	M_L (dNm)	M_H (dNm)	ΔM (dNm)	t_{s2} (min)	t_{90} (min)
Unfilled	0.7	5.8	5.1	17	27
Unfilled-CA	0.5	7.2	6.7	5	42
Sustainable filler					
c-GTR ₁₀	0.6	4.9	4.3	9	15
c-GTR ₂₀	0.8	4.4	3.6	8	16
c-GTR ₃₀	1	4.4	3.4	8	18
c-GTR ₁₀ -CA	0.8	8.4	7.6	4	22
c-GTR ₂₀ -CA	0.9	8.7	7.8	5	24
c-GTR ₃₀ -CA	1	7.7	6.7	4	24
m-GTR ₁₀	0.6	3.6	3	34	52
m-GTR ₂₀	0.8	3.8	3	57	82
m-GTR ₃₀	0.9	3.9	3	100	136
m-GTR ₁₀ -CA	0.5	8.6	8.1	10	52
m-GTR ₂₀ -CA	0.6	8.8	8.2	11	54
m-GTR ₃₀ -CA	0.5	9.4	8.9	12	62

On the contrary, t_{s2} increases for the composites filled with m-GTR due to the characteristic marching modulus behavior. An analogous behavior can be seen in silica-filled composites. The adsorption of the accelerant (CBS) on the silica surface can explain the slower cure characteristics.[18] The high content of acid hydroxyl groups can easily form hydrogen bonds between polar materials, especially basic organics, and silica. Moreover, the sulfur linkages and amine group of CBS can form hydrogen bonds with the hydroxyl groups of silica. This can weaken the strength of the N–S bonds of CBS and accelerate their dissociation. This effect is more pronounced with higher silica content. Therefore, the increased adsorption of CBS can explain the slower cure characteristics. In a similar way, the m-GTR particle surface is acidic, due to the presence of hydroxyl groups. Some of the amine accelerants and Zn complex could bond to the hydroxyl groups on the surface of the m-GTR and, thus, resulting in a deactivating effect.[20]

In an attempt to fix a realistic curing time and limit the marching trend of the m-GTR filled composites, ΔM was established as a fixed parameter. M_H , t_{s2} and t_{90} shown in Table 4.9 are associated with this value. It is well known that ΔM can be considered as an indirect measure of the cross-link density of a rubber composite. Nonetheless, different cross-link values were obtained for the three m-GTR filled composites. This unexpected behavior can be ascribed to the uncontrolled migration of sulfur from the SBR matrix to the m-GTR reducing the cross-link density. This effect is more notorious with the increment in the chemically modified GTR content. Hence, it is challenging to control the cross-link density in rubber composites filled with chemically modified GTR (m-GTR).

Regarding the CA, it has a plasticizing effect at the early stages of the vulcanization reducing the viscosity of the unfilled compound and m-GTR composites, expressed as a decrease in M_L as shown in Table 4.9. An increase in M_H and in ΔM is also observed, indicating a relatively more restrained matrix resulting from the improved interaction between the blend components. This improvement is attributed to the fact that TESPT contains 4 sulfur atoms on its molecule acting as accelerant and sulfur donor to the rubber compound.[21] Besides, the silane coupling agent is a bifunctional compound composed of two functionally active end groups, i.e., the readily hydrolysable alkoxy group and the organo-functional group. The latter, which is relatively non-polar, is more compatible with rubbers and also can participate in the sulfur vulcanization to form chemical linkages with the rubber matrix. The homolytic cleavage of S–S bonds of TESPT takes place forming free radicals at the curing temperature. These radicals may then combine with rubber chains and free sulfur.

Adding CA also reduces t_{s2} , demonstrating the accelerating effect of the coupling agent on the onset of vulcanization.[20, 22, 23] This effect is more notorious in presence of m-GTR; the alkoxy groups of the CA would react with the hydroxyl groups on the m-GTR surface during mixing. The faster cure rate suggests that the deactivation of the accelerant molecules is avoided. In addition, the organo-groups of TESPT could chemically react with the butadiene phase of SBR, favoring rubber–filler interactions, with the subsequent stabilization of the marching modulus.[22] These rubber–filler interactions are corroborated by the analysis of Payne effect. Payne effect reflects the agglomeration tendency and the reinforcing activity of a given filler.[2, 24] After adding the filler, the low strain modulus, G_0 , rises more than the high strain modulus, G_∞ , resulting in a non-linear viscoelastic behavior, known as Payne effect ($G'_0 - G'_\infty$). Figure 4.16 shows the Payne effect in the 0.1 % – 100 % strain range for the SBR composites. The increase of the Payne effect with filler loading results from the formation of filler–filler interactions.[3] This behavior has been ascribed to the decrease in inter-aggregate distances with rising filler content and the formation of a filler network.[25] The Payne effect is quantified by the difference in the G' moduli measured at 0.56 % and 100 % strains as shown in Table 4.10. As expected, this difference is negligible for the unfilled and unfilled-CA SBR compounds and more pronounced for the SBR filled with c-GTR and m-GTR if compared to their peers with CA. The addition of CA reduces the filler–filler interactions, leading to a greater potential of rubber molecules to interact with the GTR particles, and therefore, improving filler dispersion in the SBR matrix.

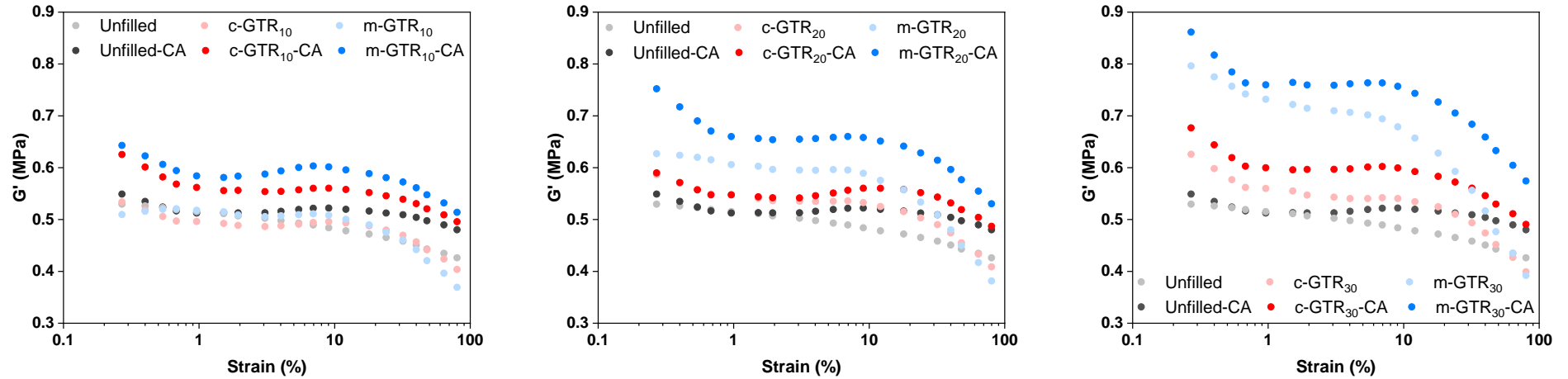


Figure 4.16 G' as a function of strain (Payne effect) for the SBR composites filled with different content of c-GTR, m-GTR with and without CA.

Table 4.10 Payne effect of unfilled, c-GTR, and m-GTR composites with and without CA

		Payne effect						
		$(G'_{0.56\% \text{ strain}} - G'_{100\% \text{ strain}})$						
		(MPa)						
Composite	Unfilled	c-GTR ₁₀	c-GTR ₂₀	c-GTR ₃₀	m-GTR ₁₀	m-GTR ₂₀	m-GTR ₃₀	
		0.063	0.100	0.154	0.169	0.146	0.232	0.361
	Unfilled-CA	c-GTR ₁₀ -CA	c-GTR ₂₀ -CA	c-GTR ₃₀ -CA	m-GTR ₁₀ -CA	m-GTR ₂₀ -CA	m-GTR ₃₀ -CA	
		0.039	0.095	0.072	0.133	0.097	0.156	0.182

Physical properties

Table 4.11 summarizes the physical properties of the vulcanized composites. The incorporation of c-GTR and m-GTR decreases their cross-link density, as corroborated from rheometric results. Such a decrease in the filled composites may be attributed to the combination of two factors. On one hand, the fact that GTR is already partially cross-linked infers that less reaction sites are available for additional cross-linking.[26] On the other hand, the migration of sulfur from the elastomeric matrix towards the vulcanized GTR particles results in a lower cross-linking degree.

Hardness and resilience are also affected by the type and amount of filler, as well as by the presence of the CA. The hardness of rubber composites deeply depends on filler properties, such as particle size and surface characteristics, and on the cross-link density of the rubber composite.[18] The functional groups present on the m-GTR surface and the acid-base interactions lead to the formation of m-GTR filler particles aggregates and to a decrease in the cross-link density of the SBR matrix. This aggregation decreases the availability of surface functional groups to improve the physical bonding between the m-GTR and the SBR matrix. Thus, it leads to a decrease in the hardness of rubber.[27] This effect is compensated with the addition of the CA in all SBR/GTR composites. Resilience, a measure of material elasticity, is found to decrease with the increase in c-GTR and m-GTR content. The resilience decreased from 65 % at 0 phr to 56 % and 61 % at 30 phr of c-GTR and m-GTR, respectively. Similar results were reported for SBR by Sreeja *et al.*[28] and Formela *et al.*[29] Lower resilience values correspond to higher energy dissipation through the filler-matrix interface, as well as by the breakdown of the filler structure. The addition of the CA for all SBR/GTR composites shows a slight increment in resilience values that suggests the increase of interface interactions between SBR and both c-GTR and m-GTR.

Table 4.11 Physical properties of SBR/c-GTR and SBR/m-GTR composites.

Physical properties	Composite						
	Unfilled	c-GTR ₁₀	c-GTR ₂₀	c-GTR ₃₀	m-GTR ₁₀	m-GTR ₂₀	m-GTR ₃₀
T _g (°C) by DSC	-55 ± 1	-52 ± 1	-53 ± 1	-53 ± 1	-52 ± 1	-52 ± 1	-52 ± 1
ν × 10 ⁻⁵ (mol/g)	2.27 ± 0.03	1.5 ± 0.6	0.64 ± 0.02	0.38 ± 0.01	0.65 ± 0.01	0.38 ± 0.01	0.24 ± 0.01
Hardness (Shore A)	33.9 ± 0.2	31.2 ± 0.2	30.5 ± 0.3	30.5 ± 0.2	27.1 ± 0.4	26.8 ± 0.3	30.9 ± 0.3
Resilience (%)	64.6 ± 0.1	61.0 ± 0.3	59.0 ± 0.2	55.8 ± 0.6	62.4 ± 0.2	61.8 ± 0.4	61.3 ± 0.1

	Unfilled-CA	c-GTR ₁₀ -CA	c-GTR ₂₀ -CA	c-GTR ₃₀ -CA	m-GTR ₁₀ -CA	m-GTR ₂₀ -CA	m-GTR ₃₀ -CA
T _g (°C) by DSC	-51 ± 1	-51 ± 1	-52 ± 1	-52 ± 1	-51 ± 1	-51 ± 1	-52 ± 1
ν × 10 ⁻⁵ (mol/g)	4.1 ± 0.4	5.3 ± 0.1	3.8 ± 0.1	3.23 ± 0.04	4.60 ± 0.06	4.2 ± 0.1	4.00 ± 0.04
Hardness (Shore A)	36.2 ± 0.2	41.8 ± 0.5	43.5 ± 0.1	42.7 ± 0.6	42.8 ± 0.2	44.3 ± 0.6	47.2 ± 0.4
Resilience (%)	66.9 ± 0.1	63.4 ± 0.2	61.1 ± 0.2	59.6 ± 0.2	65.2 ± 0.1	62.3 ± 0.2	61.8 ± 0.3

Mechanical properties

The effect of the GTR and m-GTR filler content and surface modification of GTR on the mechanical behavior of SBR vulcanizates can also be analyzed from the values compiled in Table 4.12. At deformations up to 500 %, the c-GTR and m-GTR fillers do not seem to have an effect on the mechanical response of the material. However, the effect on elongation at break and tensile strength is notorious as shown in Figure 4.17. Elongation at break increases significantly with the increase of filler content, about 356 % for c-GTR and 727 % for m-GTR at 30 phr. Such high values are consistent with the evident reduction of the cross-link density.

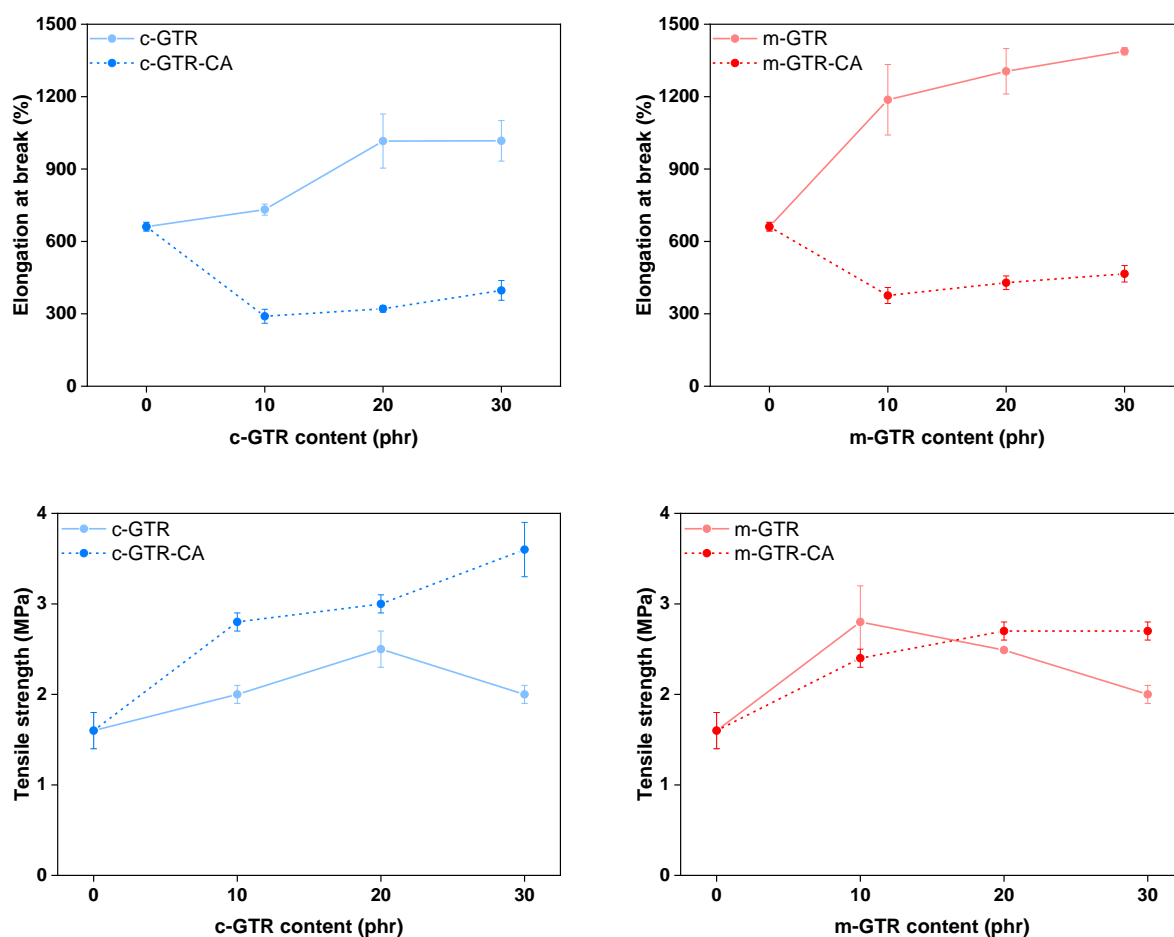


Figure 4.17 Elongation at break and tensile strength of unfilled compounds, SBR/c-GTR and SBR/m-GTR composites with and without CA.

Table 4.12 Mechanical properties of SBR/c-GTR and SBR/m-GTR composites.

Mechanical properties	Composite						
	Unfilled	c-GTR10	c-GTR20	c-GTR30	m-GTR10	m-GTR20	m-GTR30
M50 (MPa)	0.51 ± 0.01	0.57 ± 0.04	0.5 ± 0.1	0.63 ± 0.03	0.52 ± 0.03	0.59 ± 0.03	0.58 ± 0.04
M100 (MPa)	0.67 ± 0.02	0.69 ± 0.01	0.6 ± 0.1	0.66 ± 0.03	0.62 ± 0.03	0.60 ± 0.03	0.6 ± 0.1
M300 (MPa)	0.99 ± 0.01	0.97 ± 0.01	0.8 ± 0.1	0.93 ± 0.02	0.75 ± 0.03	0.80 ± 0.02	0.81 ± 0.04
M500 (MPa)	1.36 ± 0.03	1.37 ± 0.02	1.3 ± 0.1	1.26 ± 0.02	0.94 ± 0.03	1.05 ± 0.02	1.08 ± 0.01
σ _b (MPa)	1.6 ± 0.2	2.0 ± 0.1	2.5 ± 0.2	2.0 ± 0.1	2.8 ± 0.2	2.49 ± 0.02	2.0 ± 0.1
ε _b (%)	661 ± 18	732 ± 23	1016 ± 112	1017 ± 84	1187 ± 146	1305 ± 94	1388 ± 15

	Unfilled-CA	c-GTR10-CA	c-GTR20-CA	c-GTR30-CA	m-GTR10-CA	m-GTR20-CA	m-GTR30-CA
M50 (MPa)	0.61 ± 0.03	0.7 ± 0.1	0.73 ± 0.02	0.8 ± 0.1	0.74 ± 0.02	0.8 ± 0.1	0.83 ± 0.04
M100 (MPa)	0.85 ± 0.01	1.1 ± 0.1	1.05 ± 0.04	1.1 ± 0.1	1.03 ± 0.03	1.1 ± 0.1	1.1 ± 0.1
M300 (MPa)	1.8 ± 0.1	-	2.8 ± 0.2	2.7 ± 0.3	2.0 ± 0.1	2.0 ± 0.1	2.07 ± 0.04
M500 (MPa)	-	-	-	-	-	-	-
σ _b (MPa)	2.5 ± 0.2	2.8 ± 0.1	3.0 ± 0.1	3.6 ± 0.3	2.4 ± 0.1	2.7 ± 0.1	2.7 ± 0.1
ε _b (%)	418 ± 24	290 ± 29	321 ± 14	397 ± 41	376 ± 33	429 ± 28	466 ± 34

Tensile strength also increases in the presence of c-GTR and m-GTR, being the effect more evident with the chemically modified material at lower contents. Similar results were reported by Dai *et al.*[30] They found that composites filled with chemically modified CB showed higher tensile strength, but similar elongation at break values compared with unmodified CB filled composites. In another study, Zhang *et al.*[9] modified GTR with plasma treatment to improve the adhesion with a NBR matrix. The increased interfacial bonding between the plasma modified GTR and the rubber matrix improved the tensile strength while the elongation at break remained unchanged with 10 phr of modified GTR. Additionally, some authors have shown improvement in mechanical properties when GTR is incorporated into SBR, thanks to the presence of CB in the GTR.[28] Contradictory, other studies [31-33] reported the deterioration of the mechanical properties due to the migration of sulfur from the rubber matrix to the molecules of the GTR and migration of accelerants from the GTR to the rubber. In this research, although cross-link density is lower in all filled compounds, the prevailing factor for achieving better mechanical properties seems to be the CB incorporated in the GTR, which lies around 30 % as previously determined (see Section 4.3.1).

The chemical nature of the filler surface also plays an important role in the reinforcing action. Changes in the chemical structure of m-GTR due to the H₂SO₄ oxidizing treatment influence its adhesion ability to the SBR matrix, and thus alter the mechanical properties of the filled SBR vulcanizates. Such improvement can be ascribed to the creation of new oxygen-containing polar functional groups and their possible reactions, due to the improved interfacial bonding between the modified GTR and the SBR matrix.[12] The better dispersion and adhesion between the low contents of m-GTR and the SBR, can also be corroborated by the smooth surface and uniform appearance of the rubber matrix, as seen in SEM images shown in Figure 4.18. Furthermore, the H₂SO₄ chemical treatment creates more carbon-carbon double bonds (C=C) on the surface of m-GTR, as displayed in the FT-IR spectra (Figure 4.12). These unsaturated bonds can interact with the equivalent bonds existing in the butadiene part of the SBR matrix and, in lesser amount, in the NR and SBR fractions of GTR, leading to an improved interfacial adhesion. In this sense, there are two processes taking place simultaneously, the vulcanization of the virgin rubber (SBR) and the re-vulcanization of partially devulcanized GTR (NR and SBR fractions) during the vulcanization processes of rubber composites.[9] With regard to the effect of the CA, SBR/GTR-CA composites yield a decrease in elongation at break, and an increase in tensile stress at all strains and at break compared

to the unfilled compound, in accordance with curing characteristics and cross-link density shown in Table 4.9 and Table 4.11. Such results are consequence of enhanced rubber-filler interactions during mixing that could also lead to better filler dispersion in presence of a CA. Furthermore, from the micrographs, it is obvious that the presence of the CA noticeably improves filler dispersion. The combined effects of better dispersion, higher state of cure and the stronger linkage at the rubber–filler boundary are responsible for the increase in the tensile strength of the SBR/GTR-CA composites. When TESPT is added, tensile strength improves significantly (up to 125 % and 69 % for SBR/c-GTR-CA and SBR/m-GTR-CA composites, respectively) compared to unfilled SBR compounds. This superior reinforcement capacity could be due to the rigid covalent bonding of the tetra-functional silane between both c-GTR and m-GTR and SBR, which results in a stiff interphase transferring stress to the filler, and to the ability of active cross-linking sites in GTR and elemental sulfur in TESPT participating in the cross-linking process.[34] This shows the importance of an effective covalent bonding between active sites in GTR and matrix in controlling mechanical properties as well as stabilizing the rubber network.

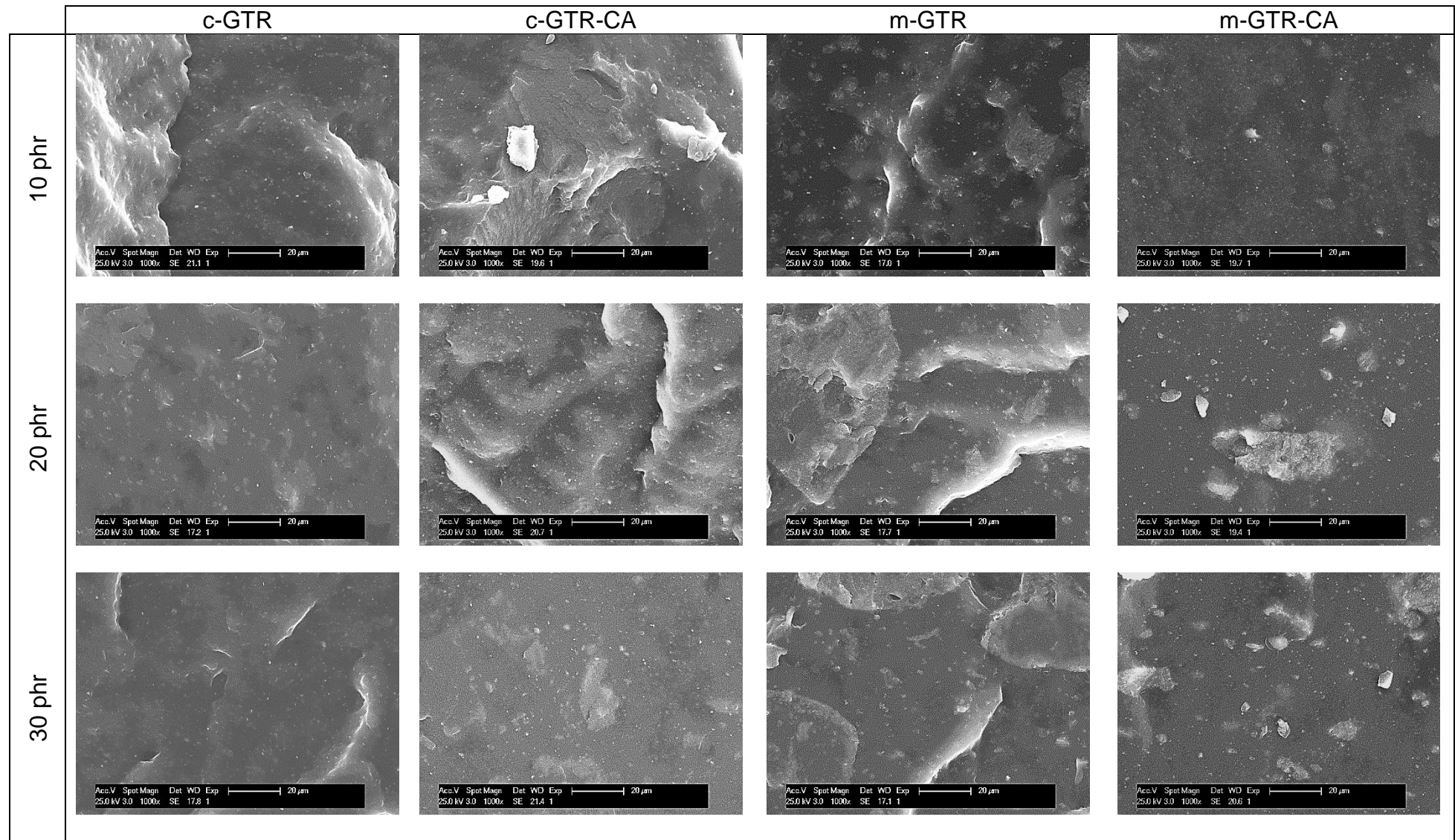


Figure 4.18 SEM fractographs of the SBR composites with different filler (c-GTR and m-GTR) with and without CA

4.4.2. Self-healing SBR/GTR composites

The successful development of sustainable self-healing SBR composites offers great opportunities to give a second lifecycle to a considerable amount of used tires. Furthermore, it offers the possibility of extending service life of rubber composites, and reducing rubber products waste. In Chapter 3, the optimal repair protocol (130 °C and 1 h) for unfilled SBR compounds was established and is then used in this Chapter. Again, all the composites were evaluated with and without thermal treatment before being damaged in order to compare them with the same network structure.

Figure 4.19 shows the tensile strength of unfilled SBR, SBR/c-GTR and SBR/m-GTR composites with and without CA at the pristine, thermally treated and healed states, as well as their healing efficiency.

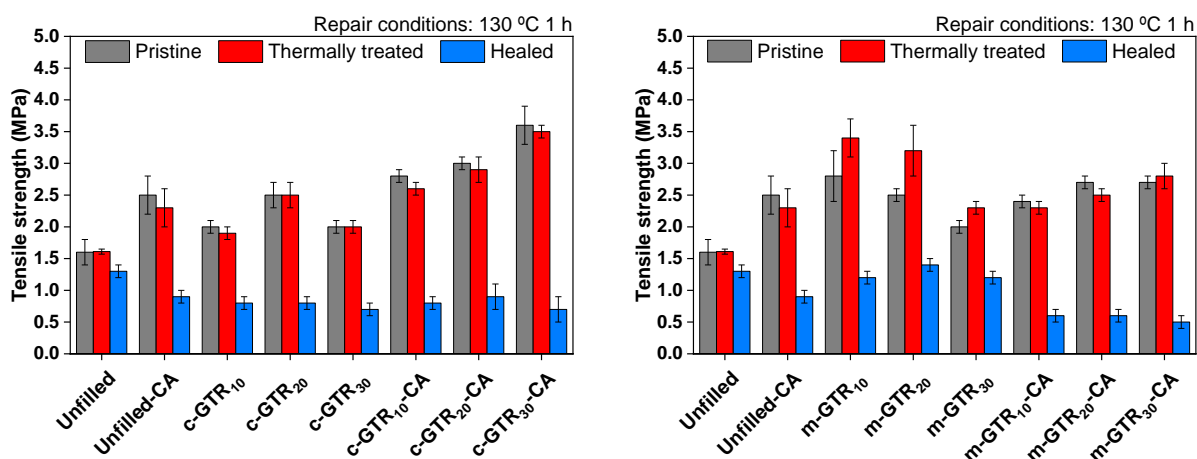


Figure 4.19 Tensile strength of SBR, SBR/c-GTR and SBR/m-GTR composites with and without CA, at the pristine, thermally treated and healed states. Repair conditions: 130 °C and 1h.

The rubber self-healing response is related to the presence of disulfide bonds. This mechanism is based on the dynamic character of the disulfides ($-S-S-$) present in sulfur vulcanized rubbers.[35-38] Moreover, the cross-link density (dependent on disulfides) not only determines the physical properties of the vulcanizates but also the molecular motions of the polymer chains on the rubber network. With the incorporation of c-GTR, it is to be expected two simultaneous effects on the self-healing capability of the rubber matrix. First, the cryo-grinding process of GTR results in scission of S-S crosslink bonds and, thus, subsequent formation of disulfide radicals.[39] The presence of these S-S radicals was corroborated by XPS in the previous section. Second, the low cross-link density with the content of c-GTR. Thus, the presence of these radicals and their recombination, plus

the low cross-link density of SBR/c-GTR composites, would favor the healing of the matrix. However, the healing efficiency of c-GTR composites shows a decrease with the increment in the c-GTR content compared to unfilled SBR compounds. This contradictory result could be due to the fact that, on one hand c-GTR is a partially cross-linked filler, and, on the other hand, GTR particles contain CB and Si as reinforcing fillers. These two simultaneous contributions restrict the mobility of the rubber chains, limiting their interdiffusion and the restoration of broken bonds at the damage zone.

In the case of m-GTR composites, the healing efficiency shows an increase with the m-GTR content compared to c-GTR composites. In addition to the low cross-link density, the surface modification of the m-GTR could be contributing to the healing capability. The surface modification induced by increasing $-OH$ groups, $S-S$, $S-O$, and sulfate compounds on the GTR surface, after the oxidizing treatment, could form ionic associates with the ZnO present in the rubber composites as shown in the scheme (Figure 4.20).

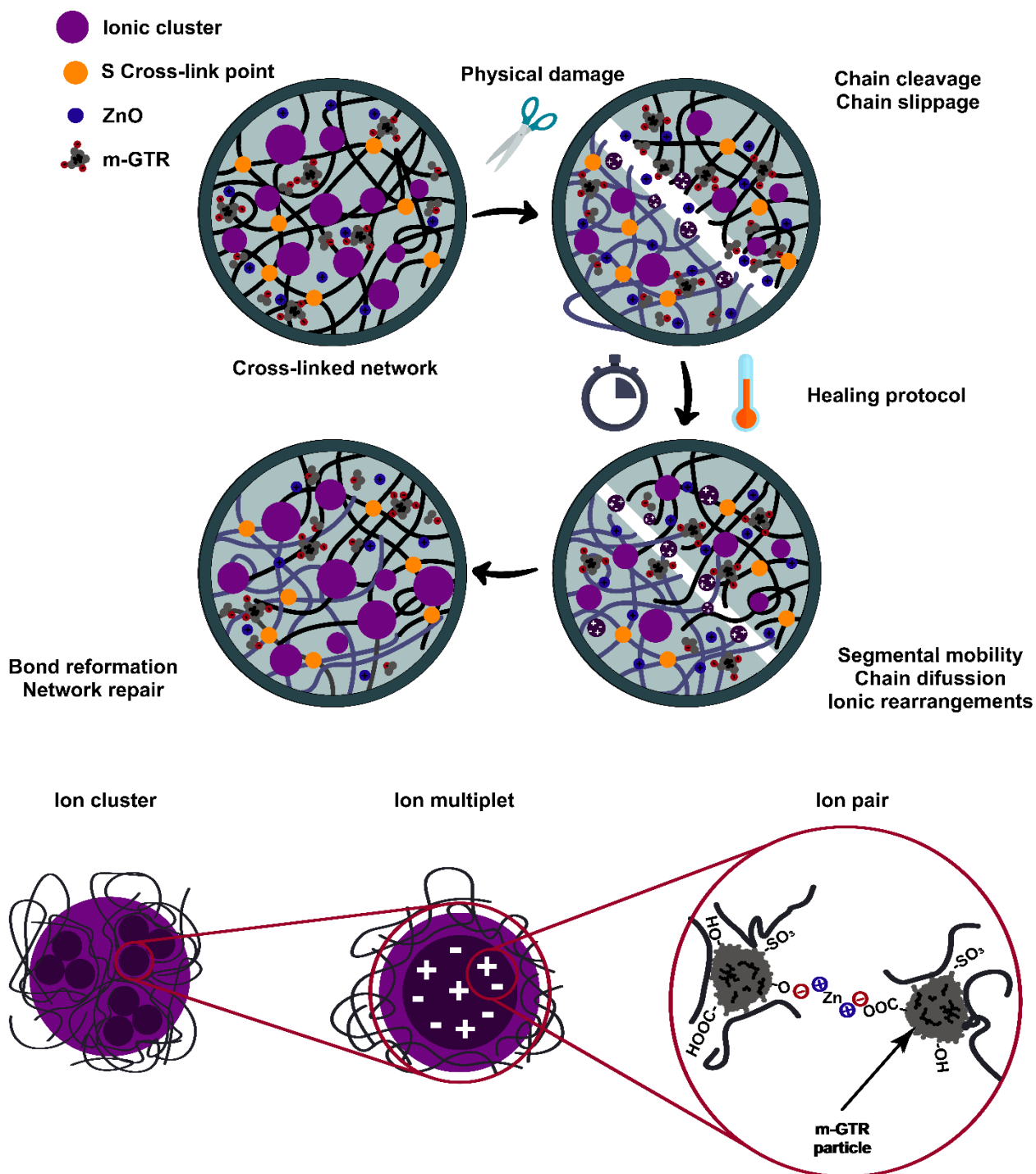


Figure 4.20 Schematic representation of self-healing by reconstruction of ionic associates.

These ionic associates would provide an ionic nature to the SBR network. This hypothesis was evaluated by means of DMA analysis, with the appearance of the so-called ionic transition.[40, 41] Figure 4.21 shows that the loss tangent ($\tan\delta$), at the frequency of 1 Hz, shows a maximum at low temperatures that corresponds to the glass transition (T_g) of SBR, while the second maximum is attributed to the ionic transition, which appears

exclusively in ionic systems at temperatures above the T_g of the polymer. The broadness of the peak reflects the heterogeneity of this transition.

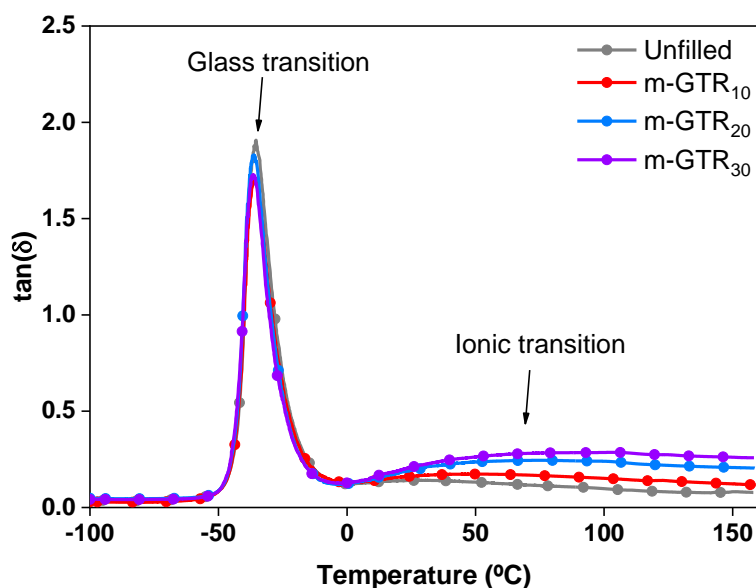


Figure 4.21 Loss tangent ($\tan\delta$) of unfilled SBR compounds and m-GTR composites.

Ionic networks are known to facilitate segment rearrangement, which may induce another healing mechanism after material damage in combination with the disulfide exchange reactions.[42] These functional groups could generate reversible ionic pairs that tend to aggregate in multiplets and clusters. These ionic clusters can act as physical cross-links in the rubber network, reducing the dynamics of the adjacent polymeric segments and creating areas of trapped polymer chains.[43] When the temperature increases, the mobility of these trapped chains is favored and, simultaneously, the ionic interactions behave as dynamic bonds.[44] Hence, the intrinsic healing character can be related to the ability of re-association of the ionic groups leading to re-clustering of the ions.[45, 46]

The increase of m-GTR content promotes more ionic reversible interactions due to the increment in the functional groups on the m-GTR surface. Similar results were reported by Utrera-Barrios *et al.*[47] They incorporated acid groups through a selective modification of GTR, by grafting of poly(acrylic acid). The incorporation of acid groups contributed to the formation of additional ionic clusters, during the vulcanization process, which resulted in a notorious increase in healing efficiency in carboxylated nitrile rubber (XNBR) composites filled with ZnO. The reformation and growth of ionic associates in the interphase of the two cut pieces are assumed to be the reason for the self-healing effect

observed. The higher chain mobility and reduced internal cohesion of the ionic associates facilitated the healing processes at elevated temperatures.[42]

Regarding the effect of the CA, all composites show a decrease in the healing efficiency. Although the homolytic cleavage and recombination of the S–S bonds of CA can also take place during the occurrence of the mechanical damage, the high cross-link density appears to be the predominant effect on the rubber chains mobility, with the subsequent reduction on healing efficiency. Furthermore, in the case of m-GTR, the alkoxy groups of the CA could react with hydroxyl, carboxyl groups, and sulfates located on the surface during mixing, limiting the formation of ionic interactions between the functional groups and the metal ions, and reducing even more the repair process.[22, 23]

In an attempt to improve the self-healing efficiency, the previously established repair conditions were modified increasing the time up to 5 h and keeping the temperature at 130 °C. As can be seen in Figure 4.22, a longer repairing time shows an important increase of the healing efficiency for all the composites, especially for the m-GTR without CA. Thus, the composite with the highest healing efficiency (20 phr of m-GTR-H₂SO₄ (HT)) was selected for further research, as discussed in the following section.

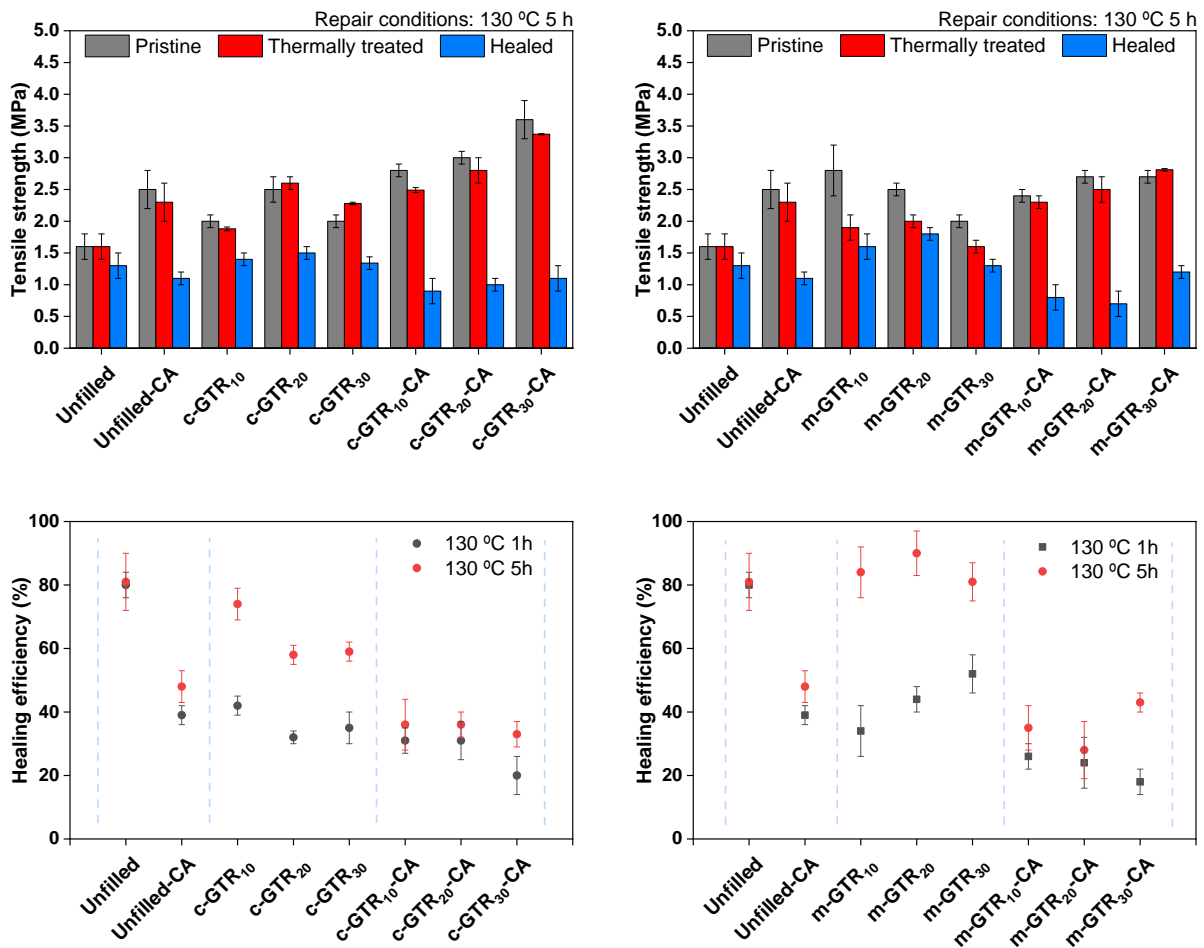


Figure 4.22 Top: Tensile strength of SBR, SBR/c-GTR and SBR/m-GTR composites with and without CA, at the pristine, thermally treated and healed states. Repair conditions: 130 °C and 5 h. Bottom: Healing efficiency of sustainable SBR/GTR composites with and without CA at different healing conditions.

4.5. Development of hybrid reinforced SBR composites

As shown for other self-healing polymers, the incorporation of conventional fillers or fibers improves stiffness and tensile properties, but, at the same time, the self-healing process is deteriorated significantly.[48] The aim of this section is to develop hybrid reinforcing filler composites as a possible strategy to solve the opposed compromise between healing capability and mechanical performance.

4.5.1. Characterization of hybrid reinforced SBR composites

Rheometric properties

Figure 4.23 and Table 4.13 present some important vulcanization characteristics of the individual and hybrid reinforced SBR composites, filled with 20 phr of m-GTR and combined with different contents of traditional fillers as carbon black (CB) and silica (Si), with and without CA.

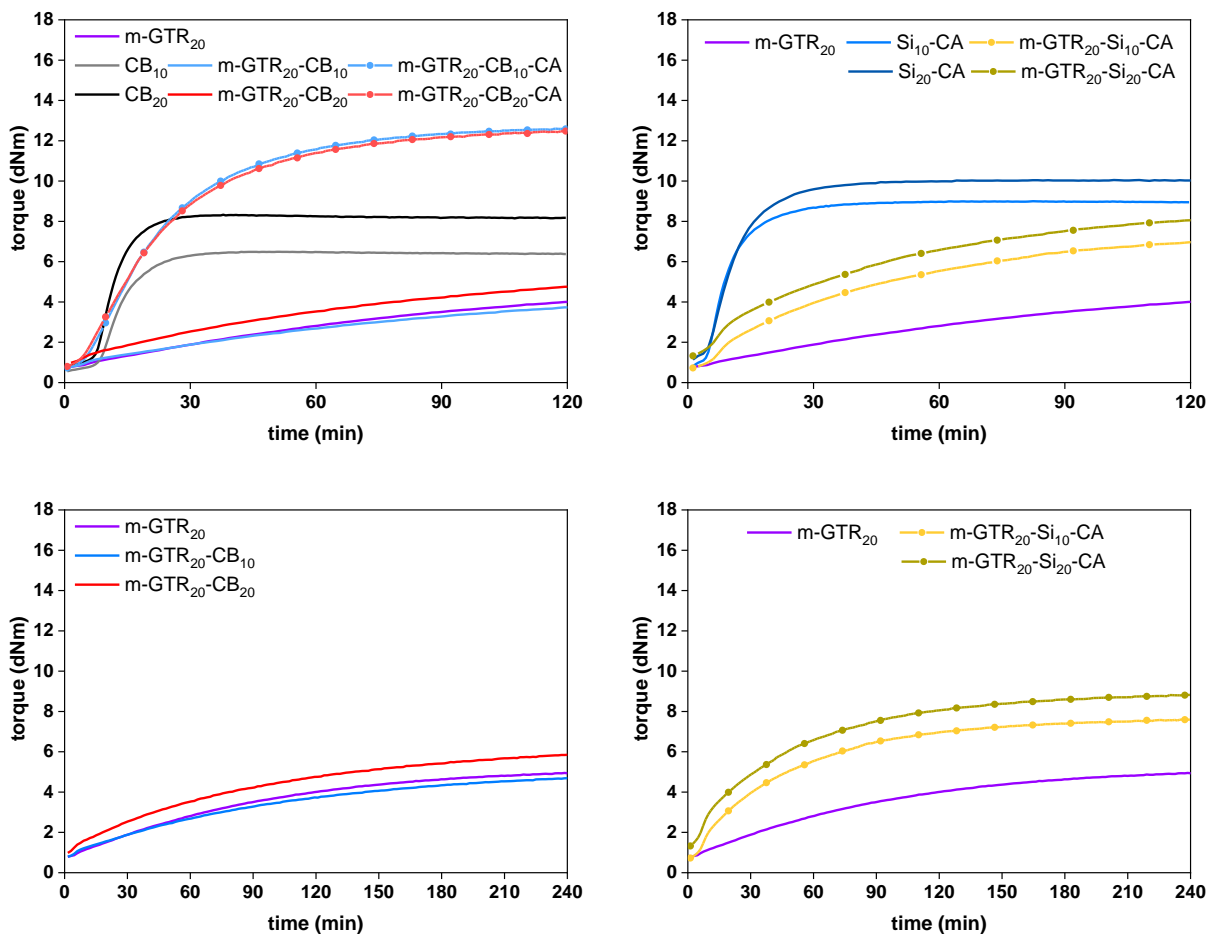


Figure 4.23 Rheometric curves of m-GTR₂₀-CB and m-GTR₂₀-Si composites with and without CA.

As expected, the addition of CB shows a substantial decrease in t_{s2} and t_{90} compared to unfilled SBR compounds, indicating that the vulcanization reaction can occur more readily, especially when the amount of CB increases.[49] This substantial decrease indicates that CB is working to deliver the heat needed to complete the process of vulcanization.[50] Furthermore, M_L increases with increasing CB content. This effect is due to the entanglement or trapping of rubber chains in the voids of CB aggregates,

during the mixing process. Those CB particles whose surfaces are covered by entangled rubber chains can be considered as physical cross-links that hinder the mobility of the chains.[51] M_H and ΔM increase with increasing CB content, indicating that strong interactions between CB and SBR are taking place.

Similar trends are found with the addition of Si. The use of CA with this traditional filler is well established because it reduces the adsorption of accelerant on the Si surface. Even though the addition of Si shows a substantial decrease in t_{s2} and t_{90} compared to the unfilled SBR, these parameters slightly increase with increasing Si content. This slight increment could be due to the amount of CA that may not be sufficient to reduce the adsorption of accelerant on the surface at high Si content.[22]

Table 4.13 Rheometric properties of SBR/c-GTR and SBR/m-GTR composites.

Composite	M_L (dNm)	M_H (dNm)	ΔM (dNm)	t_{s2} (min)	t_{90} (min)
Unfilled	0.7	5.8	5.1	17	27
m-GTR ₂₀	0.8	3.8	3	57	82
CB ₁₀	0.6	6.5	5.9	11	23
CB ₂₀	0.8	8.3	7.5	9	19
m-GTR ₂₀ -CB ₁₀	0.8	3.8	3	63	114
m-GTR ₂₀ -CB ₂₀	0.9	3.9	3	40	61
m-GTR ₂₀ -CB ₁₀ -CA	0.7	12.6	11.9	9	56
m-GTR ₂₀ -CB ₂₀ -CA	0.8	12.5	11.7	9	58
Si ₁₀ -CA	0.7	9	8.3	6	21
Si ₂₀ -CA	1	10.1	9.1	7	23
m-GTR ₂₀ -Si ₁₀ -CA	0.7	7.6	6.9	16	117
m-GTR ₂₀ -Si ₂₀ -CA	1.3	8.8	7.5	12	121

Regarding the hybrid SBR composites, the curing curves of m-GTR₂₀-CB composites, without CA, exhibit the same marching modulus behavior of the m-GTR composites described previously. This behavior indicates that the effect of m-GTR predominates over the effect provided by the CB filler. Nonetheless, the marching modulus disappears in presence of the CA, as seen in the individual composites. In the case of the m-GTR₂₀-Si composites, intermediate values of M_L , M_H , ΔM , and t_{s2} are found. However, the extremely high t_{90} values indicate the strong effect that m-GTR exerts on the curing behavior of SBR

composites. Despite the presence of the CA, it is not enough to reduce the adsorption of zinc complex and basic curatives on the Si and m-GTR surface. Therefore, reaching a plateau over time is hindered.

The Payne effect for the hybrid reinforced SBR composites was also analyzed. An increase with traditional filler loading is observed, due to the formation of filler–filler interactions between CB or Si particles (Figure 4.24). The Payne effect quantification by the difference in the G' moduli measured at 0.56 % and 100 % strains is shown in Table 4.14.

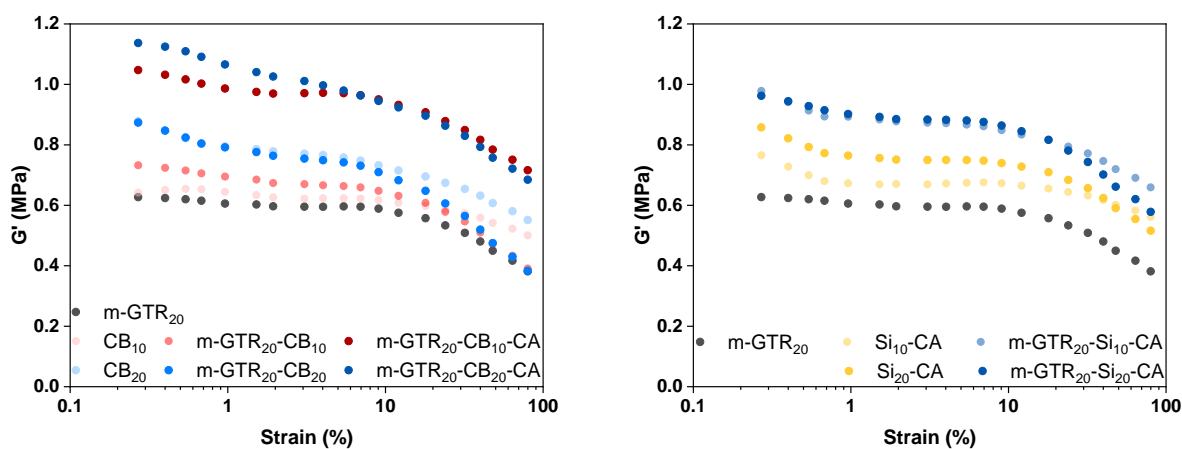


Figure 4.24 G' as a function of strain (Payne effect) for the SBR composites filled with different content of c-GTR, m-GTR with and without CA

The addition of CA reduces the filler–filler interaction of SBR/m-GTR₂₀-CB composites, leading to a greater potential of rubber chains to interact with the m-GTR and CB particles, therefore, improves filler dispersion in the SBR matrix. However, at higher content of CB the Payne effect shows a slight increase. This could be due to the presence of traditional filler (CB and Si) on m-GTR particles. In the case of SBR/m-GTR₂₀-Si-CA composites, there is a combination of different factors. On the one side, the combination of CB and Si present in m-GTR increases the content of filler, thus, the Payne effect increases. On the other side, the insufficient content of CA, which is not enough to react with the large amount of functional groups present on the m-GTR and Si surface.

Table 4.14 Payne effect individual reinforced and hybrid reinforced SBR composites with and without CA

Composite	Payne effect
	($G'_{0.56\% \text{ strain}} - G'_{100\% \text{ strain}}$) (MPa)
m-GTR ₂₀	0.232
CB ₁₀	0.158
CB ₂₀	0.263
m-GTR ₂₀ -CB ₁₀	0.313
m-GTR ₂₀ -CB ₂₀	0.433
m-GTR ₂₀ -CB ₁₀ -CA	0.297
m-GTR ₂₀ -CB ₂₀ -CA	0.442
Si ₁₀ -CA	0.142
Si ₂₀ -CA	0.246
m-GTR ₂₀ -Si ₁₀ -CA	0.268
m-GTR ₂₀ -Si ₂₀ -CA	0.342

The improved filler dispersion can also be corroborated by the smooth surface and uniform appearance of the rubber matrix and homogeneous dispersion of the CB and m-GTR particles in the SBR matrix, as shown in Figure 4.25. From the SEM micrographs, it is obvious that the presence of CA noticeably enhances the filler dispersion in m-GTR₂₀-CB composites.

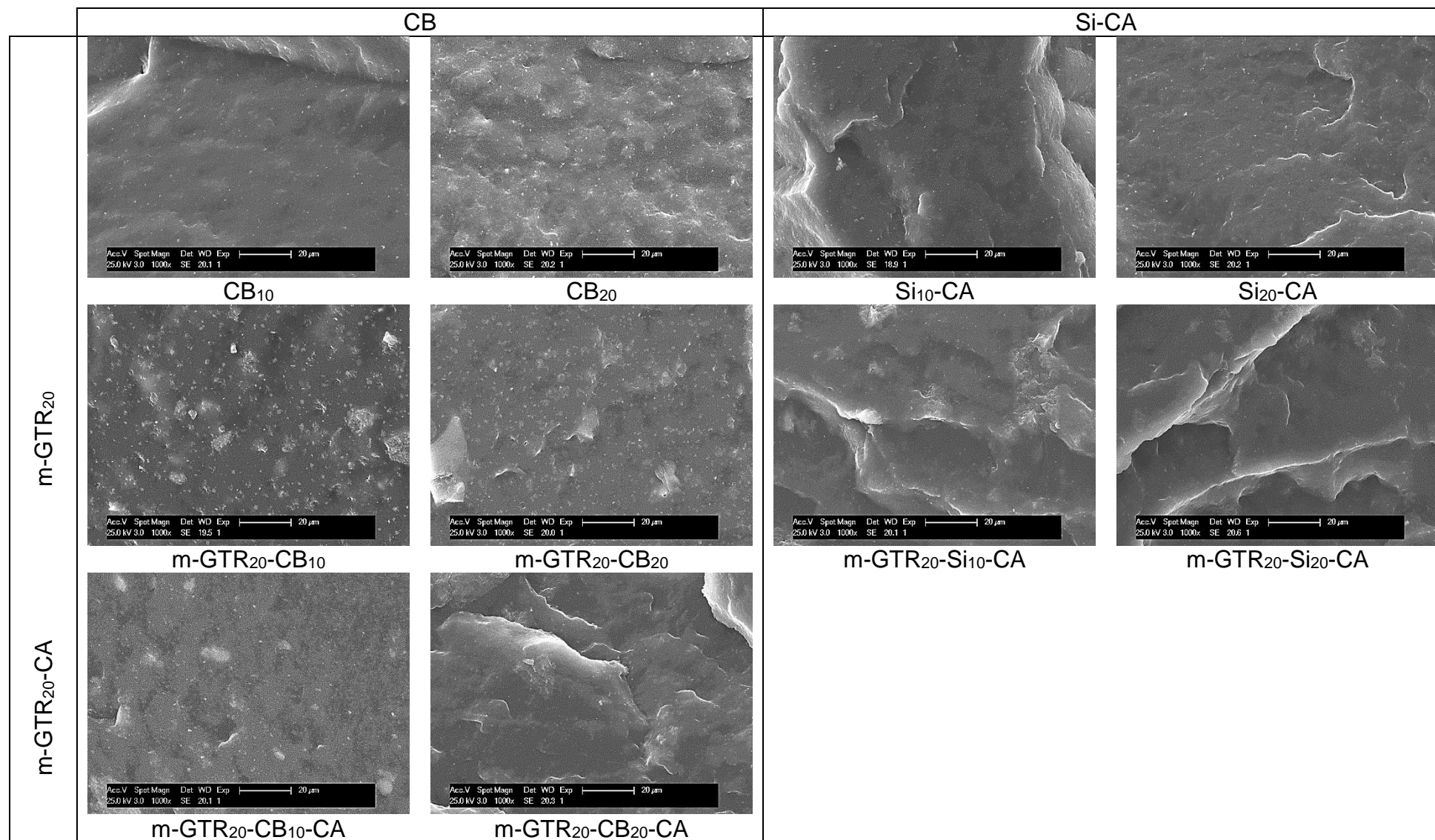


Figure 4.25 SEM fractographs of the m-GTR₂₀-CB and m-GTR₂₀-Si SBR hybrid composites.

Physical properties

The cross-link density of the individual and hybrid SBR composites are shown in Table 4.15. Adding CB and Si significantly increases the cross-link density of the pure rubber. However, the values for the m-GTR-CB hybrid composites show negligible differences compared to the individual m-GTR composite. Once again, this result indicates that the effect of m-GTR predominates over the effect provided by a traditional filler. Furthermore, the m-GTR₂₀-Si composites show intermediate values of cross-link density compared to individual filled m-GTR and Si composites.

Hardness and resilience of individual and hybrid reinforced SBR composites are also shown in Table 4.15. As expected, the addition of traditional fillers (CB and Si) increases the hardness of SBR compounds.[18, 52] Meanwhile, all the hybrid composites show intermediate values that increase in presence of a CA. The higher cross-link density and the better rubber-filler interaction are responsible for this increase. Regarding resilience, there are negligible differences between the hybrid composites and their individual counterparts. These results show that the reinforced hybrid filler systems have the possibility of increasing hardness without affecting resilience with respect to the unfilled SBR compounds; the incorporation of traditional fillers compensates the decrease in the hardness values due to the presence of m-GTR, as described in the previous section.

Table 4.15 Physical properties of m-GTR₂₀-CB and m-GTR₂₀-Si composites.

Physical properties	Composite						
	CB based						
	m-GTR ₂₀	CB ₁₀	CB ₂₀	m-GTR ₂₀ -CB ₁₀	m-GTR ₂₀ -CB ₂₀	m-GTR ₂₀ -CB ₁₀ -CA	m-GTR ₂₀ -CB ₂₀ -CA
T _g (°C) by DSC	-52 ± 1	-52 ± 1	-51 ± 1	-52 ± 1	-53 ± 1	-52 ± 1	-52 ± 1
ν × 10 ⁻⁵ (mol/g)	0.38 ± 0.01	2.50 ± 0.04	3.20 ± 0.07	0.30 ± 0.01	0.29 ± 0.01	6.6 ± 0.1	5.5 ± 0.1
Hardness (Shore A)	26.8 ± 0.3	38.2 ± 0.3	43.3 ± 0.2	34.5 ± 0.4	32.1 ± 0.3	52.7 ± 0.1	50.5 ± 0.2
Resilience (%)	61.8 ± 0.4	61.2 ± 0.2	60 ± 0.5	60.1 ± 0.1	58.4 ± 0.3	61.8 ± 0.3	60.6 ± 0.2
	Si based						
	m-GTR ₂₀	Si ₁₀ -CA	Si ₂₀ -CA	m-GTR-Si ₁₀ -CA	m-GTR-Si ₂₀ -CA		
T _g (°C) by DSC	-52 ± 1	-51 ± 1	-51 ± 1	-51 ± 1	-51 ± 1	-51 ± 1	-51 ± 1
ν × 10 ⁻⁵ (mol/g)	0.38 ± 0.01	5.20 ± 0.05	5.2 ± 0.1	2.5 ± 0.1	2.7 ± 0.1		
Hardness (Shore A)	26.8 ± 0.3	43.9 ± 0.3	46.5 ± 0.4	42.1 ± 0.5	43.7 ± 0.5		
Resilience (%)	61.8 ± 0.4	64.5 ± 0.1	62.8 ± 0.1	62.2 ± 0.3	59.5 ± 0.3		

Mechanical properties

Moduli M_{50} , M_{100} , M_{300} , M_{500} of m-GTR₂₀-CB and m-GTR₂₀-Si composites follow a similar trend than the cross-link density values, as seen in Table 4.16. Figure 4.26 shows the tensile strength and elongation at break of the composites with and without CA. As expected, results show an increase of the tensile strength and a reduction of the elongation at break, with increasing filler (CB and Si) content.

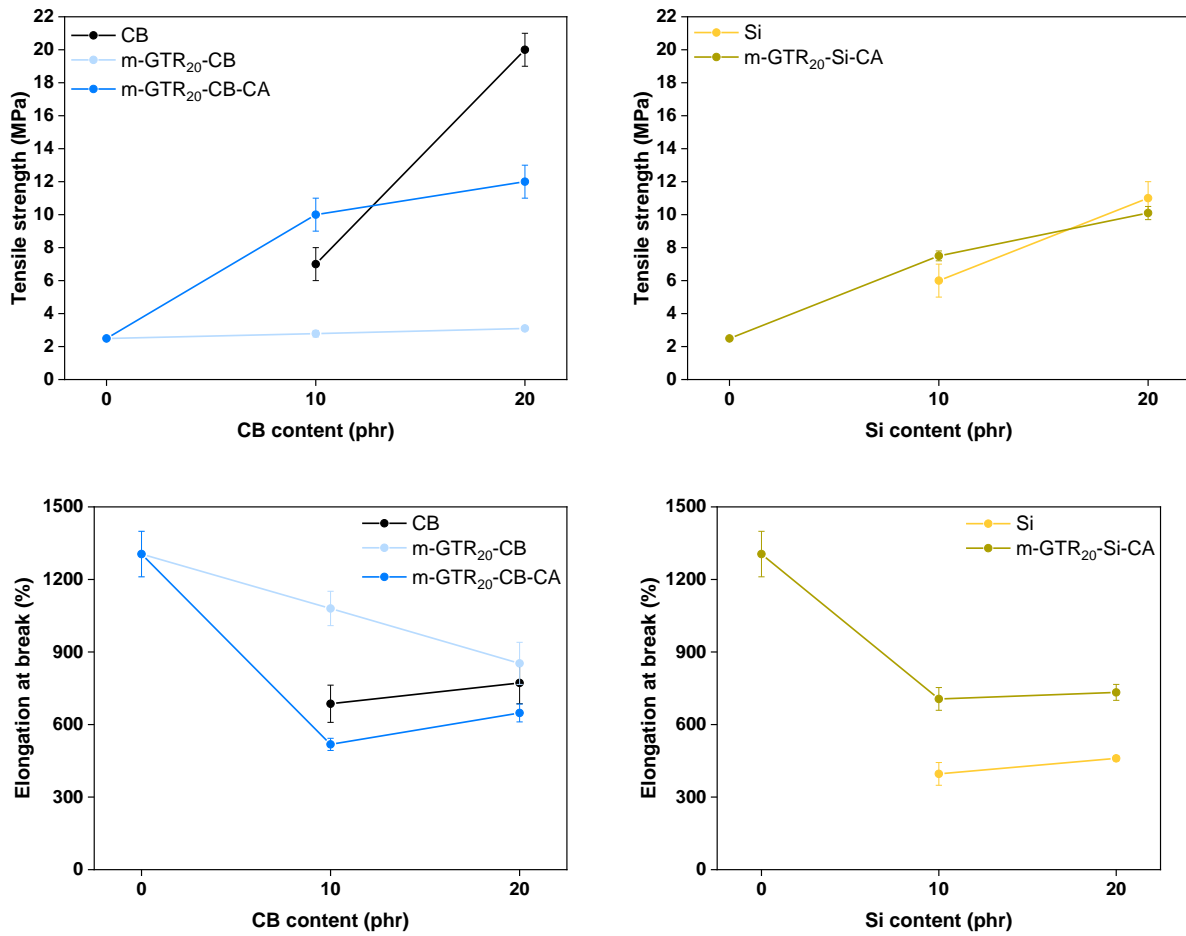


Figure 4.26 Tensile strength and elongation at break of hybrid reinforced SBR composites.

Table 4.16 Mechanical properties of m-GTR₂₀-CB and m-GTR₂₀-Si composites.

Mechanical Properties	Composite						
	CB based						
	m-GTR ₂₀	CB ₁₀	CB ₂₀	m-GTR ₂₀ -CB ₁₀	m-GTR ₂₀ -CB ₂₀	m-GTR ₂₀ -CB ₁₀ -CA	m-GTR ₂₀ -CB ₂₀ -CA
M ₅₀ (MPa)	0.59 ± 0.03	0.6 ± 0.1	0.7 ± 0.1	0.58 ± 0.04	0.6 ± 0.1	1.2 ± 0.1	0.98 ± 0.03
M ₁₀₀ (MPa)	0.60 ± 0.03	0.7 ± 0.1	0.9 ± 0.1	0.64 ± 0.04	0.6 ± 0.1	1.73 ± 0.04	1.51 ± 0.03
M ₃₀₀ (MPa)	0.80 ± 0.02	1.38 ± 0.04	2.7 ± 0.4	0.89 ± 0.02	0.9 ± 0.1	4.8 ± 0.1	4.9 ± 0.2
M ₅₀₀ (MPa)	1.05 ± 0.02	3.3 ± 0.3	10 ± 0.3	1.4 ± 0.1	1.2 ± 0.1	9.6 ± 0.3	8.7 ± 0.3
σ _b (MPa)	2.49 ± 0.02	7 ± 1	20 ± 1	2.78 ± 0.07	3.1 ± 0.1	10 ± 1	12 ± 1
ε _b (%)	1305 ± 94	686 ± 77	772 ± 86	1154 ± 99	853 ± 87	518 ± 25	648 ± 37
	Si based						
	m-GTR ₂₀	Si ₁₀ -CA	Si ₂₀ -CA	m-GTR-Si ₁₀ -CA	m-GTR-Si ₂₀ -CA		
M ₅₀ (MPa)	0.59 ± 0.03	0.8 ± 0.1	0.97 ± 0.02	0.82 ± 0.03	0.97 ± 0.04		
M ₁₀₀ (MPa)	0.60 ± 0.03	1.1 0±.1	1.30 ± 0.03	1.04 ± 0.03	1.23 ± 0.04		
M ₃₀₀ (MPa)	0.80 ± 0.02	3.2 ± 0.3	4.5 ± 0.1	2.5 ± 0.1	3.4 ± 0.2		
M ₅₀₀ (MPa)	1.05 ± 0.02	-	-	5.0 ± 0.2	6.7 ± 0.3		
σ _b (MPa)	2.49 ± 0.02	6 ± 1	11.0 ± 0.5	7.5 ± 0.4	10.1 ± 0.4		
ε _b (%)	1305 ± 94	396 ± 47	460 ± 10	706 ± 47	734 ± 33		

The effect of the thermal treatment on the cross-link density is listed in Table 4.17. It can be seen that the thermally treated composites show different behaviors. The cross-link densities of individual reinforced composites with m-GTR, traditional fillers, and hybrid reinforced m-GTR₂₀-CB composites tend to increase with the thermal treatment. This could be attributed to the thermo-oxidative process that causes the degradation of the elastomeric matrix by varying its structure.[53] Meanwhile, the hybrid composites with CA only show a slight change in their cross-link density.

Table 4.17 Cross-link density of hybrid reinforced SBR composites at pristine and thermally treated state.

Composite	$\nu \times 10^{-5}$ (mol/g)	
	Pristine	Thermally treated (T: 130 °C, t: 5 h)
m-GTR ₂₀	0.38 ± 0.01	1.99 ± 0.07
CB ₁₀	2.50 ± 0.04	3.08 ± 0.01
CB ₂₀	3.20 ± 0.07	4.72 ± 0.14
m-GTR ₂₀ -CB ₁₀	0.30 ± 0.01	1.84 ± 0.04
m-GTR ₂₀ -CB ₂₀	0.29 ± 0.01	3.09 ± 0.01
m-GTR ₂₀ -CB ₁₀ -CA	6.61 ± 0.1	6.63 ± 0.2
m-GTR ₂₀ -CB ₂₀ -CA	5.46 ± 0.1	5.73 ± 0.06
Si ₁₀ -CA	5.20 ± 0.05	5.77 ± 0.08
Si ₂₀ -CA	5.22 ± 0.09	6.00 ± 0.03
m-GTR ₂₀ -Si ₁₀ -CA	2.48 ± 0.05	3.14 ± 0.03
m-GTR ₂₀ -Si ₂₀ -CA	2.72 ± 0.09	3.45 ± 0.05

4.5.2. Self-healing of hybrid reinforced SBR composites

Figure 4.27 show the tensile strength and the healing efficiency of m-GTR₂₀-CB and m-GTR₂₀-Si composites. As expected, in traditional reinforced SBR composites, the reinforcing filler, regardless of its nature, deteriorates their self-healing capability.[48, 54] Such efficiency decrease is due the significant increase in the cross-link density that restricts the mobility of the rubber chains, hindering the bond reformation across the damaged interface. This effect is more pronounced in presence of a CA, as previously explained. Nonetheless, for the hybrid m-GTR₂₀-CB composites without CA, excellent

values of healing efficiency are achieved, 85 % and 90 % with 10 and 20 phr of CB, respectively.

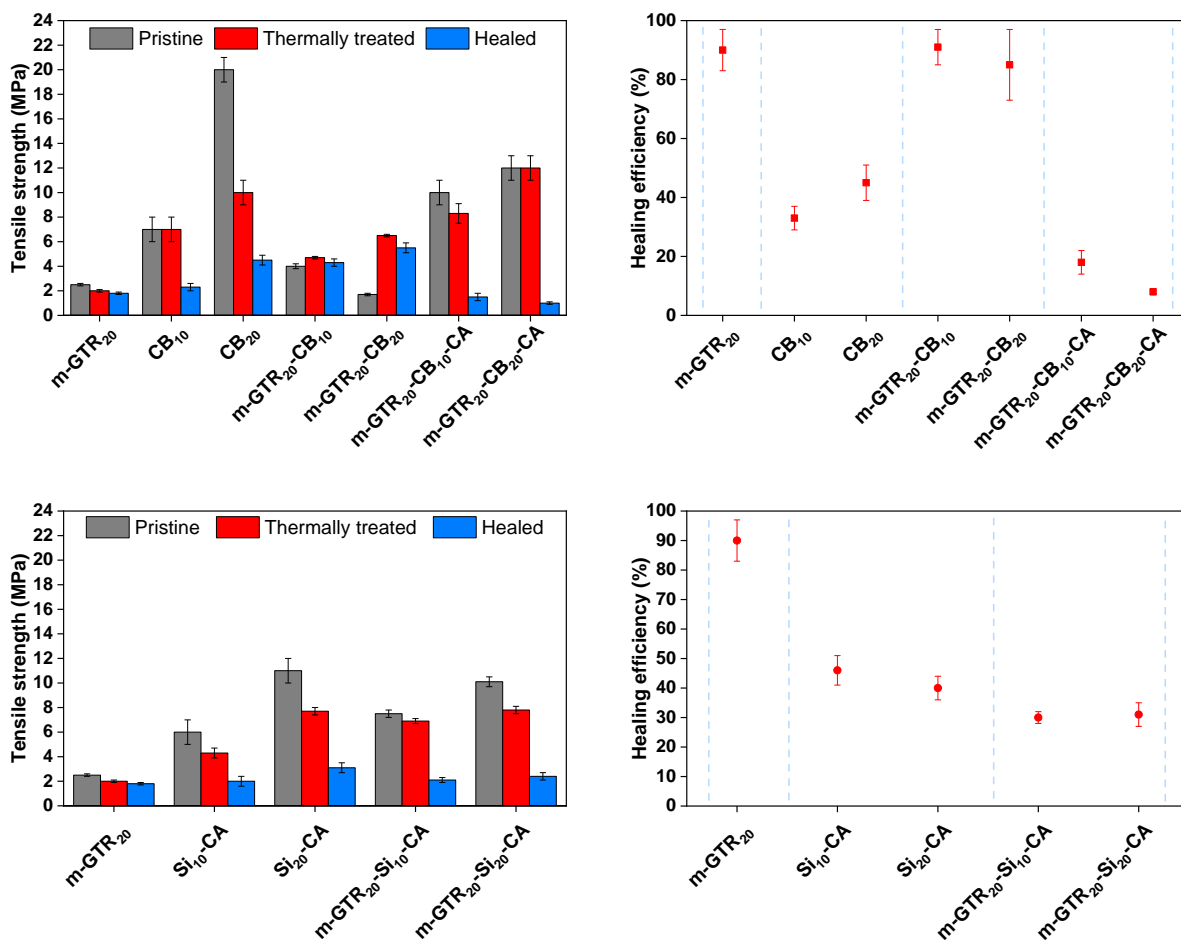


Figure 4.27 Tensile strength of thermally treated compared to healed samples and the healing efficiency of m-GTR₂₀-CB and m-GTR₂₀-Si composites

The $\tan\delta$ at the frequency of 1 Hz of hybrid reinforced SBR composites is shown in Figure 4.28. Traditional reinforced composites present similar behavior than the unfilled SBR compound, which only show the maximum associated to the T_g . Meanwhile, the hybrid reinforced composites present the second maximum attributed to the ionic transition and is more intense in the case of m-GTR₂₀-CB₂₀ composite.

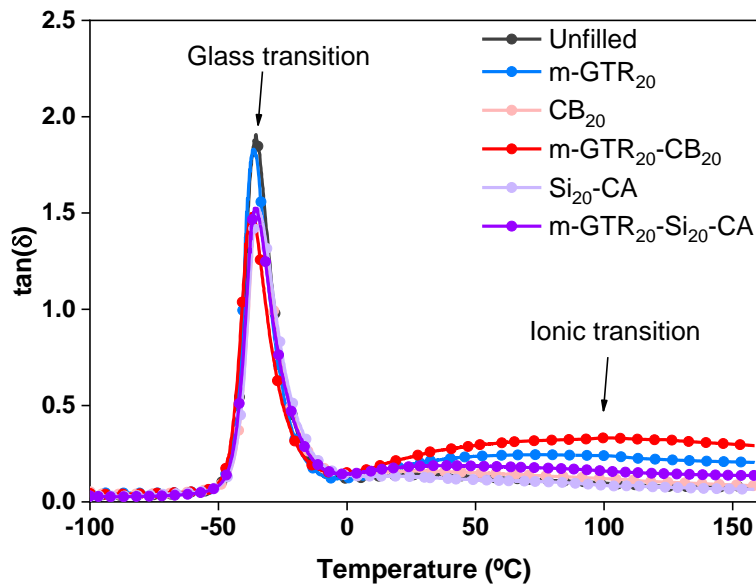


Figure 4.28 Los tangent ($\tan\delta$) hybrid reinforced SBR composites.

Figure 4.29 shows a representation of the healing capability and tensile strength of all the SBR composites developed in this thesis. The green quadrant delimits the ideal area of attention, targeting healing efficiencies higher than 70 % and tensile strengths higher than 5 MPa. The SBR composite reinforced with a combination of 20 phr m-GTR and 20 phr CB is located in this quadrant, balancing perfectly well both properties and solving the existing dichotomy between mechanical performance and reparability. This composite maintains the healing efficiency of the unfilled SBR and improves by 400 % its tensile strength.

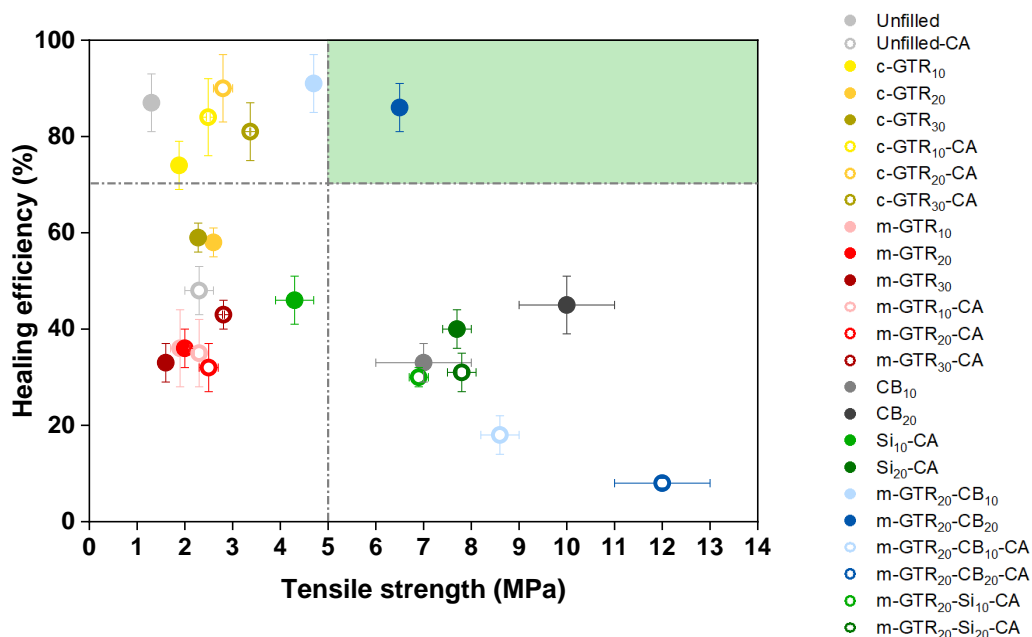


Figure 4.29 Tensile strength and healing efficiency of all the SBR composites developed.

It can be seen that the developed hybrid reinforcing SBR composite (m-GTR₂₀-CB₂₀) presents healing efficiency and tensile strength values comparable with other reported elastomeric systems that combine both covalent and non-covalent dynamic bonds (see Figure 4.30). Liu *et al.*[55] developed a dual ionic network; maleic anhydride (MAH) was grafted to NR by an anionic mechanism to construct the first ionic network, with *n*-butyllithium as the metallization reagent. Subsequently, zinc dimethacrylate (ZDMA) reacted with the MAH-modified NR, and the second ionic network was constructed. They found a healing efficiency of 75 % and a mechanical strength of 2.5 MPa. Xu *et al.*[46] prepared carboxylated styrene butadiene rubber (XSBR) composites filled with nano-chitosan (NCS). The NCS acted as a multiple-functional cross-linker as well as reinforcement for XSBR. The self-healing combined mechanism was due to ionic interactions and hydrogen bonds at ambient temperature for 24 h. More recently, Stein *et al.*[56] designed an elastomeric network of brominated poly(isobutylene-co-isoprene) rubber (BIIR) modified with uracil and imidazole moieties. The uracil group contributed to physical cross-links of the rubber through hydrogen bonding; meanwhile the imidazole group provided the formation of ionic clusters. The BIIR composites were healed at 70 °C for 1 h.

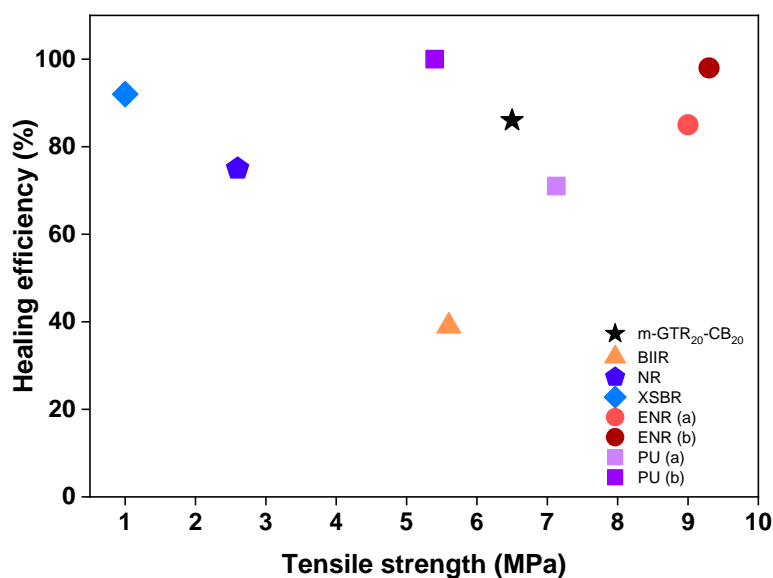


Figure 4.30 Tensile strength and healing efficiency of $m\text{-GTR}_{20}\text{-CB}_{20}$ and different rubber composites.

There are several studies published using epoxidized natural rubber (ENR). Chen *et al.*[57] prepared ENR (a) compounds with dynamic dual cross-links of boronic esters and $\text{Zn}^{2+}\text{-O}$ coordination bonds. On the one side, they covalently cross-linked the ENR with 2,2'-(1,4-Phenylene)-bis[4-mercaptan-1,3,2-dioxaborolane] (BDB) through the chemical reaction between thiols and epoxy groups. On the other side, the boronic ester transesterification enabled the composite to heal at 80 °C for 24 h. Moreover, the integration of $\text{Zn}^{2+}\text{-O}$ coordination bonds improved the mechanical performance without hindering the self-healing capability. In another investigation Cheng *et al.*[44] reported dual cross-linked self-healing ENR(b) based on thermoreversible hydrogen bonding and dynamic disulfide metathesis. They introduced aromatic disulfide compounds to promote the disulfide metathesis after a healing protocol of 120 °C for 6 h.

Xu *et al.*[58] developed polyurethane – PU(a) based on zinc–imidazole coordinated bonds and multiple hydrogen bonding. The dual dynamic cross-linked system endowed self-healing capacity at room temperature for 48 h. Moreover, at 60 °C the healing process was accelerated. PU(b) system with healing properties was developed by Chang *et al.*[59] The PU network was responsible for the crack closure due to shape memory properties while the self-healing capability was due to the dynamic disulfide bond exchange after the application of a healing protocol of 80 °C for 24 h.

Finally, a fair comparison between selected SBR composites and a generic tire tread compound is presented in Table 4.18 in terms of their mechanical properties. On the one side, it can be seen that the hybrid composite with CA presents quite similar values (m-GTR₂₀-CB₂₀-CA) compared to the generic tire tread composites. However, the self-healing capability of this composite is not adequate. On the other side, the m-GTR₂₀-CB₂₀ shows the best self-healing efficiency, meanwhile, the mechanical performance is half compared to the tire tread generic composite. Hence, these results put in evidence the compromise between mechanical properties and healing capability. It is worth mentioning that the usual CB content in a tire tread compound is around 70 phr, higher than the maximum filler content present in the developed composites (20 phr CB and 20 phr m-GTR). Hence, the sustainable hybrid reinforcing composites offer a potential versatility to the rubber industry still to be explored.

Table 4.18 Mechanical properties of hybrid reinforcing composites and a generic tire rubber compound.

	Composite		
	m-GTR ₂₀ -CB ₂₀	m-GTR ₂₀ -CB ₂₀ -CA	Tire rubber [60]
M ₃₀₀ (MPa)	2.4 ± 0.1	6.1 ± 0.3	11
σ _b (MPa)	6.5 ± 0.1	12 ± 1	14
ε _b (%)	777 ± 32	556 ± 39	400
η (%)	86 ± 5	8 ± 1	-

4.6. Summary

The aim of the present work was to study SBR composites filled with mechano-chemically modified GTR, to overcome the poor compatibility between the waste material and the rubber matrix. The mechano-chemical modification of GTR was accomplished following two procedures: i) a cryo-grinding process; ii) different oxidizing chemical treatments. The cryo-grinding process was successfully optimized, reducing the average particle size of the departing material up to 100 – 150 μm, achieving a narrow distribution and a smooth fracture surface. The oxidation on the surface of GTR was corroborated by the increase in oxygen content, being the modification with H₂SO₄ (HT) the most successful one. The interaction of the polar functional groups on the surface of GTR with the SBR matrix favored the adhesion between phases and improved the mechanical performance of the composite.

The c-GTR and m-GTR composites showed a good balance between tensile strength and healing capability when applying 130 °C for 5 h. The use of this sustainable filler provides a second life cycle to a considerable quantity of used tires. The combination of disulfide bonds and reversible ionic bonds, originating from the incorporation of functional groups on the surface of the m-GTR, were responsible for promoting a good compromise between repair efficiency and mechanical performance. The effect of combining the mechano-chemically modified GTR (m-GTR) with conventional fillers such as CB and Si was also studied. The presence of a coupling agent provided better filler dispersion and interaction with the SBR matrix, leading to an increase in the cross-link density and in mechanical strength, but limiting the healing capability. Finally, the hybrid system consisting of 20 phr m-GTR and 20 phr CB without CA was selected as the best SBR composite with a positive balance between mechanical strength and healing efficiency.

4.7. References

1. Luginsland, H.-D., J. Fröhlich, and A. Wehmeier, *Influence of Different Silanes on the Reinforcement of Silica-Filled Rubber Compounds*. Rubber Chem. Technol., 2002. **75**(4): p. 563-579.
2. Anke, B., et al., *Silica and Silanes*, in *Rubber Compounding: Chemistry and Applications*. 2004. p. 251 - 332.
3. Donnet, J.-B., *Black and White Fillers and Tire Compound*. Rubber Chem. Technol., 1998. **71**(3): p. 323-341.
4. Motiee, F., S. Taghvaei-Ganjali, and M. Malekzadeh, *Investigation of correlation between rheological properties of rubber compounds based on natural rubber/styrene-butadiene rubber with their thermal behaviors*. Int. J. Ind. Chem., 2013. **4**(1): p. 16.
5. Fernández-Berridi, M.J., et al., *Pyrolysis-FTIR and TGA techniques as tools in the characterization of blends of natural rubber and SBR*. Thermochim. Acta, 2006. **444**(1): p. 65-70.
6. Hernández, E., et al., *Sulfuric acid treatment of ground tire rubber and its effect on the mechanical and thermal properties of polypropylene composites*. J. Appl. Polym. Sci., 2017. **134**(21): p. 1-7.
7. Hoyer, S., L. Kroll, and D. Sykutera, *Technology comparison for the production of fine rubber powder from end of life tyres*. Procedia Manuf., 2020. **43**: p. 193-200.
8. Hernández Gámez, J.F., et al., *Mechanical reinforcement of thermoplastic vulcanizates using ground tyre rubber modified with sulfuric acid*. Polym. Compos., 2018. **39**(1): p. 229-237.
9. Zhang, X., et al., *Improvement of the properties of ground tire rubber (GTR)-filled nitrile rubber vulcanizates through plasma surface modification of GTR powder*. J. Appl. Polym. Sci., 2009. **114**(2): p. 1118-1125.
10. Yehia, A.A., et al., *Effect of chemically modified waste rubber powder as a filler in natural rubber vulcanizates*. J. Appl. Polym. Sci., 2004. **93**(1): p. 30-36.
11. Xinxing, Z., et al., *Improvement of the Properties of Ground Tire Rubber (GTR)-Filled Nitrile Rubber Vulcanizates Through Plasma Surface Modification of GTR Powder*. J. Appl. Polym. Sci., 2009. **114**: p. 1118-1125.
12. Cheng, X., et al., *Time effectiveness of the low-temperature plasma surface modification of ground tire rubber powder*. J. Adhes. Sci. Technol., 2015. **29**(13): p. 1330-1340.
13. Yagneswaran, S., et al., *Surface-grafting of ground rubber tire by poly acrylic acid via self-initiated free radical polymerization and composites with epoxy thereof*. Polym. Compos., 2013. **34**(5): p. 769-777.
14. Liang, H., et al., *Ground tire rubber (GTR) surface modification using thiol-ene click reaction: Polystyrene grafting to modify a GTR/polystyrene (PS) blend*. Prog. Rubber Plast. Recycl. Technol., 2019. **36**(2): p. 81-101.
15. Zefeng, W., et al., *Recycling waste tire rubber by water jet pulverization: Powder characteristics and reinforcing performance in natural rubber composites*. J. Polym. Eng., 2018. **38**(1): p. 51-62.
16. Carli, L.N., et al., *Crosslinking kinetics of SBR composites containing vulcanized ground scraps as filler*. Polym. Bull., 2011. **67**(8): p. 1621-1631.
17. Formela, K., et al., *Styrene-Butadiene Rubber/Modified Ground Tire Rubber Blends Co-Vulcanization: Effect of Accelerator Type*. Macromol. Sy., 2016. **361**(1): p. 64-72.
18. Choi, S.-S., B.-H. Park, and H. Song, *Influence of filler type and content on properties of styrene-butadiene rubber (SBR) compound reinforced with carbon black or silica*. Polym. Adv. Technol., 2004. **15**(3): p. 122-127.

19. Maridass, B. and B.R. Gupta, *Effect of Carbon Black on Devulcanized Ground Rubber Tire—Natural Rubber Vulcanizates: Cure Characteristics and Mechanical Properties*. J. Elastomers Plast., 2006. **38**(3): p. 211-229.
20. Sae-oui, P., et al., *Comparison of reinforcing efficiency between Si-69 and Si-264 in a conventional vulcanization system*. Polym. Test., 2004. **23**(8): p. 871-879.
21. Mathew, G., et al., *Improvement of properties of silica-filled styrene-butadiene rubber composites through plasma surface modification of silica*. Polym. Adv. Technol., 2004. **15**: p. 400-408.
22. Sae-oui, P., et al., *Roles of silane coupling agents on properties of silica-filled polychloroprene*. Eur. Polym. J., 2006. **42**(3): p. 479-486.
23. Nelson, P.A. and S.K.N. Kutty, *Effect of Silane Coupling Agent on Cure Characteristics and Mechanical Properties of Chloroprene Rubber/Reclaimed Rubber Blend*. Polym. Plast. Technol. Eng., 2004. **43**(4): p. 1141-1156.
24. Klüppel, M., *The Role of Disorder in Filler Reinforcement of Elastomers on Various Length Scales*, in *Filler-Reinforced Elastomers Scanning Force Microscopy*, B. Capella, et al., Editors. 2003, Springer Berlin Heidelberg: Berlin, Heidelberg. p. 1-86.
25. Fröhlich, J., W. Niedermeier, and H.D. Luginsland, *The effect of filler–filler and filler–elastomer interaction on rubber reinforcement*. Compos. - A: Appl. Sci. Manuf., 2005. **36**: p. 449-460.
26. Nelson, P.A. and S.K.N. Kutty, *Cure Characteristics and Mechanical Properties of Butadiene Rubber/Whole Tyre Reclaimed Rubber Blends*. Prog. Rubber Plast. Recycl. Technol., 2002. **18**(2): p. 85-97.
27. Heo, Y.-J., *A review: role of interfacial adhesion between carbon blacks and elastomeric materials*. Carbon Lett., 2015. **18**: p. 1-10.
28. Sreeja, T. and S. Kutty, *Styrene butadiene rubber/reclaimed rubber blends*. Int. J. Polym. Mater., 2010. **52**: p. 599-609.
29. Formela, K. and J.T. Haponiuk, *Curing characteristics, mechanical properties and morphology of butyl rubber filled with ground tire rubber (GTR)*. Iran. Polym. J., 2014. **23**(3): p. 185-194.
30. Dai, S.-Y., G.-Y. Ao, and M.-S. Kim, *Properties of carbon black/SBR rubber composites filled by surface modified carbon blacks*. Carbon Lett., 2007. **8**(2): p. 115-119.
31. Gibala, D. and G.R. Hamed, *Cure and Mechanical Behavior of Rubber Compounds Containing Ground Vulcanizates. Part I—Cure Behavior*. Rubber Chem. Technol., 1994. **67**(4): p. 636-648.
32. Gibala, D., G.R. Hamed, and J. Zhao, *Tensile Behavior of an SBR Vulcanizate Containing a Single Rubber Particle*. Rubber Chem. Technol., 1998. **71**(5): p. 861-865.
33. Li, S., J. Lamminmäki, and K. Hanhi. *Effect of ground rubber powder on properties of natural rubber*. in *Macromol. Sy.* 2004.
34. Hosseini, S.M., et al., *Comparative role of Interface in reinforcing mechanisms of Nano silica modified by Silanes and liquid rubber in SBR composites*. J. Polym. Res., 2016. **23**(9).
35. Imbernon, L., et al., *Chemically crosslinked yet reprocessable epoxidized natural rubber via thermo-activated disulfide rearrangements*. Polym. Chem., 2015. **6**(23): p. 4271-4278.
36. Nevejans, S., et al., *The underlying mechanisms for self-healing of poly(disulfide)s*. Phys. Chem. Chem. Phys., 2016. **18**(39): p. 27577-27583.
37. Martin, R., et al., *Dynamic sulfur chemistry as a key tool in the design of self-healing polymers*. Smart Mater. Struct., 2016. **25**(8): p. 084017.

38. Xiang, H.P., et al., *Crack healing and reclaiming of vulcanized rubber by triggering the rearrangement of inherent sulfur crosslinked networks*. Green Chem., 2015. **17**(8): p. 4315-4325.
39. Ghorai, S., et al., *Mechanochemical devulcanization of natural rubber vulcanizate by dual function disulfide chemicals*. Polym. Degrad. Stabil., 2016. **129**: p. 34-46.
40. Antony, P. and S.K. De, *Ionic Thermoplastic Elastomers: A review*. J. Macromol. Sci. Polymer Rev., 2001. **41**(1-2): p. 41-77.
41. Laskowska, A., et al., *Ionic elastomers based on carboxylated nitrile rubber (XNBR) and magnesium aluminum layered double hydroxide (hydrotalcite)*. Express Polym. Lett., 2014. **8**(6).
42. Das, A., et al., *Ionic modification turns commercial rubber into a self-healing material*. Acs. Appl. Mater. Inter., 2015. **7**(37): p. 20623-20630.
43. Behera, P.K., S. Mohanty, and V.K. Gupta, *Self-healing elastomers based on conjugated diolefins: a review*. Polym. Chem., 2021. **12**(11): p. 1598-1621.
44. Cheng, B., et al., *Dual cross-linked self-healing and recyclable epoxidized natural rubber based on multiple reversible effects*. ACS Sustain. Chem. Eng., 2019. **7**(4): p. 4443-4455.
45. Wemyss, A., et al., *Dynamic crosslinked rubbers for a green future: A material perspective*. Mater. Sci. Eng. R Rep., 2020. **141**: p. 100561.
46. Xu, C., et al., *Design of self-healable supramolecular hybrid network based on carboxylated styrene butadiene rubber and nano-chitosan*. Carbohydr. Polym., 2019. **205**: p. 410-419.
47. Utrera-Barrios, S., et al., *An effective and sustainable approach for achieving self-healing in nitrile rubber*. Eur. Polym. J., 2020. **139**: p. 110032.
48. Kessler, M.R., N.R. Sottos, and S.R. White, *Self-healing structural composite materials*. Compos. - A: Appl. Sci. Manuf., 2003. **34**(8): p. 743-753.
49. Chuayjuljit, S., et al., *Effects of Particle Size and Amount of Carbon Black and Calcium Carbonate on Curing Characteristics and Dynamic Mechanical Properties of Natural Rubber*. J. Met. Mater. Miner., 2002. **12**(1): p. 51-57.
50. Al-maamori, M.H., A.A.-A. Al-Zubaidi, and A.A. Subeh, *Effect of Carbon Black on Mechanical and Physical Properties of Acrylonitrile Butadiene Rubber (NBR) Composite*. Int. J. Acad. Res., 2015. **6**(2): p. 28.
51. Li, Z., J. Zhang, and S.J. Chen, *Effects of carbon blacks with various structures on vulcanization and reinforcement of filled ethylene-propylene-diene rubber*. Express Polym. Lett., 2008. **2**: p. 695-704.
52. Robertson, C.G. and N.J. Hardman, *Nature of Carbon Black Reinforcement of Rubber: Perspective on the Original Polymer Nanocomposite*. Polymers, 2021. **13**(4): p. 538.
53. Mostafa, A., et al., *The influence of CB loading on thermal aging resistance of SBR and NBR rubber compounds under different aging temperature*. Mater. Des., 2009. **30**(3): p. 791-795.
54. Hayes, S., et al., *Self-healing of damage in fibre-reinforced polymer-matrix composites*. J. R. Soc. Interface, 2007. **4**(13): p. 381-387.
55. Liu, J., et al., *Construction of a Dual Ionic Network in Natural Rubber with High Self-Healing Efficiency through Anionic Mechanism*. Ind. Eng. Chem. Res., 2020. **59**(28): p. 12755-12765.
56. Stein, S., et al., *Self-healing and reprocessable bromo butylrubber based on combined ionic cluster formation and hydrogen bonding*. Polym. Chem., 2020. **11**(6): p. 1188-1197.
57. Chen, Y., et al., *Mechanically Robust, Self-Healable, and Reprocessable Elastomers Enabled by Dynamic Dual Cross-Links*. Macromolecules, 2019. **52**(10): p. 3805-3812.

58. Xu, S., et al., *A dual supramolecular crosslinked polyurethane with superior mechanical properties and autonomous self-healing ability*. *New J. Chem.*, 2020. **44**(18): p. 7395-7400.
59. Chang, K., H. Jia, and S.-Y. Gu, *A transparent, highly stretchable, self-healing polyurethane based on disulfide bonds*. *Eur. Polym. J.*, 2019. **112**: p. 822-831.
60. Singh, G., A. Mahajan, and M. Kumar, *Comparative study of tyre rubber and v-belt rubber: composition and mechanical properties*. *IOSR J. Mech. Civ. Eng.*, 2015. **12**(5): p. 60-65.

5

“R” AS REDUCE DYNAMICS OF SBR COMPOSITES

5. “R” as Reduce – Dynamics of SBR/GTR Composites

Tire industry is constantly looking at new compound formulations to “reduce” the total weight of the vehicle and, hence, the fuel consumption. These new rubber compounds have to be analyzed in terms of the so-called “magic triangle” of tire technology. This triangle describes the intertwined relationship between three tire performance factors: rolling resistance (fuel consumption), wet grip (driving safety), and wear resistance (durability), that are intimately linked to the viscoelastic properties of the material. As an example, low hysteresis losses account for low rolling resistance.

This chapter performs an in-depth and systematic analysis of the dynamics and molecular structure of the SBR compounds to comprehend the healing capability of the rubber matrix; as well as on the three major indices of the magic triangle of tires. It specifically studies broadband dielectric spectroscopy (BDS) and dynamic mechanical analysis (DMA) of the rubber compounds under three different conditions: pristine, damaged (under cyclic deformation), and healed. A schematic representation on the content of Chapter 5 is shown in Figure 5.1.

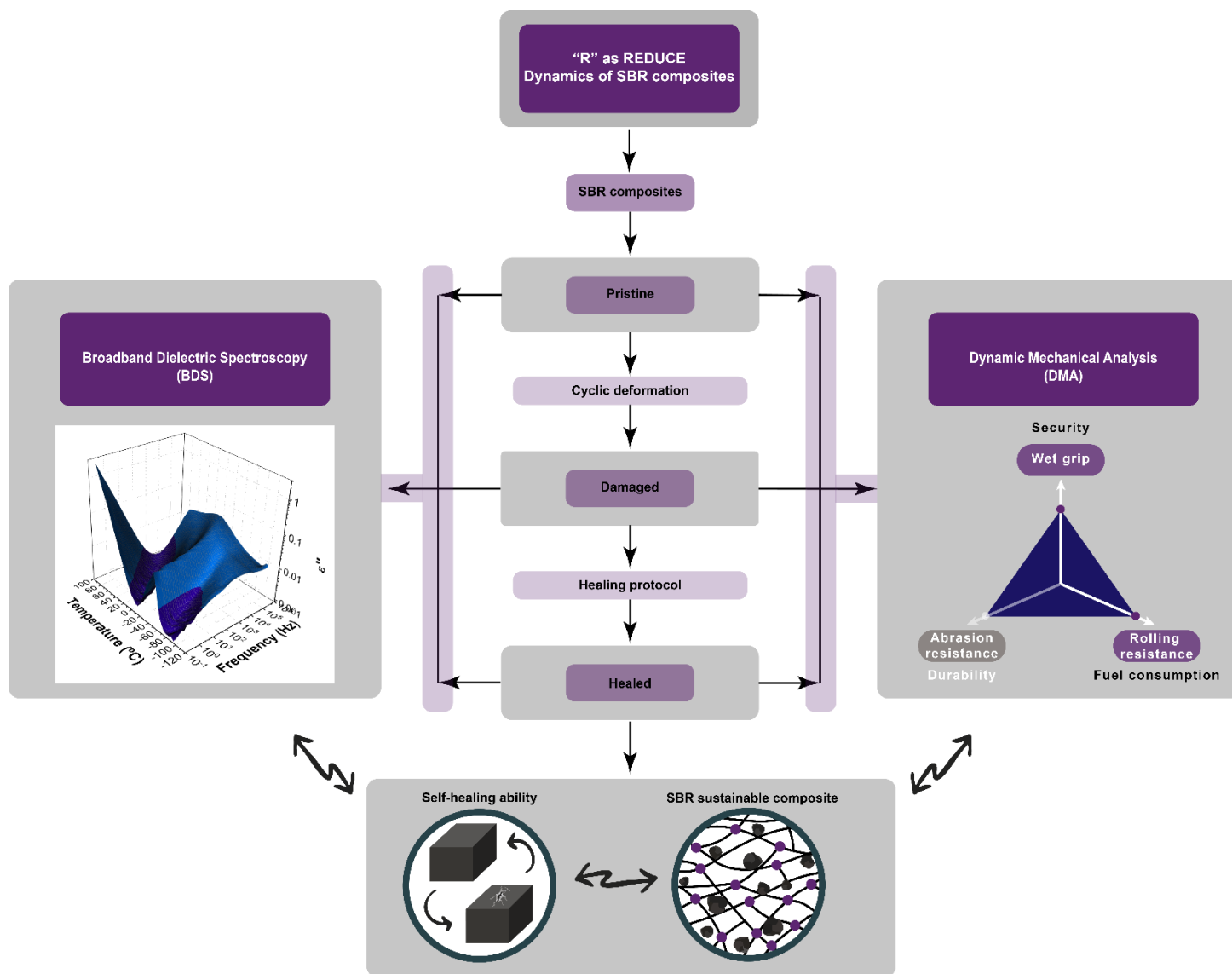


Figure 5.1 Schematic representation of Chapter 5. "R" as Reduce – Dynamics of SBR composites.

5.1. Experimental

5.1.1. Broadband dielectric spectroscopy (BDS)

Broadband dielectric spectroscopy (BDS) has proved to be a very useful tool for studying the molecular dynamics of polymers, since it enables the study over wide temperature and dynamic ranges, between 10^{-2} up to 10^9 Hz. In dielectric spectroscopy, the external source is an electric field, \vec{E} , which polarizes the material resulting in different types of responses: i) electronic polarization that causes induced dipoles due to the distortion of the electron cloud of each atom with respect to the positive nucleus; ii) atomic polarization due to slight displacements of atoms or groups of atoms of the macromolecule; and iii) the orientational polarization, which corresponds to the reorientation of the permanent dipoles in the direction of the applied electric field (Figure 5.2).[1, 2]

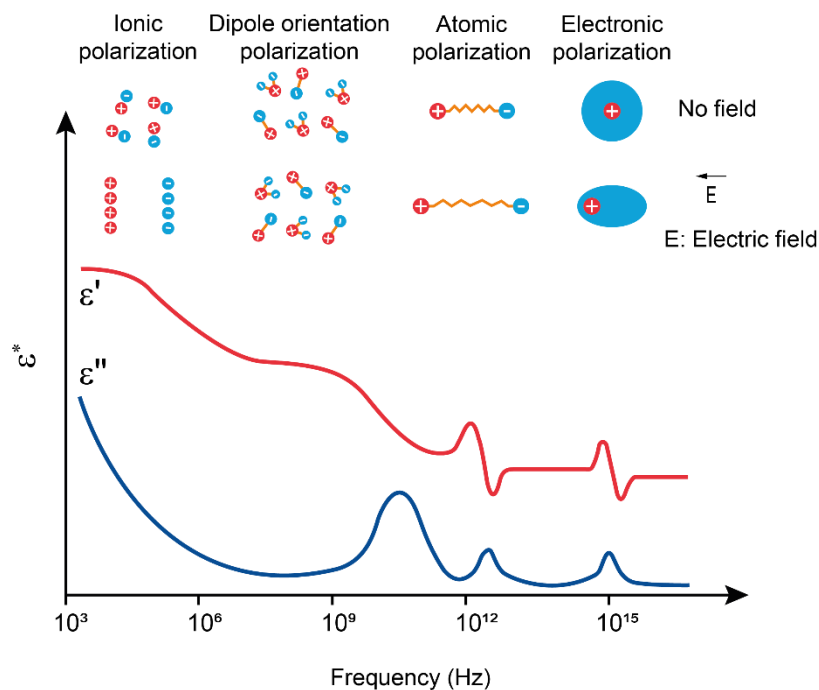


Figure 5.2 Polarization mechanism as a function of frequency.[1]

Permanent dipoles associated to the chain bonds help to study their movement as a function of the frequency of the \vec{E} and temperature. When an \vec{E} is applied, the orientational distribution changes and becomes anisotropic. In order to reach the new equilibrium state, a finite time is required since intermolecular forces hinder free rotation of the units that contribute to dipoles. For independent units, this movement can be described as a

rotational diffusion resulting in a complete reorientation in a characteristic relaxation time, τ . While for interacting dipoles, the movement to equilibrium is characterized by a distribution of relaxation times.

Thus, the dielectric orientational relaxation time can be defined as the time required for dipoles to become field-oriented when applying an electric field. For symmetric peaks, the relaxation time can be determined from the reciprocal of the loss peak frequency (when the dipolar relaxation reaches its maximum). Relaxation time as a function of the frequency is described according to the following equation:

$$\tau = \frac{1}{2\pi\omega_{max}} \quad (5.1)$$

where ω_{max} corresponds with the frequency at the maximum loss.

The polymeric properties monitored by BDS are: dielectric permittivity (ϵ') as a measure of the degree of alignment of the chain dipoles to the applied \vec{E} , and loss factor or permittivity loss (ϵ'') which represents the energy required to align the dipoles.[2] These parameters are analogous to the elastic and viscous modulus in DMA, respectively.[3] Dielectric permittivity is usually written in the complex form:

$$\epsilon^*(\omega) = \epsilon'(\omega) - i\epsilon''(\omega) \quad (5.2)$$

where ϵ^* is the complex dielectric permittivity, and ϵ' and ϵ'' the real and the imaginary part, respectively. Relaxation processes are characterized by a peak in the imaginary part and a step-like decrease of the real part of the complex dielectric function with increasing frequency.[4] A schematic representation of the frequency dependence of $\epsilon^*(\omega)$ is given in Figure 5.3.

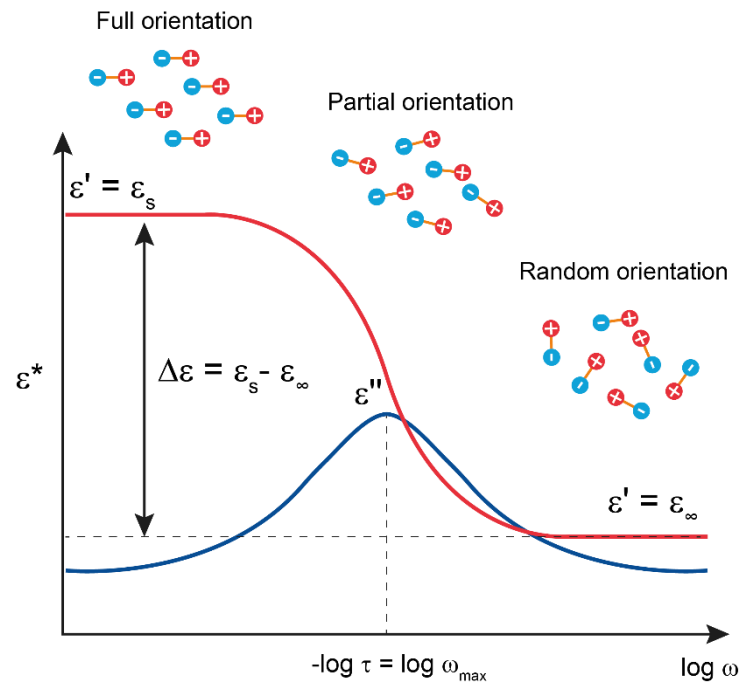


Figure 5.3 Frequency variation of the real ϵ' and imaginary ϵ'' part of the complex ϵ^* dielectric permittivity.

Both, the step in ϵ' and the loss peak in ϵ'' are centered at a characteristic frequency. At low frequencies, molecular dipoles can follow the electric field with a complete orientation giving rise to a plateau of the dielectric permittivity.

One of the most widely used functions that describe, in the frequency domain, the broadened and asymmetrically shaped dielectric relaxation of polymers is the Havriliak–Negami (HN) function, according to the following equation:

$$\epsilon^*(\omega) = \epsilon_\infty + \frac{\Delta\epsilon}{[1 + (i\omega\tau_{HN})^b]^c} \quad (5.3)$$

where $\Delta\epsilon = \epsilon_s - \epsilon_\infty$ is the relaxation strength, ϵ_s and ϵ_∞ refer to the low and the high frequency permittivity, respectively, τ_{HN} is the characteristic HN relaxation time, which corresponds to the most probable value of the distribution function of relaxation times, and b and c are so-called shape parameters ($0 < b, c \leq 1$) which describe the symmetric and the asymmetric broadening of the equivalent relaxation time distribution function, respectively. τ_{HN} is related to the frequency of maximum loss.[4-6]

Depending on the temperature dependence of the relaxation times, these processes can be described by the Arrhenius equation or the Vogel-Fulcher-Tamman-Hesse (VFTH) equation. The Arrhenius equation represents a widely used way for describing the linear inverse temperature dependence of relaxation times (τ_{max}):

$$\tau_{max} = \tau_0 \exp\left(\frac{-E_a}{RT}\right) \quad (5.4)$$

where τ_0 is an empirical parameter, E_a is the activation energy and R is the universal gas constant (8.314 K J mol⁻¹).

The non-linearity temperature dependence of the relaxation time (τ_{max}) process can be described via the empirical Vogel-Fulcher-Tamman-Hesse (VFTH) equation:

$$\tau_{max} = \tau_0 \exp\left(\frac{B}{T-T_0}\right) \quad (5.5)$$

where τ_0 and B are empirical parameters, T_0 is the so-called ideal glass transition or Vogel temperature, sometimes also called ideal glass transition temperature, which is generally 30 – 70 K below T_g . [7] To reduce the effect of data fitting to the VFT equation over a limited frequency range, a value of $\text{Log } \tau_0 \approx 14$ s is normally used. [8] This assumption does not affect the quality of the data fit into the VFT equation, but reduces the dispersion among fitting parameters.

The dielectric spectroscopy measurements were carried out on a high-resolution dielectric analyzer ALPHA (Novocontrol Technologies GmbH) as explained in Chapter 2. First, pristine samples were analyzed to evaluate the individual effects of the sulfur content, curing system, filler type and content, coupling agent, and hybrid systems. Secondly, a complete study was made to microscopically damaged and healed samples of selected SBR composites.

5.1.2. Dynamic-mechanical analysis (DMA)

DMA is one of the most widely used techniques to study the influence of molecular structure on the physical properties of polymers. This technique consists of subjecting the

sample to a small cyclic deformation, generally sinusoidal, and recording the response as a function of time or temperature.[9]

The viscoelastic behavior of a material can be modeled using a sinusoidal strain, $\varepsilon(t)$, of an angular frequency, (ω) , where the tensile stress response, $\sigma(t)$, is phase shifted, according to the following equations:

$$\varepsilon(t) = \varepsilon_0 \sin(\omega t) \quad (5.6)$$

$$\sigma(t) = \sigma_0 \sin(\omega t + \delta) \quad (5.7)$$

where ε_0 is the maximum strain, σ_0 is the maximum stress, t is the time, and δ is the phase angle (Figure 5.4).

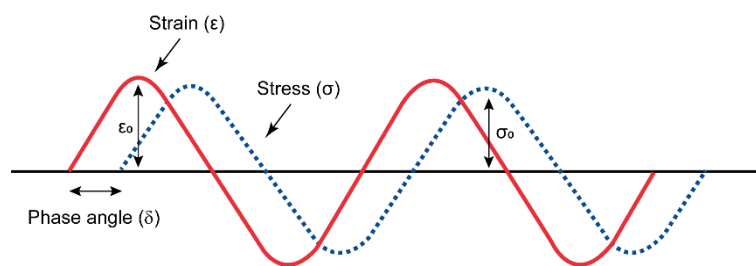


Figure 5.4 Sinusoidal strain and the corresponding delayed stress response of a viscoelastic material.

This type of test allows the determination of the storage modulus (E') and the loss modulus (E''). E' is related to the mechanical energy stored by the sample in a cycle; it is the elastic response and corresponds to the fully recoverable energy. Meanwhile, E'' is related to the energy dissipated in a cycle, the viscous response, in the form of heat when the sample is deformed. Damping is the parameter that evaluates the ratio between the loss modulus and the storage modulus, and is called the loss factor, $\tan \delta$, according to the following equations:

$$E' = \frac{\sigma_0}{\varepsilon_0} \cos(\delta) \quad (5.8)$$

$$E'' = \frac{\sigma_0}{\varepsilon_0} \sin(\delta) \quad (5.9)$$

$$\tan \delta = \frac{E''}{E'} \quad (5.10)$$

DMA measurements are also of utmost interest for the tire industry, since the prediction of tire performance is usually evaluated by considering the viscoelastic properties of rubber. The “magic triangle” principle of the tire industry is related to three main material-specific requirements relevant to the tread, such as rolling resistance, wet grip, and abrasion resistance; targeting lower fuel saving efficiency, driving safety, and extended lifetime, respectively (Figure 5.5).

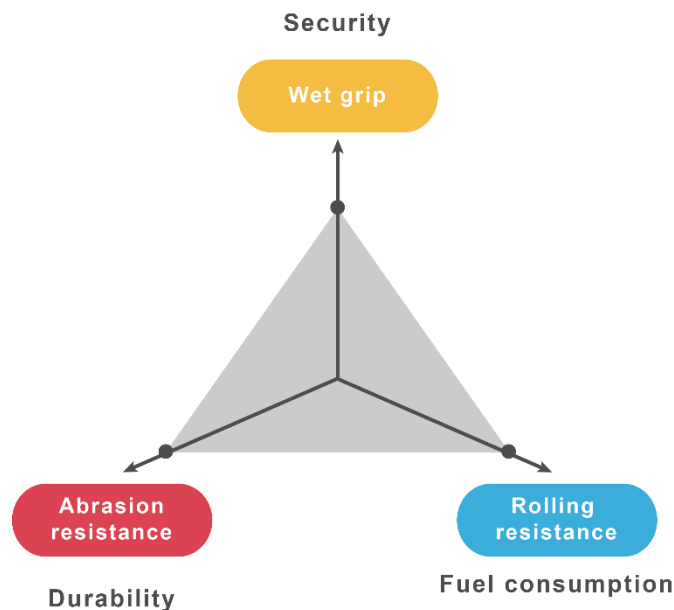


Figure 5.5 Illustration of the “magic triangle” of tires.

The $\tan \delta$ is frequently used to foresee the rolling resistance and the wet grip of tires, these two parameters being linked to fuel economy and driving safety, respectively. The basic theory behind these parameters is related to the hysteresis of the rubber compound by the continuous deformation of the sample at different temperatures. During driving, tires rotate at relatively low frequencies ($\sim 10^1 - 10^2$ Hz), whereas the temperature reached by the tire tread is $\sim 50 - 80$ °C due to the energy dissipation of rubber during the dynamic deformation. In general, the lower $\tan \delta$ value at 60 °C, the lower the rolling resistance and, thus, higher fuel-saving efficiency. On the other hand, when full brakes are applied

on a wet road, the tire tread will be subjected to periodical deformation at very high frequencies ($\sim 10^4 - 10^5$ Hz) due to the dynamic sliding contact on the road roughness. Based on the Williams–Landel–Ferry (WLF) equation, this high frequency could be estimated by measuring at lower frequencies and shifting the measured temperature toward lower temperatures. Hence, the wet grip efficiency of rubber can be predicted considering the $\tan \delta$ value at $-20 - 0$ °C; where high values imply better wet grip. The ideal condition would then be to achieve a high $\tan \delta$ at -10 °C to ensure appropriate wet traction and, simultaneously, a low $\tan \delta$ at 60 °C to guarantee low rolling resistance and better fuel economy (Figure 5.6).

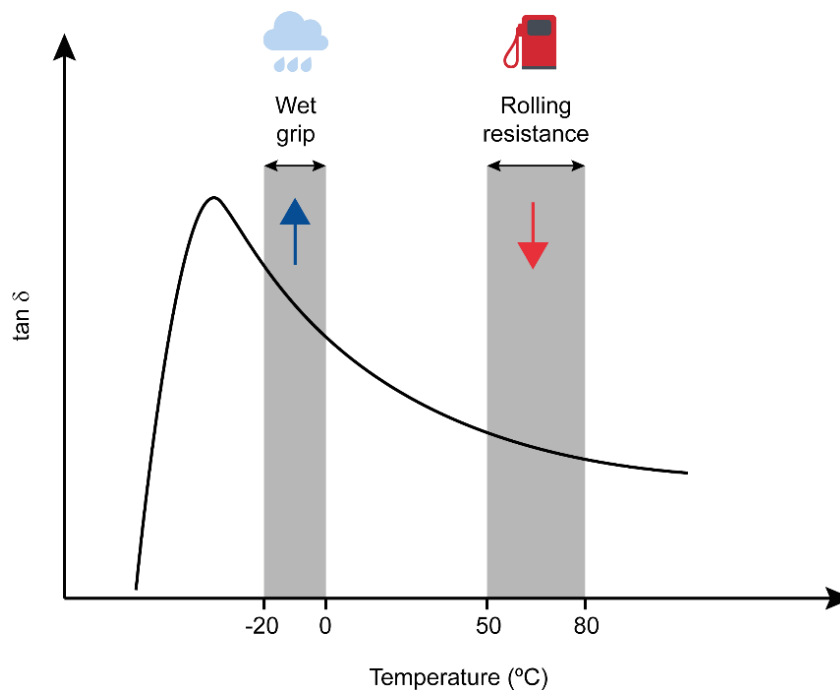


Figure 5.6 Temperature dependence of the loss factor for tire performances.[10]

The DMA measurements of vulcanized samples were carried out in a DMA Q800 device (TA Instruments) as explained in Chapter 2. Following and complementing the analysis by means of BDS, pristine samples were initially tested evaluating the effect of the different components of the SBR composites (curing system, filler, coupling agent, etc). Afterwards, a comparative analysis was done to pristine, damaged and healed samples of selected SBR composites.

5.1.3. Microscopic network damage

Rubber composites were subjected to a cyclic deformation protocol. Tests were done on a universal mechanical testing machine (Instron 3366) equipped with a 1 kN load cell at room temperature. Type 3 dumbbell-shaped samples with a thickness of 2.0 ± 0.2 mm and a width in the narrow section of 4.0 ± 0.2 mm and films ($50 \text{ mm} \times 35 \text{ mm} \times 0.3 \text{ mm}$) were tested during 20 stretching cycles at a speed of 500 mm/min up to 400 % of deformation of each composite. After being damaged by cyclic deformation, the samples were kept for 30 min at room temperature and, then, a healing protocol (130 °C and 1 h) was applied to the rubber composites. A schematic representation of the microscopic network damage is shown in Figure 5.7. Afterwards, the samples were retested by BDS and DMA.

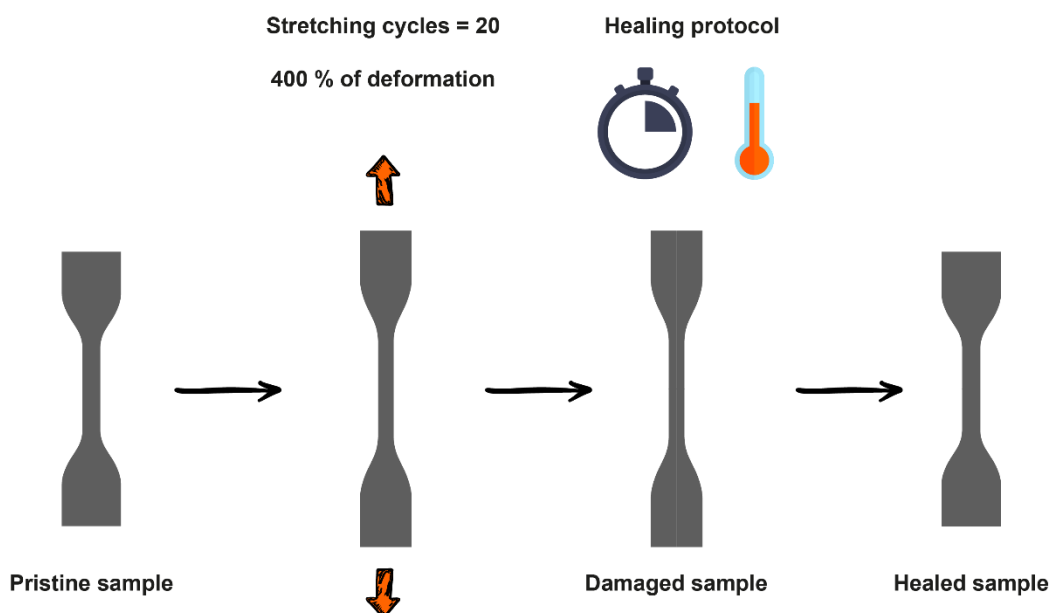


Figure 5.7 Schematic representation of microscopic network damage.

5.2. BDS analysis. Evaluation of pristine composites.

5.2.1. Effect of sulfur content

The dielectric response of several vulcanized formulations was evaluated as a first approach to study the molecular dynamics of SBR compounds. In the first series of experiments, the effect of the S content was explored, in order to understand in a systematic way, how the relaxation processes of SBR can be influenced by the cross-link density.

Figure 5.8 shows the dielectric loss (ϵ'') spectra of two selected unfilled compounds with different S content ($S_{0.7}$ and S_1), as a function of frequency at temperatures approaching the glass transition ($-55\text{ }^\circ\text{C}$). A maximum is observed, evolving towards higher frequencies as the temperature increases, a well-known characteristic of thermally activated processes. This maximum is related to a relaxation, known as segmental mode or α -relaxation, due to the cooperative rearrangements of polymer chain segments.[11]

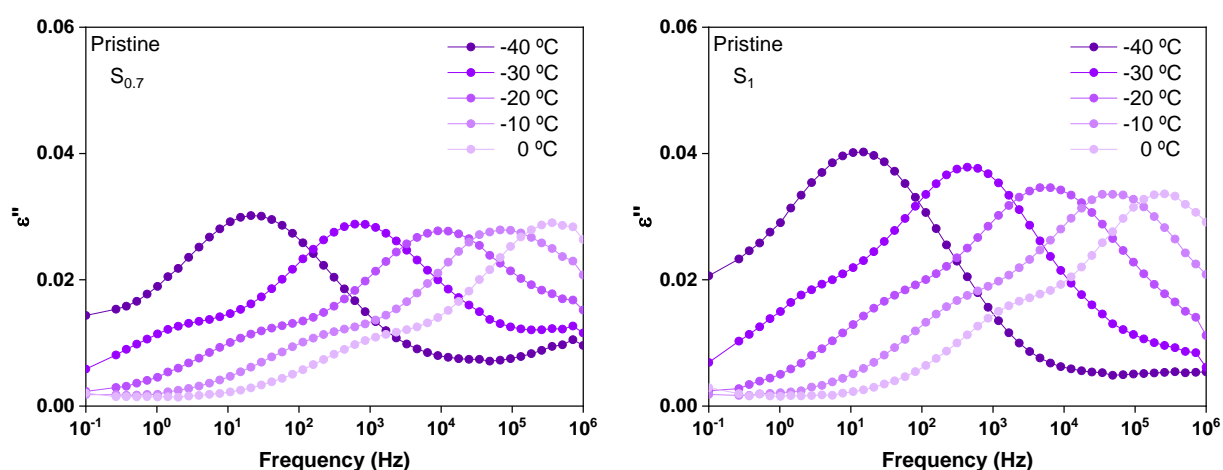


Figure 5.8 Dielectric loss (ϵ'') as function of frequency in the temperature range from -40 to $0\text{ }^\circ\text{C}$ of unfilled SBR compounds vulcanized with 0.7 and 1 phr of S.

To discuss the dependence of the dielectric loss (ϵ'') on frequency, it is useful to consider its value normalized to its maximum value. For comparison purposes, Figure 5.9 shows the normalized dielectric loss of both SBR compounds over a wide frequency range and at a selected temperature ($-20\text{ }^\circ\text{C}$). This temperature is chosen since at this point, the segmental mode process is well centered and well resolved within the frequency window, and manifests itself as a relatively broad and asymmetric peak. Nevertheless, the trends obtained at this selected temperature can well be applied to the whole temperature range where the segmental mode is present. It can be seen how the molecular mobility of the polymer segments is influenced by the cross-linking degree since the dielectric loss maximum shifts to lower frequencies as the S content increases. This shift is the result of the inherent constraints to the segmental motions, imposed by higher cross-linking points.[8, 12] The cross-link density and T_g values compiled in Table 5.1 further support this explanation. Similar results were reported by Hernández *et al.*[13] on NR compounds.

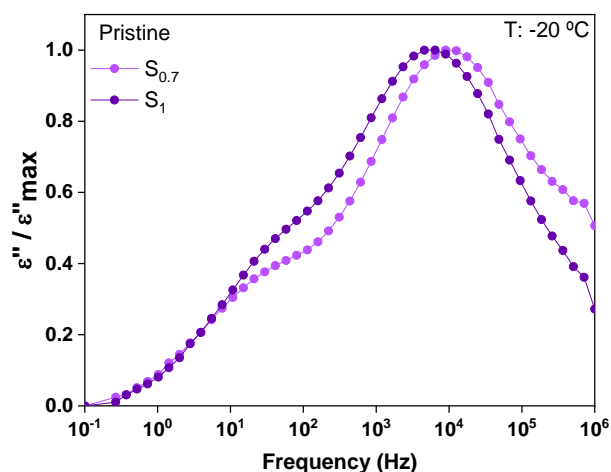


Figure 5.9 Normalized dielectric loss, ϵ'' , at $-20\text{ }^{\circ}\text{C}$ of unfilled SBR compounds vulcanized with 0.7 and 1 phr of S.

Table 5.1 T_g and cross-link density of SBR compounds with different content of S.

Compound	S _{0.7}	S ₁
T_g ($^{\circ}\text{C}$) by DSC	-53 ± 1	-50 ± 1
$\nu \times 10^{-5}$ (mol/g)	0.76 ± 0.01	2.27 ± 0.03

5.2.2. Effect of curing system

DCP vulcanized SBR was evaluated and compared to a S vulcanized SBR compound (S₁). From the analysis of Figure 5.10a and Figure 5.10b, it can be seen that SBR_S and SBR_{DCP} show the same main peak ascribed to the α -relaxation. One can also notice that the S system presents more restricted dynamics, evidenced by the shift of the maximum to lower frequencies (Figure 5.10c) as a consequence of a more cross-linked network (see Table 5.2).

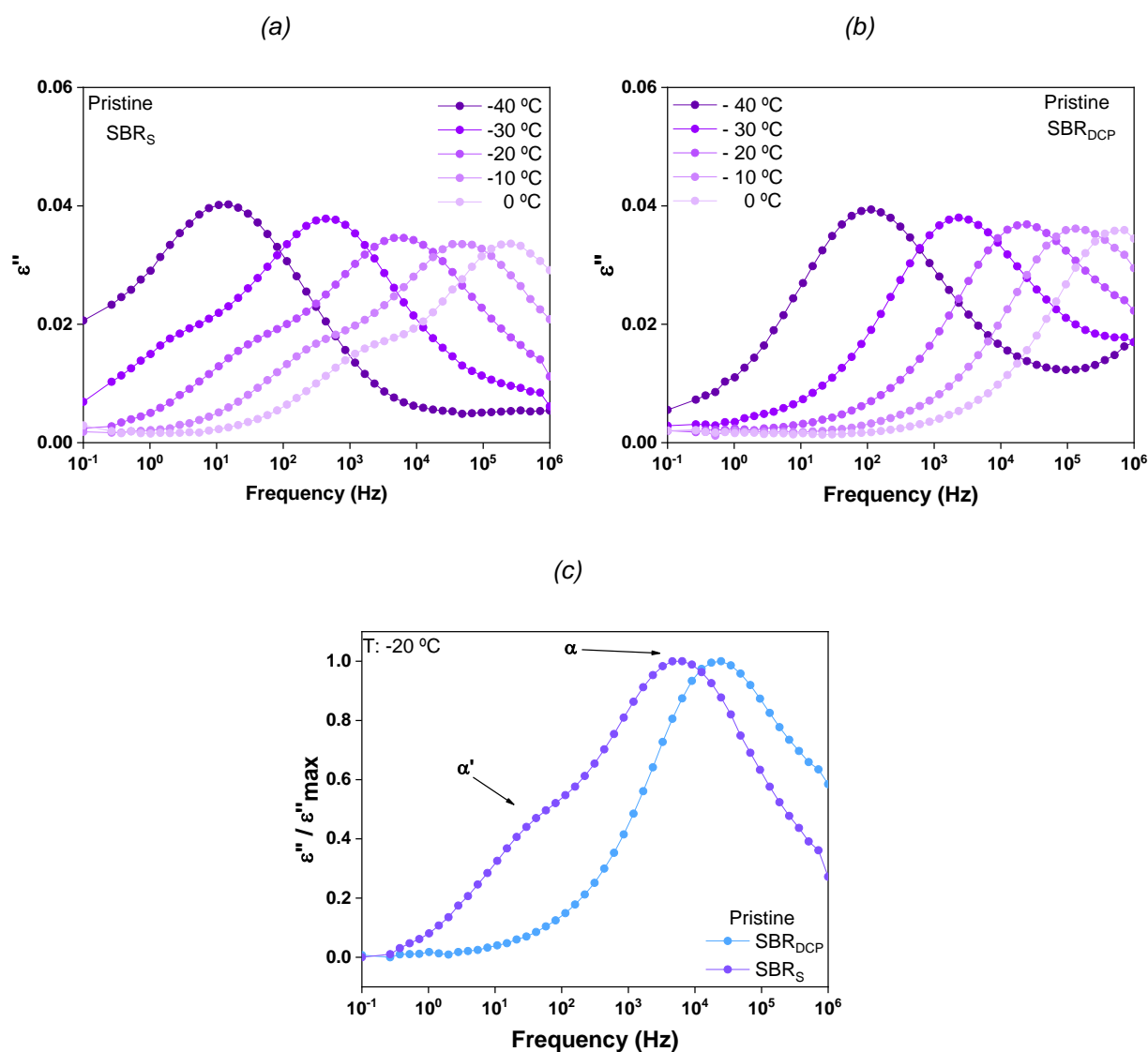


Figure 5.10 Dielectric loss (ϵ'') as function of frequency from -40 to 0 °C of (a) SBR_S and (b) SBR_{DCP}.
 (c) Normalized dielectric loss at -20 °C of SBR_S and SBR_{DCP} compounds.

Table 5.2 T_g and cross-link density of SBR_{DCP} and SBR_S compounds.

Compound	SBR _{DCP}	SBR _S
T_g (°C) by DSC	-54 ± 1	-50 ± 1
$\nu \times 10^{-5}$ (mol/g)	1.68 ± 0.03	2.27 ± 0.03

Other interesting observation worth analyzing is that the α -relaxation of SBR_{DCP} shows a single broad peak as normally observed for most polymers.[2] Meanwhile, in SBR_S it is not possible to describe the main peak by a single process. Instead, it is made up of two distinct contributions, showing an asymmetric relaxation peak due to a shoulder on the

low-frequency side. This asymmetric relaxation peak clearly contains two contributions, the α -relaxation (faster process) and α' -relaxation (slower process). This second contribution, absent in SBR_{DCP}, could be related to the presence of some vulcanization additives or due to some new product generated during the vulcanization process, since the main differences between the SBR_s and SBR_{DCP} are associated to the vulcanization system. Similar results were reported by Rathi *et al.*[14] and Ortega *et al.*[15] Ortega *et al.* studied the role of vulcanizing additives on the α -relaxation of neat and vulcanized SBR. They assigned the low-frequency broadening of the dielectric loss peak to an extra contribution due to the presence of some additives, particularly the accelerants such as CBS. CBS has associated a relative strong dipole moment that can be detected by dielectric spectroscopy in a temperature range close to the α -relaxation of SBR.[15] Furthermore, it can be assumed that the dipoles of the CBS couple to the SBR chain segments instead of having an independent relaxation process. Therefore, at the end of the vulcanization process, the sulfur bridges link two rubber chains but other products, like the accelerant, could remain in the compound without being chemically attached to the rubber chain or contributing to the final molecular dynamics of the compound.[16]

The relaxation processes are commonly modeled by the HN function. A typical fit of the dielectric data to the HN function is shown in Figure 5.11 for a selected temperature (T: -20 °C). Two HN equations were applied for SBR_s to obtain a good fit for the α -process but the fitting parameters for the α' -process are not considered in the discussion of the molecular dynamics of the compounds. The solid lines represent the HN fitting curve that has been deconvoluted into individual relaxation processes represented as lines with symbols. A conductivity contribution, shown as dashed lines, was used in the fitting protocol to achieve a better fit of the low frequency tail of the dielectric spectra. The relaxation parameters: $\Delta\varepsilon$, $\tau_{HN(\alpha)}$, b , and c are listed in Table 5.3. In the selected temperature range, the τ_{HN} of the SBR_s are higher than those of the SBR_{DCP}, evidencing the more restricted network in presence of S.

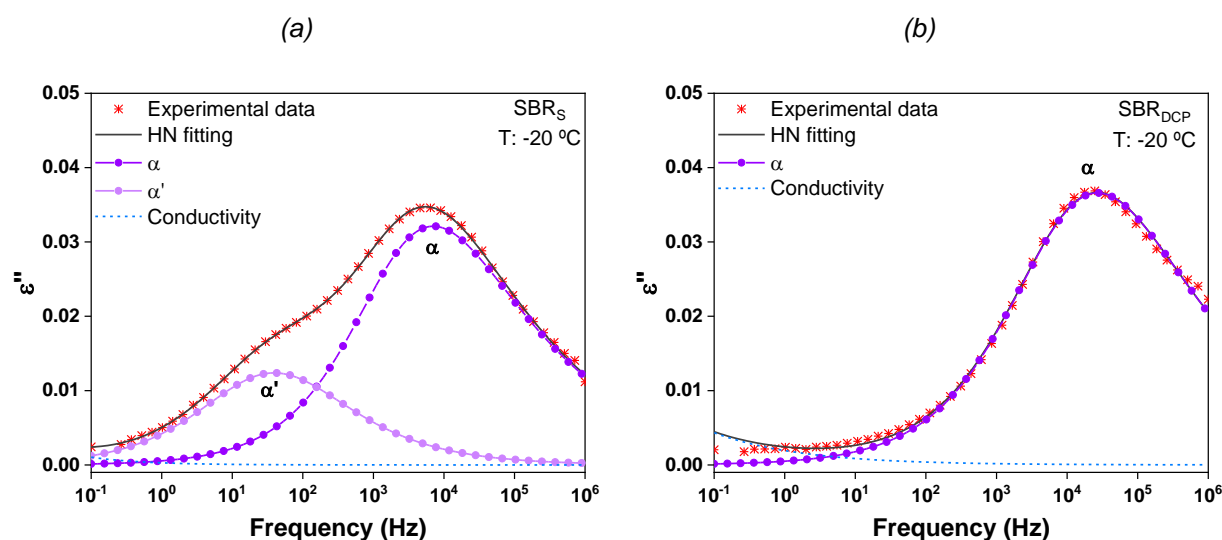


Figure 5.11 Deconvolution results for the dielectric loss (ϵ'') of SBR compounds vulcanized by (a) sulfur (S) and (b) DCP. Solid lines represent the HN fitting curve, symbol lines the individual processes, and dashed lines the conductivity contribution.

Table 5.3 Havriliak-Negami (HN) parameters for the segmental mode of SBR_S and SBR_{DCP} compounds at T: -20, -10 and 0 °C.

Compound	T (°C)	$\Delta\epsilon$	$\tau_{HN(\alpha)}$ (s)	b	c
SBR _S	-20	1.65×10^{-1}	6.55×10^{-5}	6.15×10^{-1}	4.98×10^{-1}
	-10	1.61×10^{-1}	7.67×10^{-6}	8.77×10^{-1}	4.93×10^{-1}
	0	2.33×10^{-1}	3.39×10^{-6}	9.23×10^{-1}	1.23×10^{-1}
SBR _{DCP}	-20	1.99×10^{-1}	1.61×10^{-5}	5.71×10^{-1}	5.52×10^{-1}
	-10	1.92×10^{-1}	2.68×10^{-6}	5.67×10^{-1}	5.59×10^{-1}
	0	1.86×10^{-1}	5.30×10^{-6}	5.50×10^{-1}	5.88×10^{-1}

The calculation of the relaxation times, τ , allows the determination of the temperature dependence of the relaxation processes. A characteristic relaxation time is obtained from a curve fit to the peak maximum frequency at each temperature. Figure 5.12 shows the α -relaxation times plotted as a function of the inverse temperature. The temperature dependence of the relaxation time displays the characteristic curvature of a VFTH dependence, ascribed to cooperative relaxations motions.[17] The parameters for these fits are listed in Table 5.4.

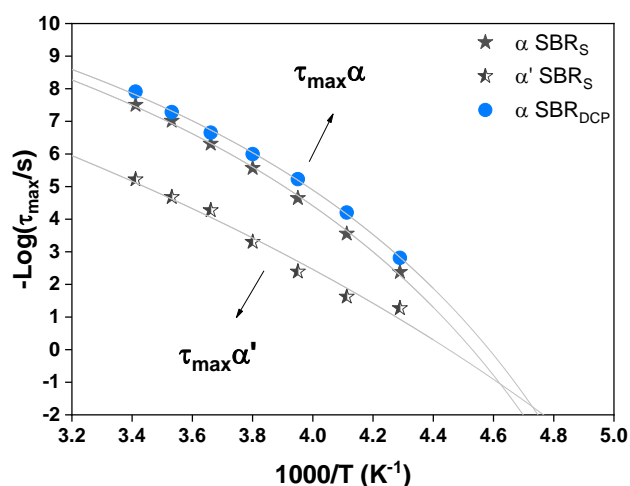


Figure 5.12 Temperature dependence of the average relaxation time of SBR compounds.

Table 5.4 VFTH fitting parameters of DCP and S vulcanized SBR compounds.

Compound	B	T ₀ (K)	T _g (°C) at τ _{100s}
SBR _S	2046	157	-60
SBR _{DCP}	1914	159	-62

As can be noticed, the relaxation times of the α -relaxation for SBR_{DCP} and SBR_S are quite similar in the whole temperature range. A slight displacement to higher temperatures is observed when vulcanization is carried out by sulfur, meaning that more temperature (or time) is needed for promoting the motions of rubber chain segments. This shift correlates well to the higher cross-link density reached by SBR_S compared to SBR_{DCP} compound.

By convention, the extrapolation of the VFTH fit to the temperature at which τ is equal to 100 s, (τ_{100s}), (10^{-2} Hz), provides a dielectric estimation of the glass transition temperature, T_g , similar to that measured by DSC. The corresponding T_g for each system is listed in Table 5.4 with very similar values to those measured by DSC (Table 5.2). The extrapolation to 100 s can sometimes be misleading, as it is far from the experimentally obtained results. However, for the systems studied, the values obtained for 100 s are very complimentary and maintain a similar trend.

5.2.3. Effect of filler type and content

Figure 5.13 shows the normalized dielectric loss spectra as a function of frequency of SBR composites (sulfur-based with 1 phr S, S₁) filled with different content of c-GTR and m-GTR at -20 °C. It can be seen that in the SBR composites filled with c-GTR, the α -relaxation remains unaffected. However, the slow process (α' -relaxation) is more pronounced and broader as the c-GTR content increases. This indicates that higher inter-molecular interactions take part in the relaxation process, increasing hindrance of large scale motions.[11] This effect could be attributed to the migration of unreacted cross-linking precursor fragments (accelerants and activators) from the c-GTR towards the virgin matrix.

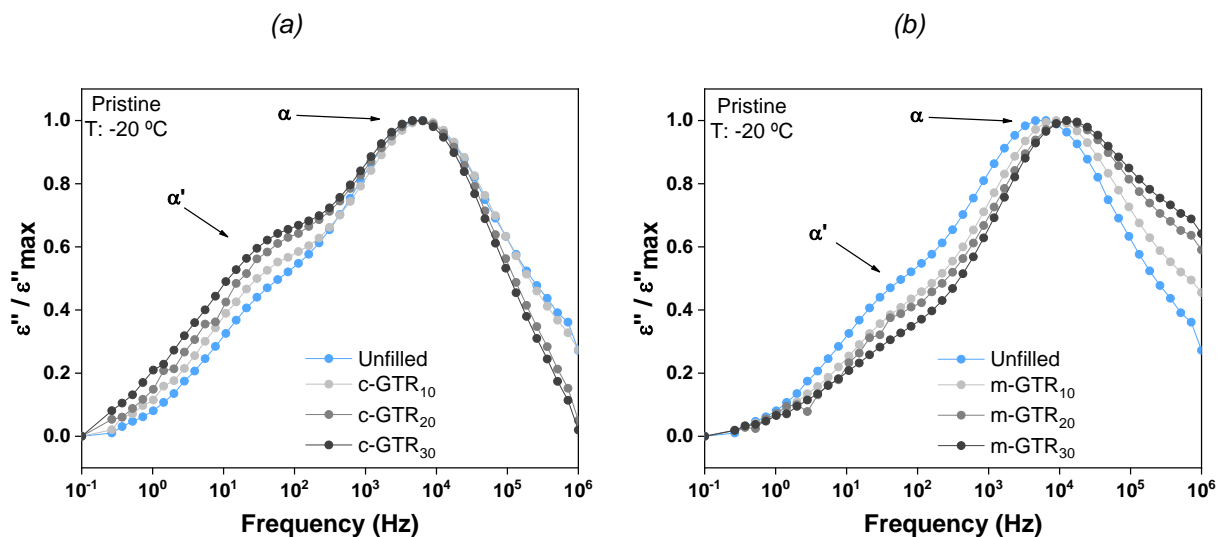


Figure 5.13 Normalized dielectric loss at -20 °C of unfilled SBR and SBR composites with different content of (a) c-GTR and (b) m-GTR.

In contrast, SBR mixed with m-GTR shows a shift of the α -relaxation to higher frequencies as the m-GTR content increases. Furthermore, there is a decrease in the α' -relaxation intensity. This behavior could be ascribed to the adsorption of the CBS by the m-GTR particles due to the hydroxyl groups on their surface, as previously detailed in Chapter 4. Therefore, the vulcanization process is hindered, resulting in m-GTR composites with lower cross-link density and less restricted chain dynamics. Another aspect to consider is the broadening on the high frequency side. The phenomenological model of Schönhals and Schlosser[18] proposes that the shape of the dielectric loss peak is related to the behavior of the polymer at low and high frequencies, controlled by inter-

and intra-molecular interactions, respectively. The application of such a model to the studied SBR suggests that the variations on the high-frequency side can be attributed to inhomogeneities in the local surrounding of the polymer chain segments (intra-molecular interactions).[11] Miura *et al.*[19] reported the dielectric relaxation of poly *o*-chlorostyrene – PoCS, polystyrene – PS, PoCS/PS blend and P(oCS/S) random copolymer. They found that the shape of the relaxation process of the polymer blend was broader than that of the copolymer due to the heterogeneity of the blend at the segmental level.

As previously mentioned in Chapter 4, the addition of both c-GTR and m-GTR tends to decrease the cross-link density. Thus, it is reasonable to expect that changes in the cross-link density can be observed in the dynamics. As studied in the previous section, a decrease in cross-link density increases the segmental mobility of rubber molecules. However, the dielectric loss spectra of the SBR composites showed different behaviors depending on the type of sustainable filler used. The α -relaxation process remains unaffected for c-GTR filled composites, meanwhile m-GTR filler composites show a shift to higher frequencies, as a result of an accelerated dynamics. Published studies report decreases, increases, or no change in the segmental relaxation and T_g (parameters deeply related to each other) after the addition of CB, Si, or other reinforcing filler, despite their good dispersion, high surface area and significant levels of “bound” polymer from chemically modified polymer–filler interfaces.[20, 21] No universal conclusions have yet been reached. Therefore, the nature of the interfacial interactions between the filler particles and the polymer may be the reason for the discrepancies between structure and dynamics.[22]

The series of plots in Figure 5.14 show the experimental data of the dielectric loss versus frequency for c-GTR and m-GTR composites fitted in terms of the phenomenological HN function at a selected temperature. Similar to the previous analysis, a superposition of two HN functions corresponding to each one of the experimentally determined relaxations (α and α'), plus a conductivity contribution, were considered to fit the dielectric data. The α -relaxation parameters are listed in Table 5.5.

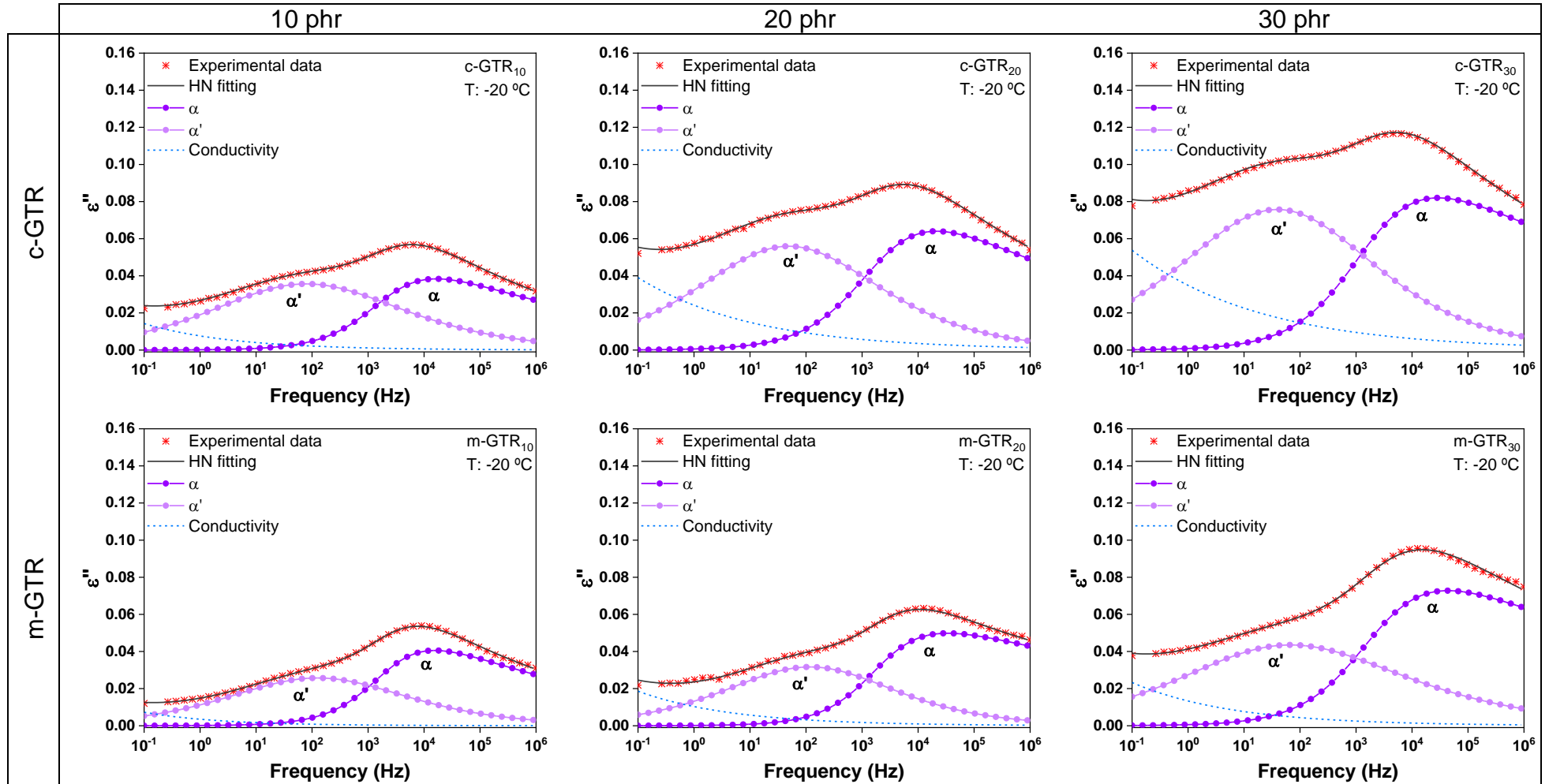


Figure 5.14 Deconvolution results for the dielectric loss (ϵ'') of c-GTR and m-GTR composites. Solid lines represent the HN fitting curve, symbol lines the individual processes, and dashed lines the conductivity contribution.

Table 5.5 Havriliak-Negami (HN) parameters for the α -relaxation of c-GTR and m-GTR composites at T : -20, -10 and 0 °C.

Composite	T (°C)	$\Delta\varepsilon$	$\tau_{HN(\alpha)}$ (s)	b	c
c-GTR ₁₀	-20	2.96×10^{-1}	7.84×10^{-5}	7.42×10^{-1}	1.77×10^{-1}
	-10	2.71×10^{-1}	1.08×10^{-6}	5.96×10^{-1}	3.22×10^{-1}
	0	1.94×10^{-1}	8.00×10^{-7}	4.58×10^{-1}	6.91×10^{-1}
c-GTR ₂₀	-20	5.58×10^{-1}	8.34×10^{-5}	6.82×10^{-1}	1.25×10^{-1}
	-10	5.31×10^{-1}	1.54×10^{-5}	6.50×10^{-1}	1.73×10^{-1}
	0	2.64×10^{-1}	4.31×10^{-7}	4.72×10^{-1}	3.39×10^{-1}
c-GTR ₃₀	-20	9.04×10^{-1}	1.01×10^{-4}	6.49×10^{-1}	1.30×10^{-1}
	-10	7.32×10^{-1}	1.69×10^{-5}	6.18×10^{-1}	1.69×10^{-1}
	0	5.99×10^{-1}	9.91×10^{-7}	3.76×10^{-1}	7.54×10^{-1}
m-GTR ₁₀	-20	3.03×10^{-1}	7.73×10^{-5}	7.86×10^{-1}	1.69×10^{-1}
	-10	2.86×10^{-1}	9.87×10^{-6}	7.83×10^{-1}	1.76×10^{-1}
	0	2.78×10^{-1}	1.97×10^{-6}	7.44×10^{-1}	4.53×10^{-1}
m-GTR ₂₀	-20	6.14×10^{-1}	8.02×10^{-5}	7.78×10^{-1}	1.38×10^{-1}
	-10	6.79×10^{-1}	1.19×10^{-5}	7.96×10^{-1}	1.42×10^{-1}
	0	4.04×10^{-1}	1.70×10^{-6}	8.23×10^{-1}	1.42×10^{-1}
m-GTR ₃₀	-20	9.93×10^{-1}	6.36×10^{-5}	7.46×10^{-1}	7.75×10^{-1}
	-10	9.03×10^{-1}	1.03×10^{-5}	7.06×10^{-1}	7.89×10^{-1}
	0	8.76×10^{-1}	2.83×10^{-6}	6.77×10^{-1}	9.28×10^{-1}

Figure 5.15 shows the α -relaxation times plotted as a function of the inverse temperature. The parameters for the VFTH fitting are listed in Table 5.6. The type of filler (c-GTR or m-GTR) exerts a different effect on the relaxation. The c-GTR composites overlap with the unfilled SBR at higher temperatures; meanwhile, at lower temperatures, the c-GTR favors the dynamics of the relaxation process. On the contrary, the m-GTR composites show faster segmental dynamics in the whole temperature range. This behavior correlates well with the cross-linked structure of all the studied composites, as previously discussed. However, the extrapolated T_g values from the VFTH fitting do not follow the trend of the experimental results obtained by DSC.

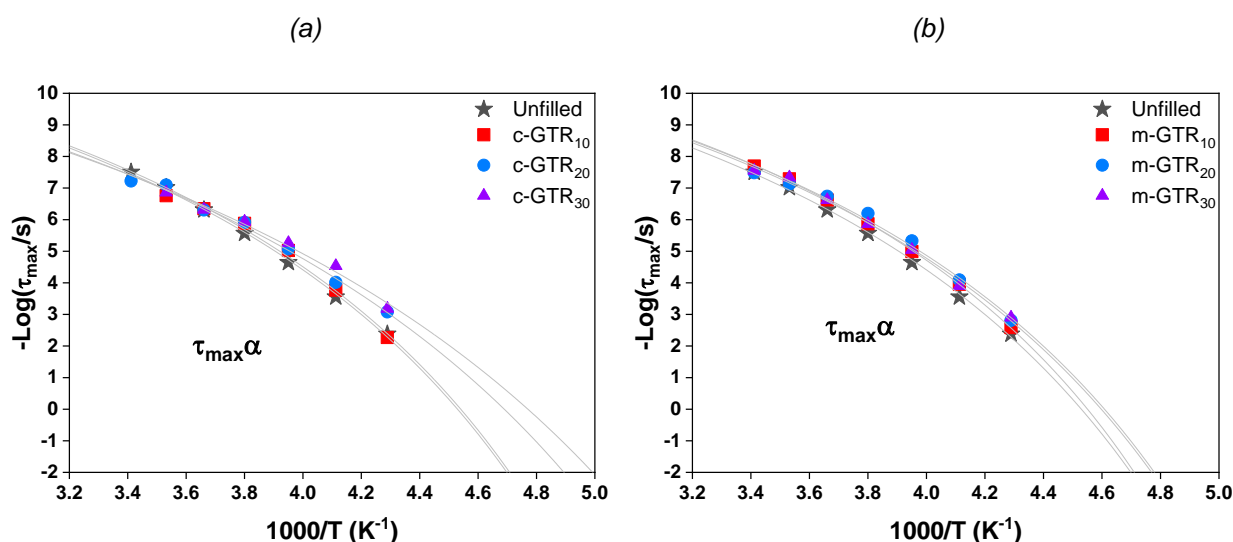


Figure 5.15 Temperature dependence of the average relaxation time for the α -relaxation process of (a) c-GTR and (b) m-GTR composites.

Table 5.6 VFTH fitting parameters of unfilled, c-GTR and m-GTR composites.

Compound	B	T ₀ (K)	T _g (°C) at τ_{100s}
Unfilled	2046	157	-60
c-GTR ₁₀	2018	158	-62
c-GTR ₂₀	2295	142	-60
c-GTR ₃₀	2399	135	-69
m-GTR ₁₀	1794	160	-64
m-GTR ₂₀	1994	155	-64
m-GTR ₃₀	1740	154	-71

We also evaluated the effect of combining traditional and sustainable fillers on the dynamics of SBR composites. We have chosen the SBR hybrid composite reinforced with 20 phr m-GTR and 20 phr CB. The individually reinforced composites were also analyzed for a comparative purpose. The series plots in Figure 5.16 show the dielectric relaxations as a function of the frequency of the selected SBR composites in the temperature range from -40 to 20 °C

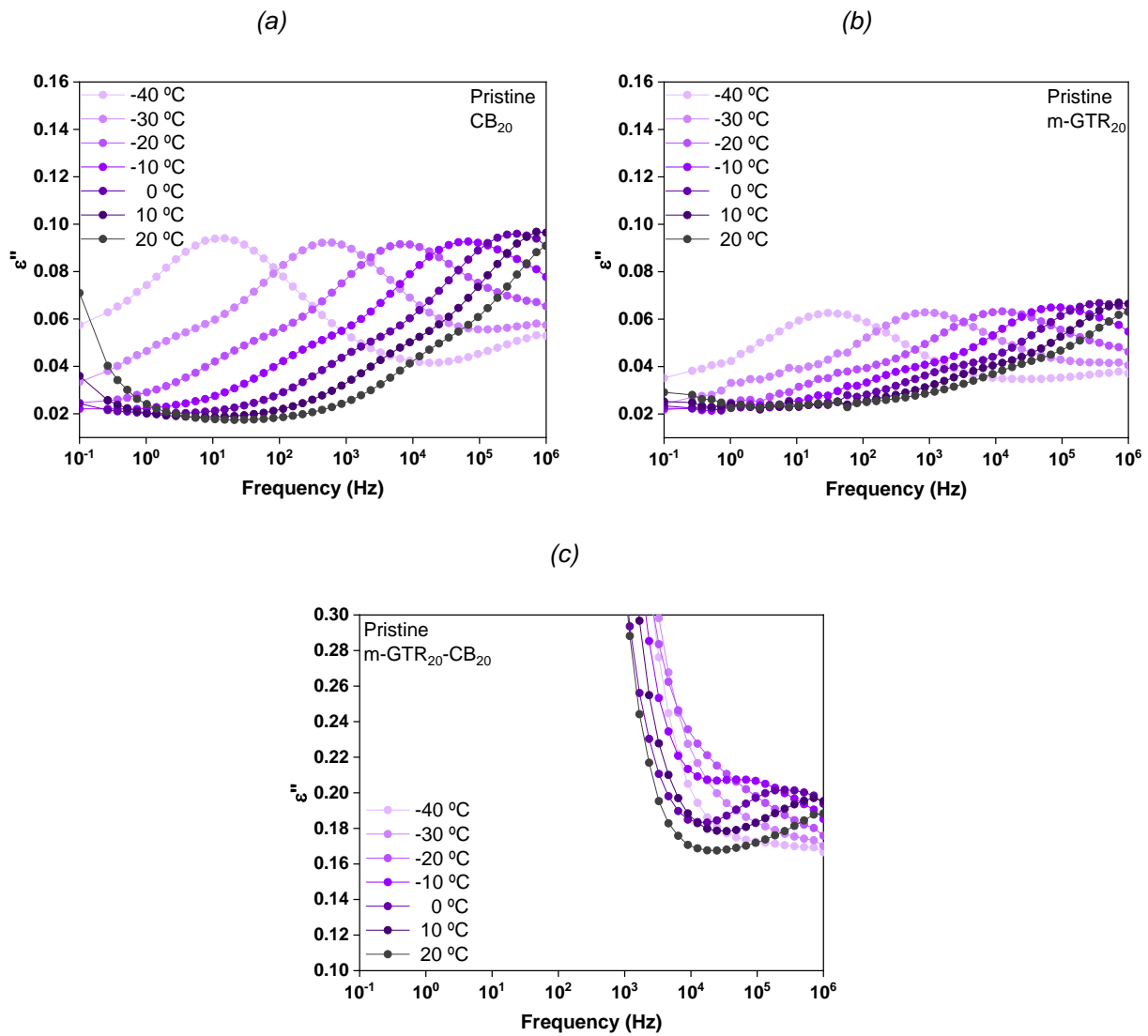


Figure 5.16 Dielectric loss (ϵ'') as a function of the frequency in the temperature range from -40 to 20 °C for: (a) CB_{20} , (b) $m-GTR_{20}$ and (c) $m-GTR_{20}-CB_{20}$ composites.

Both individually reinforced composites show a dielectric loss maximum that evolves with temperature. Meanwhile, the hybrid composite ($m-GTR_{20}-CB_{20}$) shows a drastic increase in the dielectric loss and in the conductivity contribution in the low to medium frequency range. At low frequencies, the accelerated movement of ions generate long capacitances that translate into high dielectric constants and into a considerable increase in conductivity. Figure 5.17 shows the conductivity of the selected SBR composites. The individual reinforced composites show the typical behavior of an isolating material with a linear dependence of conductivity with frequency. An important increase in conductivity (5 orders of magnitude) is observed for the hybrid system. Besides, the electrical percolation threshold is reached, evidenced by the plateau at low frequencies. This conductivity could be due to two contributions. First, the volume fraction of the filler particles (CB and m-GTR) that when combined, becomes sufficient to provide a

continuous conductive path through the polymer matrix.[23, 24] Second, the presence of functional groups (OH, COOH, and SO₃) in the surface of m-GTR particles which are highly polar groups. Similar results were reported by Ward *et al.*[25] in Si filled SBR composites. They assigned the low frequency absorption in the dielectric loss spectra to the presence of silanol groups on the surface of Si, which are highly polar groups, and act as charge carriers.

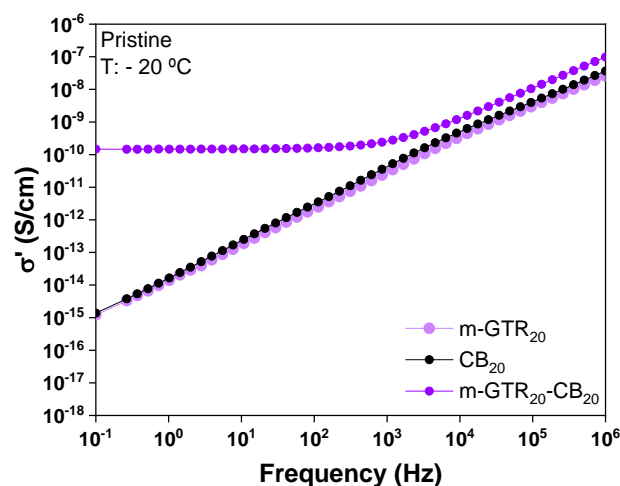


Figure 5.17 Electrical conductivity (σ') as function of frequency for $m\text{-GTR}_{20}$, CB_{20} and $m\text{-GTR}_{20}\text{-CB}_{20}$ composites at $-20\text{ }^\circ\text{C}$

Figure 5.18 shows the normalized dielectric loss against frequency for individual and hybrid composites. The CB and m-GTR filled composites show similar behavior, while the hybrid reinforcing composite shows a broader α -relaxation and an α' -relaxation masked by the conductivity contribution. The broadening on the segmental relaxation can be associated to the chemical heterogeneity of the different chain segments, due either to different chemical composition/bonds or to different chemical species around the chain segments. In this case, the broadening is ascribed to the heterogeneity between the matrix and the different filler particles. Similar results were reported by Rathi *et al.*[14] and Hernandez *et al.*[13] Rathi *et al.* found broadening of the segmental relaxation comparing SBR vulcanizates with SBR/BR (polybutadiene) blends. Meanwhile, Hernandez *et al.* found that the different accelerants and A/S ratios play an important role on the broadening of the segmental relaxation due to the differences on the length of the sulfur bonds.

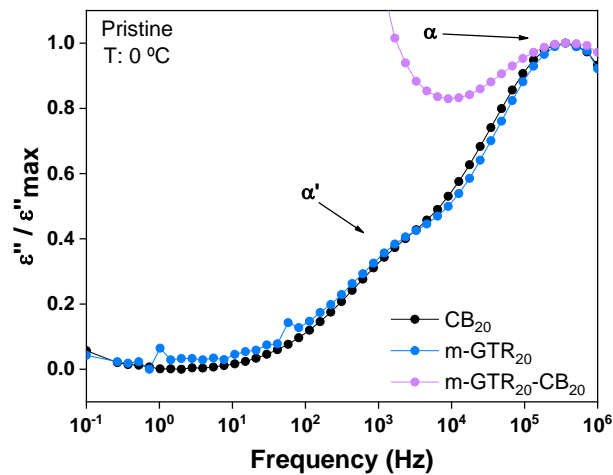


Figure 5.18 Normalized dielectric loss of $m\text{-GTR}_{20}$, CB_{20} and $m\text{-GTR}_{20}\text{-CB}_{20}$ composites and at 0 °C.

Figure 5.19 shows the experimental data of dielectric loss versus frequency fitted in terms of the HN function at a selected temperature, for individual and hybrid composites. Due to the conductivity contribution in the hybrid composite, it was not possible to make an appropriate HN fitting in the same temperature range.

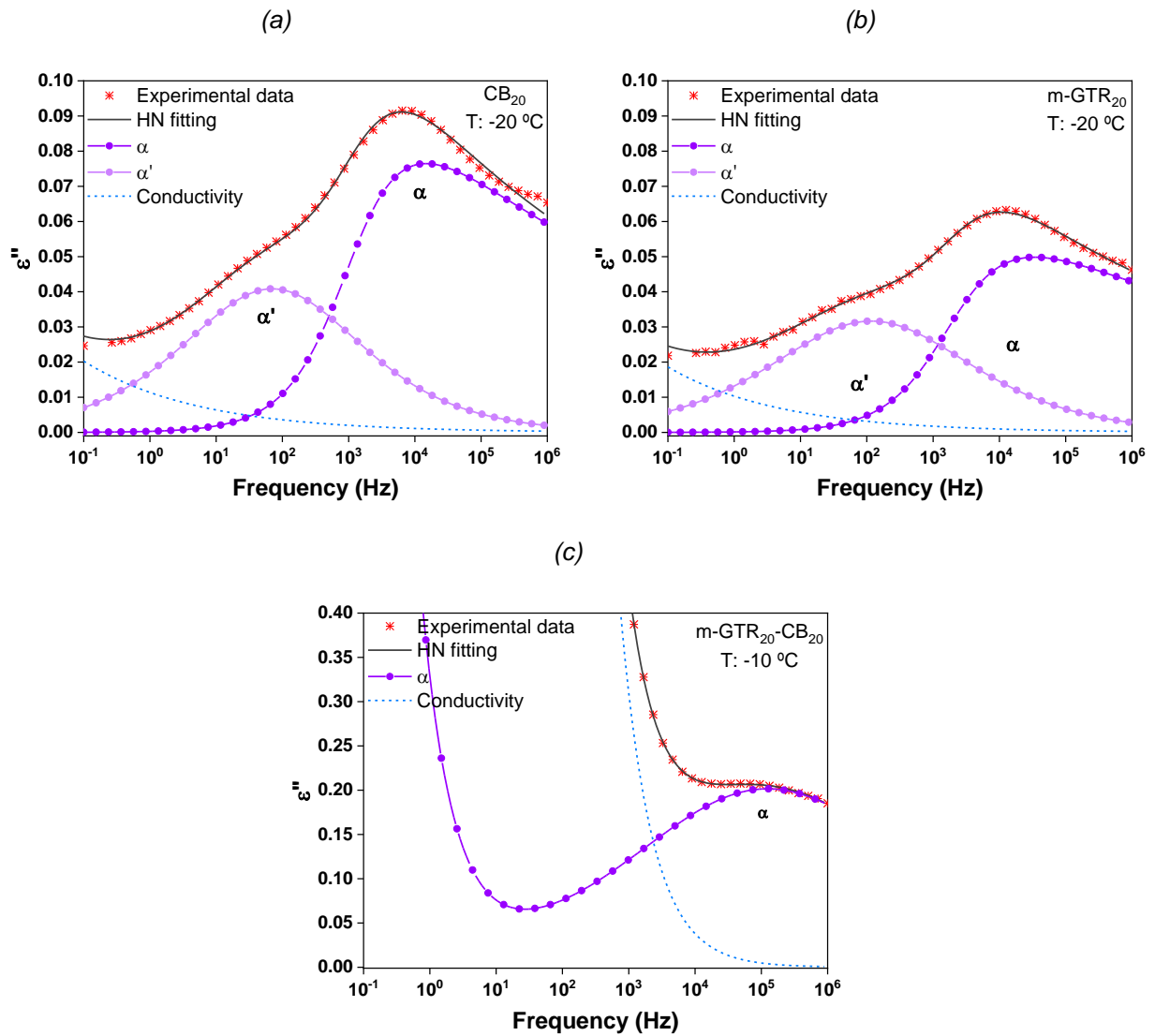


Figure 5.19 Deconvolution results for dielectric loss (ϵ'') of (a) CB_{20} , (b) $m-GTR_{20}$ and (c) $m-GTR_{20}-CB_{20}$ composites. Solid lines represent the HN fitting curve, symbol lines the individual processes, and dashed lines the conductivity contribution.

The temperature dependence of the average relaxation time of unfilled SBR, CB_{20} , and $m-GTR_{20}$ composites is shown in Figure 5.20. The parameters for the VFTH and Arrhenius fitting are listed in Table 5.7.

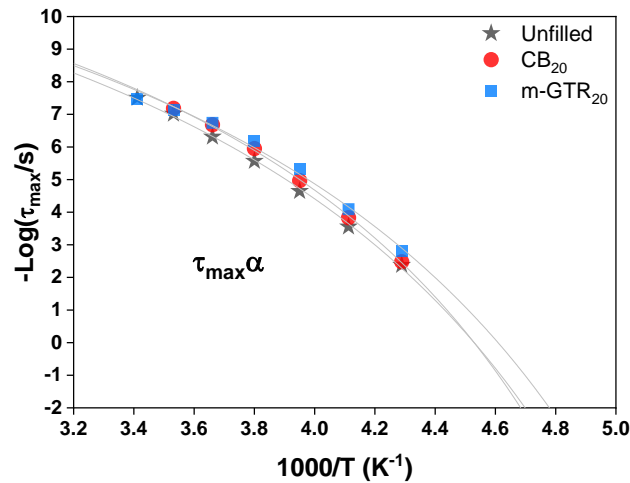


Figure 5.20 Temperature dependence of the average relaxation time of the α -relaxation of CB_{20} , $m-GTR_{20}$ and $m-GTR_{20}-CB_{20}$ composites.

The curves corresponding to the α -relaxation times of the individual filler composites almost overlap with the unfilled SBR, meaning that none of these fillers affect the segmental dynamics of the rubber. The higher values of T_0 indicate a higher temperature requirement for its activation compare to unfilled compound, $m-GTR_{20}$, and CB_{20} composites.

Table 5.7 VFTH fitting parameters of unfilled, of CB_{20} , and $m-GTR_{20}$ composites.

Compound	B	T_0 (K)	T_g ($^{\circ}C$) at τ_{100s}
Unfilled	2046	157	-60
CB_{20}	1876	162	-60
$m-GTR_{20}$	1994	155	-64

5.2.4. Effect of coupling agent (CA)

Figure 5.21 shows the normalized dielectric loss of unfilled SBR and selected SBR composites filled with 20 phr of c-GTR and 20 phr of m-GTR with and without CA. As expected, the addition of the CA shifts the α -relaxation of all the systems to lower frequencies. These more restrictive relaxation processes correlate well with the increment in the cross-link density. As explained in Chapter 4, the CA can participate in the sulfur vulcanization forming additional chemical linkages with the rubber matrix. Besides, the

enhanced rubber-filler interactions in presence of a CA are also responsible for the higher cross-link density in the filled SBR composites; resulting in more restricted dynamics.

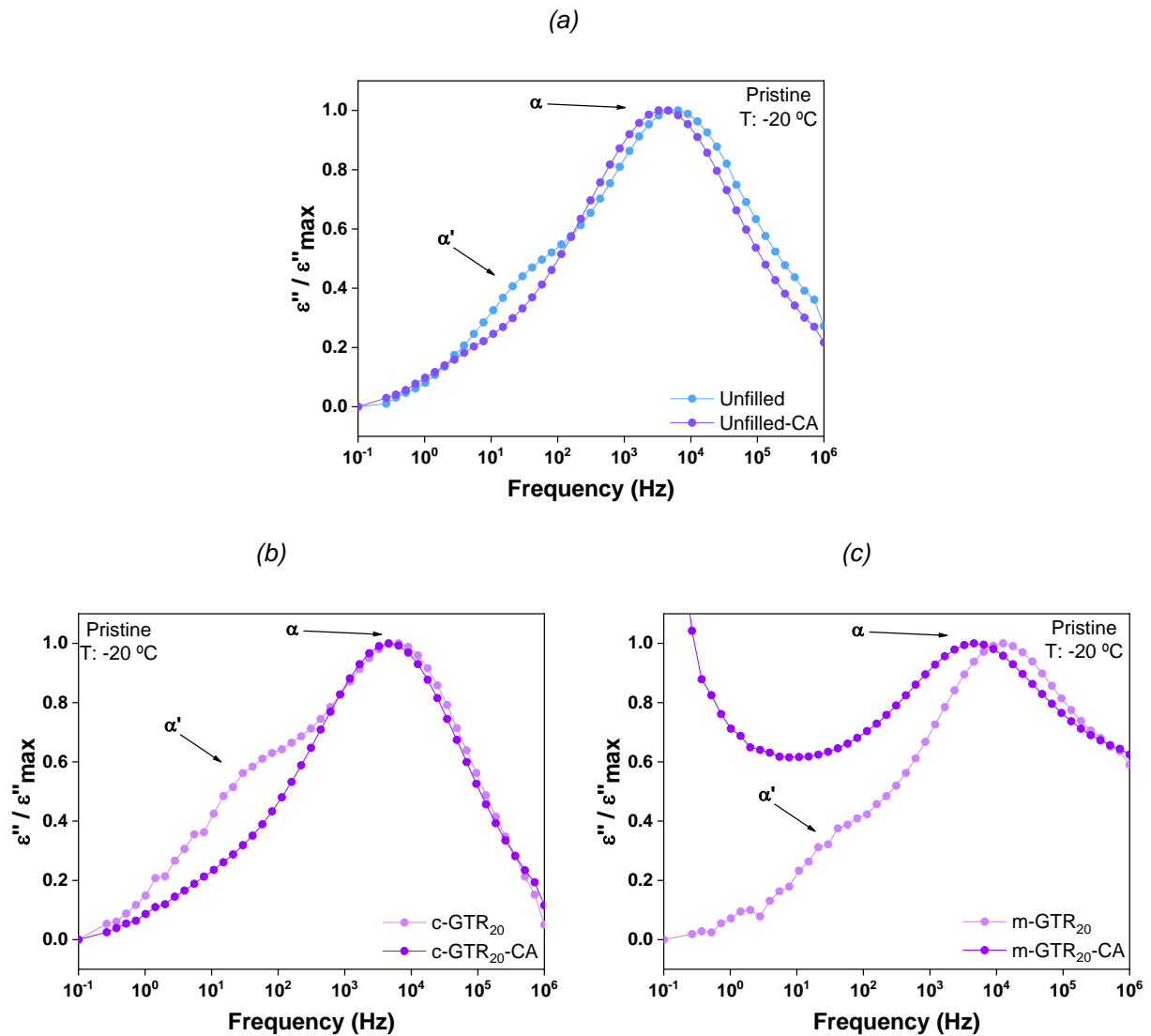


Figure 5.21 Normalized dielectric loss at $-20\text{ }^\circ\text{C}$ of (a) unfilled SBR, (b) c-GTR₂₀, (c) m-GTR₂₀ composites with and without CA.

The CA reduces the intensity of the α' -relaxation for the unfilled SBR and the c-GTR₂₀ composite. This can be explained in terms of the improved interactions between the unreacted cross-linking precursor fragments or blend components (responsible for the appearance of the α' -relaxation) and the rubber matrix.

The most notorious effect is observed in the low frequency region of the m-GTR₂₀ composites. The addition of the CA produces a significant rise in ϵ'' , partially hiding the α' -relaxation process. This increase can be associated with the material conductivity. The

dependence of the electrical conductivity with frequency is shown in Figure 5.22. All the composites show the characteristic behavior of an isolating rubber, with very low values of conductivity and a linear increase with frequency. However, the m-GTR₂₀-CA composite shows the highest value of conductivity.

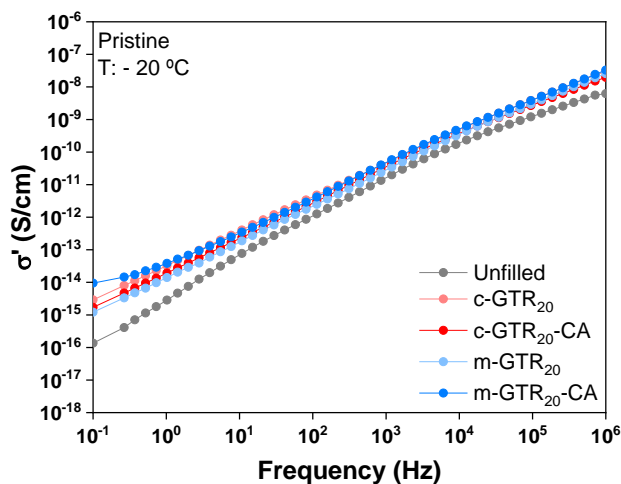


Figure 5.22 Electrical conductivity (σ') as function of frequency for unfilled, c-GTR₂₀ and m-GTR₂₀ composites with and without CA at -20 °C.

The series of plots in Figure 5.23 show the experimental data of dielectric loss versus frequency for unfilled, c-GTR₂₀ and m-GTR₂₀ composites with CA fitted to the HN function at a representative temperature. The relaxation parameters are compiled in Table 5.8.

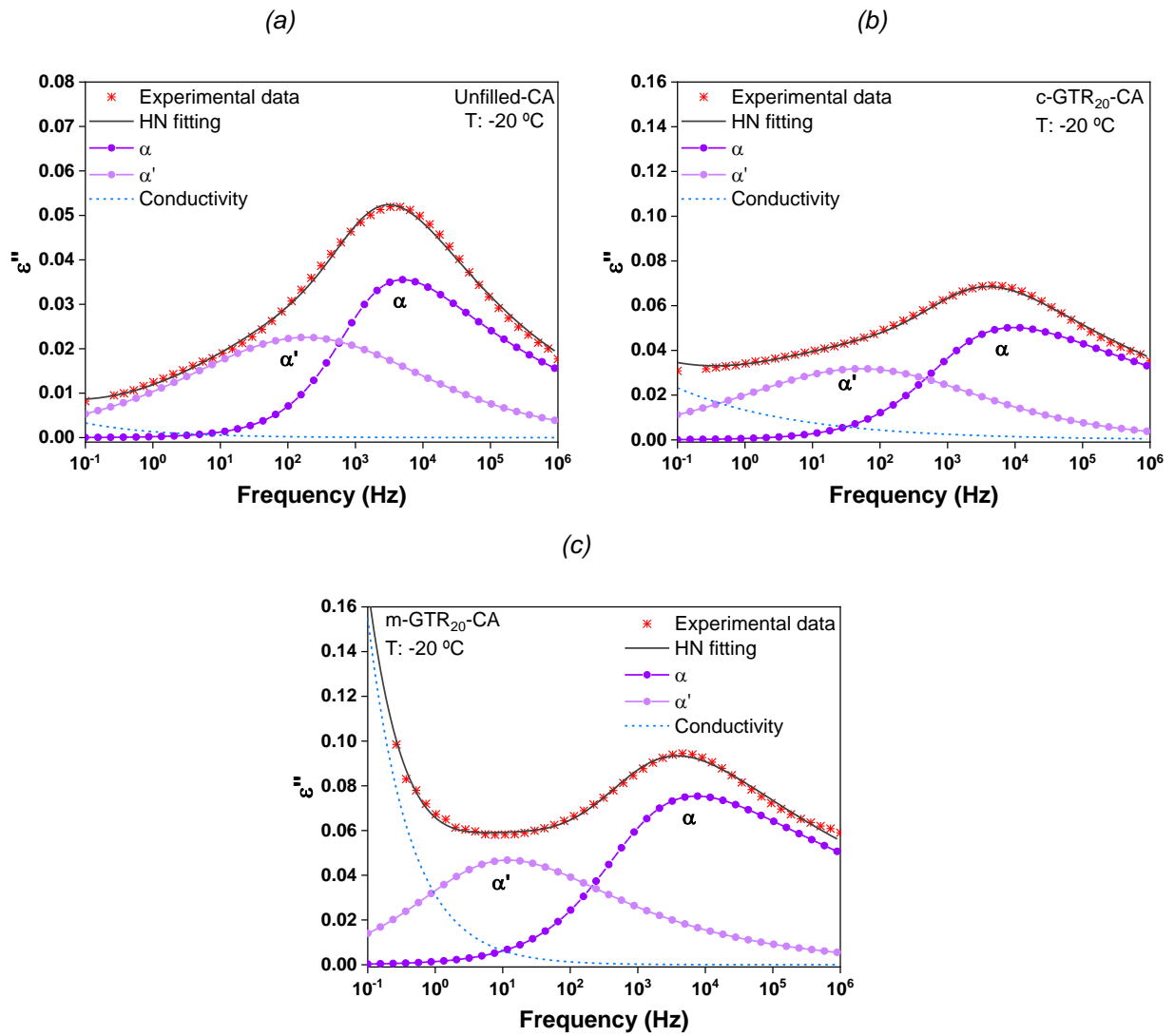


Figure 5.23 Deconvolution results for dielectric loss (ϵ'') of unfilled, c-GTR and m-GTR composites with CA. Solid lines represent the HN fitting curve, symbol lines the individual processes, and dashed lines the conductivity contribution.

Table 5.8 Havriliak-Negami (HN) parameters for the segmental mode of unfilled, c-GTR₂₀ and m-GTR₂₀ composites with CA at T: -20, -10 and 0 °C.

Composite	T (°C)	$\Delta\varepsilon$	$\tau_{HN(\alpha)}$ (s)	b	c
Unfilled-CA	-20	2.11×10^{-1}	1.45×10^{-4}	7.84×10^{-1}	2.69×10^{-1}
	-10	1.59×10^{-1}	1.45×10^{-5}	6.86×10^{-1}	4.11×10^{-1}
	0	1.62×10^{-1}	2.99×10^{-6}	6.85×10^{-1}	4.15×10^{-1}
c-GTR ₂₀ -CA	-20	3.95×10^{-1}	1.49×10^{-4}	6.28×10^{-1}	2.55×10^{-1}
	-10	2.92×10^{-1}	1.91×10^{-5}	6.81×10^{-1}	1.97×10^{-1}
	0	3.75×10^{-1}	4.48×10^{-6}	7.08×10^{-1}	2.02×10^{-1}
m-GTR ₂₀ -CA	-20	4.62×10^{-1}	2.39×10^{-4}	7.29×10^{-1}	1.71×10^{-1}
	-10	4.03×10^{-1}	2.18×10^{-5}	7.32×10^{-1}	1.76×10^{-1}
	0	3.13×10^{-1}	2.70×10^{-6}	6.77×10^{-1}	2.73×10^{-1}

Figure 5.24 shows the α -relaxation times plotted as a function of inverse temperature. The relaxation times of the composites with CA show a shift to higher temperatures compared to their peers without CA. This shift correlates well to the higher cross-link density reached when the CA is added in the SBR composites. Hence, the segmental mode process tends to slow down.

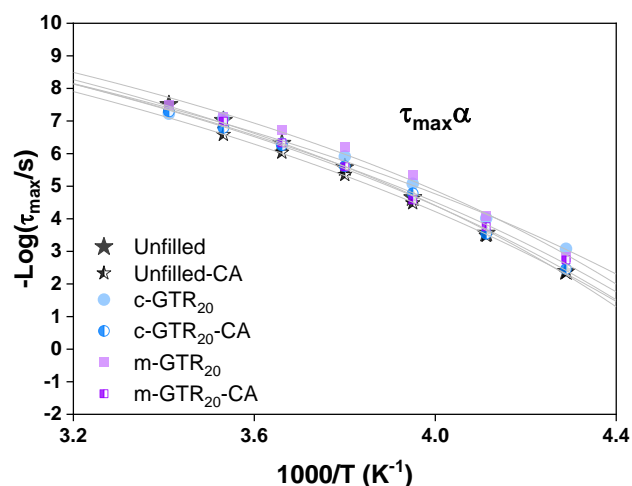


Figure 5.24 Temperature dependence of the average relaxation time of unfilled, c-GTR₂₀ and m-GTR₂₀; composites with and without CA.

5.3. DMA analysis. Evaluation of pristine composites.

The temperature dependence of the storage modulus (E') and damping factor ($\tan\delta$) at a fixed frequency is a good measuring tool to evaluate the effect of the underlying structural properties, such as the cross-link degree and the rubber–filler interactions, on the mechanical performance of a rubber matrix. The curves of E' and $\tan\delta$ as a function of temperature are shown for selected SBR composites in Figure 5.25 and Figure 5.26, respectively. As expected, the E' increases with filler content, regardless of the type of filler (c-GTR, m-GTR or CB). The presence of CB, either in the form of individual filler or as part of the GTR, restricts the mobility of the rubber chains, providing rigidity to the vulcanized rubber.[26-28] It is well known that the E' of a filled polymer composite is influenced by the effective interfacial interaction between the polymer matrix and the filler particles. In general, a strong interfacial interaction contributes to a higher E' of the composite.[29] The addition of CA further increases E' . This effect is due to the combination of enhanced rubber–filler interactions during mixing and the increment in cross-link density in presence of a CA.[30, 31]

The combination of fillers (CB + m-GTR) does exert a stiffening effect of the rubber matrix. However, the resulting E' is lower than that observed for individual CB reinforced composites. It seems that the presence of m-GTR limits the typical reinforcement effect of CB. This behavior is in agreement with the cross-link density results discussed in Chapter 4, where the values of the m-GTR-CB hybrid composites show negligible differences compared to the individually reinforced composites. Once again, this result indicates that the effect of m-GTR dominates over the effect provided by a traditional filler. Nonetheless, the addition of the CA raises the E' of the hybrid composites (m-GTR-CB-CA) to values similar to those of the individual CB composites. As previously discussed (Chapter 4), the addition of a CA reduces the filler–filler interactions in the SBR composites, leading to a greater potential of rubber chains to individually interact with the m-GTR and CB particles, improving filler dispersion in the SBR matrix and mechanical performance.

The $\tan\delta$ is referred to as the internal damping and it is an indicator characterizing the dynamic behavior of materials. The maximum peak in the $\tan\delta$ curves can be used to study the glass transition and is associated with the movement of side groups or low molecular-weight units within the rubber molecules. The $\tan\delta$ relates the damping of a material to its impact resistance, which mainly depend on the nature of the matrix, the

filler, and their interface.[10, 29] It can be seen that the unfilled compound shows the highest $\tan\delta$ value in the glass transition region, which indicates a large degree of mobility and good damping properties. The filler loading effects at different temperature regions are governed by different mechanisms. At temperatures near the $\tan\delta$ peak (transition zone), two opposite effects are to be considered. First, the presence of CB in c-GTR and m-GTR gives a low hysteresis for a specific energy input, since individual filler particles may not absorb energy significantly.[10] Secondly, in this transition zone, the total rubber fraction in the compound is responsible for the high portion of energy dissipation among rubber molecules, resulting in high hysteresis. For this set of composites, the governing factor seems to be the CB content, since the value of $\tan\delta$ decreases as the c-GTR and m-GTR loading increases. This might be attributed to the filler retarding the mobility of rubber chains, restricting the segmental motions of the rubber molecules, by the strong filler-rubber interactions.[32] This behavior is also seen in the hybrid composites, with and without CA. As explained previously, the CA improves the filler-rubber interactions. Hence, a low $\tan\delta$ value suggests a relatively high filler-rubber interaction. Finally, the T_g , taken as the temperature of the maximum of the $\tan\delta$ curve, did not change noticeably as a function of filler type and amount.

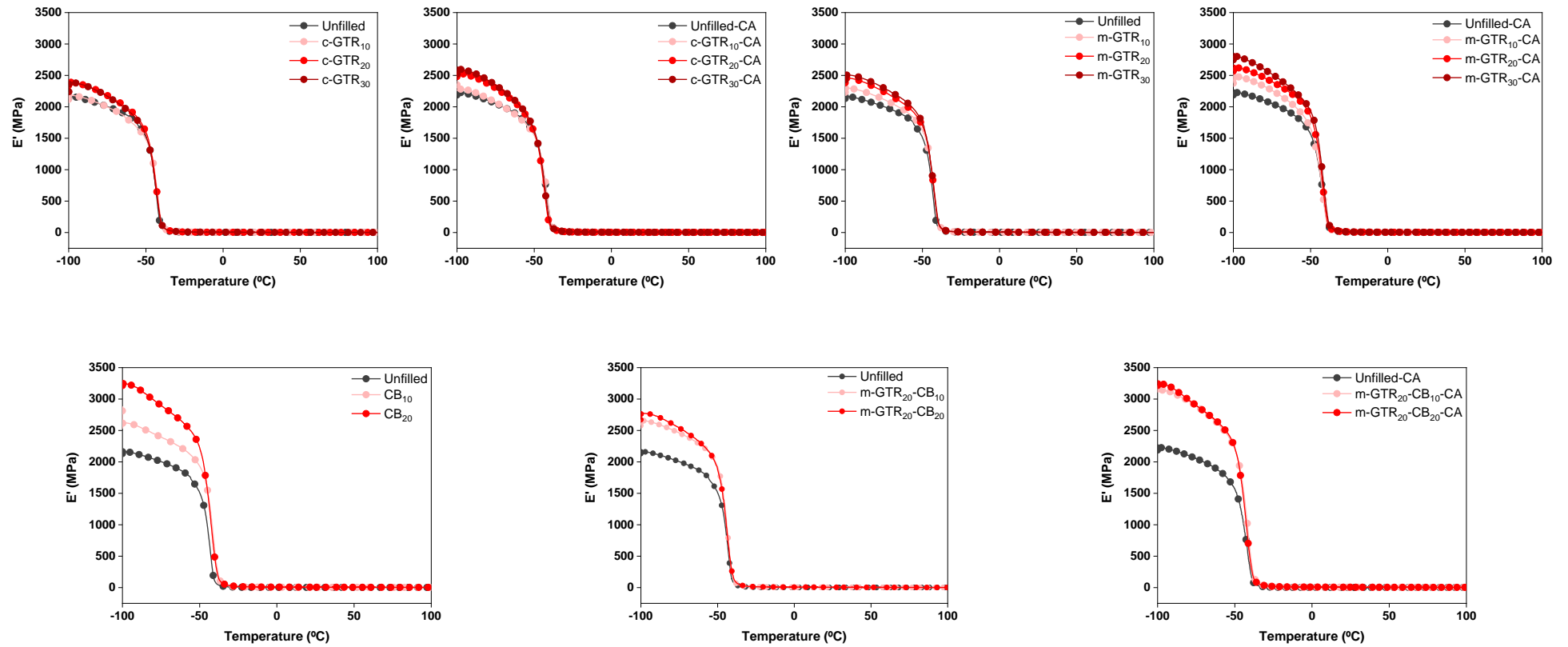


Figure 5.25 Storage modulus (E') of SBR composites.

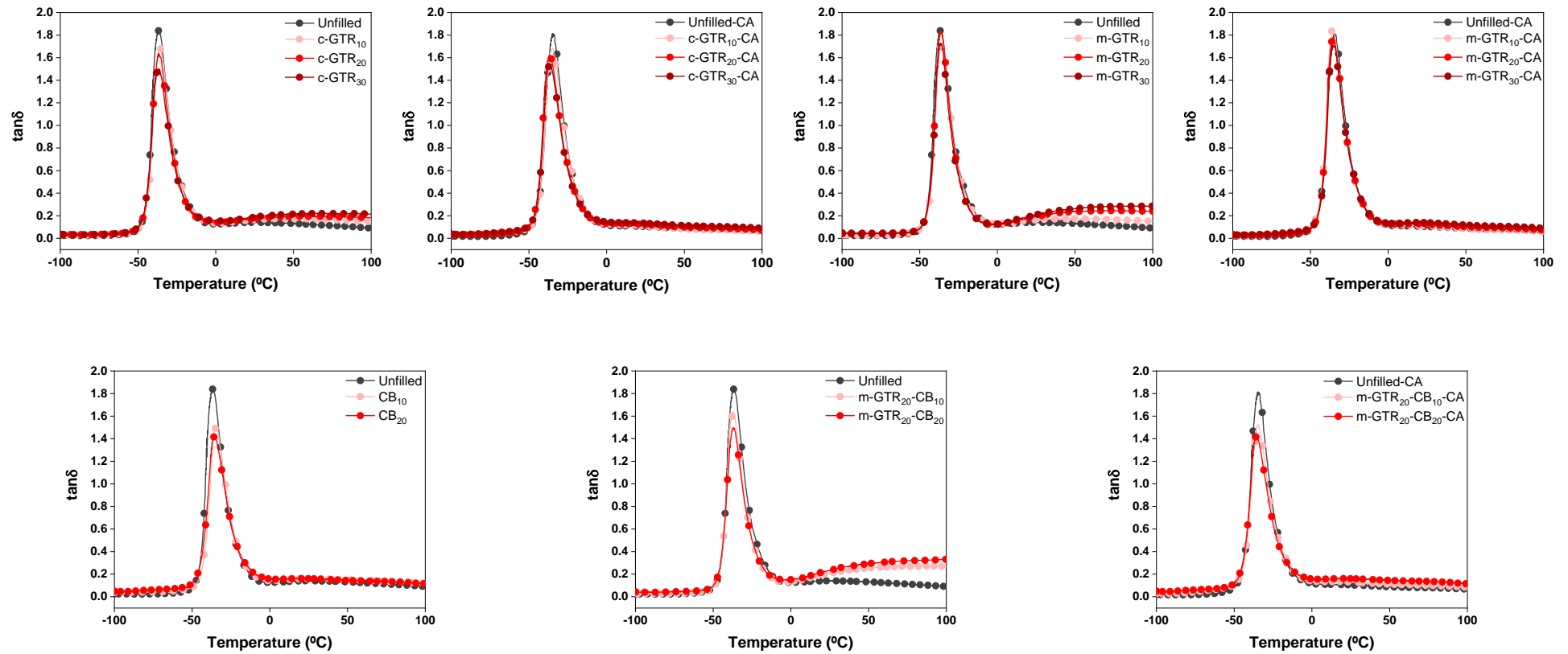


Figure 5.26 Damping factor ($\tan\delta$) of SBR composites.

The values of $\tan\delta$ at low (-10 °C) and high (60 °C) temperatures are used as a predictive tool for the wet grip and rolling resistance of tread compounds, respectively (Figure 5.27). The material should demonstrate high hysteresis at low temperatures, in order to obtain high wet grip. High c-GTR contents (20 and 30 phr) have equivalent or slightly higher values of $\tan\delta$ (10 % for 30 phr) than the unfilled sample. Meanwhile, the high m-GTR contents show a slight decrease of the wet grip (14 % for 30 phr). On the one side, as explained in Chapter 4, the incorporation of c-GTR decreases the cross-link density of SBR composites, providing flexibility to the rubber molecules and improving hysteresis; hence, wet grip. On the other side, the polar groups present on the surface of the m-GTR particles promote their agglomeration hindering the energy dissipation, hence low hysteresis.[10] Ren *et al.*[33] found similar behavior on SBR compounds filled with CB and fly ash. Regarding the hybrid reinforcing composite (m-GTR₂₀-CB₂₀), $\tan\delta$ values are not particularly negatively influenced. All these results indicate that the use of a sustainable filler like GTR, at the studied contents, does not harm the wet grip properties of SBR. Meanwhile, high contents of c-GTR and m-GTR content (20 and 30 phr) present higher values of $\tan\delta$ at 60 °C and, hence, a detrimental effect on the rolling resistance.[34] Such result is ascribed to the presence of some agglomerates, as explained in Chapter 4. Moreover, in terms of tread composition, low rolling resistance is favored by compounds of lower hysteresis. Other authors have also found that filler dispersion is the dominant factor governing the rolling resistance of vulcanizates.[35] The hybrid reinforced composite shows a large increase in $\tan\delta$ values; which is ascribed to the presence of higher CB content in the system, which causes high energy losses.

The addition of the CA to any of the SBR composites also favors the overall performance,[34] showing an improvement in wet grip and rolling resistance if compared to the composites without CA. These results confirm that the use of CA enhances the rubber–filler interactions and reduces the filler–filler interactions, improving the filler dispersion. Therefore, the CA reduces the mobility of the rubber molecular chains, as well as the filler–filler friction, resulting in a low hysteresis and low temperature rise.[36]

Similar results were found in a SBR/NR blends with bio-based epoxidized soybean oil, where the oil acted as a CA and enhanced the interactions with silica improving the wet grip and lowering the rolling resistance.[37] Finally, the rebound check-resilience results presented in Chapter 4 are consistent with the $\tan\delta$ values. The composites with CA show higher resilience than their corresponding peers.

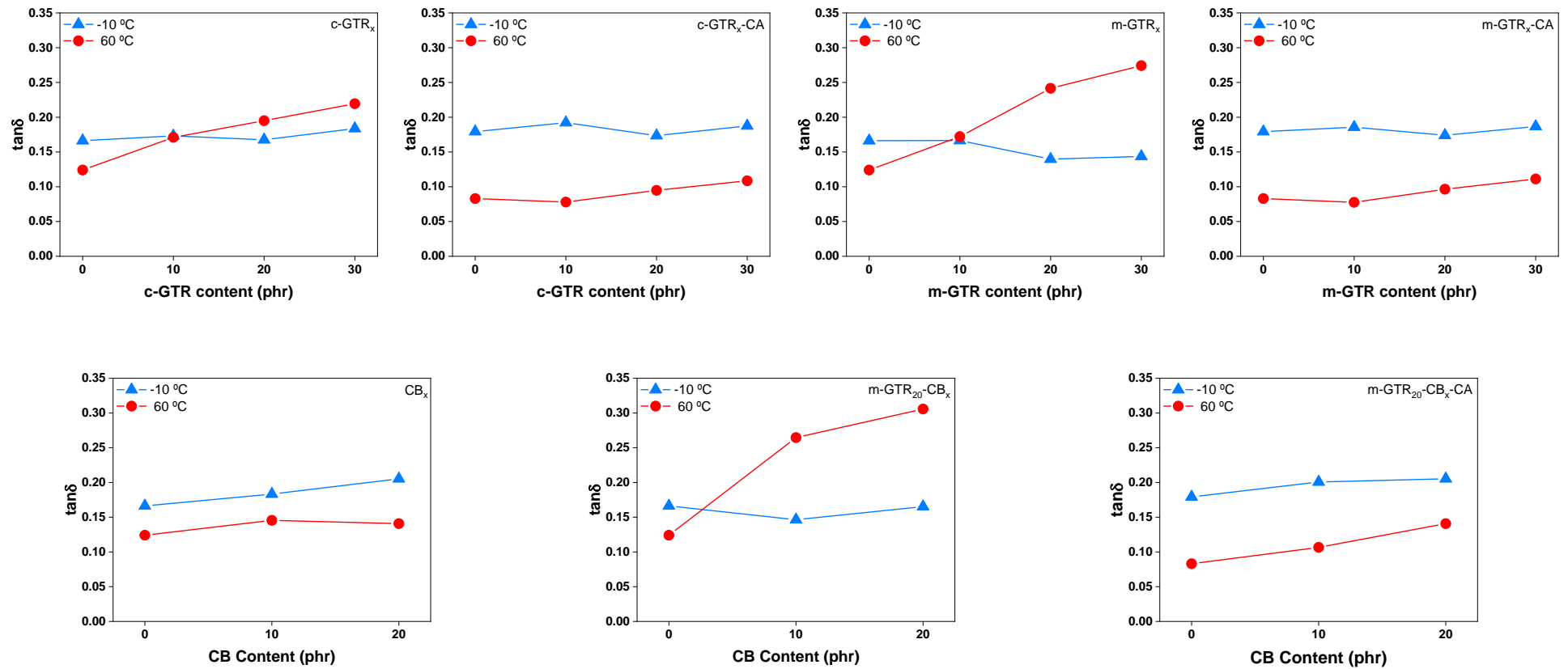


Figure 5.27 Damping factor ($\tan\delta$) of SBR composites at low (-10 °C) and high (60 °C) temperatures.

5.4. Dynamics of self-healing SBR composites

5.4.1. Analysis of network damage

Selected SBR composites were subjected to a network damage by means of 20 strain cycles. For ease of visual comparison, only the first, second and last (20th) load cycles of the pristine samples are shown in Figure 5.28. The stress–strain curves change differently from cycle to cycle for all the evaluated systems. A small decrease in the maximum stress level is observed for the unfilled SBR compound. Similar results were reported by Hernández *et al.* for NR compounds.[38] In their research, they found that a 50 %-cured NR showed lower value of the overall stress level and a lower Young’s modulus from the second cycle onward. Meanwhile, a fully cured rubber did not show substantial difference in the instantaneous modulus between all cycles, although a small decrease in the maximum stress level was still observed. Such a behavior is attributed to the cyclic deformation to which the material was subjected and can be interpreted based on the Mullins effect. This effect is characterized by a softening induced by the deformation of an elastomer after a first load during a protocol of several load cycles.[39] The main physical interpretations that explain the Mullins effect are (i) the breaking of bonds (e.g., sulfur crosslinks) or chain scission of rubber molecules, (ii) the physical disentanglement of rubber chains, (iii) the breakage of filler aggregates, and (iv) the consideration that the elastomeric material is constituted by a soft phase and a rigid one (groups of molecular chains joined by segments of short-chain entanglements or intermolecular forces), being the latter broken and transformed into soft regions during deformation.[39-41] A schematic representation of Mullins effect is given in Figure 5.29

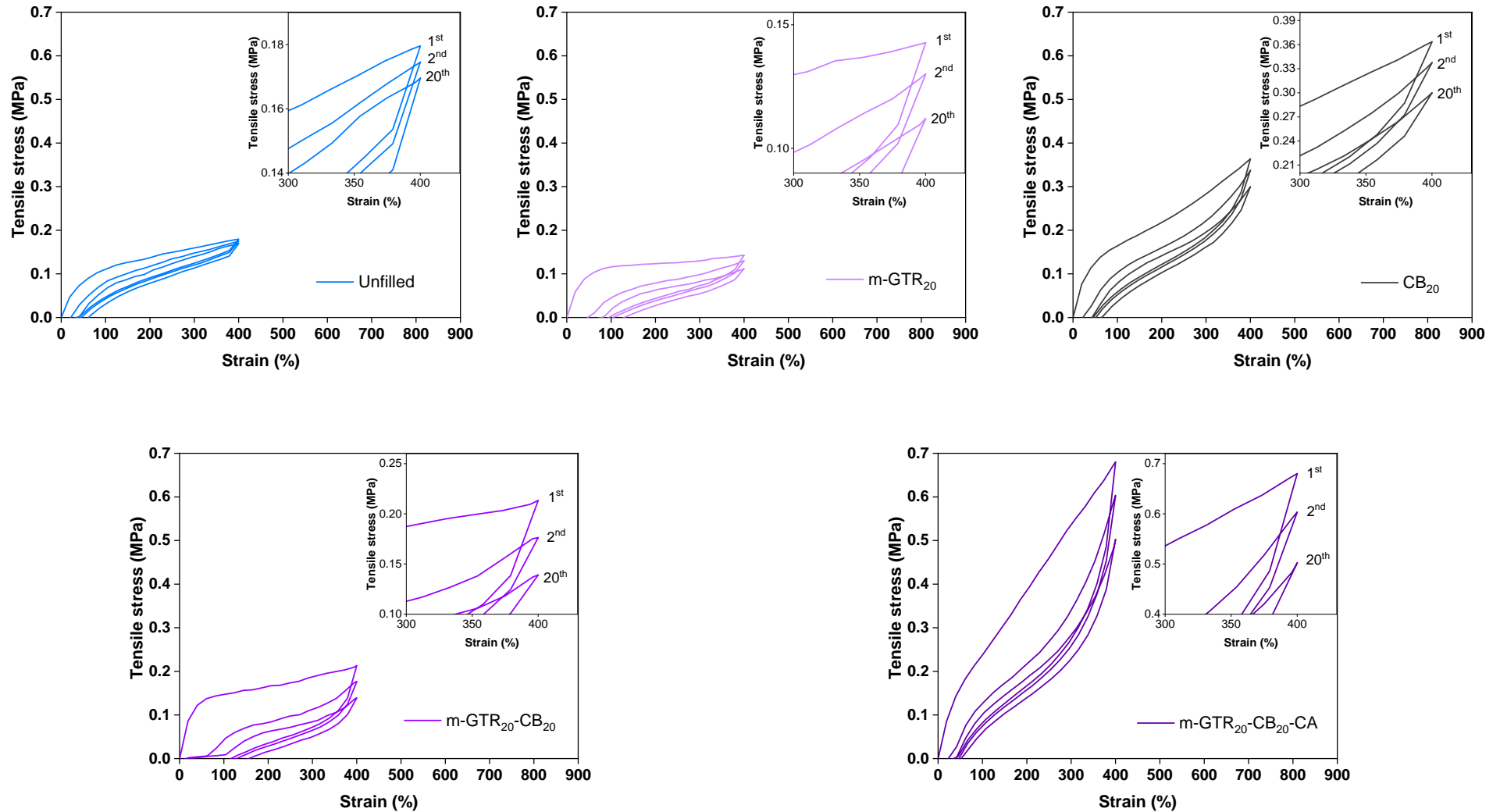


Figure 5.28 Stress-strain curve of Unfilled SBR under cyclic straining showing the 1st, 2nd, and 20th cycle. Inset correspond to end point of each cycle.

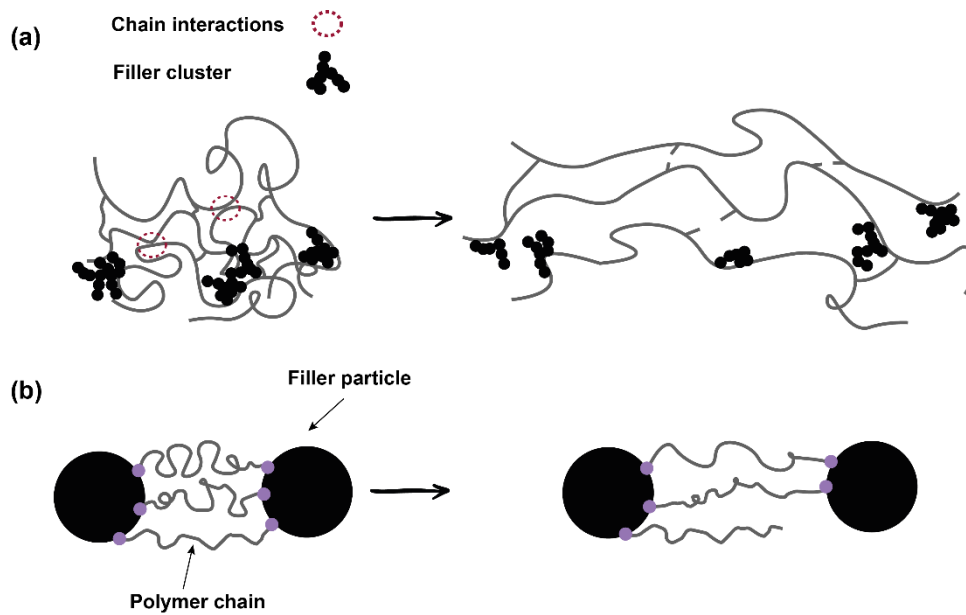


Figure 5.29 Schematic representation of Mullins effect: (a) Weak links, cross-links and filler cluster breakdown, and (b) Filler particle-chain junctions breakdown.[39]

Regarding the filled SBR composites, all of them show a bigger reduction of the maximum stress level independently of the type of filler. During stretching, some polymer chains are extended until their limit of extensibility and, subsequently, some chain breaking occurs. In the same way, some weak interactions are not able to stand, and they break down too. As the number of breakdowns increases, the number of junction points between chains decreases.

The disentanglement of the network chains with the breakdown of the interactions between the filler particles and the rubber matrix is carried out, resulting in a decrease in the overall stiffness of the composites.[39] This is corroborated by the comparison of the manually calculated moduli M_{300} (tensile stress at strain of 300 %) for SBR composites for the 1st, 2nd, and 20th cycle (Table 5.9). The M_{300} retention, calculated as the ratio between the first and last straining cycle, confirms that the unfilled SBR retains 89 % of its initial stiffness; meanwhile, the hybrid reinforced composite composed of 20 phr of m-GTR and 20 phr of CB seems to be the system more affected by this microscopic damage produced in the network structure by the cyclic deformation.

Table 5.9 Moduli M_{300} for the 1st, 2nd and 20th loading cycles and percentage retention after the last cycle.

Composites	M_{300} (MPa)			% M_{300} retention
	1 st cycle	2 nd cycle	20 th cycle	20 th cycle/1 st cycle
Unfilled	0.161	0.151	0.143	89
m-GTR ₂₀	0.131	0.102	0.086	66
CB ₂₀	0.292	0.232	0.205	70
m-GTR ₂₀ -CB ₂₀	0.190	0.117	0.088	46
m-GTR ₂₀ -CB ₂₀ -CA	0.551	0.363	0.300	55

Summarizing, when exposed to cyclic deformation, unfilled SBR shows lower mechanical properties and less damage. However, reinforced systems exhibit higher mechanical performance but higher accumulation of damage. Having determined the microscopic damage of the developed SBR composites, the next section is dedicated to understand the molecular processes by BDS and DMA tests.

5.4.2. Correlating dynamics and structure with healing

The interrelation between dynamics and molecular structure has been analyzed by means of BDS and DMA tests, in order to elucidate the physical properties of the developed composites and their possible repair mechanism after a cyclic deformation damage.

The effect of damage and healing on the α -relaxation is used in this study to analyze and understand the changes occurring at the molecular level, under the three different test conditions (pristine, damaged and healed). By plotting the normalized dielectric loss in a broad frequency range, one can easily discriminate how the shape (symmetry, broadness) of the relaxation spectra varies and how the maximum shifts to lower or higher frequencies (Figure 5.30).

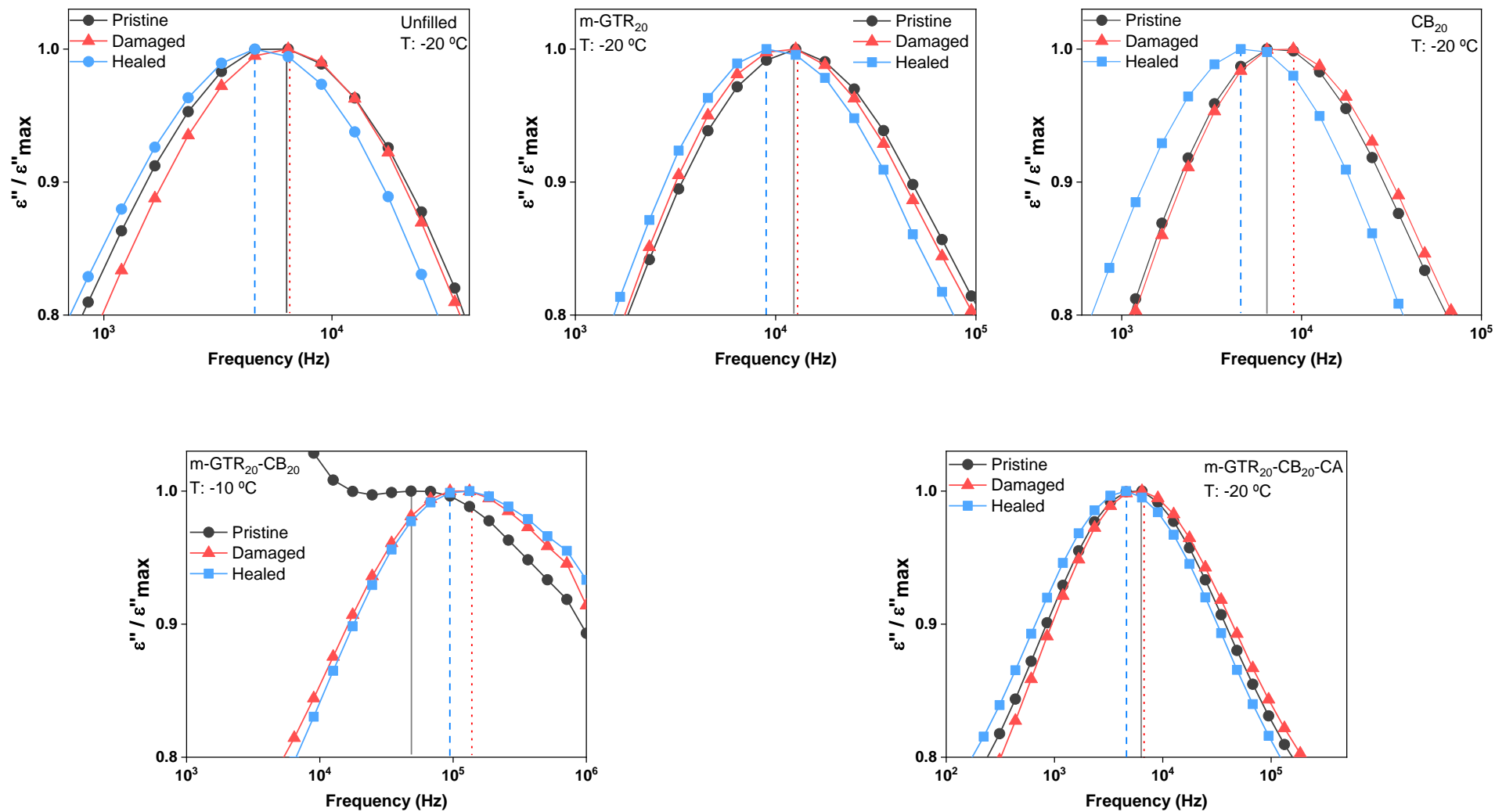


Figure 5.30 Normalized dielectric loss vs frequency of SBR composites in the region of the segmental mode for pristine, damaged and healed states.

It can be seen that the damaged state induces a slightly faster dynamic, as follows from the shift of the position of the maximum of the dielectric loss to slightly higher frequencies. This behavior can be explained by the state of the polymer network after damage and after healing. When damage takes place, the cross-link density of the rubber compound decreases due to a partial destruction of the network, the rubber network undergoes chain scission, and so the chain dynamics are less hindered due to the increase of unconnected chains produced during scission.[38]

In contrast, the maximum in the healed state shifts to lower frequencies compared to the pristine state. Thus, the healing protocol slows down the dynamics of the SBR composites (higher network constraint), which can be attributed to the reformation of bonds restricting and/or restoring the initial dynamics of the system, but also to some redistribution of the structure which leads to the formation of a new network with different architecture with respect to the pristine SBR. These results correlate well with the increase in the cross-link density due to the application of the thermal healing treatment, explained in Chapter 3. Unexpectedly, the hybrid reinforced m-GTR₂₀-CB₂₀ composite presents a significant change between the virgin, damaged, and repaired states. Upon damage, the electrical percolation path is lost, and the notorious rise in ϵ'' at low frequencies ascribed to the CB content and the contribution of the CB present in the GTR is not seen. The softening of the composite after damage and the drop of conductivity can be correlated and associated to the rupture of the CB structure and conductive network breakdown (Figure 5.31).[42, 43] After the repair process, the conductivity remains low, indicating that the filler network is not recovered.[44]

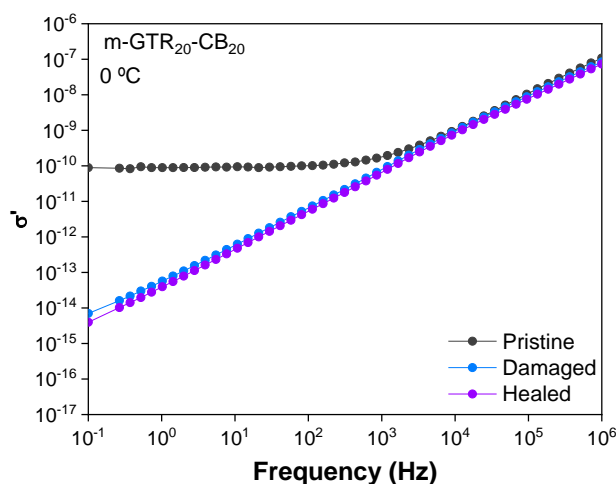


Figure 5.31 Electrical conductivity (σ) as a function of the frequency at a temperature of 0 °C for the virgin, damaged and healed states of m-GTR₂₀-CB₂₀ composite.

The changes on dynamic properties depending on the sample condition (pristine, damaged and healed) were also evaluated by means of DMA. Figure 5.32 shows E' as a function of temperature for SBR composites under the three different states. A decrease in E' is observed in all the damaged samples. This behavior is attributed to the cyclic deformation to which the material was subjected. Consequently, for the unfilled SBR compound, the decrease in E' could mainly be due to the broken chains transformed into dangling chains, which do not contribute to the material stiffness.[39] Instead, the decrease in E' for the SBR reinforced composites can be a consequence of the disentanglement of chains and breakage of the rubber network, together with the fracture of filler aggregates and/or rupture of the CB network.[44] After the thermal healing protocol, an increase and, thus, a recovery of E' is observed. Recovery caused by heating could be explained by the arrangement of a new network at sufficiently high temperature thanks to the formation of entanglements between dangling chains.[45] Similar behavior was reported in NR by Sattar *et al.*[46] They ascribed the redistribution of the structure to the formation of a new network with different architecture and higher modulus. Several authors[47, 48] have established that for intrinsic macroscopic healing to occur, three main steps should be followed: firstly, a self-adhesion step (interface formation); secondly, a long-range chain diffusion at short time scales (interphase formation); and finally, a homogenization process at longer times (randomization). The full randomization only occurs if fracture does not reappear at the same site of the initial damage. Thus, a valid explanation to the total recovery of stiffness in unfilled SBR could be the interdiffusion of the dangling chains, which was promoted by the reversibility of the

disulfide and polysulfide bonds of the vulcanized network, reestablishing the chemical bonds through the damaged network.[49-51] In the case of the filled SBR composites, there is an almost complete recovery of stiffness with temperature, which suggests that heating the samples increases the molecular mobility and free chains adsorbed at the CB and GTR aggregates surface, creating stronger rubber–filler interactions. Both new entanglements and the layer of bonded rubber at the rubber–filler interface are believed to play a key role, resulting in the recovery of the stiffness and, hence, the healing of the filled SBR composites.[44, 45]

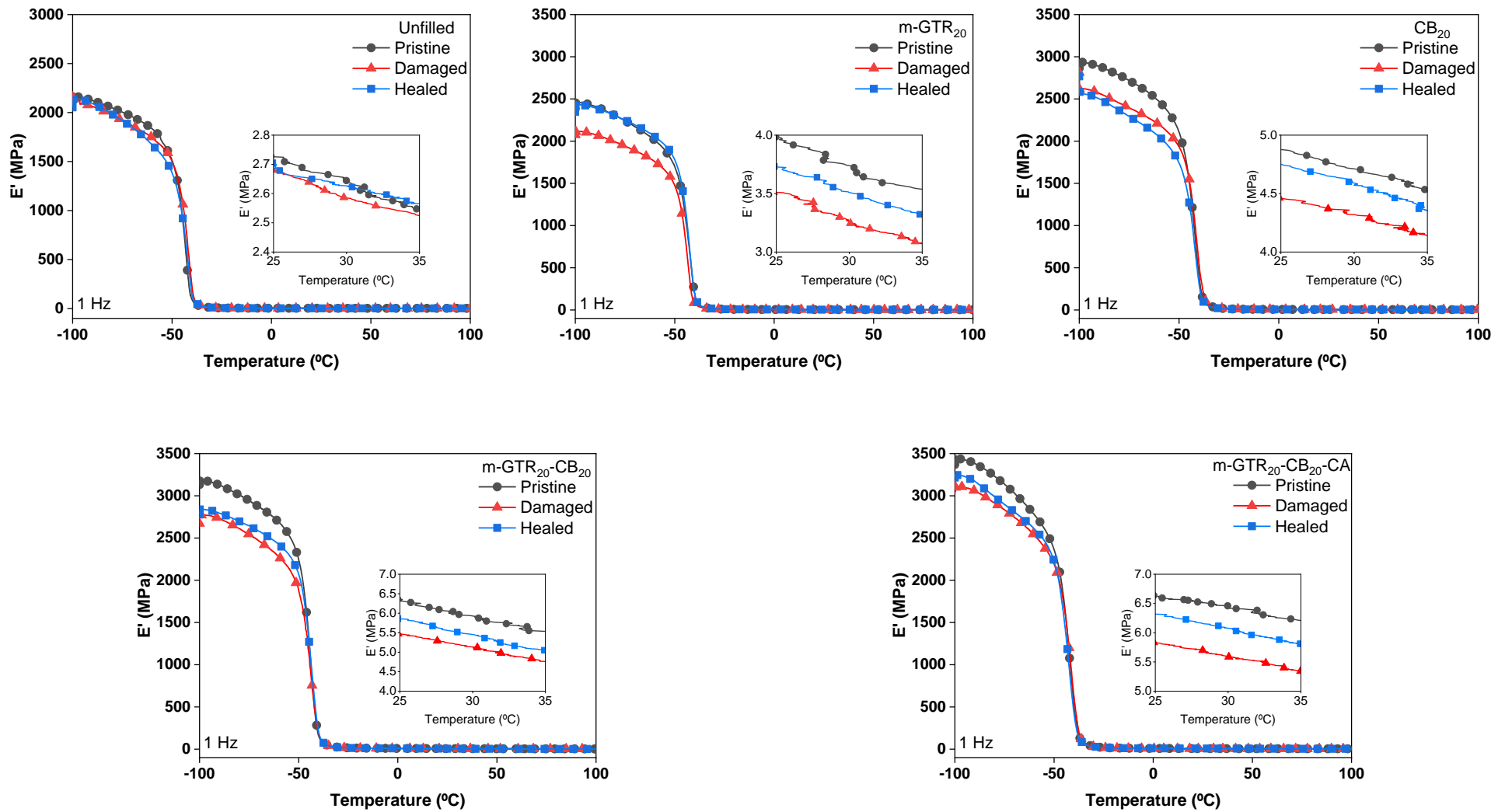


Figure 5.32 Storage modulus (E') as a function of temperature for SBR composites for pristine, damaged and healed states.

The microscopic healing efficiency was measured at different temperature regions ($-80\text{ }^{\circ}\text{C} < T_g$) and ($30\text{ }^{\circ}\text{C} > T_g$) (Figure 5.33), as the recovery of the E' between the healed and pristine state. It can be seen that there is an almost complete recovery of E' (more than 80 %) at both temperatures.

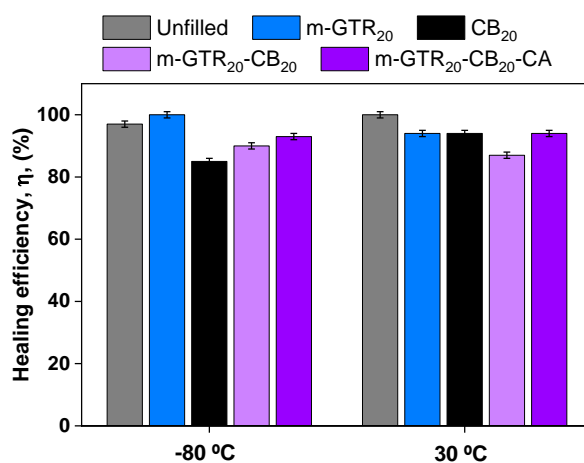


Figure 5.33 Microscopic healing efficiency of unfilled, m-GTR₂₀, CB₂₀, m-GTR₂₀-CB₂₀, and m-GTR₂₀-CB₂₀-CA at $-80\text{ }^{\circ}\text{C}$ and $30\text{ }^{\circ}\text{C}$.

The healing efficiency of the microscopic cyclic damage was compared with the results of macroscopic damage discussed in Chapter 3 (Figure 5.34). At first glance, all samples present a complete recovery of the studied property (E') of the microscopic damage using the same healing temperature but shorter times, 1 h instead of 5 h. Thus, the microscopic network damage is easier to repair than a macroscopic induced damage.

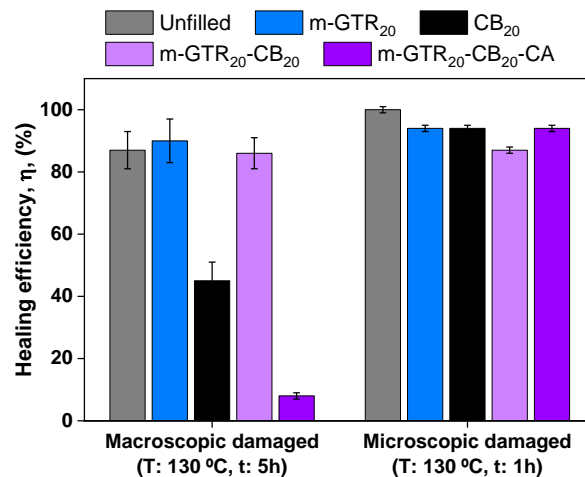


Figure 5.34 Healing efficiency as function of macroscopic and microscopic damage of unfilled, m-GTR₂₀, CB₂₀, m-GTR₂₀-CB₂₀, and m-GTR₂₀-CB₂₀-CA.

5.4.3. Healing as part of the magic triangle of tires

As detailed previously, the “magic triangle” principle of the tire industry is related to three main material-specific requirements relevant to the tread, such as rolling resistance, wet grip, and abrasion resistance; targeting lower fuel consumption, driving safety, and extended lifetime, respectively. In this section, the extended lifetime requirement (abrasion resistance) was redefined to include the healing ability of the rubber after being exposed to a cyclic deformation damage. Thus, selected SBR composites were studied in order to analyze the recovery of the viscoelastic properties associated with the final performance of the tires (wet grip and rolling resistance).

Figure 5.35 presents the values of $\tan\delta$ at low ($-10\text{ }^{\circ}\text{C}$) and at high ($60\text{ }^{\circ}\text{C}$) temperatures under pristine, damaged and healed conditions. In the damaged state, $\tan\delta$ tends to increase at both temperatures for all the SBR composites. This increase at low temperatures is ascribed to a higher energy dissipation, due to the increased rubber chains slippage and to the disruption of the filler network.[35] Meanwhile, the $\tan\delta$ increase at $60\text{ }^{\circ}\text{C}$ is related to the loss of conformational entropy with the cyclic deformation, the disentanglement of network chains, and the destruction of the filler network.[34] After the healing protocol, $\tan\delta$ shows a different response depending on the temperature region. On the one side, the wet grip values tend to increase for unfilled, m-GTR₂₀ and CB₂₀ composites; meanwhile, for hybrid reinforcing composites (m-GTR₂₀-CB₂₀) with and without CA it remains unaltered. The non-recovery of the filler network in

the hybrid composites is corroborated by the loss of the electrical conductivity after damage by cyclic deformation. On the other side, rolling resistance values tend to decrease. This behavior could be due to the creation of a new network with entanglements with lower volume of immobilized rubber and enhanced rubber–filler interactions.[45] Generally, the formation of a filler network and the associated rupture leads to energy losses that provoke an increase in the rolling resistance.[52] At the healed state, it is most likely that greater spacing is created between the filler particles, which would result in less filler–filler interactions and, hence, less hysteresis due to the Payne effect.

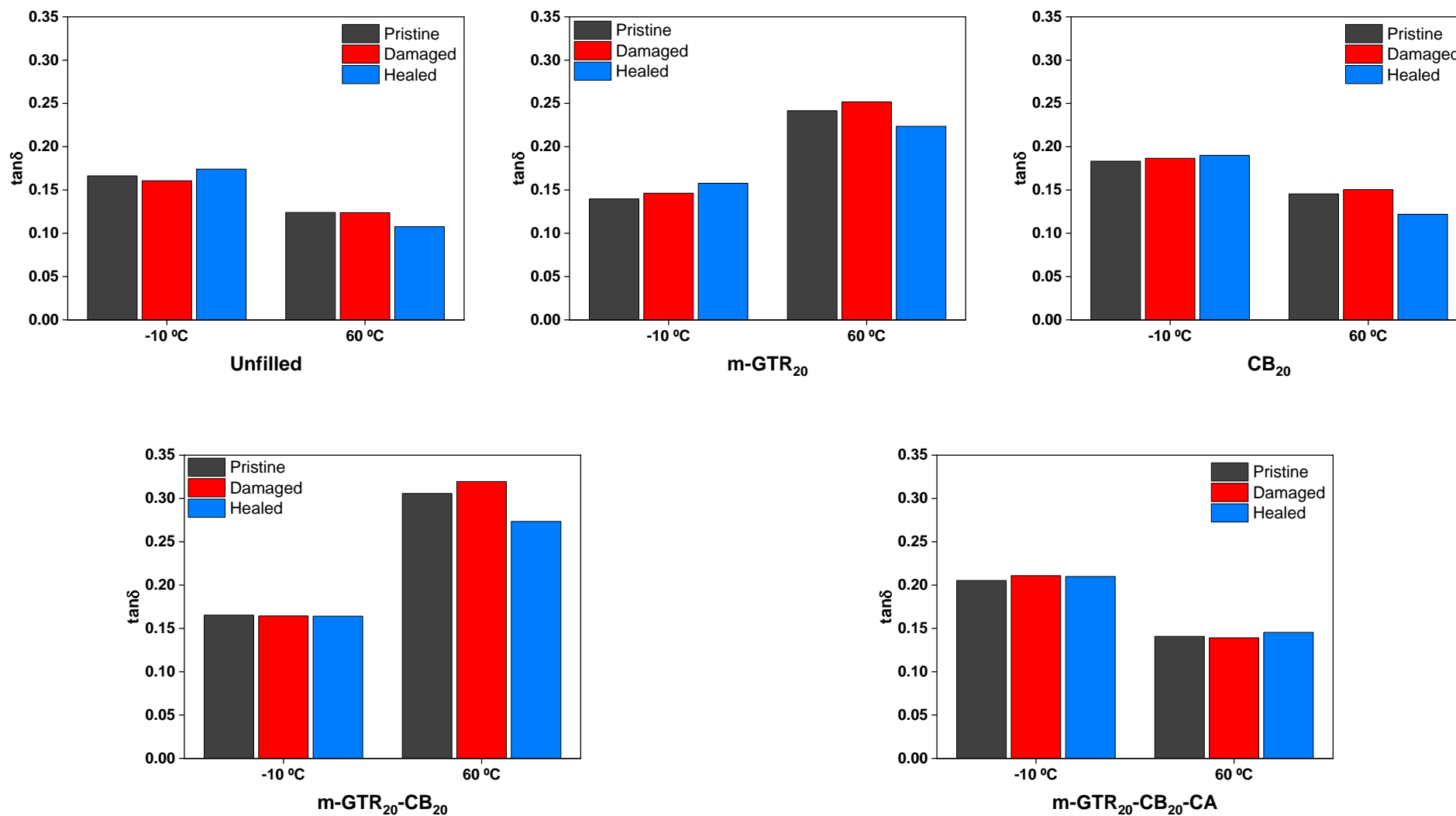


Figure 5.35 Damping factor ($\tan\delta$) of SBR composites under virgin, damaged, and repaired conditions at low (-10 °C) and high (60 °C) temperatures.

Finally, the representation of the magic triangle is presented in Figure 5.36. The radar plot shows that the hybrid composite (m-GTR₂₀-CB₂₀-CA) combines excellent healing capability (94 %) and excellent wet grip and rolling resistance compared to the CB₂₀ composite; thus, it could be a very good choice as potential material to be considered within the tire industry. It will extend the lifetime of the tire, assuring safety on the road, and giving it a sustainable feature thanks to the inclusion of tire waste.

The rolling resistance of the hybrid composite was similar to the conventional CB filled composite. Nonetheless, this parameter seems to be the less important in the upcoming years. We are in the middle of the biggest revolution in the automotive sector that it is likely to happen much more quickly than we anticipate, favoring the substitution of fuel and diesel by electric vehicles.

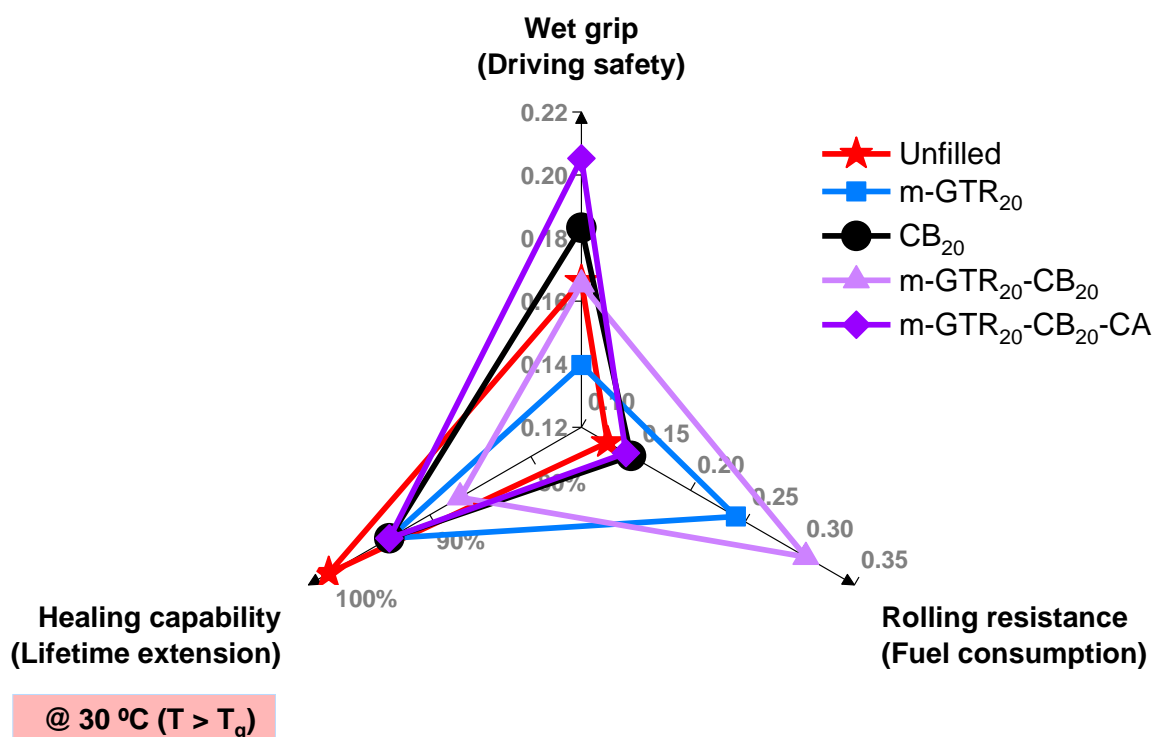


Figure 5.36 Rolling resistance, wet grip, and healing capability of SBR composites.

5.5. Summary

In the present chapter, we attempt to comprehend the changes in structure and dynamics of the SBR composites herein developed. The effect of the different additives and fillers present in each rubber compound were systematically studied. It can be concluded that all the factors that favor the formation of a more cross-linked network (presence of a CA, high S content and presence of fillers) tend to restrict the segmental dynamics of the SBR rubber. A second less restrictive process is also detected and influenced by inter- and intra-molecular interactions between the additives, filler and rubber matrix.

We also analyzed the composites under three different conditions: virgin, damaged by cyclic deformation, and thermally healed. The interpretation of healing in terms of dynamic properties is of high practical interest, since most rubber products are used in a frequency-dependent environment. Based on a series of systematic and complementary experiments by BDS and DMA, it is shown that SBR composites fully recover their stiffness at different temperature regions (-80 °C and 30 °C). All the composites show faster dynamics after damaged by cyclic deformation; meanwhile, the dynamics tends to slow down after the healing protocol. Moreover, the structure of the healed rubber network becomes more heterogeneous, suggesting chain interdiffusion and the reversibility of the disulfide bonds correlated to the healing process. It is worth mentioning that microscopic damaged composites require shorter periods of healing to achieve a high healing efficiency compared to macroscopic damaged composites.

The magic triangle of tires was also customized, substituting abrasion resistance for healing ability. The presence of a sustainable filler combined with a conventional one and with a CA optimizes the three triangle indices overcoming the delicate balance between rolling resistance, wet grip, and healing efficiency. In conclusion, the material herein studied could be useful for developing new applications that are economically and environmentally viable for the tire industry, combining repairability and sustainability.

5.6. References

1. Deshmukh, K., et al., *Dielectric Spectroscopy*, in *Spectroscopic Methods for Nanomaterials Characterization*, S. Thomas, et al., Editors. 2017, Elsevier Inc. p. 237 - 299.
2. Kremer, F. and A. Schönhals, *Theory of Dielectric Relaxation*, in *Broadband dielectric spectroscopy*. 2002, Springer Science & Business Media.
3. Forrest, M.J., *Analytical Techniques*, in *Rubber Analysis: Characterisation, Failure Diagnosis and Reverse Engineering.*, M.J. Forrest, Editor. 2018, Smithers Rapra.
4. Kremer, F. and A. Schönhals, *Analysis of Dielectric Spectra*, in *Broadband dielectric spectroscopy*. 2002, Springer Science & Business Media.
5. Havriliak, S. and S. Negami, *A complex plane representation of dielectric and mechanical relaxation processes in some polymers*. *Polymer*, 1967. **8**: p. 161-210.
6. Havriliak, S. and S. Negami. *A complex plane analysis of α -dispersions in some polymer systems*. in *J. Polym. Sci., Part C: Polym. Symp.* 1966. Wiley Online Library.
7. Fischer, E.W., *Light scattering and dielectric studies on glass forming liquids*. *Phys. A: Stat. Mech. Appl.*, 1993. **201**(1-3): p. 183-206.
8. Kramarenko, V.Y., et al., *Influence of cross-linking on the segmental dynamics in model polymer networks*. *J. Chem. Phys.*, 2000. **113**(1): p. 447-452.
9. Menar, K.P., *Dynamic Mechanical Analysis: A practical introduction*. 2008: CRC Press.
10. Wang, M.-J., *Effect of Polymer-Filler and Filler-Filler Interactions on Dynamic Properties of Filled Vulcanizates*. *Rubber Chem. Technol.*, 1998. **71**(3): p. 520-589.
11. Lindemann, N., J.E.K. Schawe, and J. Lacayo-Pineda, *Kinetics of the glass transition of styrene-butadiene-rubber: Dielectric spectroscopy and fast differential scanning calorimetry*. *J. Appl. Polym. Sci.*, 2021. **138**(5): p. 49769.
12. Abd-El-Messieh, S. and K. Abd-El-Nour, *Effect of curing time and sulfur content on the dielectric relaxation of styrene butadiene rubber*. *J. Appl. Polym. Sci.*, 2003. **88**(7): p. 1613-1621.
13. Hernández, M., et al., *Influence of the vulcanization system on the dynamics and structure of natural rubber: Comparative study by means of broadband dielectric spectroscopy and solid-state NMR spectroscopy*. *Eur. Polym. J.*, 2015. **68**: p. 90-103.
14. Rathi, A., et al., *Identifying the effect of aromatic oil on the individual component dynamics of S-SBR/BR blends by broadband dielectric spectroscopy*. *J. Polym. Sci. B Polym. Phys.*, 2018. **56**(11): p. 842-854.
15. Ortega, L., et al., *The effect of vulcanization additives on the dielectric response of styrene-butadiene rubber compounds*. *Polymer*, 2019. **172**: p. 205-212.
16. Bandzierz, K.S., et al., *Effect of polymer chain modifications on elastomer properties*. *Rubber Chem. Technol.*, 2019. **92**(1): p. 69-89.
17. *Dielectric Spectroscopy of Polymeric Materials: Fundamentals and Applications*. Vol. 119. 1997, Washington, DC.: American Chemical Society. 12029-12029.
18. Schönhals, A. and E. Schlosser, *Dielectric relaxation in polymeric solids Part 1. A new model for the interpretation of the shape of the dielectric relaxation function*. *Colloid Polym. Sci.*, 1989. **267**(2): p. 125-132.
19. Miura, N., et al., *Comparison of polymer blends and copolymers by broadband dielectric analysis*. *Polymer*, 2001. **42**(14): p. 6129-6140.
20. Robertson, C.G., et al., *Flocculation, reinforcement, and glass transition effects in silica-filled styrene-butadiene rubber*. *Rubber Chem. Technol.*, 2011. **84**(4): p. 507-519.

21. Robertson, C. and C. Roland, *Glass Transition and Interfacial Segmental Dynamics in Polymer-Particle Composites*. Rubber Chem. Technol., 2008. **81**.
22. Robertson, C.G., et al., *Influence of Particle Size and Polymer-Filler Coupling on Viscoelastic Glass Transition of Particle-Reinforced Polymers*. Macromolecules, 2008. **41**(7): p. 2727-2731.
23. Karásek, L., et al., *Percolation Concept: Polymer-Filler Gel Formation, Electrical Conductivity and Dynamic Electrical Properties of Carbon-Black-Filled Rubbers*. Polym. J., 1996. **28**(2): p. 121-126.
24. Roland, C., *Electrical and dielectric properties of rubber*. Rubber Chem. Technol., 2016. **89**(1): p. 32-53.
25. Ward, A.A., et al., *Dielectric Behaviour of Silica Filled Vinyl Solution-SBR in the Presence of Silane Coupling Agent*. KGK-Kaut. Gummi. Krunst., 2006(12): p. 654 - 658.
26. Ramarad, S., et al., *Waste tire rubber in polymer blends: A review on the evolution, properties and future*. Prog. Mater. Sci., 2015. **72**: p. 100-140.
27. De, D., D. De, and G. Singharoy, *Reclaiming of ground rubber tire by a novel reclaiming agent. I. Virgin natural rubber/reclaimed GRT vulcanizates*. Polym. Eng. Sci., 2007. **47**(7): p. 1091-1100.
28. Zedler, Ł., et al., *Processing, physico-mechanical and thermal properties of reclaimed GTR and NBR/reclaimed GTR blends as function of various additives*. Polym. Degrad. Stabil., 2017. **143**: p. 186-195.
29. Thongsang, S., et al., *Dynamic mechanical analysis and tribological properties of NR vulcanizates with fly ash/precipitated silica hybrid filler*. Tribol. Int., 2012. **53**: p. 134–141.
30. Hosseini, S.M., et al., *Comparative role of Interface in reinforcing mechanisms of Nano silica modified by Silanes and liquid rubber in SBR composites*. J. Polym. Res., 2016. **23**(9).
31. Tao, Y.-C., et al., *Reactions of silica-silane rubber and properties of silane-silica/solution-polymerized styrene-butadiene rubber composite*. Rubber Chem. Technol., 2016. **89**(3): p. 526-539.
32. Pongdong, W., et al., *Influence of Filler from a Renewable Resource and Silane Coupling Agent on the Properties of Epoxidized Natural Rubber Vulcanizates*. J. Chem., 2015. **2015**: p. 796459.
33. Ren, X. and E. Sancaktar, *Use of fly ash as eco-friendly filler in synthetic rubber for tire applications*. J. Clean. Prod., 2019. **206**: p. 374-382.
34. Mohanty, T.R., et al., *Role of calcium stearate as a dispersion promoter for new generation carbon black-organoclay based rubber nanocomposites for tyre application*. Polym. Compos., 2013. **34**(2): p. 214-224.
35. Thaptong, P., P. Sae-oui, and C. Sirisinha, *Influences of styrene butadiene rubber and silica types on performance of passenger car radial tire tread*. Rubber Chem. Technol., 2017. **90**(4): p. 699-713.
36. Wang, X., et al., *Analysis of effect of modification of silica and carbon black co-filled rubber composite on mechanical properties*. E-Polym., 2021. **21**(1): p. 279-288.
37. Kim, M.C., et al., *Preparation of novel bio-elastomers with enhanced interaction with silica filler for low rolling resistance and improved wet grip*. J. Clean. Prod., 2019. **208**: p. 1622-1630.
38. Hernández, M., et al., *Monitoring Network and Interfacial Healing Processes by Broadband Dielectric Spectroscopy: A Case Study on Natural Rubber*. Acs. Appl. Mater. Inter., 2016. **8**(16): p. 10647-10656.

39. Marckmann, G., et al., *A theory of network alteration for the Mullins effect*. J. Mech. Phys., 2002. **50**(9): p. 2011-2028.
40. Suzuki, N., M. Ito, and F. Yatsuyanagi, *Effects of rubber/filler interactions on deformation behavior of silica filled SBR systems*. Polymer, 2005. **46**(1): p. 193-201.
41. Diani, J., B. Fayolle, and P. Gilormini, *A review on the Mullins effect*. Eur. Polym. J., 2009. **45**(3): p. 601-612.
42. Zhan, Y., Y. Meng, and Y. Li, *Electric heating behavior of flexible graphene/natural rubber conductor with self-healing conductive network*. Mater. Lett., 2017. **192**: p. 115-118.
43. Kraus, G., C.W. Childers, and K.W. Rollmann, *Stress softening in carbon black-reinforced vulcanizates. Strain rate and temperature effects*. J. Appl. Polym. Sci., 1966. **10**(2): p. 229-244.
44. Diaz, R., J. Diani, and P. Gilormini, *Physical interpretation of the Mullins softening in a carbon-black filled SBR*. Polymer, 2014. **55**(19): p. 4942-4947.
45. Yan, L., et al., *Mullins effect recovery of a nanoparticle-filled polymer*. J. Polym. Sci. B Polym. Phys., 2010. **48**(21): p. 2207-2214.
46. Sattar, M.A., S. Gangadharan, and A. Patnaik, *Design of dual hybrid network natural rubber-SiO₂ elastomers with tailored mechanical and self-healing properties*. ACS Omega, 2019. **4**(6): p. 10939-10949.
47. Wool, R.P. and K.M. O'Connor, *A theory crack healing in polymers*. J. Appl. Phys., 1981. **52**(10): p. 5953-5963.
48. Maes, F., et al., *Activation and deactivation of self-healing in supramolecular rubbers*. Soft Matter, 2012. **8**(5): p. 1681-1687.
49. Hernández, M., et al., *Turning vulcanized natural rubber into a self-healing polymer: Effect of the disulfide/polysulfide ratio*. ACS Sustain. Chem. Eng., 2016. **4**(10): p. 5776-5784.
50. AbdolahZadeh, M., et al., *Healable dual organic-inorganic crosslinked sol-gel based polymers: Crosslinking density and tetrasulfide content effect*. J. Polym. Sci. A Polym. Chem., 2014. **52**(14): p. 1953-1961.
51. Canadell, J., H. Goossens, and B. Klumperman, *Self-healing materials based on disulfide links*. Macromolecules, 2011. **44**(8): p. 2536-2541.
52. Medalia, A.I., *Effect of Carbon Black on Dynamic Properties of Rubber Vulcanizates*. Rubber Chem. Technol., 1978. **51**(3): p. 437-523.

6

SUMMARY AND FINAL REMARKS

6. Summary and final remarks

6.1. General conclusions

In this doctoral thesis, SBR eco-friendly composites that combine self-healing properties with the use of waste rubber as alternative filler were developed, following circular economy principles. The main results have served for defining an environmentally friendly scenario for addressing the rubber waste disposal problem, extending service life of products and reducing rubber waste by re-bonding the damaged materials.

The following conclusions can be extracted from this work.

Repair

This work presents experimental results that validate self-healing concepts in SBR compounds. The healing mechanism arises from the combination of two different processes. First, the chain interdiffusion and formation of physical entanglements take place, during the initial stages of healing process. Second, long-range interactions and disulfide exchange reactions, as intrinsic self-healing mechanism, result in the almost full recovery of mechanical stress beyond low strains. Hence, vulcanizing additives, such as ZnO and SA, affect healing in its early stages. Meanwhile, S is the fundamental component that promotes the almost full recovery of a macroscopic damage.

Temperature and time also affect the repair mechanism, achieving higher healing efficiencies as time and/or temperature increased, thanks to the enhanced mobility and interdiffusion of molecular chains. Moreover, the SBR compound herein developed exhibited repeatable healing after multiple cycles, resulting an acceptable recovery of tensile strength of 60 % after 3 cycles.

Recycle

A fundamental, extensively and systematic study has been carried out to understand the healing mechanism of SBR composites and the influence of cryo grounded GTR (c-GTR) and modified GTR (m-GTR) as sustainable filler in the rubber properties of the developed composites.

A successful mechano-chemical modification of GTR was accomplished with a combination of a cryo-grinding process and a chemical treatment. The cryo-grinding

process was successfully optimized, reducing the average particle size of the departing material up to 100 – 150 μm . The most effective modification of the GTR particles was performed with H_2SO_4 (HT), corroborated by the increase in oxygen content on the surface of the GTR.

The c-GTR and m-GTR composites showed a good balance between tensile strength and healing capability when applying 130 $^\circ\text{C}$ during 5 h, and confirm the great potential of c-GTR and m-GTR as sustainable filler in rubber materials. A good compromise between healing efficiency and mechanical performance was promoted by the combination of disulfide bonds and reversible ionic bonds, which come from the functional groups on the surface of the m-GTR. The use of a CA provided better filler dispersion and interaction with the SBR matrix, leading to an increase in mechanical strength, but limiting the healing capability.

Hybrid reinforcing SBR composites, combining m-GTR and conventional fillers such as CB and Si, were also developed in order to overcome the limitations of c-GTR and m-GTR. The hybrid system consisting of 20 phr m-GTR and 20 phr CB turned out as the best SBR composite with a positive balance between mechanical strength and healing efficiency.

Reduce

The magic triangle of tires was customized, substituting wear resistance for healing ability. It was demonstrated that the good properties of the m-GTR₂₀-CB₂₀ sustainable composite had some limitations when applied in tire tread composites. However, in presence of a CA, the three triangle indices were optimized, overcoming the delicate balance between rolling resistance, wet grip, and healing efficiency; hence, reducing fuel consumption, increasing driving safety and extending lifetime.

Correlations between the dynamics and the molecular structure of the developed composites were also established in an attempt to understand the physical properties and the possible repair mechanism at the microscopic scale. The presence of CA, fillers and high S content tend to restrict the segmental dynamics of the SBR matrix due to the formation of a more cross-linked network. Meanwhile, accelerants affect the inter- and intra-molecular interactions between the rest of the additives, fillers and rubber matrix.

Selected composites were analyzed under three different conditions: pristine, damaged by cyclic deformation, and thermally healed. When damaged, the composites show faster dynamics; meanwhile, after the application of the healing protocol, the dynamics tends to slow down, and the rubber network becomes more heterogeneous due to the chain interdiffusion and reversibility of disulfide bonds, which enable the full recover of stiffness at different temperature regions (-80 °C and 30 °C). Moreover, it was found that a microscopic damage requires shorter periods of healing to achieve a high healing efficiency, if compared to macroscopic damaged composites.

6.2. Outlook and future work

This thesis gives a fundamental insight into the self-healing mechanism of SBR compounds and the influence of sustainable fillers (c-GTR and m-GTR) and their combination with conventional fillers (CB and Si), on the properties of the rubber matrix. The promising results reported herein represent a major contribution from the point of view of the application of circular economy principles to tire rubbers. However, many challenges remain to be studied or solved.

The analysis of the effect of the different additives in a rubber formulation should be completed, considering the individual action of the components of the activating complex (ZnO and SA).

Other surface modification processes, such as thermal, plasma, ozone, among others, should be taken into consideration, in search of better rubber-filler interactions, mechanical performance and healing capability.

The hybrid m-GTR-CB systems have already shown great advantages over the individually filled systems. The investigation of a broader range of filler combinations could lead to optimized composites with improved properties. Moreover, the focus should be on using higher amounts of GTR as sustainable filler, which would provide a second life cycle to a considerable quantity of used tires with no additional cost.

Finally, in order to study the feasibility of the development of these sustainable self-healing SBR composites within the framework of the circular economy, one should carry out a life cycle assessment (LCA); a robust and science-based tool for the analysis of the environmental and economic impact of their complete manufacturing process. The circular economy model needs proven methodologies to ensure that it generates tangible benefits for the environment and society. Therefore, LCA can complement the CE model

with robust measurements, helping to ensure the feasibility of implementation at the product level, validating their assumptions, and obtaining feedback for improvement.

APPENDIX

Appendix

Publications related to this Doctoral Thesis

1. **Araujo-Morera, J.**; Verdejo, R.; Lopez-Manchado, M.A. and Hernández Santana, M. Sustainable mobility: The route of tires through the circular economy model". *Waste Management*. **2021**, 126(3), 309-322. **(Open Access. Q1. Number of cites:10)**
2. **Araujo-Morera, J.**; Verdugo-Manzanares, R.; González, S.; Verdejo, R.; Lopez-Manchado, M.A. and Hernández Santana, M. On the Use of Mechano-Chemically Modified Ground Tire Rubber (GTR) as Recycled and Sustainable Filler in Styrene-Butadiene Rubber (SBR) Composites. *Journal of Composites Science*. **2021**, 5(3), 68. **(Open Access. Number of cites:6) (Selected as front cover)**
3. Utrera-Barrios, S.; Verdugo Manzanares, R.; **Araujo-Morera, J.**; González, S.; Verdejo, R.; López-Manchado, M.Á.; Hernández Santana, M. Understanding the Molecular Dynamics of Dual Crosslinked Networks by Dielectric Spectroscopy. *Polymers*. **2021**, 13, 3234. **(Open Access. Q1)**
4. Utrera-Barrios, S.; **Araujo-Morera, J.**; Pulido de Los Reyes, L.; Verdugo-Manzanares, R.; Verdejo, R.; Lopez-Manchado, M.A.; Hernández Santana, M. An effective and sustainable approach for achieving self-healing in nitrile rubber. *European Polymer Journal*. **2020**, 139(10), 110032. **(Q1. Number of cites:10)**
5. **Araujo-Morera, J.**; Hernández Santana, M.; Verdejo, R.; Lopez-Manchado, M.A. Giving a Second Opportunity to Tire Waste: An Alternative Path for the Development of Sustainable Self-Healing Styrene–Butadiene Rubber Compounds Overcoming the Magic Triangle of Tires. *Polymers*. **2019**, 11(12), 2122. **(Open Access. Q1. Number of cites:20)**

6. Hernández Santana, M.; Huete, M.; Lameda, P.; **Araujo, J.**; Verdejo, R.; Lopez-Manchado, M.A. Design of a new generation of sustainable SBR compounds with good trade-off between mechanical properties and self-healing ability. *European Polymer Journal*. **2018**, 106(9), 273-283. **(Q1. Number of cites:23)**

7. **Araujo-Morera, J.**; Verdejo, R.; Lopez-Manchado, M.A. and Hernández Santana. Unravelling the effect of healing conditions and vulcanizing additives on the healing performance of rubber networks. *Polymer*. **2021**. **(Q1. Under review)**

8. Alonso Pastor, L.; Núñez Carrero, K.; **Araujo-Morera, J.**; Hernández Santana, M. and Pastor, J. Setting relationships between structure and devulcanization of ground tire rubber and their effect on self-healing elastomers. *Polymers*. **2021**. **(Open Access. Q1. Under review)**

Other articles

1. González, F.J.; Montesinos, A.; **Araujo-Morera, J.**; Verdejo, R.; Hoyos, M. 'In-Situ' Preparation of Carbonaceous Conductive Composite Materials Based on PEDOT and Biowaste for Flexible Pseudocapacitor Application. *Journal of Composites Science*. **2020**, 4(3), 87. **(Open Access)**

2. Cuervo-Rodríguez, R.; Muñoz-Bonilla, A.; **Araujo, J.**; Echeverría, C.; Fernández-García, M. Influence of side chain structure on the thermal and antimicrobial properties of cationic methacrylic polymers. *European Polymer Journal*. **2019**, 117(8), 86-93. **(Q1. Number of cites:7)**

Dissemination articles

1. **Araujo-Morera, J.**; Utrera-Barrios, S. Cauchos autorreparables: La nueva frontera en el desarrollo de elastómeros inteligentes y sostenibles. *Revista SLTCaucho | Industria y Tecnología en América Latina*. **2021**, 41(2), 6-8.
2. **Araujo-Morera, J.**; Verdejo, R.; Lopez-Manchado, M.A.; Hernández Santana, M. La autorreparación: estrategia clave en el modelo de economía circular de los neumáticos. *Revista de Plásticos Modernos*. **2020**, 120(12), 5-11.
3. Utrera-Barrios, S.; Pulido de los Reyes, L.; Verdugo Manzanares, R.; **Araujo-Morera, J.**; Verdejo, R.; Hernández Santana, M. Neumáticos fuera de uso: una carga sostenible para el desarrollo de nuevos elastómeros con capacidad autorreparadora. *Revista de Plásticos Modernos*. **2020**, 120(12), 17-21.
4. **Araujo-Morera, J.**; Utrera-Barrios, S.; Peñas-Caballero, M.; Hernández Santana, M.; Verdejo, R.; Lopez-Manchado, M.A. La autorreparación, un aliado efectivo contra el impacto medioambiental de los polímeros. *Ambiente y Medio*. **2020**, 8, 16-24
5. Peñas-Caballero, M.; **Araujo-Morera, J.**; Hernández Santana, M.; Verdejo, R.; Lopez-Manchado, M.A. El futuro del sector transporte: materiales compuestos auto-reparables. *Revista de Plásticos Modernos*. **2019**, 117(2), 20-25.
6. Hernández Santana, M.; **Araujo, J.**; Pulido de Los Reyes, L.; Verdejo, R.; Lopez-Manchado, M.A. La auto-reparación: proceso clave para prolongar la vida útil de los elastómeros. *Consortio Nacional de Industriales del Caucho | Revista del Caucho*. **2018**, 2(547), 15-19.
7. Hernández Santana, M.; **Araujo, J.**; Pulido de Los Reyes, L.; Verdejo, R.; Lopez-Manchado, M.A. La auto-reparación: proceso clave para prolongar la vida útil de los elastómeros. *Revista SLTCaucho*. **2018**, 25(4), 32-35.

Oral contributions

1. Compuestos elastoméricos autorreparables: Estrategia clave en el desarrollo de una economía circular. XVI Jornadas Latinoamericanas de Tecnología del Caucho. Buenos Aires, Argentina. November **2021**.
2. Can we make rubber biocomposites that self-heal and help save the planet?. Department of Technology Management and Economics. Division of Environmental System Analysis. Chalmers University of Technology. Göteborg, Sweden. September **2021**. **(Invited talk)**
3. Autorreparación: una nueva estrategia para prolongar la vida útil de los elastómeros. Sociedad Latinoamericana de Tecnología del Caucho. Buenos Aires, Argentina. November **2020**. **(Invited talk)**
4. Development of sustainable and self-healing SBR composites. International Rubber Conference (IRC). London, UK. September **2019**.

Dissemination activities

1. **Araujo-Morera, J.**; Utrera-Barrios, S.; Peñas-Caballero, M.; Fernández-Benito, Amparo. La metamorfosis del neumático. Photopol 2019. Categoría: Sostenibilidad, valorización y reciclado de polímeros. **(Second prize)**



Contents lists available at ScienceDirect

Waste Management

journal homepage: www.elsevier.com/locate/wasman

Sustainable mobility: The route of tires through the circular economy model



Javier Araujo-Morera, Raquel Verdejo*, Miguel Angel López-Manchado, Marianella Hernández Santana*

Institute of Polymer Science and Technology ICTP-CSIC, Juan de la Cierva 3, Madrid 28006, Spain

ARTICLE INFO

Article history:

Received 30 December 2020

Revised 6 March 2021

Accepted 15 March 2021

Available online 29 March 2021

Keywords:

Tires

Circular economy

Sustainability

Recycle

End-of-life tire management

Sustainable mobility

ABSTRACT

Until nowadays, the concept of the 3Rs (Reduce, Reuse, Recycle) has tried to develop responsible consumption habits. Nonetheless, the rise of ecological thinking has generated the appearance of four new Rs in addition to these basic 3Rs; the currently 7Rs (Reduce, Reuse, Recycle, Redesign, Renew, Repair and Recover) which refer to the actions necessary to achieve the change towards a circular economy (CE) model. This model aims at extending the lifetime of the resources through their rational and efficient use to generate value repeatedly, reducing costs and waste. In this review, we examine the route followed by tires from the CE perspective, analyzing end-of-life strategies that aim to improve the circular flow of tire rubber materials. We discuss the most relevant studies on the “7Rs” concepts applied to tires, comparing different scientific approaches, as well as their industrial and commercial implementation. We also illustrate the drawbacks and feasibility of each of the R-hierarchy strategies. From the early stages of production to the post-consumption step, the path that tires trail within this CE model evidences the commitment and efforts towards the development of effective management schemes for achieving a real sustainable mobility.

© 2021 Elsevier Ltd. All rights reserved.

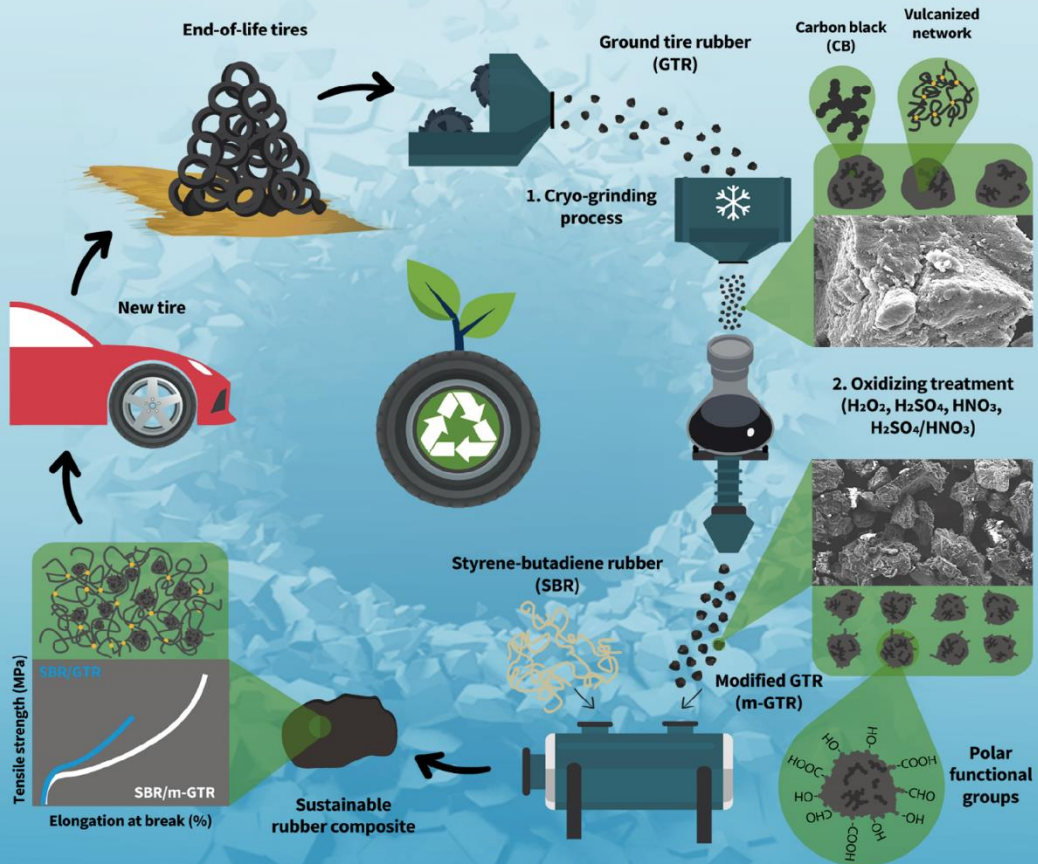
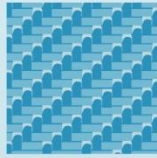
Contents

1. Introduction	310
2. The tire industry	310
3. Circular economy applied to tires	312
3.1. Redesign	312
3.2. Renew	313
3.3. Reduce	315
3.4. Reuse	315
3.5. Repair	316
3.6. Recover	317
3.6.1. Pyrolysis	317
3.6.2. Gasification	317
3.6.3. Incineration	317
3.7. Recycle	318
3.7.1. Uses of GTR	318
3.7.2. Reclaim/Devulcanization	318
4. Conclusions	319
5. Outlook and perspectives	319
CRediT authorship contribution statement	320
Declaration of competing interest	320
Acknowledgements	320
References	320

* Corresponding author.

E-mail addresses: r.verdejo@csic.es (R. Verdejo), marhema@ictp.csic.es (M. Hernández Santana).<https://doi.org/10.1016/j.wasman.2021.03.025>

0956-053X/© 2021 Elsevier Ltd. All rights reserved.



Mechano-Chemically Modified GTR as Sustainable Filler in SBR Composites

Volume 5 · Issue 3 | March 2021



mdpi.com/journal/jcs
ISSN 2504-477X



Article

On the Use of Mechano-Chemically Modified Ground Tire Rubber (GTR) as Recycled and Sustainable Filler in Styrene-Butadiene Rubber (SBR) Composites

Javier Araujo-Morera , Reyes Verdugo-Manzanares, Sergio González, Raquel Verdejo , Miguel Angel Lopez-Manchado and Marianella Hernández Santana *

Institute of Polymer Science and Technology (ICTP-CSIC), Juan de la Cierva 3, 28006 Madrid, Spain; jaraujo@ictp.csic.es (J.A.-M.); reyes@ictp.csic.es (R.V.-M.); sergio@ictp.csic.es (S.G.); rverdejo@csic.es (R.V.); lmanchado@ictp.csic.es (M.A.L.-M.)

* Correspondence: marherna@ictp.csic.es



Citation: Araujo-Morera, J.; Verdugo-Manzanares, R.; González, S.; Verdejo, R.; Lopez-Manchado, M.A.; Hernández Santana, M. On the Use of Mechano-Chemically Modified Ground Tire Rubber (GTR) as Recycled and Sustainable Filler in Styrene-Butadiene Rubber (SBR) Composites. *J. Compos. Sci.* **2021**, *5*, 68. <https://doi.org/10.3390/jcs5030068>

Academic Editor:
Francesco Tomabene

Received: 5 February 2021
Accepted: 26 February 2021
Published: 3 March 2021

Publisher's Note: MDPI stays neutral with regard to jurisdictional claims in published maps and institutional affiliations.



Copyright: © 2021 by the authors. Licensee MDPI, Basel, Switzerland. This article is an open access article distributed under the terms and conditions of the Creative Commons Attribution (CC BY) license (<https://creativecommons.org/licenses/by/4.0/>).

Abstract: The management of end-of-life tires (ELTs) is one of the main environmental issues that society faces nowadays. Recycling of ELTs appears as one feasible option for tackling the problem, although their incorporation as ground tire rubber (GTR) in other rubber matrices is limited due to poor compatibility. In this research, we report a successful combination of a cryo-grinding process with a chemical treatment for modifying the surface of GTR. Various cryo-grinding protocols were studied until a particle size of 100–150 μm was achieved. Chemical treatments with different acids were also analyzed, resulting in the optimal modification with sulfuric acid (H_2SO_4). Modified GTR was added to a styrene-butadiene rubber (SBR) matrix. The incorporation of 10 phr of this filler resulted in a composite with improved mechanical performance, with increments of 115% and 761% in tensile strength and elongation at break, respectively. These results validate the use of a recycled material from tire waste as sustainable filler in rubber composites.

Keywords: circular economy; sustainability; recycling; ground tire rubber; surface treatment; chemical modification; styrene-butadiene rubber

1. Introduction

The rational use of raw materials and polymer waste management, especially end-of-life tires (ELTs), is a global problem. One possible solution to this disposal issue is to recycle the waste and reuse it. Recycling of resources and products is one of the main strategies of the circular economy (CE) model, providing an alternative to the traditional linear economy. The CE model aims to take care of the environment and achieve a sustainable society, keeping resources in use for as long as possible and reducing costs and waste [1]. By using recycled rubber, it is possible to give a second lifecycle to a considerable number of used tires.

The first stage in any tire recycling route should involve the consideration of the production of ground tire rubber (GTR), a fine granular material obtained from worn tires. The grinding is generally carried out by impact, shearing, or cutting actions under various environmental conditions, transforming the used tires into a powder of the desired particle size. Dry or wet ambient mechanical grinding and cryogenic grinding are some of the various methods used to obtain GTR [2,3].

Direct recycling options for GTR cover a wide variety of successful applications. The use of GTR in the cement and concrete industry is an area of research that has developed considerably in the last decades [4]; in this application, the GTR improves fracture resistance, decreases density, favors thermal and acoustic isolation properties, and reduces the transmission of crack and vibrations. Also, the asphalt industry uses GTR as filler for treating road surfaces [5,6] since it reduces the noise generated by vehicles, improves crack

Article

Understanding the Molecular Dynamics of Dual Crosslinked Networks by Dielectric Spectroscopy

Saul Utrera-Barrios [†], Reyes Verdugo Manzanares [†], Javier Araujo-Morera [‡], Sergio González, Raquel Verdejo [‡], Miguel Ángel López-Manchado [‡] and Marianella Hernández Santana ^{*‡}

Institute of Polymer Science and Technology (ICTP-CSIC), Juan de la Cierva 3, 28006 Madrid, Spain; sutrera@ictp.csic.es (S.U.-B.); reyes@ictp.csic.es (R.V.M.); jaraujo@ictp.csic.es (J.A.-M.); sergio@ictp.csic.es (S.G.); r.verdejo@csic.es (R.V.); lmanchado@ictp.csic.es (M.Á.L.-M.)

* Correspondence: marherna@ictp.csic.es

[†] S.U.-B. and R.V.M. contributed equally to this work.

Abstract: The combination of vulcanizing agents is an adequate strategy to develop multiple networks that consolidate the best of different systems. In this research, sulfur (S), and zinc oxide (ZnO) were combined as vulcanizing agents in a matrix of carboxylated nitrile rubber (XNBR). The resulting dual network improved the abrasion resistance of up to ~15% compared to a pure ionically crosslinked network, and up to ~115% compared to a pure sulfur-based covalent network. Additionally, the already good chemical resistance of XNBR in non-polar fluids, such as toluene and gasoline, was further improved with a reduction of up to ~26% of the solvent uptake. A comprehensive study of the molecular dynamics was performed by means of broadband dielectric spectroscopy (BDS) to complete the existing knowledge on dual networks in XNBR. Such analysis showed that the synergistic behavior that prevails over purely ionic vulcanization networks is related to the restricted motions of rubber chain segments, as well as of the trapped chains within the ionic clusters that converts the vulcanizate into a stiffer and less solvent-penetrable material, improving abrasion resistance and chemical resistance, respectively. This combined network strategy will enable the production of elastomeric materials with improved performance and properties on demand.

Keywords: nitrile rubber; metal oxides; ionic crosslinks; dual networks; molecular dynamics; dielectric spectroscopy



check for updates

Citation: Utrera-Barrios, S.; Verdugo Manzanares, R.; Araujo-Morera, J.; González, S.; Verdejo, R.; López-Manchado, M.Á.; Hernández Santana, M. Understanding the Molecular Dynamics of Dual Crosslinked Networks by Dielectric Spectroscopy. *Polymers* **2021**, *13*, 3234. <https://doi.org/10.3390/polym13193234>

Academic Editor: Luca Vaghi

Received: 12 September 2021

Accepted: 22 September 2021

Published: 24 September 2021

Publisher's Note: MDPI stays neutral with regard to jurisdictional claims in published maps and institutional affiliations.



Copyright: © 2021 by the authors. Licensee MDPI, Basel, Switzerland. This article is an open access article distributed under the terms and conditions of the Creative Commons Attribution (CC BY) license (<https://creativecommons.org/licenses/by/4.0/>).

1. Introduction

Elastomers usually undergo a crosslinking process of their polymeric chains (known as vulcanization), which gives them their characteristic elastic behavior. Typically, the vulcanizing agent depends on the elastomer nature, but sulfur is the most widespread used in diene rubbers, forming covalent crosslinks. Sulfur vulcanization allows a precise control over material processing. By varying the proportions of sulfur and of the rest of the ingredients in the vulcanization system (accelerants and activators), networks can be obtained on demand. Peroxide vulcanization is also widely used in rubber matrices for the creation of covalent networks [1].

Special synthetic elastomers such as carboxylated rubbers admit other vulcanization agents like metal oxides (mainly zinc oxide, ZnO, and magnesium oxide, MgO) that generate ionic crosslinks (ion pair) [2]. The rise of carboxylated elastomers as promising elastomeric materials was a consequence of the early work of Brown and Gibbs [3]. In 1955, they presented the first study of properly crosslinked carboxylated elastomers, considering the role of the carboxylic group in the vulcanization. At that time, the carboxylation of elastomers was a novel synthesis proposal that opened the possibility of an alternative crosslinking to that of sulfur. The benefits of the carboxylic group over different properties that were being discovered were adequately collected in multiple reviews of the literature [2,4]. However, it was not until the work of Eisenberg, in which a molecular model (currently in



Contents lists available at ScienceDirect

European Polymer Journal

journal homepage: www.elsevier.com/locate/europolj

An effective and sustainable approach for achieving self-healing in nitrile rubber



Saul Utrera-Barrios, Javier Araujo-Morera, Laura Pulido de Los Reyes, Reyes Verdugo Manzanares, Raquel Verdejo, Miguel Ángel López-Manchado, Marianella Hernández Santana*

Institute of Polymer Science and Technology (ICTP-CSIC), Juan de la Cierva 3, Madrid 28006, Spain

ARTICLE INFO

Keywords:
Carboxylated nitrile rubber
Self-healing
Ionic crosslinks
Ground tire rubber
Sustainability

ABSTRACT

Nitrile rubber is considered the workhorse of the automotive rubber industry, thanks to its chemical resistance and mechanical performance. However, applications such as hoses, seals or gaskets are prone to damage, limiting their lifetime. In this work, carboxylated nitrile rubber (XNBR) was ionically crosslinked with zinc oxide (ZnO), forming ionic domains grouped into ionic clusters. These clusters have the advantage of being reversible under the application of an external stimulus such as temperature, conferring the material a certain self-healing capability and enabling a lifecycle extension. Ground tire rubber selectively modified by grafting of poly(acrylic acid) (gGTR), was added to XNBR-ZnO compounds with the aim of improving the healing properties of the rubber matrix. The incorporation of acid groups contributed to the formation of additional ionic clusters during the crosslinking process, resulting in a notorious increase in healing efficiency from 15% for the XNBR-ZnO to 70% for the XNBR-ZnO-gGTR compound. Chemical and mechanical resistance were also evaluated, showing that the addition of a waste material like gGTR keeps mechanical strength suitable for many applications; meanwhile, it does not deteriorate its resistance to aliphatic solvents such as motor oil and gasoline. These promising results open the path for developing sustainable rubber products with extended lifetime and applicable within the automotive industry.

1. Introduction

Nitrile rubber (NBR) is a random copolymer of acrylonitrile and butadiene. It is commonly considered one of the pillars of the automotive rubber industry because of its good mechanical properties, its resistance to lubricants and greases and its relative low cost. A wide range of choices is also possible as far as the NBR chemical structure is concerned. As an example, carboxylated nitrile rubber (XNBR) contains carboxyl groups as active functional groups, resulting in a rubber more abrasion resistant and more convenient for industrial seal applications.

The different molecular structure and the presence of active functional groups also enable following different crosslinking routes. Several strategies have been put forward for the formation of rubber networks composed of chemical (covalent) and/or physical (non-covalent) crosslinks [1–4]. Under deformation, physical crosslinks usually dissociate before the chemical crosslinks since their bond energies are generally lower. After the deformation is removed, physical crosslinks can form again but the damage caused by the rupture of

chemical crosslinks remains [5].

Ionic elastomers consist of a physically crosslinked network formed by ionic-rich domains due to the formation of a salt as a consequence of the approximation of the Zn^{2+} ion of the oxide with two COO^- of XNBR [1]. These ionic domains gather in higher structures known as multiplets which in turn form clusters that can dissociate and associate with temperature, demonstrating their reversible nature [1,6–9]. The latter are characterized by having high proportions of trapped chains, which restrict mobility and lead to the appearance of a new transition (i.e. the ionic transition) above the glass transition temperature (T_g). This dynamic characteristic enables them to be considered as healing moieties [10,11], understanding self-healing as the ability to repair damages and partially restore the original material properties [12–15]. The strategy of incorporating ionic domains as healing moieties has been used in different elastomers. The most widespread approach is the direct incorporation of zinc dimethacrylate (ZDMA), a complex formed by the combination of one Zn^{2+} with two $-OOC-C(CH_3)=CH_2$ (an ion pair) with a powerful electrostatic interaction that enables the

* Corresponding author.

E-mail address: marherna@ictp.csic.es (M. Hernández Santana).

<https://doi.org/10.1016/j.eurpolymj.2020.110032>

Received 19 August 2020; Received in revised form 10 September 2020; Accepted 11 September 2020

Available online 17 September 2020

0014-3057/ © 2020 Elsevier Ltd. All rights reserved.

Article

Giving a Second Opportunity to Tire Waste: An Alternative Path for the Development of Sustainable Self-Healing Styrene–Butadiene Rubber Compounds Overcoming the Magic Triangle of Tires

Javier Araujo-Morera , Marianella Hernández Santana * , Raquel Verdejo  and Miguel Angel López-Manchado 

Institute of Polymer Science and Technology (ICTP-CSIC), Juan de la Cierva 3, 28006 Madrid, Spain; jaraujo@ictp.csic.es (J.A.-M.); rverdejo@ictp.csic.es (R.V.); lmanchado@ictp.csic.es (M.A.L.-M.)

* Correspondence: marherna@ictp.csic.es

Received: 25 November 2019; Accepted: 13 December 2019; Published: 17 December 2019



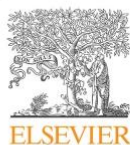
Abstract: Current regulations demand tires with long lifetime and reduced fuel consumption without sacrificing car safety. However, tire technology still needs to reach a suitable balance between these three indicators. Here, we address them by developing a self-healing tire compound using styrene–butadiene rubber (SBR) as the matrix and reclaimed tire waste as the sustainable filler. The addition of ground tire rubber (GTR) to the matrix simultaneously improved the rolling resistance and maintained both wet grip and healing ability. We provide an in-depth analysis of the healing behavior of the material at a scale close to the relevant molecular processes through a systematic dynamic-mechanical and dielectric analysis. We found that SBR and SBR/GTR compounds show a complete recovery of stiffness and relaxation dynamics after being damaged by cyclic deformation, resulting in a heterogeneous repaired rubber network. This new development could well overcome the so-called magic triangle of tires, which is certainly one of the key objectives of the tire industry.

Keywords: styrene–butadiene rubber; sustainability; self-healing; ground tire rubber; magic triangle; molecular dynamics

1. Introduction

One of the most serious environmental problems facing society today is the accumulation of a great quantity of used tires in landfill sites, and the increasing automotive production over the years is continuously aggravating it [1]. Recycling and recovering used tires can be considered reasonable strategies to solve this concern. However, some limitations have to be defeated, since a tire is composed of various materials and additives incorporated in the rubber compound, turning it into a very complex system [2,3]. The more stringent environmental regulations and the fluctuating price of raw materials are the driving forces for the development of several innovative recycling technologies [4]. The recycling of waste tires has important implications in energy conservation, environmental protection, costs reduction, and in promoting the “4R” principle (Re-use, Reduce, Recycle, and Recover) [2,5,6]. One of the main ways to consume tire waste is in the production of technically less demanding rubbers by mixing rubber powder (i.e., grinding the rubber waste to form granulates) with new rubbers (or plastics) [7]. Sports and playing surfaces, floors and walkway tiles, concrete mixtures [8], asphalt mixtures [9], thermal and acoustic isolation, and footwear, among others, are traditional fields of application of ground tire rubber (GTR).

More recently, dedicated efforts have been put forth to convert GTR into other added value products with improved performance [1]. Research concerning the incorporation of GTR in natural rubber



Contents lists available at ScienceDirect

European Polymer Journal

journal homepage: www.elsevier.com/locate/europolj

Design of a new generation of sustainable SBR compounds with good trade-off between mechanical properties and self-healing ability



Marianella Hernández Santana*, María Huete, Patricia Lameda, Javier Araujo, Raquel Verdejo, Miguel A. López-Manchado

Institute of Polymer Science and Technology (ICTP-CSIC), Juan de la Cierva 3, Madrid 28006, Spain

ARTICLE INFO

Keywords:
Styrene-butadiene rubber (SBR)
Self-healing
Ground tire rubber (GTR)
Mechanical properties
Silane
Sustainable

ABSTRACT

Self-healing polymers typically face an enforced trade-off between repairability and mechanical properties, with a high degree of self-healing being achieved mainly by materials having low mechanical strength and stiffness. This study focuses on the development of SBR compounds that can combine together self-healing properties with the use of ground tire rubber (GTR) as alternative sustainable filler. The self-healing efficiency of GTR filled SBR compounds is compared to conventional carbon black filled compounds. The influence of the vulcanization system and the addition of silane-based coupling agents are also assessed. Results show that SBR compounds vulcanized by means of a semi-efficient sulfur based system recover around 50% of their mechanical strength, being the self-healing response related to the presence of disulfide bonds. Contrary to carbon black compounds, GTR samples present similar healing efficiency to the unfilled SBR samples, improving mechanical properties in 50%. Moreover, the coupling agent enhances even more (up to 80%) the mechanical strength of the SBR-GTR compounds without adversely affecting the healing efficiency. These results can thus be seen as a starting model material for developing new sustainable applications economically and environmentally convenient with good mechanical properties as well as healing ability.

1. Introduction

Elastomers are a special class of polymeric materials with a wide range of application. Apart from their common use in our daily life as tires or shoes they are also extensively used in other industrial sectors like the aerospace or the biomedical industry. Such a widespread usage is due to the unique properties these materials display, namely their large elastic deformation and their excellent noise and vibration damping capabilities. While these materials can sustain large deflections with little or no permanent deformation, elastomers can also fail through fracture and fatigue processes. This inherent weakness makes the prospect of self-healing materials more than ever attractive. Intrinsic self-healing polymers make use of reversible moieties to obtain on-demand or autonomous repair of macroscopic, microscopic or even molecular damages leading to the loss of certain functionality [1].

Developments of self-healing rubbers started with the pioneering work of Cordier et al. in 2008 [2]. They reported the synthesis of an autonomous healing rubber based on supramolecular assembly. Since then, many different healing routes have been developed and new families of self-healing rubbery-like materials and crosslinked elastomers

have evolved [3–19]. All self-healing methods have the aim to generate crosslinks in networks, either by physical interactions (molecular interdiffusion/rearrangements), and/or by chemical reactions of various kinds of functional groups (dynamic bonds). In general terms, the first steps of healing involve physical interactions, while at later stages, the chemical reactions occur. Over time the rearrangement of the chains on the damaged surface progresses into diffusion on a low level, and then further into a seemingly random and complete diffusion of the chains, making the material appear as one again [20]. As an example, Yamaguchi et al. designed polyurethanes (PU) in which the chemically controlled chain ends facilitated the autonomous healing of a fully cut polymer at $T > T_g$ in about 10 min [3]. It was hypothesized that the relatively long distance between the free end of the molecule and its first physical crosslink point (“the dangling length”) facilitate the observed crack disappearance. In a later review paper, the healing efficiency of similar PU was presented and defined as the tear strength of the healed material over the virgin material [18]. The phenomenon of healing facilitated by dangling chains has also been investigated leading to high healing degrees at room temperature in a mechanically interesting thermoplastic elastomer [15]. In their work the authors used

* Corresponding author.

E-mail address: marherna@ictp.csic.es (M. Hernández Santana).

<https://doi.org/10.1016/j.eurpolymj.2018.07.040>

Received 20 April 2018; Received in revised form 18 July 2018; Accepted 24 July 2018

Available online 25 July 2018

0014-3057/ © 2018 Elsevier Ltd. All rights reserved.

Article

'In-Situ' Preparation of Carbonaceous Conductive Composite Materials Based on PEDOT and Biowaste for Flexible Pseudocapacitor Application

Francisco J. González * , Andreina Montesinos, Javier Araujo-Morera , Raquel Verdejo and Mario Hoyos * 

Instituto de Ciencia y Tecnología de Polímeros, ICTP-CSIC, Juan de la Cierva, 3, 28006 Madrid, Spain; montesinosandreina@gmail.com (A.M.); jaraujo@ictp.csic.es (J.A.-M.); r.verdejo@csic.es (R.V.)

* Correspondence: fgonzalez@ictp.csic.es (F.J.G.); hoyos@ictp.csic.es (M.H.); Tel.: +34-915-622-900 (M.H.)

Received: 4 June 2020; Accepted: 1 July 2020; Published: 3 July 2020



Abstract: Composite materials of poly(3,4-ethylenedioxythiophene) (PEDOT)/activated carbon (AC) were prepared by 'in-situ' polymerization and subsequently deposited by spray-coating onto a flexible electrolyte prepared in our laboratories. Two activated carbons were tested: a commercial activated carbon and a lab-made activated carbon from brewer's spent grain (BSG). The porous and spongy structure of the composite increased the specific surface area, which helps to enhance the energy storage density. This procedure to develop conductive composite materials using AC prepared from biowaste has the potential to be implemented for the preparation of polymer-based conductive inks for further applications as electrodes in pseudocapacitors.

Keywords: conductive composite materials; biowaste; brewer's spent grain; activated carbon; conjugated polymer; 'in-situ' polymerization; electrodes; flexible pseudocapacitor

1. Introduction

Energy demand has drastically increased around the world with the growing population and due to the rapid development of wearable electronics and microelectronic devices [1]. Unfortunately, the use of renewable energies, such as solar and wind sources presents the inconvenience of its intermittent nature. In this context, energy storage devices have become a key academic and industrial research topic towards a low cost and zero environmental impact energy source, which can be supplied on demand [2]. As a consequence, there is a great interest on developing novel materials for energy storage devices using preferably low cost materials and sustainable methodologies [3,4].

During the past decade, the global supercapacitors market has been growing rapidly as an energy storage source compared to batteries [5]. In comparison to batteries, they are able to charge energy in a faster way and can have much more charge–discharge cycles. Most employed supercapacitors are known as electronic double-layer capacitors (EDLC) due to the electrical double layer generated during the charge process.

In order to increase the capacity of supercapacitors, different active materials have been used. Particularly, conjugated polymers (CPs) have shown promising characteristics as electrodes for supercapacitors. Unlike EDLC, the charge–discharge mechanism in these materials is due to the faradaic reactions, which occur on the bulk and surface between the electrode and the electrolyte [6]. This pseudo-capacitance gives the name of pseudocapacitors, where other materials such as metal oxides have been also used. These pseudocapacitors can be considered intermediate materials between batteries and EDLC in terms of capacity but with much lower cycles and lower power density compared to EDLC [7].



Contents lists available at ScienceDirect

European Polymer Journal

journal homepage: www.elsevier.com/locate/europolj

Influence of side chain structure on the thermal and antimicrobial properties of cationic methacrylic polymers



Rocío Cuervo-Rodríguez^a, Alexandra Muñoz-Bonilla^{b,c}, Javier Araujo^b, Coro Echeverría^{b,c}, Marta Fernández-García^{b,c}

^a Facultad de Ciencias Químicas (UCM), Av. Complutense s/n, Ciudad Universitaria, 28040 Madrid, Spain

^b Instituto de Ciencia y Tecnología de Polímeros (ICTP-CSIC), C/Juan de la Cierva 3, 28006 Madrid, Spain

^c Interdisciplinary Platform for Sustainable Plastics towards a Circular Economy, SUSPLAST-CSIC, Spain

ARTICLE INFO

Keywords:

Cationic copolymers
Thiazole
Stability
Charge density
Thermal
Blends
Antimicrobial

ABSTRACT

A novel methacrylic monomer, 2-(((2-(4-methylthiazol-5-yl)ethoxy)carbonyl)oxy)ethyl methacrylate (MTZ), containing in the lateral chain both hydrolytically sensitive carbonate and thiazole groups has been firstly described. Posterior, it was free-radical polymerized and copolymerized with acrylonitrile in anhydrous solution of dimethylsulfoxide, with the purpose of investigate the influence of its chemical and structural characteristics on the antimicrobial activity. Cationic antimicrobial polymers were subsequently obtained by alkylation reaction with methyl and butyl iodide agents. Their thermal behavior was analyzed in all series, modified and unmodified copolymers in terms of glass transition temperature and thermal stability. The antimicrobial activity in solution was tested against Gram-positive *Staphylococcus aureus* and *Staphylococcus epidermidis*, Gram-negative *Escherichia coli* and *Pseudomonas aeruginosa* bacteria, and *Candida parapsilosis* yeast and further correlated with their zeta potential. Then, blends of these cationic polymers with commercial polyacrylonitrile as matrix material were prepared and their effectiveness as antimicrobial coating was determined against Gram-negative *Escherichia coli* bacteria. In addition and due to the presence of the carbonate groups in the copolymer structures, these systems could be further used as antimicrobial releasing coatings in alkaline conditions.

1. Introduction

The rising prevalence of drug-resistant pathogenic microorganisms together with the dwindling supply of new antibiotics is one of the most serious global health concerns in modern medicine [1,2]. This context has encouraged scientist to research for new antimicrobial agents as an alternative to traditional antibiotics. In the last years, cationic polymers have aroused considerable attention as antimicrobial agents due to their outstanding properties. Compared to small cationic compounds, polymers such as those based on quaternary ammonium, phosphonium, imidazolium, and pyrrolidinium groups exhibit higher antimicrobial activity, chemical stability, lower toxicity and low propensity to induce resistance [3–6]. Unlike traditional antibiotics, the mechanism of action against bacteria is mainly by membrane disrupting, which is assumed to be the reason of this low susceptibility to generate resistance, as this pathway is more difficult for bacteria to circumvent. Although the mode of action is not completely understood, the mechanism seems to involve adsorption of the polymers onto the negatively charged bacterial membrane through electrostatic interactions, disruption of the wall also by penetration and insertion of

hydrophobic segments into the inner part of the membrane, and cell lysis and release of cytoplasmic components, which finally leads to bacterial death [7]. Typically, Gram-negative bacteria with an additional outer membrane result less susceptible to cationic polymers than Gram-positive with a single membrane [8]. Most of the bacterial membrane are negatively charged while mammalian cells have a net neutral charge on the surfaces provided by zwitterionic phospholipids, a fact that gives selectivity and then low cytotoxicity [9]. Therefore, from this mechanism it is clear that in addition to positive charge, the antimicrobial polymers should have hydrophobic segments, i.e. an appropriate hydrophilic/hydrophobic balance, to facilitate their permeation through the apolar lipid bilayers of the bacteria wall. Indeed, host defense antimicrobial peptides (HD-AMP) with amphiphilic structure have been a source of inspiration to design and develop new synthetic antimicrobial peptides and polymers [10–13]. Conventional synthetic polymers including amphiphilic polymethacrylates, polystyrenes or poly(vinyl pyridine)s mimicking AMP, offer many advantages over synthetic peptides made from artificial amino acids, such as stability and versatility, but principally their synthesis allows cost effective large scale production. Synthetic polymers can be easily synthesized from a

E-mail addresses: sbonilla@ictp.csic.es (A. Muñoz-Bonilla), marta fg@ictp.csic.es (M. Fernández-García).

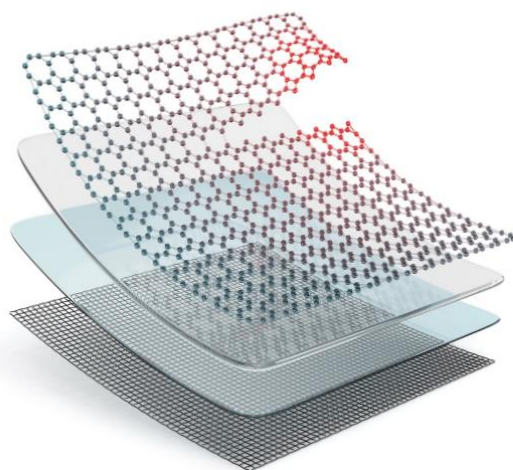
<https://doi.org/10.1016/j.eurpolymj.2019.05.008>

Received 11 April 2019; Received in revised form 3 May 2019; Accepted 7 May 2019

Available online 08 May 2019

0014-3057/ © 2019 Elsevier Ltd. All rights reserved.

Cauchos autorreparables: La nueva frontera en el desarrollo de elastómeros inteligentes y sostenibles



Desde el inicio de la Ciencia y Tecnología de Polímeros, hace cien años, la búsqueda de nuevos y mejores materiales ha seguido un enfoque tradicional, es decir, el desarrollo de materiales cada vez más resistentes (en términos de desempeño mecánico) con tiempos de vida útil diversos.

Este enfoque ha estado asociado al modelo de **economía lineal**, modelo basado en el principio de extraer, fabricar, consumir y desechar, por el cual un material al finalizar su vida útil se convierte en un desecho, con consecuencias ambientales cada vez más evidentes.

En este contexto, se han buscado alternativas que permitan contrarrestar los efectos negativos de la economía lineal, y apareció un nuevo enfoque en la Ciencia de Materiales basado en el modelo de **economía circular**.

El modelo de economía circular reemplaza el principio de desechar por restaurar, para alcanzar

un uso racional y eficiente de los recursos y prolongar los tiempos de vida útil de los materiales. **La búsqueda de estrategias que permitan el desarrollo de nuevos materiales con propiedades inteligentes que alarguen esos tiempos, es un factor clave** en la evolución hacia una sociedad sostenible; y en este proceso, la naturaleza ha servido como modelo de inspiración.

Uno de los ejemplos más prometedores de materiales bioinspirados son los materiales autorreparables (Figura 1). **Estos son capaces de repararse o restaurar sus propiedades de forma automática, autónoma o al aplicar un estímulo externo, prolongando su vida útil, ahorrando energía, materias primas y reduciendo la generación de residuos.**

La capacidad autorreparadora se puede encontrar en la naturaleza, específicamente en estrellas de mar, moluscos, insectos e incluso en nuestra piel. El desarrollo de materiales con esta capacidad

COLUMNISTAS INVITADOS

MSc-Ing. Saúl Utrera-Barrios (ESP)
sutrera@ictp.csic.es

MSc-Ing. Javier Araujo-Moreira (ESP)
jaraujo@ictp.csic.es

COORDINADOR

Dr. Mariano Escobar (ARG)
Dpto. Diseño de Materiales,
INTI - CONICET.
ritc@sltcaucho.org

alimatic
SILOS
 Instalaciones de Silos



Sistema semiautomático de carga de silos hasta 8.000 Kgs./h.



Células de carga **alimatic** precisión ±100 Kgs.



Panel de control integrado con control de consumos

Instalaciones completas llave en mano de silos para almacenado de materias primas

ALIMATIC, S.L.
 C/ Andorra, 19 B y C
 08830 SANT BOI DE LLOBREGAT (Barcelona) SPAIN
 Tel. +34 93 652 56 80 - Fax +34 93 652 56 86
 e-mail: alimatic@alimatic.com

La autorreparación: estrategia clave en el modelo de economía circular de los neumáticos

Autores: Javier Araujo-Morera, Raquel Verdejo, Miguel A. López-Manchado, Marianella Hernández Santana*

Instituto de Ciencia y Tecnología de Polímeros (ICTP-CSIC)
 * marherna@ictp.csic.es



Resumen

El modelo de economía circular (EC) tiene como objetivo alargar la vida útil de los recursos mediante su uso racional y eficiente, con el fin de generar valor de forma repetida, reduciendo costes y residuos. Los principios de la EC (Rediseñar, Renovar, Reducir, Reutilizar, Reparar, Recuperar y Reciclar) pueden

aplicarse a los neumáticos durante todo su ciclo de vida, que abarca desde el proceso de producción hasta la etapa de post-consumo. Dentro del contexto de Reparar, la autorreparación, cuyo objetivo es recuperar propiedades después de sufrir un daño, sigue siendo una tecnología incipiente en cuanto a neumáticos se refiere. Sin embargo, los esfuerzos

actuales llevados a cabo por la industria y por el sector académico sin duda conducirán a la mejora y desarrollo de una sociedad donde la movilidad sea realmente sostenible gracias a la aplicación de la estrategia de autorreparación.

Palabras clave: neumáticos; autorreparación; economía circular; movilidad sostenible.



Índice

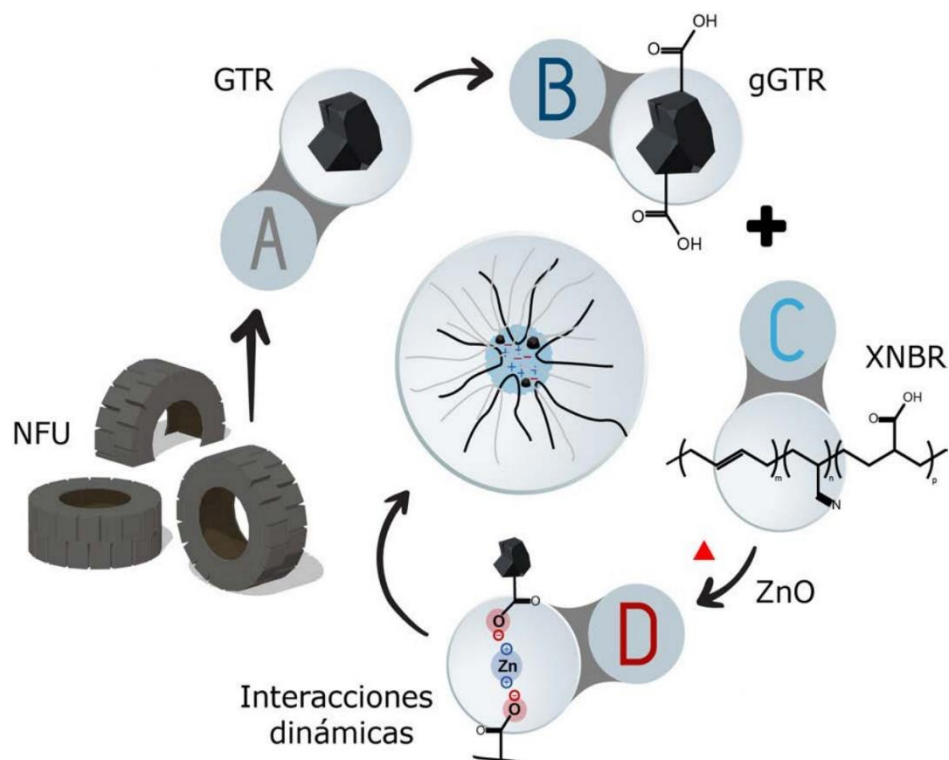
Noticias

Neumáticos fuera de uso: una carga sostenible para el desarrollo de nuevos elastómeros con capacidad autorreparadora

Autores: Saul Utrera-Barrios; Laura Pulido de los Reyes; Reyes Verdugo Manzanares; Javier Araujo-Morera; Raquel Verdejo; Marianella Hernández Santana*

Instituto de Ciencia y Tecnología de Polímeros (ICTP-CSIC), Juan de la Cierva 3, 28006, Madrid, España.

* marherna@ictp.csic.es



Resumen

La revalorización de los residuos plásticos, y en concreto de los residuos de neumáticos, supone generar un nuevo ciclo de vida útil a estos materiales reduciendo así la generación de desechos. Dicha revalorización ha supuesto, generalmente, el desarrollo de materiales de bajo valor añadido y poco atractivos comercialmente. En este trabajo, por el contrario, se busca aportar un alto valor añadido a dichos residuos mediante su empleo en el-

tómeros inteligentes con capacidad autorreparadora. La funcionalización e incorporación de polvo de neumático fuera de uso (GTR) ha permitido aumentar la capacidad de reparación de un caucho nitrilo carboxilado de un 20 a un 70% mediante la formación de entrecruzamientos iónicos reversibles.

Palabras clave: caucho nitrilo carboxilado, neumáticos fuera de uso, materiales autorreparables, entrecruzamientos iónicos, propiedades mecánicas.

Abstract

The revalorization of plastic waste, and specifically of tire waste, means generating a new useful life cycle for these materials, thus reducing the generation of rubbish. This revalorization has generally led to the development of low benefit and commercially unattractive materials. In this work, on the contrary, it is sought to provide a high added value to that waste through its use in smart elastomers with self-healing capacity. The functionaliza-

tion and incorporation of end-of-life tire powder (GTR) have made it possible to increase the reparability of a carboxylated nitrile rubber from 20 to 70% through the formation of reversible ionic crosslinks.

Keywords: carboxylated nitrile rubber, ground tire rubber, self-healing materials, ionic crosslinks, mechanical properties.



Índice

Noticias

REVISTA DE PLÁSTICOS MODERNOS Vol. 120 Número 762 Diciembre 2020

17

LA AUTORREPARACIÓN, UN ALIADO EFECTIVO CONTRA EL IMPACTO MEDIOAMBIENTAL DE LOS POLÍMEROS

J Araujo-Morera; S Utrera-Barrios; M Peñas-Caballero;

M Hernández Santana; R Verdejo ✉; MA López-Manchado

Instituto de Ciencia y Tecnología de Polímeros (ICTP-CSIC), Juan de la Cierva, 3, 28006 Madrid, España

✉ r.verdejo@csic.es

Resumen

La mala disposición y manejo de los desechos de polímeros representa uno de los problemas más graves para el medioambiente y, dentro de los polímeros, los termoestables y elastómeros se encuentran en desventaja frente a los termoplásticos, porque no se pueden reprocesar fácilmente debido a su estructura entrecruzada. Una alternativa para solucionar este problema es el desarrollo de una nueva generación de materiales autorreparables, capaces de recuperar o restaurar daños de forma automática y autónoma. Esta nueva generación de materiales se presenta como un elemento indispensable en el contexto ambiental actual, ya que mejoran la eficiencia en el uso de recursos y extienden su ciclo de vida, por lo que suponen una contribución importante a la reducción del impacto medioambiental de los polímeros.

Palabras clave: Autorreparación; Materiales Poliméricos; Materiales Compuestos;
Enlaces: Reversibilidad.

1. Introducción

Los polímeros, generalizados como “plásticos”, son considerados los materiales del siglo XXI. Esto se debe a su relativo bajo costo, facilidad de transformación, bajo peso, durabilidad y a la versatilidad de características y propiedades que presentan [1]. Estas ventajas convierten a los plásticos en materiales de uso habitual en una amplia gama de aplicaciones, entre las que se encuentran las pertenecientes al sector automotriz, construcción, aeroespacial, farmacéutico, entre otros [2].

Actualmente, la mala gestión de desechos y el uso irracional de materias primas, se han convertido en uno de los problemas de mayor relevancia para el medioambiente, empeorando progresivamente como consecuencia del desarrollo y crecimiento económico de la Sociedad [1]. La masiva fabricación de productos plásticos y la mala disposición al final de su ciclo de vida útil, que generalmente termina siendo en vertederos o en el ambiente, ha derivado en un grave impacto medioambiental que representa uno de los retos y desafíos tecnológicos y económicos más significativos de nuestros tiempos [3, 4].

El futuro del sector transporte: materiales compuestos auto-reparables

Autores: M. Peñas-Caballero*; J. Araujo-Morera*; M. Hernández Santana*; R. Verdejo; M. López-Manchado

Instituto de Ciencia y Tecnología de Polímeros (ICTP-CSIC), Juan de la Cierva 3, Madrid 28006, Spain

*marherna@ictp.csic.es

*Ambos autores han contribuido igualmente en este trabajo.

Resumen

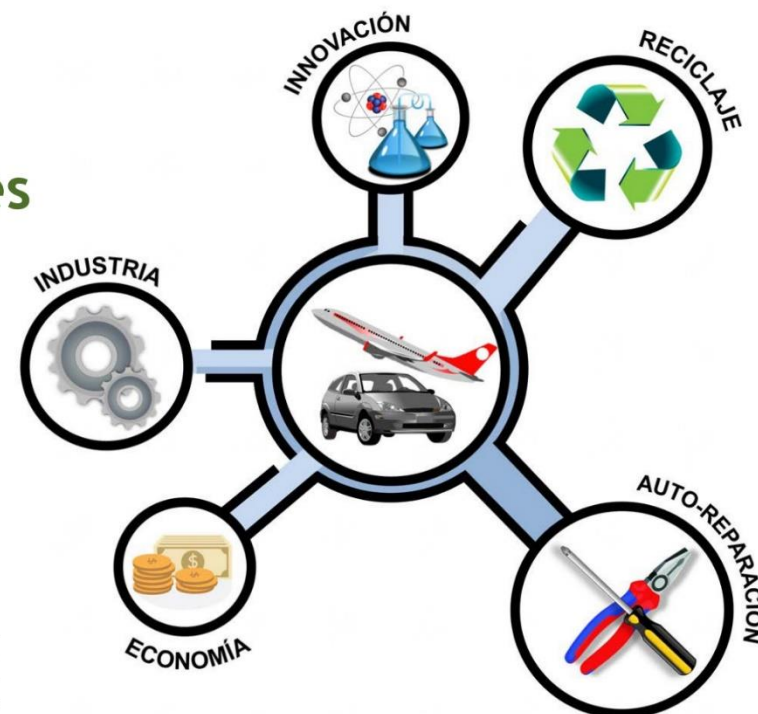
La auto-reparación, es la capacidad de un material, de repararse de forma autónoma, tras sufrir un daño por su uso, agresiones externas, etc. Este comportamiento es una alternativa eficiente para aumentar la vida útil de un material. En este trabajo, se analiza la capacidad auto-reparadora de matrices termoestables y elastómeros, materiales ampliamente usados en el sector transporte. Los resultados preliminares revelan una capacidad de reparación del 50%. Estos resultados marcan el inicio en el desarrollo de materiales innovadores, que reducirán los contenidos de residuos y permitirán su reutilización, todo ello englobado dentro de los principios de economía circular.

Palabras Clave: auto-reparación; termoestables; elastómeros; resinas epoxi; reciclaje; economía circular; industria; sector transporte; innovación.

Abstract

Self-healing is the ability a material has for repairing autonomously, after suffering damage. This behavior is an efficient alternative for extending the lifetime of a material. In this work, we analyze the self-healing capacity of thermoset matrices and elastomers, materials widely used in the transport sector. Preliminary results reveal a self-healing capacity of 50%. These results will, with no doubt, play a key role for the development of innovative materials that will reduce the amount of waste and allow their reuse, all according to circular economy principles.

Keywords: self-healing; thermosets; elastomers; epoxy resin; recycling; circular economy; industry; transport sector; innovation.



Introducción

Desde mediados del siglo XVIII, con el inicio de la Revolución industrial, hasta nuestros días el sistema económico de consumo de la Sociedad se ha basado en la extracción de materia prima, la producción de bienes, el consumo y la generación de residuos. Este hecho se conoce como Economía Lineal (**Figura 1a**), la cual es responsable del grave impacto medioambiental que existe en la actualidad, siendo insostenible e incompatible con un mundo de recursos limitados. Es así como surge la necesidad de cambiar el siste-

ma hasta entonces conocido, por una alternativa más eficiente tanto económica como ambientalmente denominada Economía Circular [1]. Los principios de la Economía Circular se basan en reducir, reusar, reciclar y reparar componentes y materiales, tal como se esquematiza en la **Figura 1b**. De tal manera que se mantienen los recursos en uso durante el mayor tiempo posible, extrayendo el valor máximo de ellos mientras están en uso, recuperando y regenerándolos en toda la cadena de valor del producto y el ciclo de vida de la cuna a la cuna [2-4].



Índice

Noticias



La auto-reparación: proceso clave para prolongar la vida útil de los elastómeros

Marianella Hernández Santana*; Javier Araujo; Laura Pulido; Raquel Verdejo; Miguel A. López-Manchado
 Instituto de Ciencia y Tecnología de Polímeros (ICTP-CSIC), Juan de la Cierva 3, 28006 Madrid
 *e-mail: marherna@ictp.csic.es

Resumen

En el marco de la nueva legislación Europea, se hace necesario replantear el uso de los polímeros y extender su ciclo de vida útil. El diseño de materiales poliméricos auto-reparadores, capaces de reparar daños de una manera más o menos independiente, es una alternativa eficiente para extender ese ciclo de vida, así como para reducir la cantidad de desechos plásticos. En los últimos años, se ha despertado un gran interés por los materiales elastoméricos auto-reparadores en los cuales el reto es obtener una red entrecruzada con enlaces covalentes débiles que puedan conferir capacidad de auto-reparación a la vez que buenas propiedades mecánicas. Una de las líneas de investigación prioritarias del grupo de Compuestos Poliméricos del Instituto de Ciencia y Tecnología de Polímeros del Consejo Superior de Investigaciones Científicas (ICTP-CSIC) se centra en el desarrollo de compuestos elastoméricos auto-reparadores capaces de superar ese reto.

Palabras clave: elastómero; auto-reparación; nanocompuestos; desechos

INTRODUCCIÓN

Tradicionalmente, los científicos han enfocado su investigación en el diseño de materiales que sean robustos y capaces de resistir daños mecánicos y químicos. La estrategia ha funcionado muy bien en las últimas décadas, desarrollándose materiales altamente resistentes.

Sin embargo, a pesar de presentar un desempeño favorable, los materiales siguen siendo susceptibles de sufrir daños y fallar en algún momento de su vida útil. Los materiales auto-reparadores surgen para resolver esta limitación dado que buscan restaurar, de manera parcial o total, daños mecánicos localizados y extender así su vida útil (ver Figura 1).



Os invitamos a participar,
 simplemente enviando un email a:
innovacion@consorcio Caucho.es



**PRÓXIMA COMISIÓN DE
 MEDIOAMBIENTE, ENERGÍA, TUTELA
 DE PRODUCTO y PRL:**

**21 DE NOVIEMBRE
 en las instalaciones de FEIQUE (MADRID)**

**TODOS LOS ASOCIADOS
 estáis invitados**



Convenio de colaboración con Revista del Caucho de España

Este acuerdo con **Revista del Caucho de España**, que pertenece al Consorcio Nacional de Industriales del Caucho, nos permite intercambiar artículos técnicos y de índole social entre las dos publicaciones.

La auto-reparación: proceso clave para prolongar la vida útil de los elastómeros

Autores: Marianella Hernández Santana*; Javier Araujo; Laura Pulido; Raquel Verdejo; Miguel A. López-Manchado Instituto de Ciencia y Tecnología de Polímeros (ICTP-CSIC), Juan de la Cierva 3, 28006 Madrid
*E-mail: marherna@ictp.csic.es

Resumen

En el marco de la nueva legislación Europea, se hace necesario replantear el uso de los polímeros y extender su ciclo de vida útil.

El diseño de materiales poliméricos auto-reparadores, capaces de reparar daños de una manera más o menos independiente, es una alternativa eficiente para extender ese ciclo de vida, así como para reducir la cantidad de desechos plásticos.

En los últimos años, se ha despertado un gran interés por los materiales elastoméricos auto-reparadores en los cuales el reto es obtener una red entrecruzada con enlaces covalentes débiles que puedan conferir capacidad de auto-reparación a la vez que buenas propiedades mecánicas.

Una de las líneas de investigación prioritarias del grupo de Compuestos Poliméricos del Instituto de Ciencia y Tecnología de Polímeros del Consejo Superior de Investigaciones Científicas (ICTP-CSIC) se centra en el desarrollo de compuestos elastoméricos auto-reparadores capaces de superar ese reto.

Palabras clave: elastómero; auto-reparación; nanocompuestos; desechos

CAUCHO CONECTADO 4.0



Introducción

Tradicionalmente, los científicos han enfocado su investigación en el diseño de materiales que sean robustos y capaces de resistir daños mecánicos y químicos.

La estrategia ha funcionado muy bien en las últimas décadas, desarrollándose materiales altamente resistentes.

Sin embargo, a pesar de presentar un desempeño favorable, los materiales si-



Figura 1. Representación esquemática del desempeño de materiales convencionales, resistentes y auto-reparadores en el tiempo.



PHOTOPOL2019

Accesit

Sostenibilidad, valorización
y reciclado de polímeros

"La metamorfosis del neumático"

Javier Araujo-Morera,

Mónica Peñas-Caballero,

Saúl Utrera-Barrios,

Amparo Fernández-Benito.

